ELECTROCHEMICAL STUDIES

OF

SOLID SOLUTION ELECTRODES

A Thesis

presented for the degree of

Doctor of Philosophy

in the Faculty of Science of the

University of St Andrews

TO MY PARENTS

WITHOUT WHOSE SUPPORT

THIS THESIS

WOULD NOT HAVE BEEN SUBMITTED.

DECLARATION

I declare that this thesis is my own composition, that the work of which it is a record has been carried out by me, and that it has not been submitted in any previous application for a Higher Degree.

This thesis describes results of research carried out in the Department of Chemistry, United College of St Salvator and St Leonard, University of St Andrews under the supervision of Dr C.A. Vincent since 1st October 1978.

Michael Smith

CERTIFICATE

I hereby certify that Michael Smith has spent twelve terms of research work under my supervision, has fulfilled the conditions of Ordinance Number 12 of St Andrews University, and is qualified to submit the accompanying thesis in application for the degree of Doctor of Philosophy.

C.A. Vincent
Director of Research

ACKNOWLEDGEMENTS

I would like to thank Dr C.A. Vincent for his help and encouragement throughout this work, and the University of St Andrews for a Research Scholarship award, and travel grants.

Thanks are also due to Professor Lord Tedder and Professor Wyatt for providing research facilities.

I gratefully acknowledge the help provided by Mr J.S. McKechnie and other members of staff during the course of this research.

Finally, I record my thanks to Paula who tolerated much before the thesis was presented.

SUMMARY

Using a method based on the analysis of the voltage transient recorded during the application of a galvanostatic pulse to a solid state, three electrode cell, diffusion coefficients of silver electroactive species in $Ag_xTiS_{1.8}$ and Ag_xNbS_2 were obtained. The activation energy of the diffusion process was found to be approximately 30 kJ $mole^{-1}$ for $TiS_{1.8}$ and between 34 kJ $mole^{-1}$ and 24 kJ $mole^{-1}$, decreasing with increasing guest concentration, for NbS_2. Non-linearity at extended times in the experimental timescale was ascribed to finite length effects, variation of the thermodynamic enhancement factor during the pulse, or a combination of these influences.

Temperature and composition variation of the cell emf, for $Ag_xTiS_{1.8}$ and Ag_xNbS_2 systems, permitted thermodynamic parameters and the compositional variation of the enhancement factors to be obtained.

Investigation of the effect of the temperature of oven pre-treatment on compressed powder samples of a lithium ion conducting vitreous electrolyte on the bulk conductivity was carried out using a scanning electron microscope and ac conductivity measurements.

Electronic conductivity measurements, using Wagner's method were undertaken on samples of iodotungstate and iodoarsenate glass with a view to confirmation of the low levels necessary for the use of these electrolytes in galvanic cells.

TABLE OF CONTENTS

CHAPTER 1: SOLID SOLUTION ELECTRODE MATERIALS

1.1 Introduction to Solid Solution Electrodes (SSE)

In the last decade interest in the development of more efficient and convenient methods of energy storage and utilisation has prompted study of several new types of battery systems. Rapid increase of the number of portable devices in everyday use, (calculators, watches, radios, tape recorders, cameras etc.),which use microcircuit technology and in many cases have fairly modest power requirements, has extended the market for miniature, efficient, primary and secondary power cells. The existence of this market has redirected considerable financial and research resources toward the investigation of novel or improved miniature cells. Ambient temperature lithium cells are of particular interest as lithium has important advantages of lightness and high electrochemical potential.

Various lithium organic electrolyte batteries are currently under investigation as high energy density secondary power sources. The use of a lithium metal electrode in organic electrolyte cells has given rise to problems associated with its poor stripping-plating efficiency.[1] Several authors[2-5] have proposed the replacement of the lithium electrode with an "intercalation electrode". These electrodes operate by a topochemical reaction which permits the reversible incorporation of metal ions into a "host" crystal lattice, and are included in the general class of "solid solution electrodes".[2] (SSE). These materials behave as very non-ideal solutions and it is this property, amongst others, which makes them of considerable interest as a new class of electrode materials.

Since the early seventies a considerable research effort has been invested in this new class of compounds.

1.2 Properties of Ideal Solid Solution Electrode Materials (SSE)

The concept of SSE materials was introduced by Steele[2], and Armand[6], who discussed the requirements, summarised below, for a mixed conducting, non-stoichiometric electrode, A_xMX_y, incorporating the electroactive species A.

The electrode material should show a high conductivity of both ionic species A, and electrons, in order that diffusion coefficients of A in the host be high, (leading to high current densities) and that electronically conducting diluents should not be required. The host should have a substantial capacity for the guest species and the free energy of formation of the A_xMX_y compound should be fairly constant over the range of composition. In all electrode systems the electrode material should be capable of forming stable interfaces with the electrolyte used, and transfer across the electrode/electrolyte interface should be rapid.

If these criteria are fulfilled by two different electrode materials for the same guest species, and a suitable electrolyte is available then a cell such as that shown in Figure 1(a) may be visualised, the so-called "rocking chair" cell, in which two SSE materials are used with the active species transferred between them in charge/discharge cycles. Individual potential versus composition profiles for the two electrodes, (Figures 1(b) and 1(c)), potential versus composition of anode and cathode combined, (Figure 1(d)), and the cell potential versus composition (Figure 1(e)), for a hypothetical ideal cell are included to illustrate the operation of this type of cell. Quite recently investigations of cyclable cells using this design have reported encouraging results.[4,5]

A large number of compounds which satisfy some, if not all, of the "good SSE criteria" have been reported. Of these the most promising candidates have either "layer" or "open-channel framework" type lattices. This chapter serves as a review of the properties of the transition metal dichalcogenides (generally designated TCh_2), probably the most thoroughly researched group of SSE compounds.

1.3 Transition Metal Dichalcogenides; The Host Structure (TCh_2)

TCh_2 compounds may be broadly classified as layered or non-layered. The layered compounds indicated in Figure 2, adopt one of the two types of 6:3 coordination. As shown in Figures 3(a) and (b), the metal ion situated between two sheets of chalcogen atoms may be in either a trigonal prismatic or octahedral site, depending on the relative position of the

FIGURE 1(a)

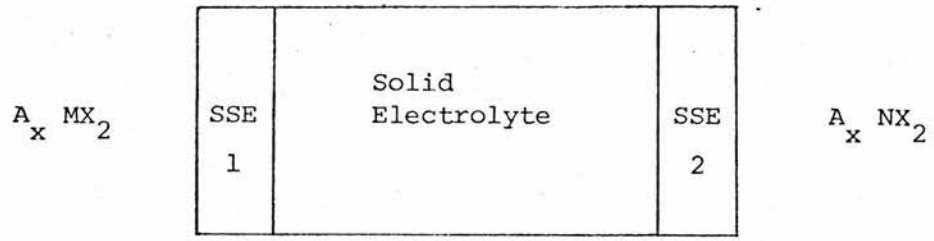

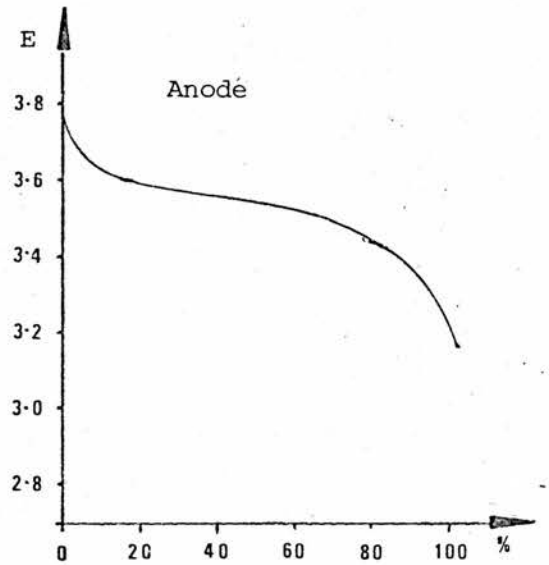

FIGURE 1(b): Potential Versus Percentage Anode Capacity A_xMX_2

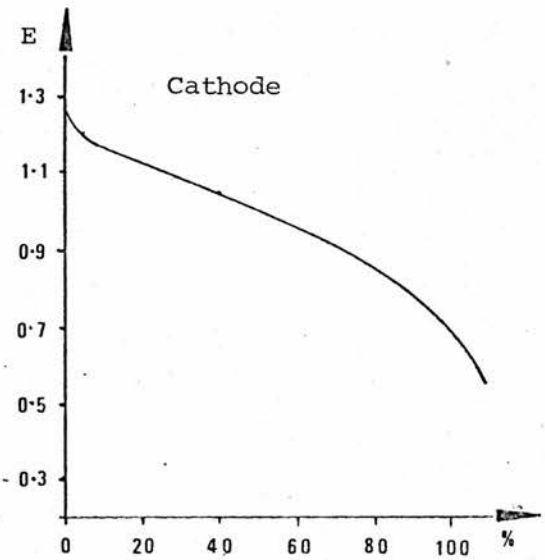

FIGURE 1(c): Potential Versus Percentage Cathode Capacity A_xNX_2

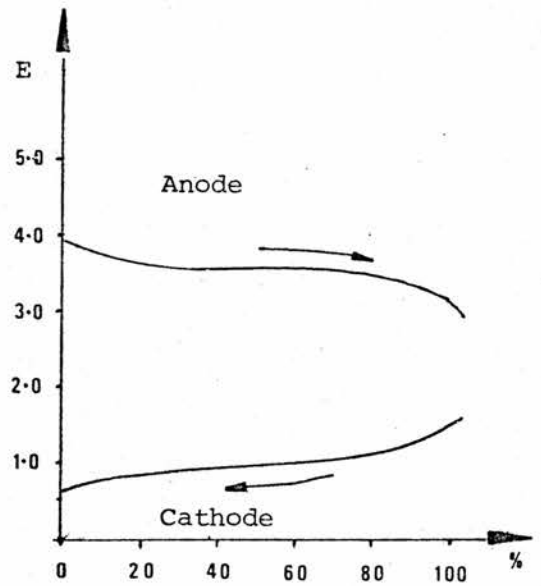

FIGURE 1(d): Individual Electrode Potentials During Cell Operation

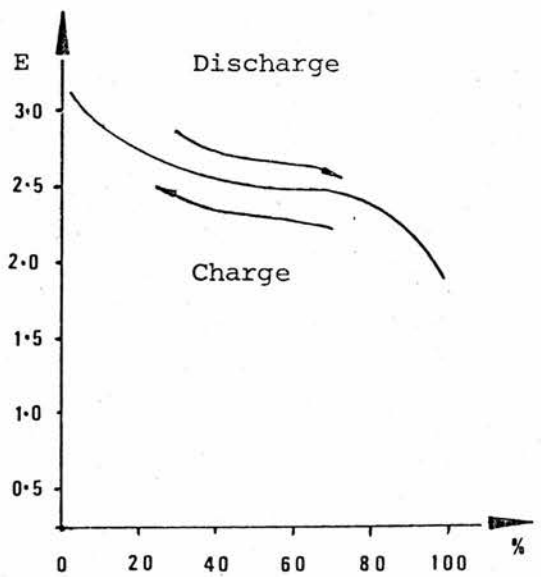

FIGURE 1(e): Overall Cell Potential.

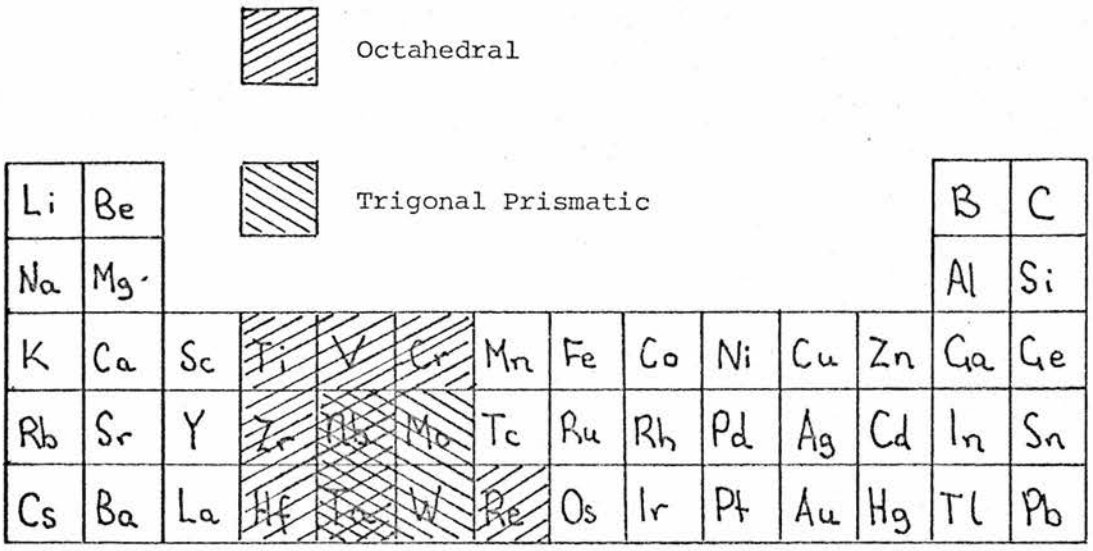

FIGURE 2: Periodic Table showing the Transition metals that form layered chalcogenides with octahedral or trigonal prismatic coordination

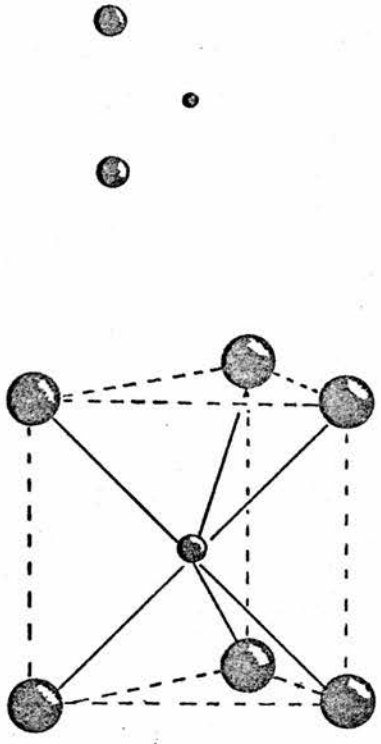

FIGURE 3(a): Trigonal Prismatic Stacking Order

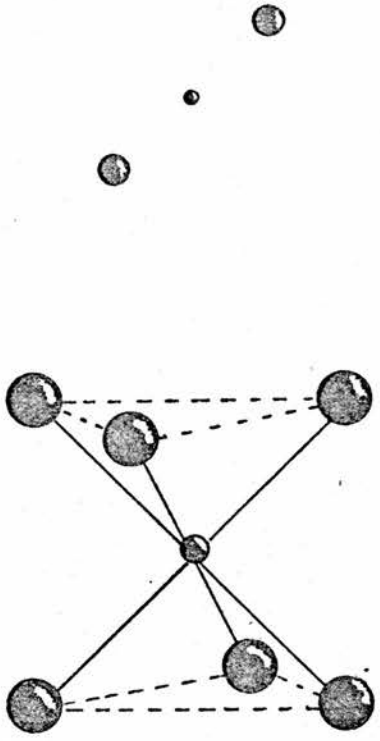

FIGURE 3(b): Octahedral Stacking Order

chalcogen sheets. The host structure is made up of ordered stacks of Ch-T-Ch layers. As there are very many permutations of relative layer position within stacks of several layers, and compounds exist with mixed coordination, (trigonal prismatic and octahedral in different layers), it follows that the structures of this class of compounds are numerous and complicated.

In reference to different structures of one compound, free use is frequently made of the terms polymorph and polytype. As defined by Verma and Krishna[7], polymorphism is the ability of some compounds to exist in more than one structural form. Polytypism is defined as a special kind of one dimensional polymorphism shown by only a few groups of compounds, one of which is the layered TCh_2 compounds.

Various systems of nomenclature and representation have been developed to uniquely describe complicated layer structures. The "ABC" notation is the simplest and describes the relative positions of atoms within a TCh_2 layer. The three sites in the plane of a hexagonally close packed sheet of atoms are designated A, B or C, (Figure 4), to indicate the anion, a, b or c, lower case, indicates the transition metal position, and [a], [b], and [c], the intercalated guest species.

Where a description of the layer disposition is required, this may be achieved by indicating the number of layer units in the c-direction of the lattice repeat unit, 1, 2, 3 etc., and the symmetry of the chalcogenide atoms round the transition metal atom by T (trigonal), H (hexagonal) or R (rhombohedral). If there is more than one polytype of a given compound they may be distinguished by subscription or a lower case letter, this letter indicating the order of discovery.

Three dimensional representation of the compounds is usually very difficult. It is more common to find $(11\bar{2}0)$ sections.

These three methods of description are probably more readily understood with reference to examples. These methods of representation of a selection of TCh_2 compounds are included in Figure 5.

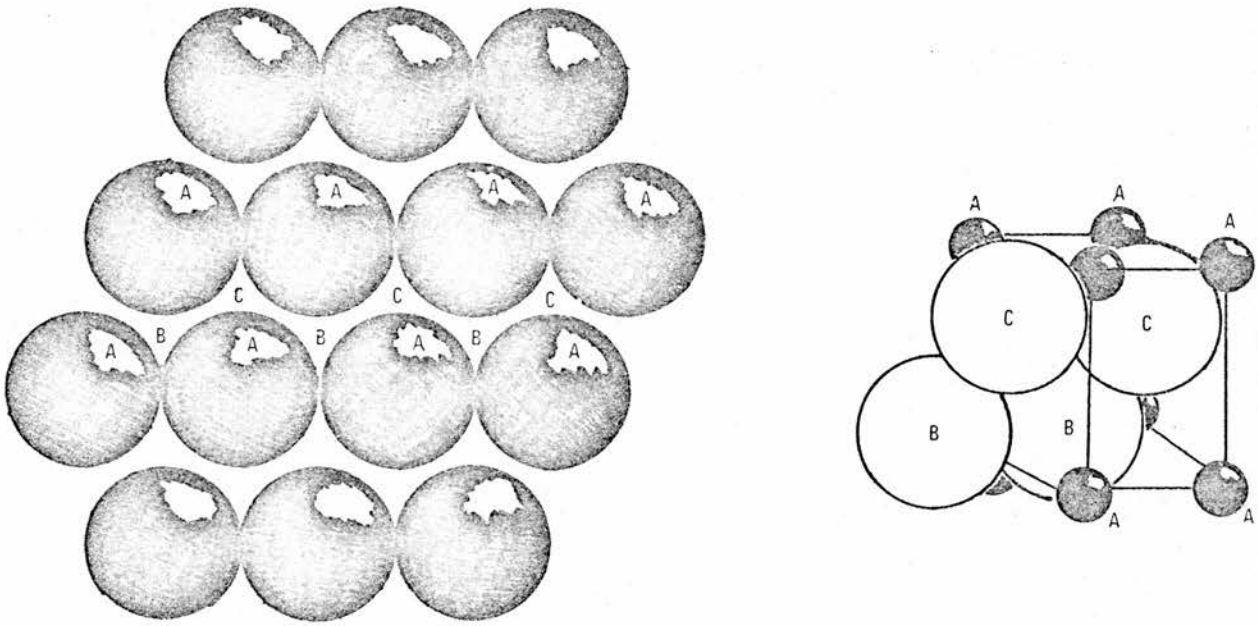

FIGURE 4: A B C notation, 001 section through lattice showing atomic positions and three-dimensional representation

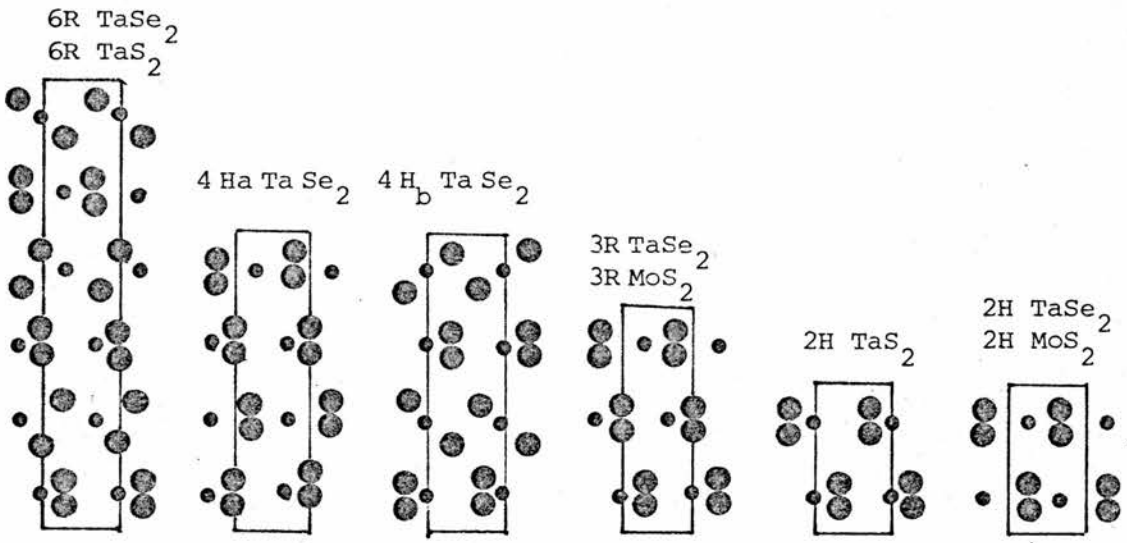

FIGURE 5: Sections through (1120) plane of polymorphic or polytypic phases, illustrating nomenclacture schemes.

1.4 Synthesis of TCh_2 Compounds

TCh_2 compounds may be synthesised in single crystal and polycrystalline form by a variety of methods.[8] Various chemical transport techniques[9] have been used in the production of large single crystals used in x-ray analysis investigations of structure. Preparations involving reduction of metal oxides with CS_2 or reaction of metal chlorides with H_2S at elevated temperatures have also been successful for certain compounds. Probably the simplest and most commonly used method for the production of polycrystalline samples is that of direct combination of the elements in sealed quartz ampoules, at elevated temperatures. Different polytypes of a given TCh_2 compound may be synthesised depending on oven temperatures, reaction duration and annealing or quenching procedures.

An important aspect of the structure, as far as applications as electrode materials are concerned, is the stoichiometry of the resultant compound. Compounds of the type $T_{1+x}\ Ch_2$ may be formed under certain conditions, with quite different electrochemical properties. This feature of the compound structure is therefore very important and will be discussed further in the next section.

1.5 Structure of the Intercalates $A_x TCh_2$

Layered TCh_2 compounds of transition elements form compounds arising from intercalation of molecules or ions into the host structure in such a manner as to permit return to the initial compound through appropriate physical or chemical treatment. A large number of elements in the Periodic Table react directly or indirectly with these structures to form well-defined compounds. In addition to the many inorganic compounds reported, there are a variety of organic intercalation products, where the organic molecule is considered to bond weakly with the TCh_2 layers. Molecules of the Lewis base type, amides, N-heterocycles, S, P and N oxides, have been reported as forming stable compounds.[10]

The structural consequences, on the host, of the intercalation reaction are either a) a lateral movement of layers to form a different polytype, or b) vertical dilation of the Van der Waals gap to accommodate

the guest species. These modifications are shown schematically in Figure 6. Figure 7 shows the geometries of the two types of site available to the guest species, (a) Trigonal prismatic, or (b) Octahedral/Tetrahedral.

In some cases intercalation compounds have been reported as forming stage type phases.[11] These staged phases have been found in many layered phases, notably graphitic compounds.[12] In these structures, not all the van der Waals gaps are occupied, Figure 8.

Metal rich phases of TCh_2 compounds may also form intercalation compounds. The rate of guest intercalation into this host has been reported as less rapid than with a near stoichiometric host. The excess metal is resident in the van der Waals gap and a correlation between metal rich non-stoichiometry and an inhibition of c-axis dilation on intercalation has been found.[12] An explanation has been proposed in terms of a "structure pinning" effect due to the excess metal bonding with adjacent sulphur layers. This has a derogatory influence on the rate of diffusion of the guest species in the lattice and also on the electrode material capacity.

1.6 Synthesis of the Intercalated Compounds.

Reported synthetic methods may be classified into three groups.

(a) Solid State Reactions

The intercalated compounds may be prepared by heating weighed mixtures of the elements, or mixtures of the host material with the guest metal, in evacuated, sealed quartz ampoules under appropriate conditions of temperature and reaction time. As before, the heating and cooling history determines the phase structure of the product. In some cases these direct reaction methods have led to the formation of impurity phases.

(b) Liquid Reagent Methods

The first alkali metal intercalates were formed by reaction of a solution of alkali metal in ammonia with transition metal sulphides. Reactions using liquid reagents may be conveniently carried out in evacuated, sealed vessels. This method with solutions in ammonia, however, has two major disadvantages. The product of the reaction is a

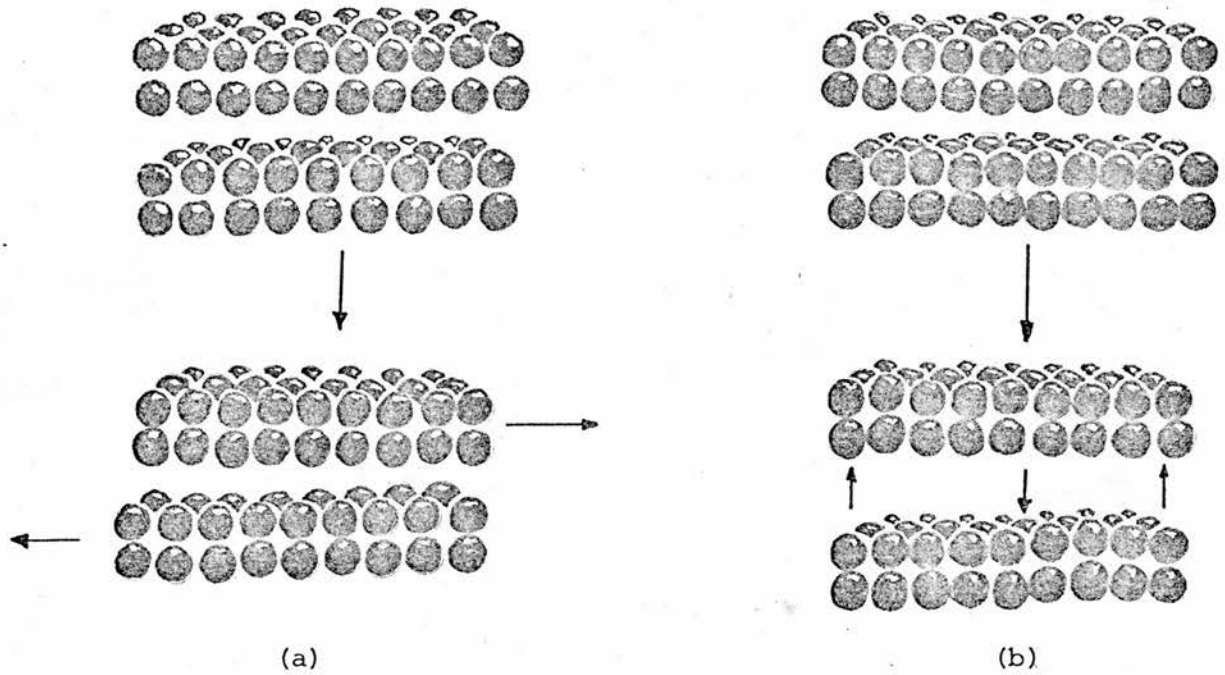

(a) (b)

FIGURE 6: On intercalation of guest species, (a) lateral shift of host layers, (b) c - lattice parameter dilation of host lattice.

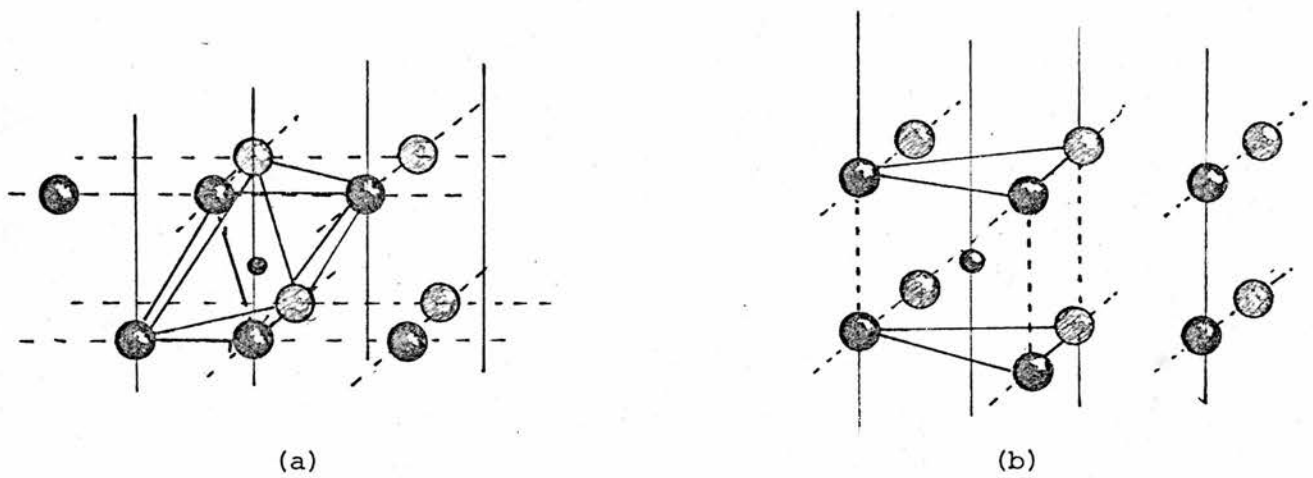

(a) (b)

FIGURE 7: (a) Octahedral and (b) Trigonal Prismatic sites in $A_x TCh_2$ complexes

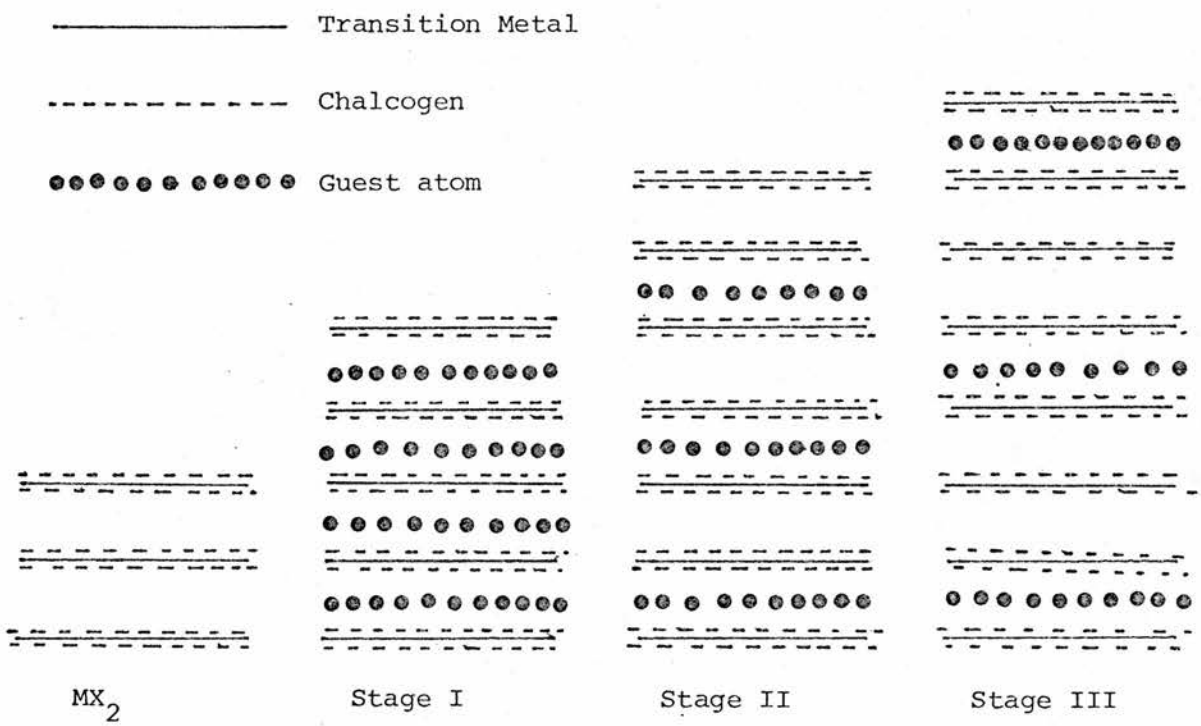

FIGURE 8: Schematic representation of first, second and third stage complexes

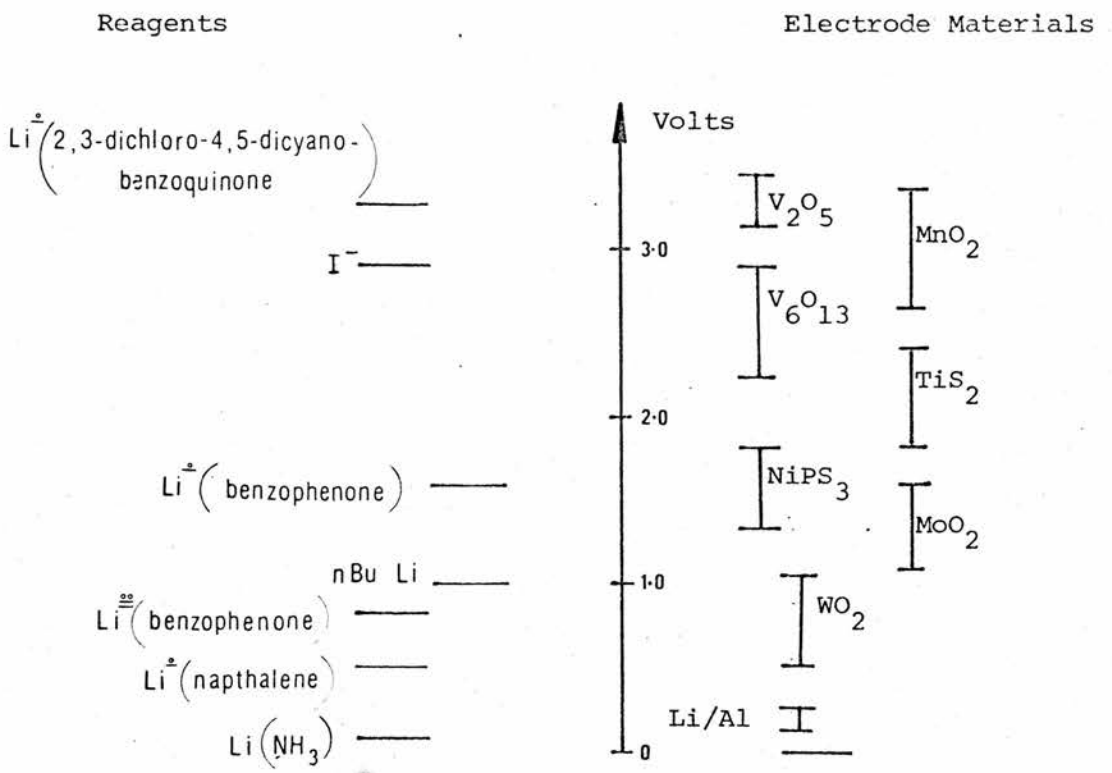

FIGURE 9: Potentials of a variety of electrode materials and reagents

co-intercalation compound with ammonia, the ammonia must be subsequently removed by heating or vacuum treatment, and disruption of the lattice may occur during these processes. A more serious problem arises from the high activity of the metal in the ammonia solution. This may result in the reduction of the TCh_2 compound to lower chalcogenides or to the transition metal itself.

A more efficient liquid reagent is n-butyllithium. The TCh_2 compound is added to an excess of approximately 0.2 molar butyllithium in hexane, in a dry box, under an argon atmosphere. The products are octane, traces of butane and butene, and Li_xTCh_2.

Various alternative liquid reagents for lithiation have been proposed. In principle, any oxidising agent stronger than the electrode material may be used to remove lithium ions and electrons from the structure, and any source of lithium ions may be used to intercalate lithium. In practice, however, there are several restrictions on the suitability of oxidising and reducing agents for intercalating and de-intercalating the host structure. Solutions of organic radical anions, generated by lithium reduction seem to be particularly suitable for lithiation reactions. Figure 9,[13] shows a range of reagents arranged in order of increasing reducing strength and related to a range of electrode materials of decreasing ease of reduction. Careful matching of reagent to substrate results in pure products with a reduction of unwanted side reactions.

Electrolysis Methods

This method has been used to prepare several intercalated layer compounds in both single crystal and polycrystalline samples from solid, and liquid, electrolyte cells. The TCh_2 sample is made the cathode in a cell with an electrolyte to transport the guest ion and an anode either of the metal guest or a suitable source of the metal. This method has the advantage of producing phases of precisely known stoichiometry of the guest species. The reaction rate is controlled by the current and the state of reaction is related to the cell potential.

1.7 Alternative Layer Structures

The obvious advantages of layered compounds, in which diffusion can occur in two dimensions of the crystal lattice, has led to consideration of other layered structure materials in SSE applications.

Graphite, one of the earliest layered compounds studied, has the advantages of high capacity and diffusion coefficient in the host structure. However, the very high activity of the guest species, in the case of reactive alkali metals, is a severe handicap.

FeOCl,[14] a layered compound with the attraction of low cost, exhibits no change in the lattice parameters as lithium is inserted. The host structure has been reported as capable of reversibly incorporating 0.5 moles of lithium per mole of FeOCl. No information on the transport properties of this material is available, however. This is the topic of an Anglo/Danish advanced battery program.

Initial results reported for the $NiPS_3$ host structure, suggesting that a maximum capacity of up to 3 lithium atoms per mole of host material, (1000 Wh/Kg) were very encouraging. However, subsequent research indicates that only 1.5 lithium atoms per mole are reversibly incorporated. A range of these compounds, formula MPX_3, have been investigated by Rouxel.[15] The results indicate that certain members of this series could perform satisfactorily over a limited range of guest concentrations. Further assessment of the role of the solvent in liquid electrolyte cells and rate of guest species diffusion in the host are at present underway.

The possibility of using $Li_xM_yV_{1-y}S_2$ electrode materials (where M is Cr or Fe) has been investigated by Murphy *et al*[16] in liquid electrolyte systems. This type of compound may be considered to be based on the Li_xVS_2 system. The results appear to indicate that the substitution of some of the vanadium metal atoms in this host structure by chromium results in an extension of the maximum lithium capacity to 0.6 moles per mole of host. Replacement of vanadium by iron results in an extension of the lithium capacity to 0.8. In both these systems the potential versus composition profiles versus a lithium reference

electrode were considerably improved relative to Li_xVS_2. Further investigations of these systems are required before a rationalisation of the effect of substitution of host metal atoms on the electrode behaviour can be attempted.

1.8 Alternative Tunnel Structures

A remarkable number of transition metal oxide electrode systems have been reported. These materials show a range of behaviour in most of the aspects of importance as solid solution electrodes (electronic conductivity, potential composition profile with respect to a lithium reference, charge/discharge cycle behaviour, and rate of diffusion of the guest species within the host lattice). Few of the structures of these materials have been studied in depth, partly because of the difficulties in the production of single crystals, and because of the complicated nature of their structure. In general, it seems unlikely that these oxides, with channel type structures, will be capable of sustaining high rates of discharge and are therefore more likely to be restricted to high potential, low current applications.

1.9 Conclusions

Sections 1.7 and 1.8 are only intended to give an insight into the variety of sources of electrode materials. Very many other systems have been investigated but the fact that such a large proportion of the literature of this field of study is reported on aspects of the TCh_2 systems, reflects the general belief that these are the most important electrode materials.

So far only the TiS_2 system has been developed to the extent of commercial viability. A $LiAl/TiS_2$ secondary cell is currently available from Exxon Enterprises Inc. This battery uses a lithium-aluminium alloy electrode, in which the lithium activity is very high, coupled to a TiS_2 electrode, and is capable of five deep cycles. The preparation of the TiS_2 material has been optimised to give the best possible operating characteristics of the cell.[17]

It seems likely that within the next few years the continued research effort in this field will result in the development of a variety of more efficient miniature power cells.

Candidate solution electrode materials may be assessed by using galvanic cells to obtain equilibrium partial thermodynamic quantities. This information permits recognition of the limits of stoichiometry of cell operation and provides a record of activity of the mobile ion as a function of composition.

The chemical difussion coefficient, which places an upper limit on the current density obtainable from a given cell geometry, may be investigated by means of electrochemical relaxation techiniques.

These electrochemical techniques were used to investigate samples of transition metal dichalcogenide materials.

1. Besenhard J.O., J. Electroanal Chem., Vol 94, (1978) 77

2. Steele B.C.H., "Fast Ion Transport in Solids", Ed. W. Van Gool, (North Holland, Amsterdam, 1973) 103

3. Whittingham M.S., J. Electrochem. Soc., Vol 123, (1976) 315

4. Murphy D.W., Carides J.N., Di Salvo F.J., Cros C., Waszezak J.V., Mat. Res. Bull, Vol 12 (1977) 825

5. Lazzari M., Scrosati B., J. Electrochem. Soc., Vol 126 (1980) 773

6. Armand M.B., "Fast Ion Transport in Solids", Ed. W. Van Gool, (North Holland, Amsterdam, 1973) 665

7. Verma A.R., Krishna P., "Polymorphism and Polytypism in Crystals", (John Wiley & Sons Inc., New York, London, 1966)

8. Leith R.M.A., "Preparation and Crystal Growth of Materials with Layered Structures", (D. Reidel Publishing Company, Dordrecht, Holland, Boston - U.S.A., 1977)

9. Balchin A.A., "Crystallography and Crystal Chemistry of Materials with Layered Structures", Ed. F. Levy, (D. Reidel Publishing Company, Dordrecht, Holland, Boston - U.S.A., 1976)

10. Whittingham M.S., Prog. Solid St. Chem., Vol 12, (1978) 41

11. Rouxel J., "Intercalated Layered Materials", Ed. F. Levy, (D. Reidel Publishing Company, Dordrecht, Holland, Boston - U.S.A. 1979)

12. Whittingham M.S., Gamble F.R., Mat. Res. Bull., Vol 10, (1975) 363

13. Christian P.A., Murphy D.W., Sicence, Vol 205, (1979) 651

14. Coic L., Palvadeau P., Portier J., Rouxel J., Mat. Res. Bull., Vol 13, (1978) 221

15. Brec R., Rouxel J., Second International Meeting on Solid Electrolytes, St. Andrews (1978).

16. Carides J.N., Cros C., Di Salvo F.J., Murohy D.W., Wazzczak J.V., Mat. Res. Bull., Vol 12 (1977) 825

17. Whittingham M.S., U.S. Patent number 4,007.055 (1975)

CHAPTER 2: EXPERIMENTAL DETAILS

Preparation of Materials: Solid Electrolytes.

2.1 Silver Iodide(γ Ag I)

Silver iodide was prepared by dropwise addition of approximately 0.5 molar potassium iodide to a slight excess of silver nitrate, of the same concentration, under conditions of minimum light and slight acidity. Stirring was maintained throughout the addition. The product, a bright yellow, fine precipitate, was recovered by filtration and washed thoroughly with distilled water and analar acetone. The solid obtained was dried and stored in darkness over phosphorous pentoxide dessicant.

2.2 Silver tungstate ($Ag_2 WO_4$)

Silver tungstate was prepared[1] by precipitation from approximately 0.5 molar solutions of sodium tungstate and silver nitrate under conditions of minimum light. During the dropwise addition of the silver nitrate solution to the sodium tungstate, the solution temperature was maintained at approximately 80°C and the pH retained between 9 and 10 by the occasional dropwise addition of dilute sodium hydroxide.[2] The white product obtained was filtered, washed with distilled water and analar acetone, then dried and stored, in darkness, over phosphorous pentoxide dessicant.

2.3 Silver Arsenate ($Ag_3 AsO_4$)

Silver arsenate was prepared, by precipitation, by dropwise addition of approximately 0.5 molar sodium hydrogen arsenate to silver nitrate in slight excess, of the same concentration under conditions of constant stirring and minimum light. The dark brown precipitate obtained was filtered, washed with distilled water and analar acetone, then dried and stored, in darkness, over phosphorous pentoxide dessicant.

2.4 Aluminium Orthophosphate $Al(PO_3)_3$

Orthophosphoric acid was standardised by titration against standard base. Aluminium orthophosphate was prepared by reacting orthophosphoric acid with alumina in the correct ratio[3], at 100°C for several hours. The solid phosphate was prepared by dehydration, in an open crucible, in a muffle furnace at 650°C, for several hours. The white solid product was stored under vacuum.

2.5 Iodotungstate Glass Electrolyte $(Ag_6I_4WO_4)$[4]

The iodotungstate glass was prepared by melting a finely ground mixture of silver iodide and silver tungstate, in a 4:1 molar ratio, in a pyrex melting tube with a narrow bore side arm. The melt was quenched, either by decanting the liquid through the side arm, in fine drops, into a dewar of liquid nitrogen, or by splat forming between two polished brass plates. The samples of electrolyte were finely ground in an agate mortar and pestle, and stored in the dark, over phosphorous pentoxide dessicant.

Ionic conductivity of samples of electrolyte was typically 4·0 $S.m^{-1}$ at room temperature with a transport number of unity.[5]

2.6 Iodoarsenate Glass Electrolyte $(Ag_7I_4AsO_4)$

The iodoarsenate glass was prepared[6] by a method identical to that used for the iodotungstate glass. The ionic conductivity of the glass was typically $0.412 S.m^{-1}$ at room temperature with a transport number of unity.[6]

2.7 Aluminophosphate Glass Electrolyte

Lithium fluoride, lithium oxide and aluminium orthophosphate in mole percent ratios, 50:30:20 respectively, were melted in a covered platinum crucible at 900 - 940°C for approximately 30 minutes. The melts were clear, colourless and very fluid. Fume extraction was

carried out during the heating process. The melts were cast onto a metal plate and quenched by splat forming. The splats were finely ground and annealed at 350°C to room temperature at a rate of cooling of approximately one degree per minute.

The conductivity of a splat formed cell with blocking aluminium electrodes was 0.21 $S.m^{-1}$ at 300°C with a transport number of unity.[7]

2.8 Transition Metal Dichalcogenides (TCh_2)

Niobium disulphide of various polymorphs[8] was prepared by the reaction of elemental niobium and sulphur, in the appropriate molar ratio, in an evacuated quartz ampoule, under various experimental conditions. The phases formed during the reaction of the elements are dependent on the precise history of maximum reaction temperature and cooling programme. The stoichiometry of the sample obtained to some extent is controlled by the volume of ampoule left available for the gaseous sulphur. Problems were encountered with ampoules more than half-filled with the solid starting mixture. At high temperatures the quartz ampoules were in some cases incapable of containing the pressure of gas produced with the result that the ampoule exploded. Suitable precautions must be taken when preparing these materials. In general slow heating rates, about 50°C per hour, are appropriate to permit the gaseous sulphur to react to form the disulphide as the heating process continues.

Polycrystalline samples of transition metal dichalcogenides were also supplied by laboratories in Milan[9] and Rome[10].

Analysis of these materials may be undertaken by various techniques. A sample of known weight may be oxidised in an oxygen gas flow, under appropriate oven temperatures, to obtain the oxide of the transition metal[11]. If the stoichiometry and final weight of the oxide is known, the stoichiometry of the original sulphide material may be calculated.

In some cases however, the product obtained by oxidation is not well defined and alternative methods of analysis must be employed.

According to a recent paper,[12] linearity, accuracy and sensitivity of noibium analysis by atomic absorption spectroscopy is improved by a background matrix of 1% hydrofluoric acid and 0.2% aluminium. Standards of 1000, 750, 500, 250 and 100 µg/ml of niobium in 1% hydrofluoric acid and 0.2% aluminium were prepared. A known weight of niobium sulphide was oxidised by the addition of a minimum volume, (approximately 5ml), of a stock solution of 40ml hydrochloric acid and 15ml nitric acid. The addition of 1ml of concentrated hydrofluoric acid was sufficient to dissolve the white niobium oxide. The appropriate amount of aluminium standard was added and the solution made up to volume for analysis.

Samples of niobium, tantalum and titanium sulphides were sent to Bernhard, West Germany for an independent sulphur analysis.

X-ray analysis of polycrystalline samples of TiS_2, $TiS_{1.80}$, TaS_2, and $Nb_{1+x}S_2$ by powder diffraction was carried out in Milan.[9]

2.9 Vanadium Oxide (V_6O_{13})

Vanadium oxide was prepared,[13] by thermal decomposition of ammonium vanadate at temperatures below 450°C in a flow of argon gas. Heating was continued for approximately 24 hours after which the sample was allowed to cool under a continuous flow of inert gas. The fine, black powder obtained was stored over phosphorous pentoxide dessicant.

A sample of known weight was dissolved in a minimum volume of nitric acid and vanadium analysis by atomic absorption spectroscopy carried out. The results indicated that the stoichiometry of the sample was $V O_{2.17} \pm 0.02$

2.10 Lithiated Vanadium Oxide $Li_x V_6 O_{13}$

Lithiation of vanadium oxide, ($V_6 O_{13}$), was carried out with an excess of 1.6 molar n-butyl lithium in hexane at room temperature, in a dry box with an argon atmosphere. The product was filtered, washed with redistilled, dry hexane and dried. The sample was stored over phosphorous pentoxide dessicant.

Atomic absorption analysis of the product for lithium indicated that the value of x in $Li_x V_6 O_{13}$ was close to unity.

Cell Preparation

2.11 3 Electrode Cell; (Diffusion Coefficient Measurement)

The configuration of the 3 electrode cell is shown in Figure 2. Figures 3 and 4 give step by step details of the pressing procedure, with dimensional details of the dies included in Figure 5.

Slight modifications to quantities used, or pressures with which segments are applied, may be necessary for different electrode materials or electrolytes. The technique described in detail below was found to be suitable for the transition dichalcogenide electrode materials and silver iodotungstate electrolyte.

A finely ground mixture of approximately 0.12g of electrolyte and 0.07g powdered silver metal, (particle size < 100μ) was pressed at ½ tonne pressure to form the outer reference ring of the cell. (Figure 3(a)) The internal former was pressed clear of the cell using one of the alternative base plates as shown in Figure 3(b).

The die arrangement shown in Figure 3(c) was then used to press approximately 0.15g of pure electrolyte, at 1 tonne, to form the electrolyte separating ring. The internal former was then pressed clear of the electrolyte ring using the die arrangement of Figure 3(d).

The working electrode, approximately 0.02 g of an electrolyte/electrode material ground mixture, in a 2 parts electrolyte to 1 part electrode material ratio, was then pressed into the pill, as shown in Figure 4(a), at hand pressure. The plunger guide, inserted in the die, was made of teflon to prevent short circuit of the cell, between working and reference electrodes during this process. Figure 4(a) does not show the presence of a teflon insulating disc, cut from thin teflon sheet and located between the cell and the lower anvil, used to prevent cell shorting at this and later stages of cell fabrication.

Figure 4(b) shows the arrangement of die pieces used to press about 0.3g of electrolyte, at 2 tonnes pressure, onto the reference and working electrode section.

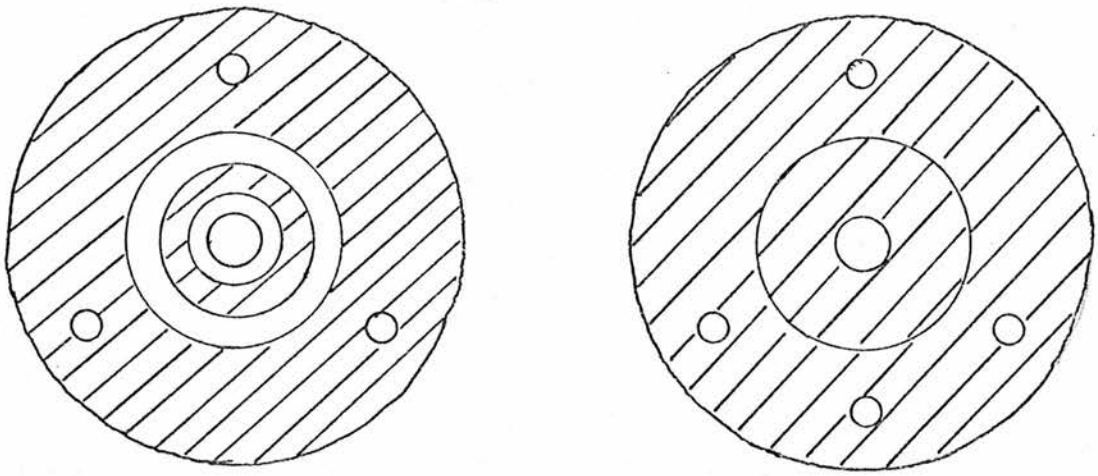

FIGURE 1: Detail of Cell-Holder

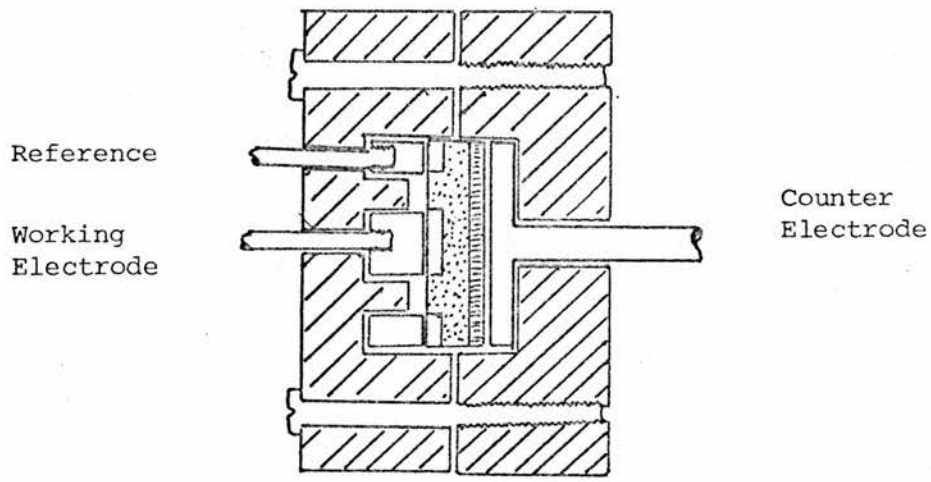

FIGURE 2: Detail of 3 Electrode Cell. (1) Working Electrode Mixture, (2) Reference Ring, (3) Electrolyte Ring, (4) Counter Electrode

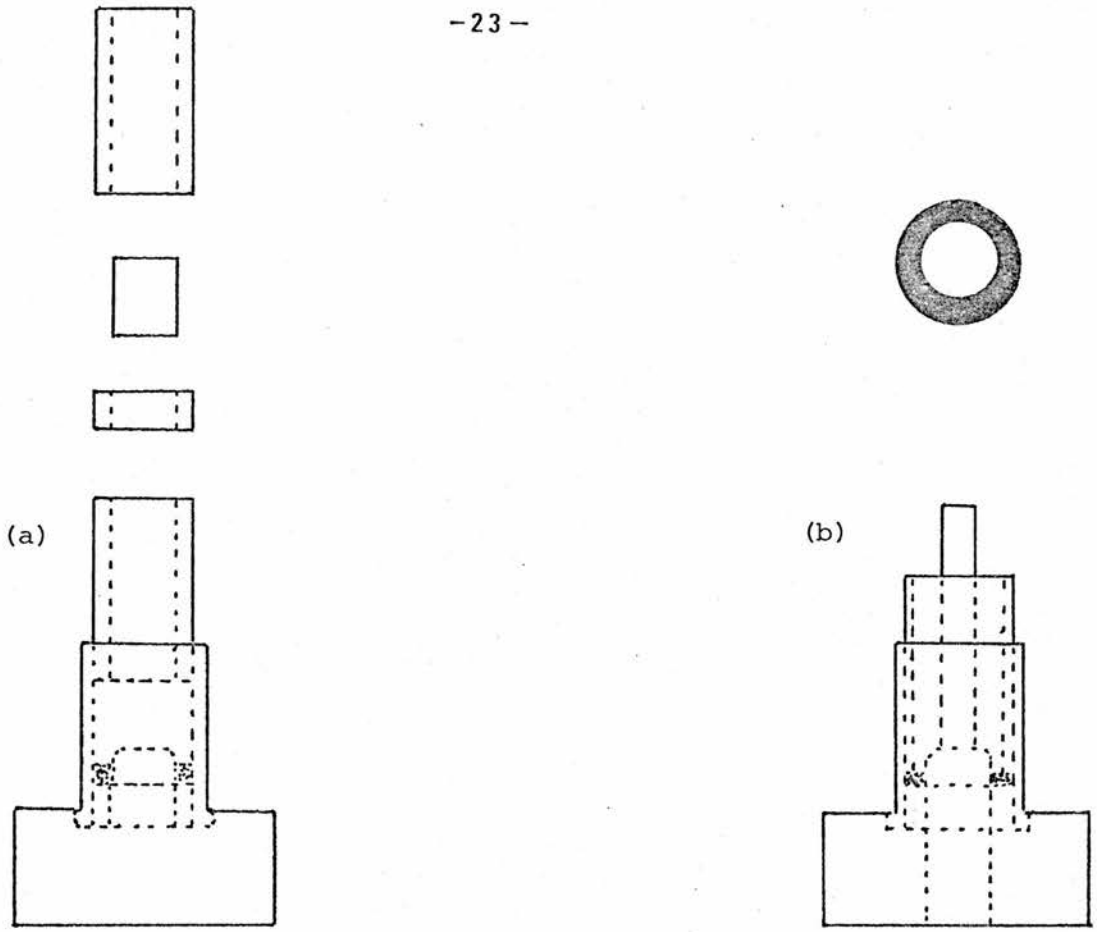

FIGURE 3: Detail of Cell Pressing Procedure

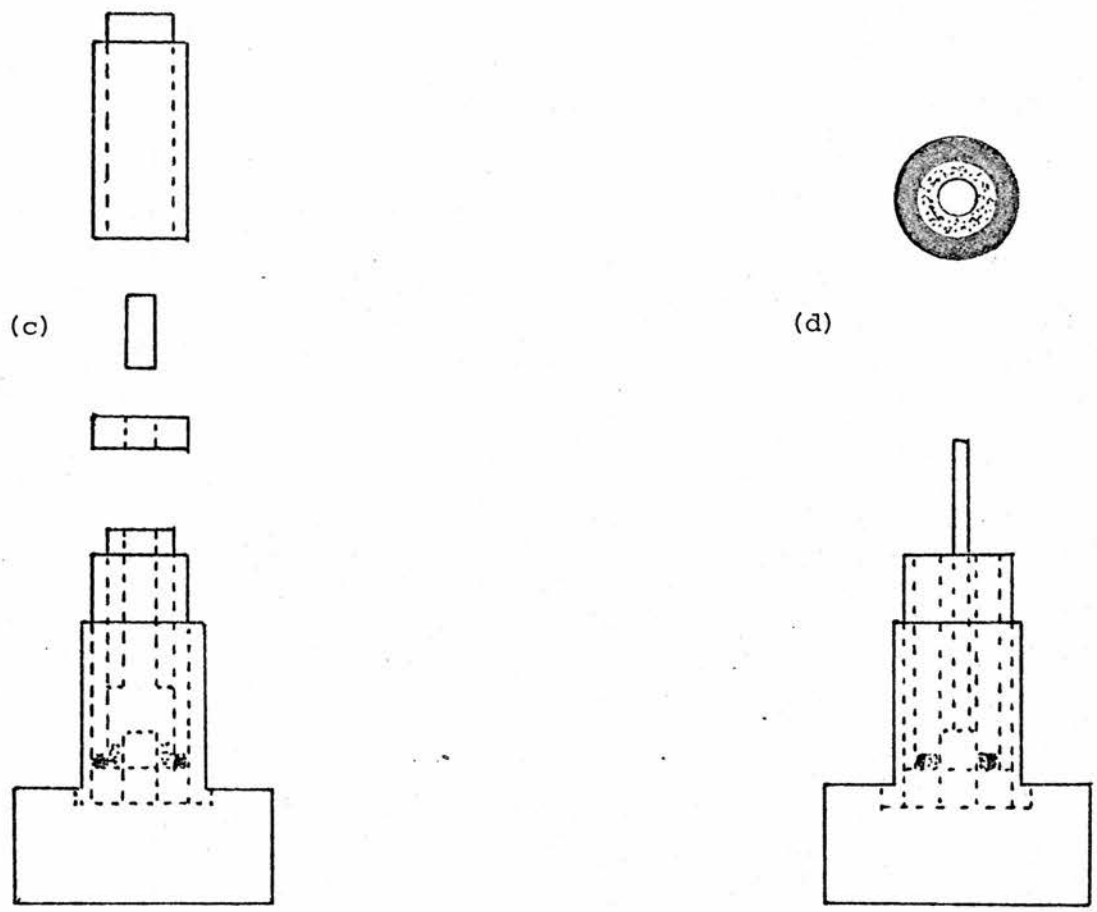

Figure 4(c) shows the final arrangement used to apply the counter electrode, 0.3g of a silver powder/electrolyte mixture, of the same composition as used for the reference electrode, at about 3 tonnes pressure. At this stage, if the teflon insulating disc is not in position, the cell short circuits through the low resistance path offered by the die pieces and press anvils.

The completed cell was then removed from the die as shown in Figure 4(d) and stored in a sample bottle, in darkness, over phosphorous pentoxide dessicant until immediately prior to installation in the cell-holder.

2.12 Cell Holder and Pyrex Cell Envelope

The cell was mounted in an asbestos cell holder, using gold electrode contacts, detail of which is shown in Figure 1. The contacts to the external circuit were made through the pyrex tube-head stopper by means of tungsten rods sealed into 7mm cones. The detail of the cell holder pyrex envelope is shown in Figure 6. This arrangement allowed the experimental environment of the cell to be carefully controlled. A continuous flow of dry, thermostatted nitrogen was supplied to the cell envelope.

Thermostatting of the cell envelope, for diffusion coefficient experiments was achieved with the use of a Townson-Mercier oil bath, a horizontal tube oven with an electronic temperature controller, or a pyrex envelope with a jacket through which the thermostatting liquid was pumped. This latter arrangement was required for systems where the cell temperature was to be maintained between 15 and 40°C, and used a heavily insulated box to maintain the pyrex envelope in a draught-free environment.

Where the cell temperature was maintained at temperatures of less than 100°C the inert gas flow to the cell was thermostatted prior to entry to the pyrex cell envelope by passage through a molecular sieve drier and thermostatting coils submerged in the bath liquid.

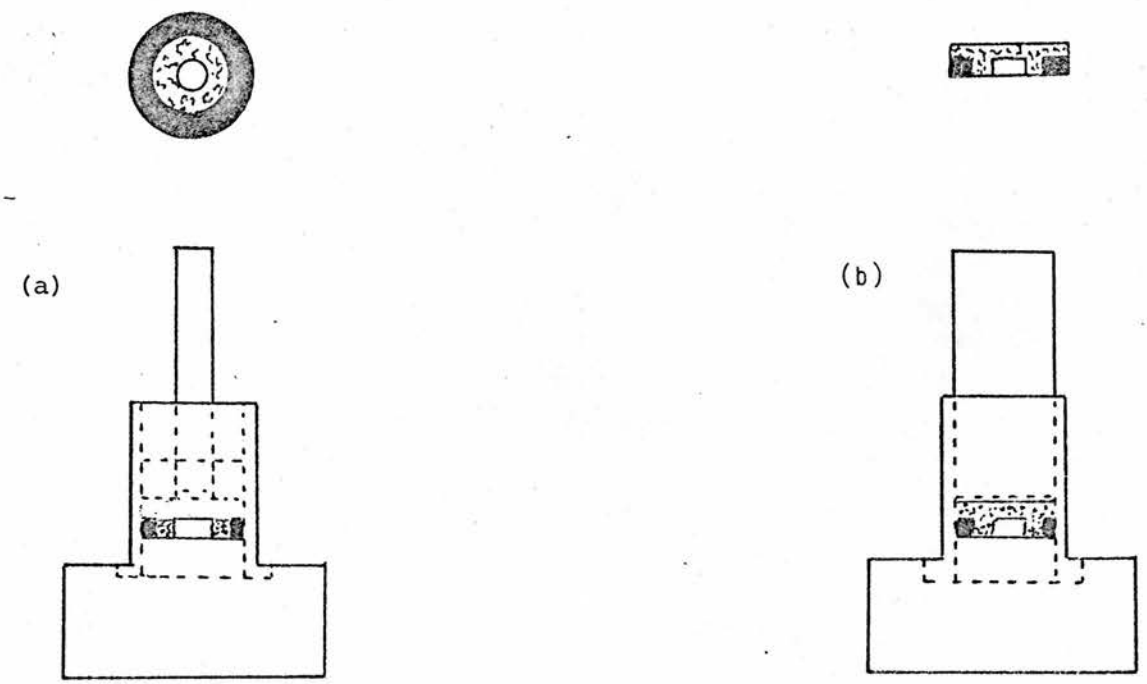

FIGURE 4: Detail of Cell Pressing Procedure

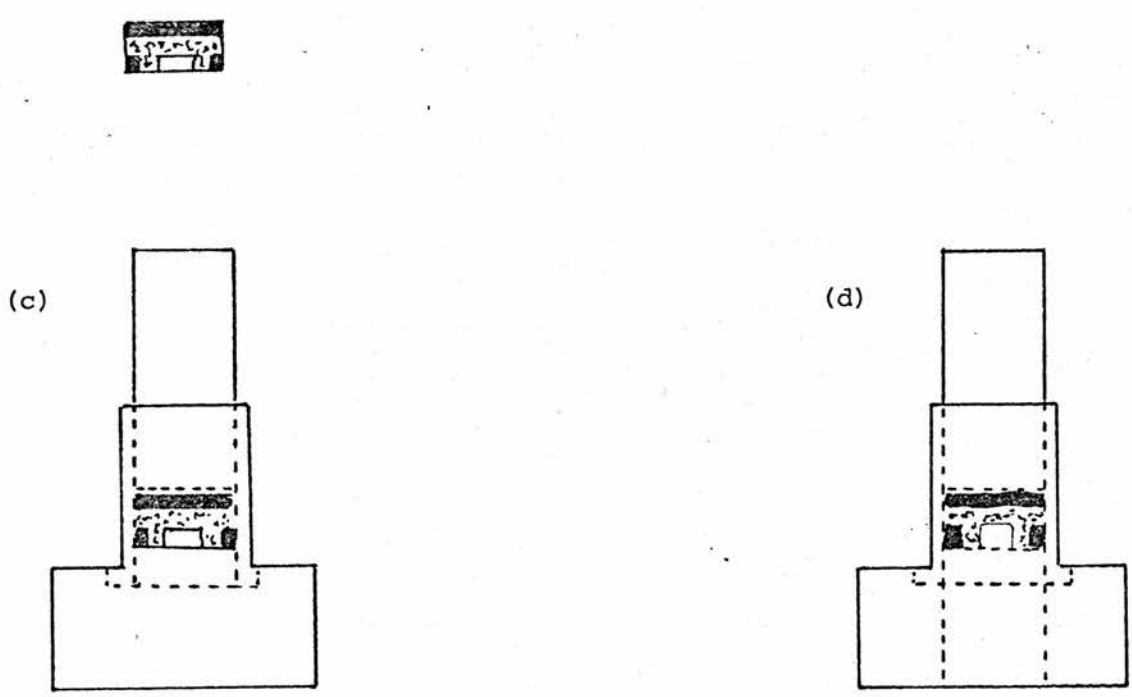

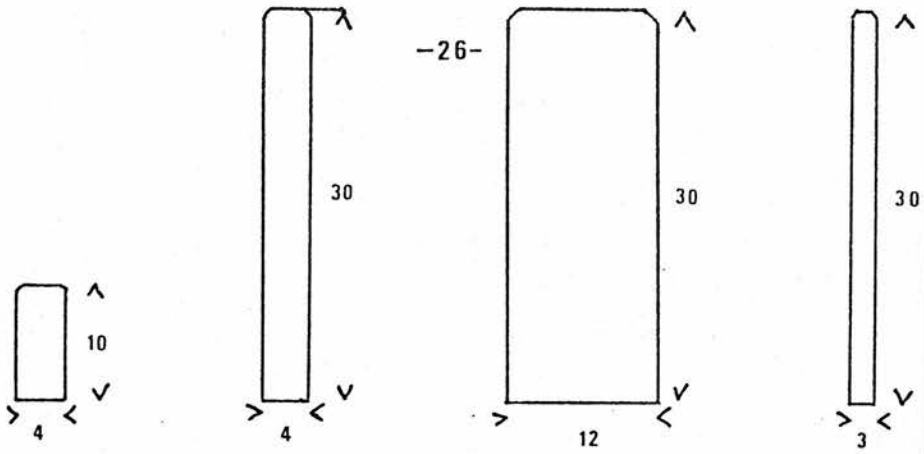

FIGURE 5: Detail of Die Dimensions (mm)

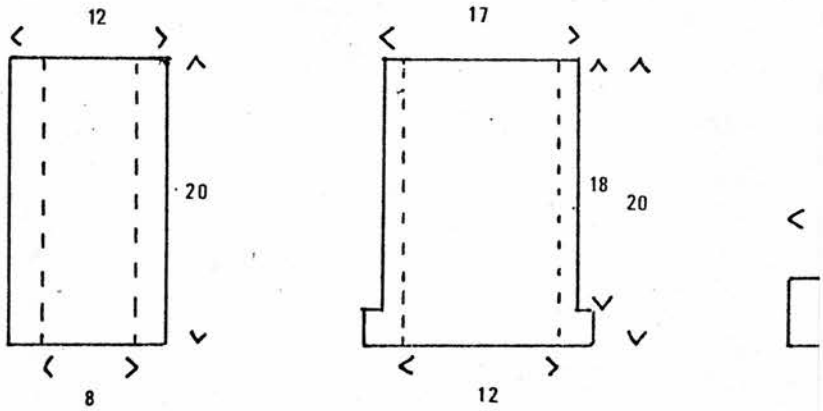

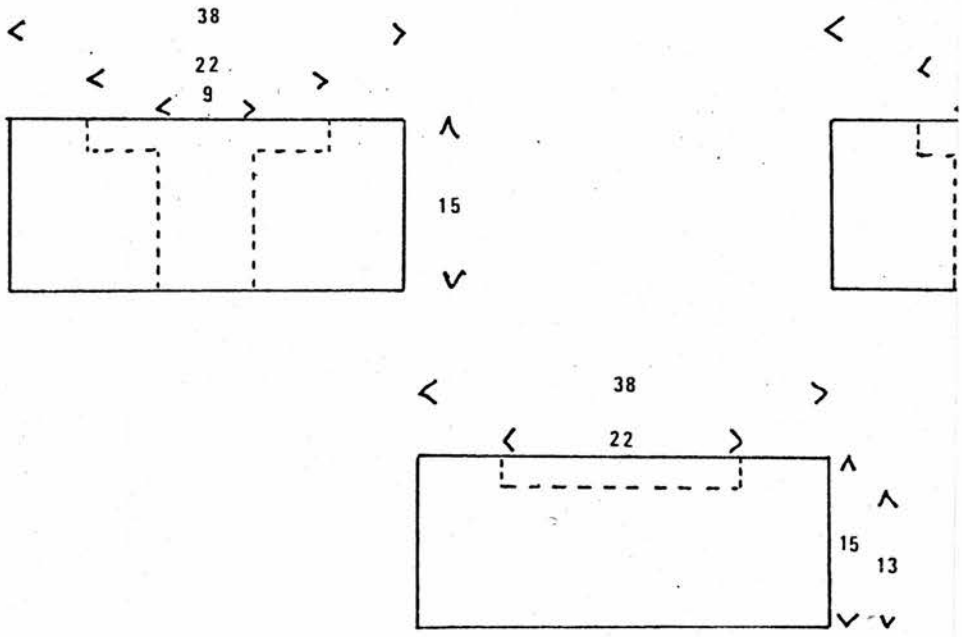

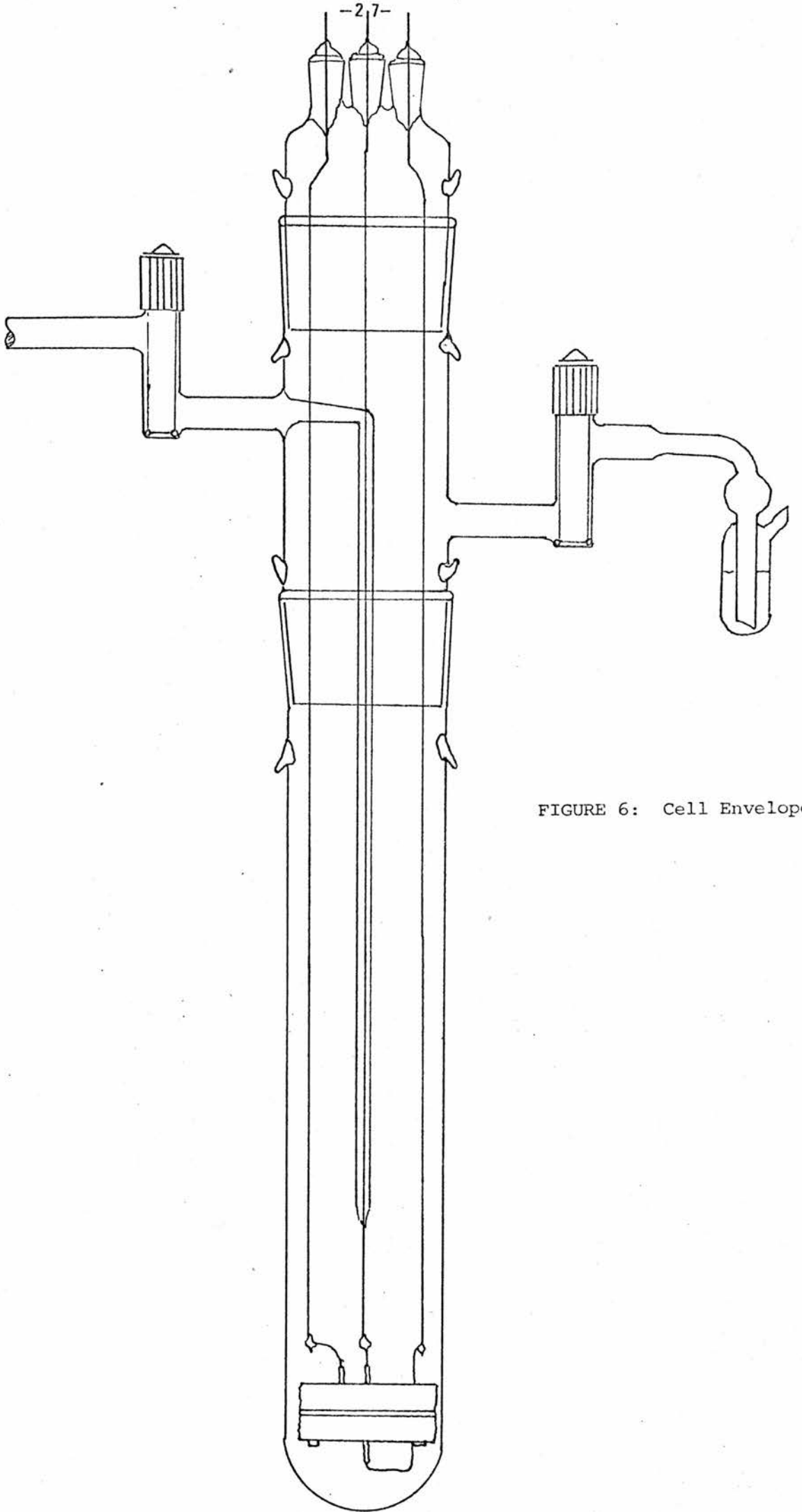

FIGURE 6: Cell Envelope

2.13 Conductivity Spectra Cells

The conductivity of the electrolytes was assessed by preparing a cell with either two non-blocking electrodes, for the silver ion conducting glasses, or two blocking electrodes for the lithium ion conducting glasses.

For the iodotungstate and iodoarsenate electrolytes the electrodes were prepared from a 2:1 mixture of electrolyte and silver powder finely ground in an agate mortar and pestle. Approximately 0.2g of the mixture was pressed at ½ tonne pressure in a 13mm Specac die. A layer of approximately 0.3g of electrolyte was pressed over the electrode layer at 1 tonne pressure. Finally, a further 0.2g of the electrode mixture was pressed onto the cell at 3 tonnes pressure.

The area of the electrodes was assumed to be the geometric area, and the length of the cell, for purpose of calculation of the cell constant, was obtained either by sectioning the cell and using a travelling microscope to determine the electrolyte layer depth, or by preparing a suitable calibration graph and reading off the cell length for weight of electrolyte used.

The lithium glass conductivity cells were prepared either by splat forming discs between two polished brass plates, or by oven treatment of compressed powder pills.

The compressed powder pills were prepared by compressing approximately 0.2g of lithium glass electrolyte in a 13mm Specac die at 3 tonnes pressure. The pill was removed from the die and maintained at various temperatures, for fixed lengths of time, in a tube oven. On removal from the oven the pill was allowed to cool and the electrodes applied.

The conductivity spectra of the lithium glass samples were determined using various blocking electrodes. Results were compared using commercial samples of colloidal silver, colloidal graphite or evaporated aluminium electrodes.

2.14 Cell Holder and Pyrex Cell Envelope

Figure 7 shows detail of the cell-holder and pyrex envelope design. The envelope was located in a horizontal tube furnace with an electronic temperature control unit, and was flushed with argon prior to heating, a slow flow of gas being maintained during the experiments.

Screened electrical connections were made with the external circuit through B.N.C. connectors sealed into the 7mm cones on the tube-head stopper with "Araldite" epoxy resin.

2.15 Open Circuit Potential Versus Composition Cells. (12mm diameter)

The 12mm diameter cells were fabricated using the same procedure as that described for the three electrode cells. In this case, however, the reference ring of the cell was not required and instead of using the silver powder/electrolyte mixture as described in Section 2.11, a pure electrolyte ring was used.

These cells were used to obtain thermodynamic data, from records of the temperature dependence of the cell open circuit potential, and the variation of potential with guest concentration.

Data was obtained for cells with NbS_2, TaS_2, $TiS_{1.80}$ and $TiS_{2.0}$ working electrodes.

2.16 Cell Holder for Open Circuit Potential Measurements (12mm cell)

The cell-holder shown in Figure 8 was used to thermostat these cells. The water jacket of the cell-holder was supplied by the circulating pump of a Grant bath with a thermostatted flow of water at temperatures between 10 and 35°C. At higher temperatures a Haake bath was used with a digol bath liquid.

The cell was clamped between gold electrodes in a plastic insulating sleeve in the centre of the brass body of the cell-holder. Fine holes bored through the electrode supports, provided close access to the cell for a thermocouple. The rubber O-rings mounted on the electrode insulator, when compressed against the insulating sleeve by tightening the knurled adjusters of the electrode supports, provide a good seal, isolating the cell from the atmosphere. The cell-holder was maintained in a chamber with a dry atmosphere as a further precaution.

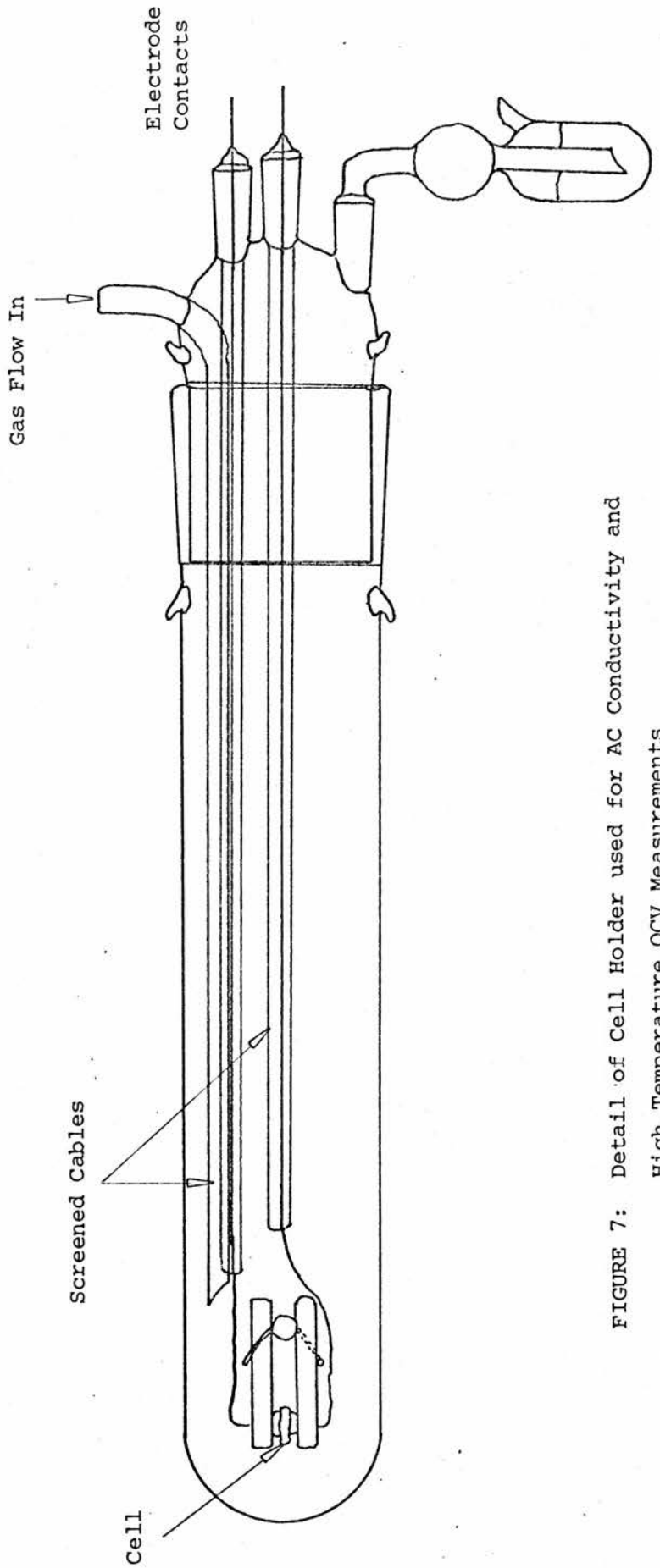

FIGURE 7: Detail of Cell Holder used for AC Conductivity and High Temperature OCV Measurements

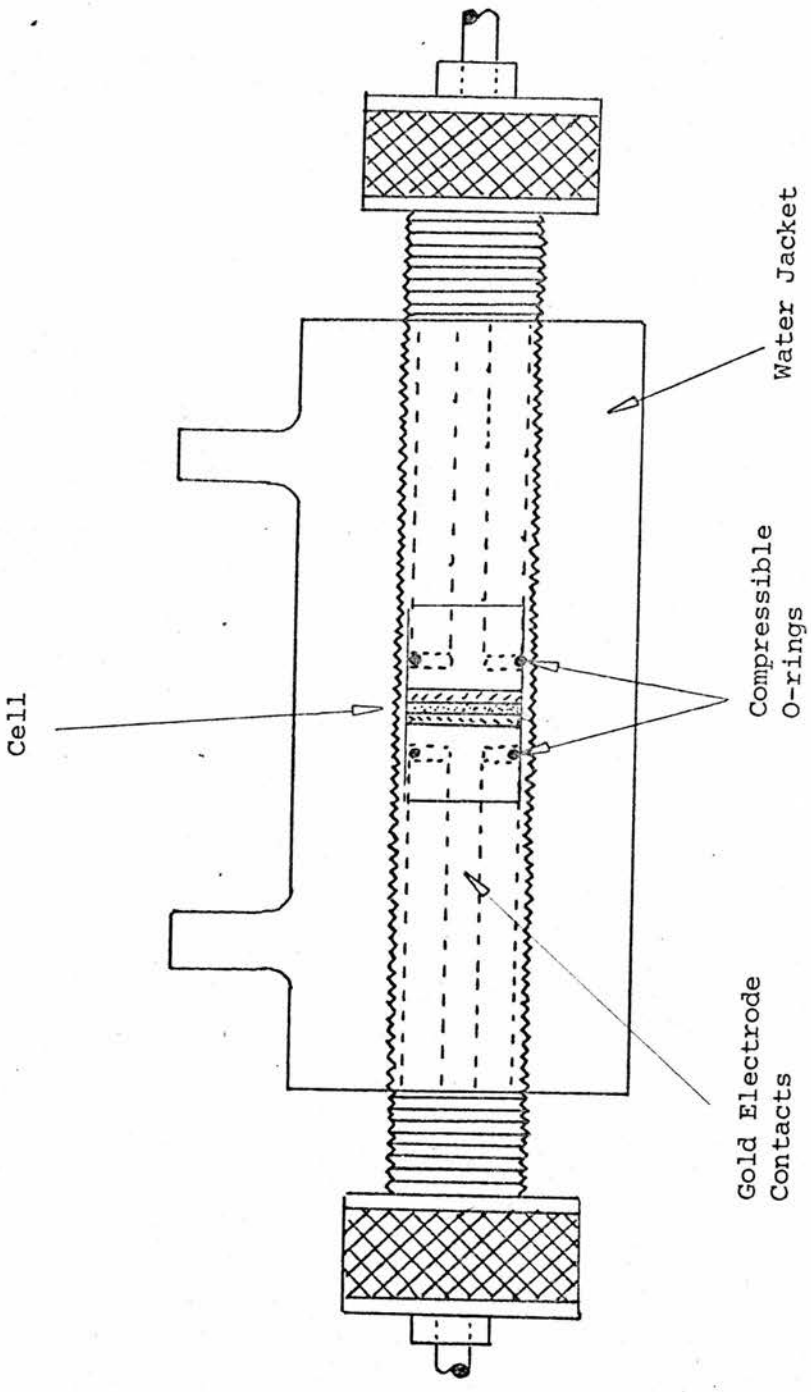

FIGURE 8: Detail of Thermostatted Cell-Holder

2.17 Open Circuit Voltage Versus Composition Cells (5mm cell)

The 5mm cells were used in the investigation of various transition metal oxide electrode materials of possible use in secondary battery systems.

Approximately 0.1g of a mixture of lithium ion conducting glass electrolyte and electrode material, in 2:1 ratio, was pressed in a Specac 5mm die at approximately ½ tonne pressure. A very thin layer of electrolyte, (usually about 20mg weight), was then pressed onto the electrode and the half cell was then removed from the die. The second electrode was then prepared by pressing about 0.1g of the other electrolyte/electrode material mixture at 1 tonne pressure in the die.

The cell was assembled and located in the cell-holder shown in Figure 7. The cell was subjected to an oven pre-treatment at 410 - 420°C prior to analysis of the charge/discharge cycle at 250°C.

2.18 Electronic Conductivity Cells

These cells were assembled in a 13mm Specac die. Approximately 0.15g of a finely ground electrolyte/silver powder mixture, 2:1 ratio, was pressed in the die at a ½ tonne pressure. The electrolyte layer, approximately 0.3g, was then transferred to the die and pressed at about 2 tonnes pressure. Finally, a mat of carbon fibres was placed in the die and pressed at 3 tonnes to ensure good contact between the fibres and the electrolyte layer was achieved. Under these conditions the fibres were partially embedded in the electrolyte material.

The cells were mounted in a simple two electrode cell-holder with a carbon fibre mat at the blocking electrode. After mounting, the cells and cell holder assembly was carefully examined to ensure no shorting of electrodes through carbon fibres or mat occurred.

The cell holders were located in pyrex cell envelopes, shown in Figure 9, and a controlled atmosphere supplied to the cell. Where dry gas was required the gas was passed slowly through a Birlec 25 litre drying tower, and where wet gas was appropriate this was supplied with the use of distilled water saturaters before entry to the cell envelope. The gas was in both cases equilibrated at bath temperature using thermostatting coils immersed in the bath fluid. The cell envelopes were immersed in a 50 litre insulated bath with an "Ether" temperature controller.

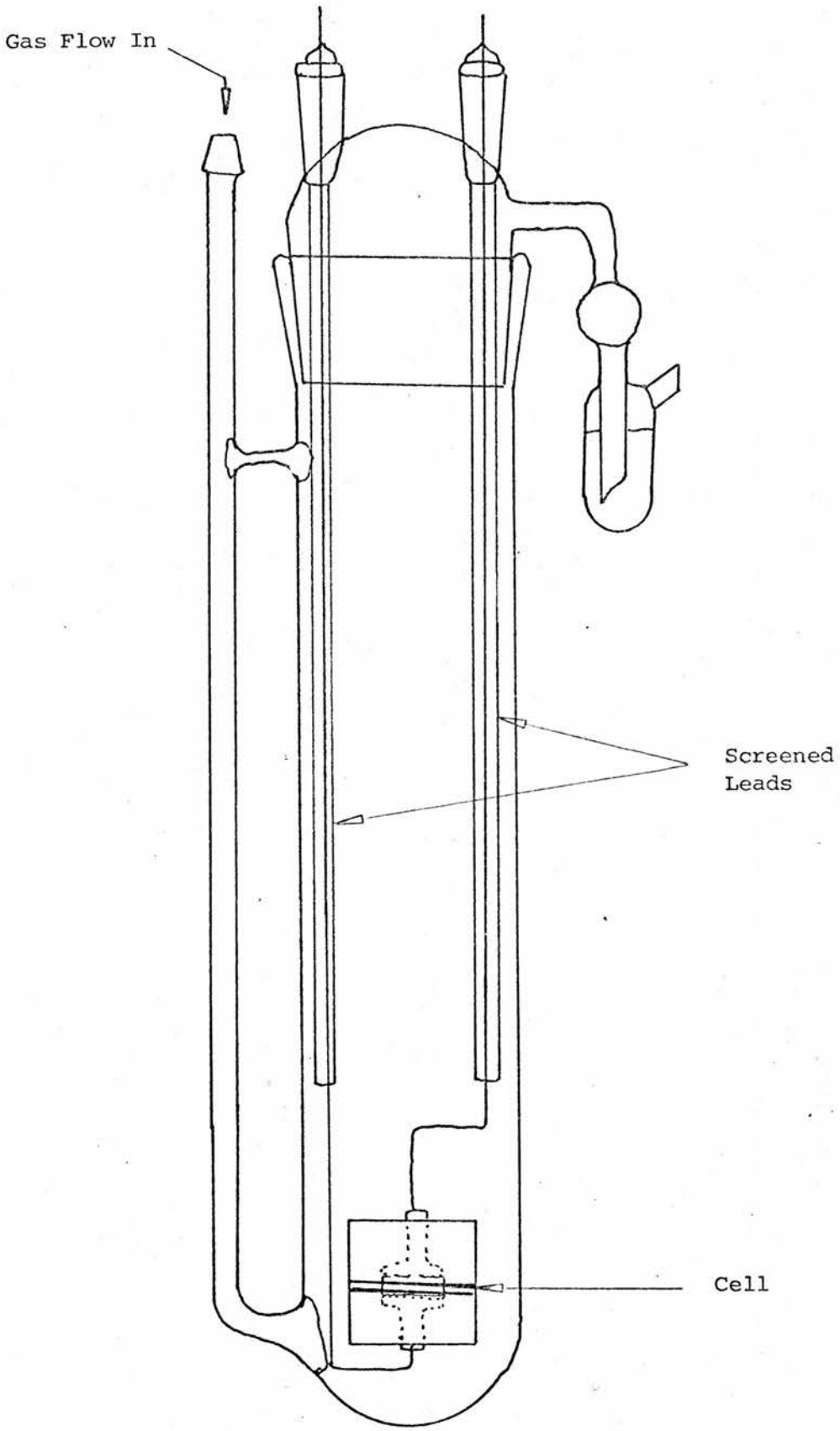

FIGURE 9: Electronic Conductivity Cell Envelope

2.19 Temperature Measurement

All the cell-holders used were designed to accommodate a copper/constantan thermocouple, close to the cell location, for temperature measurement. The temperature reading device was either a Comark Type 1625 electronic thermometer, with an internal standard, or a Solartron 7065 microprocessor voltmeter, with an ice triple point cell as an external standard.

In both cases the readings given by these devices were checked with the use of standard mercury thermometers and found to agree to within 0.2^{o}C, over the temperature range of interest.

2.20 Instrumentation

(a) Diffusion Coefficient Measurements

The block circuit diagram of the experimental setup used in these measurements is included in Figure 10.

1) Northern Scientific (NS575) Digital Signal Analyser

The digital signal analyser provided a means by which the voltage transient response of the three electrode cell to the galvanostatic current pulse could be recorded with respect to time. Several pulses were applied to the cell with sufficient interval between consecutive pulses to permit recovery. The data obtained from each pulse was stored in the memory of the device and the sum of the signals was displayed on the cathode ray tube output. When a suitable signal total was obtained, the contents of the memory were transferred, using the serial ASCII RS-232 output of the device, to a Tektronix 4052 minicomputer.

2) Tektronix 4052 Minicomputer and 4662 Interactive Plotter

The data obtained from the digital signal analyser was presented in the form of two graphs, (1) voltage transient, and (2) voltage parameter versus time parameter. The gradient of the second graph was used to calculate the diffusion coefficient. A brief description of the method of program operation is included with reference to the program listings available in Appendix 1. Both programs were written in Tektronix basic.

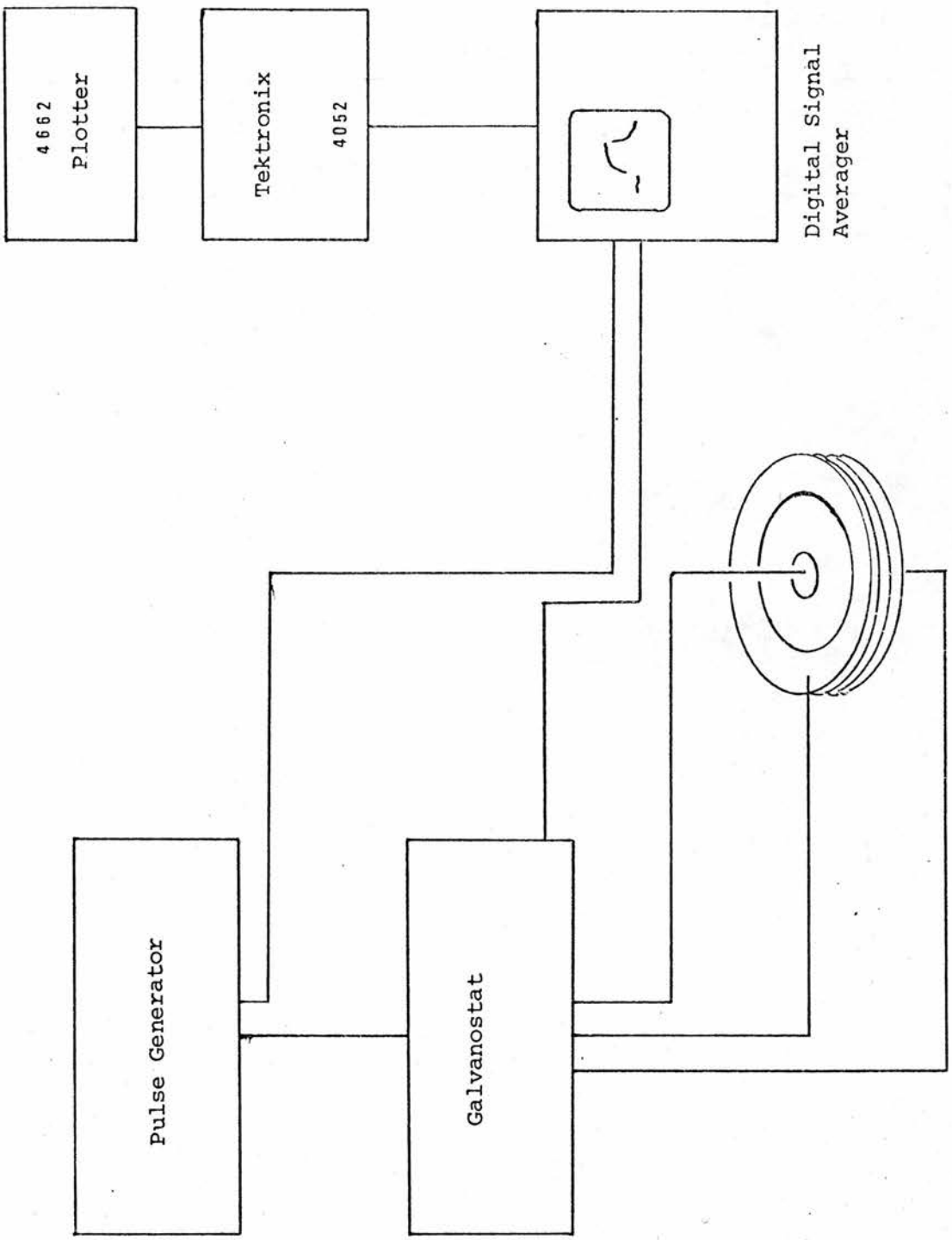

FIGURE 10: Block Circuit Diagram. Apparatus Diffusion Coefficient Measurement

The listings of the programs are partitioned by remark statements to indicate the function of sections and subroutines within the program. The important features of the programs are further explained.

Program 1; Data Receive and Formatting Program.

Various parameters required for the calculations carried out in the program were input, with cell test identification information, from the minicomputer keyboard. The computer is equipped with a tape facility which may be used for either data, or program storage, by appropriate file marking. The first function the program performed was to set parameters for reception of data from the NS-575. The data was received as multicharacter strings which were written onto the appropriate tape file. After closing this file the computer read the data, line by line, into core as a primary data array. A printed copy of the primary data set, titled and with relevant calculation parameters was then output on the line printer.

As a result of the location of the experiment, in a laboratory with other electrical equipment, a certain amount of mains noise interference was superimposed on the transient signal obtained from the test cell. In early experiments the amplitude of this noise relative to the voltage transient was reduced by summing consecutive pulses. As the noise associated with each pulse was shifted in phase from that of the previous pulse, after several pulses the noise level was usually considerably reduced.

An alternative method, adopted after the arrival of the minicomputer, involved the incorporation of a "noise removal" subroutine into the data receive program. This program made use of the fact that the noise was periodic. (50 herzt) The first few cycles of the data record were obtained prior to the cathodic current pulse and used to generate an array, the members of which were the difference between the noisy signal and a noise free signal. By repetitive subtraction of this array from the complete data set of the record of the voltage transient, the background noise was removed from the signal. In most cases the improvement in the quality of the data obtained by this method was considerable. Typical examples of signals obtained before and after implementation of the noise removal subroutine are included in Figures 11 and 12.

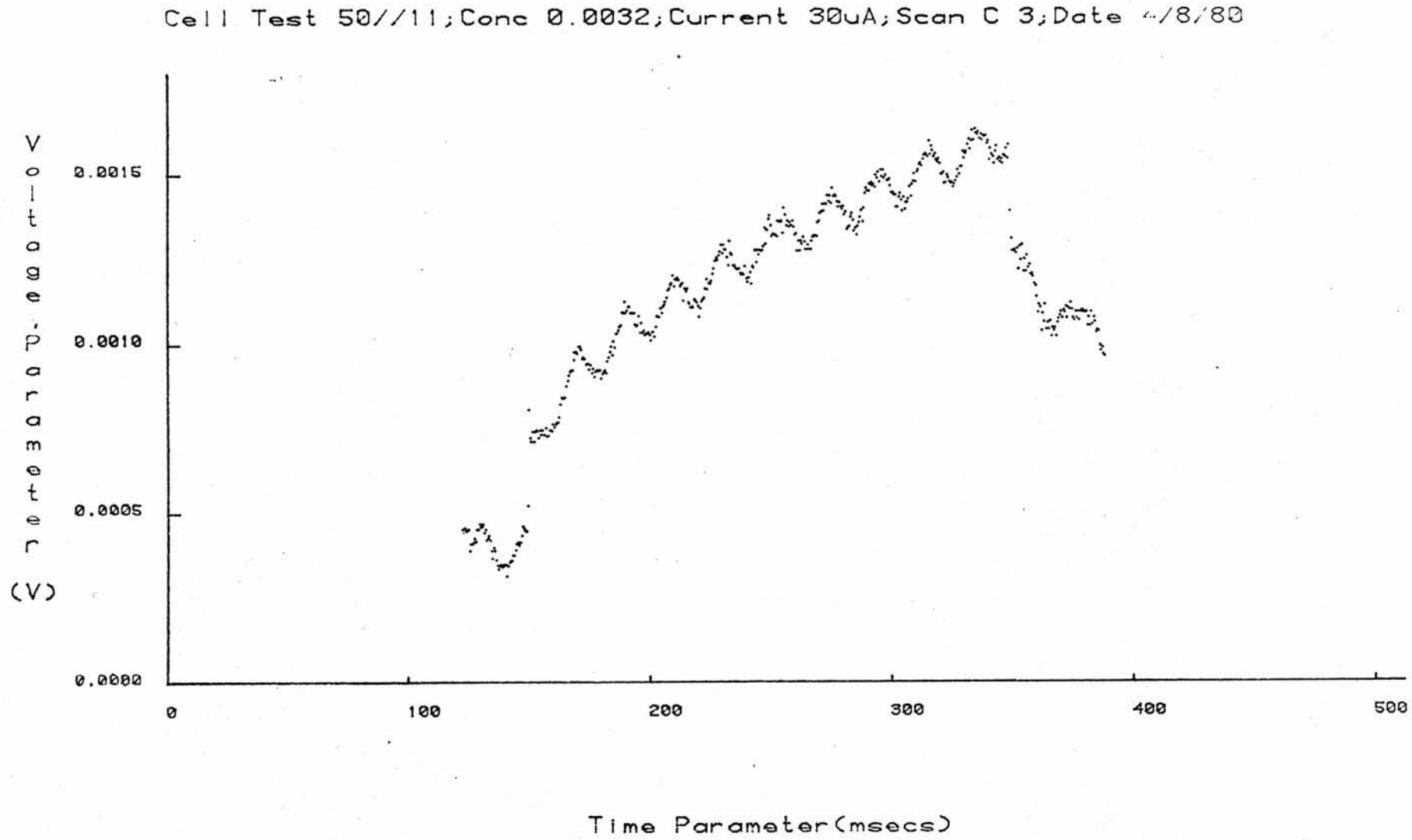

Fifure 11(a): Transient Pulse before Noise Removal

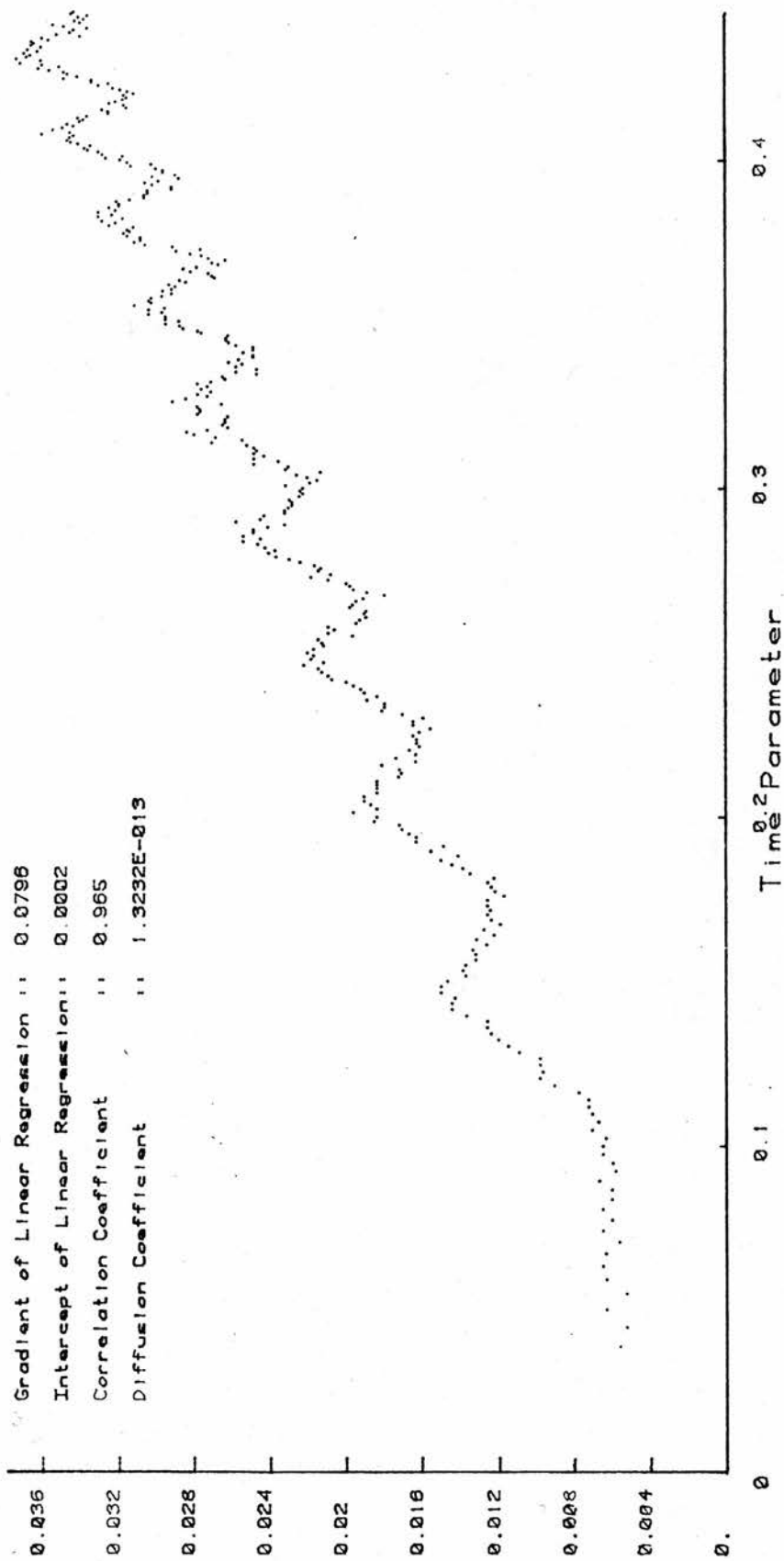

Figure 11(b): Voltage Parameter versus $t^{\frac{1}{2}}$ before Noise Removal

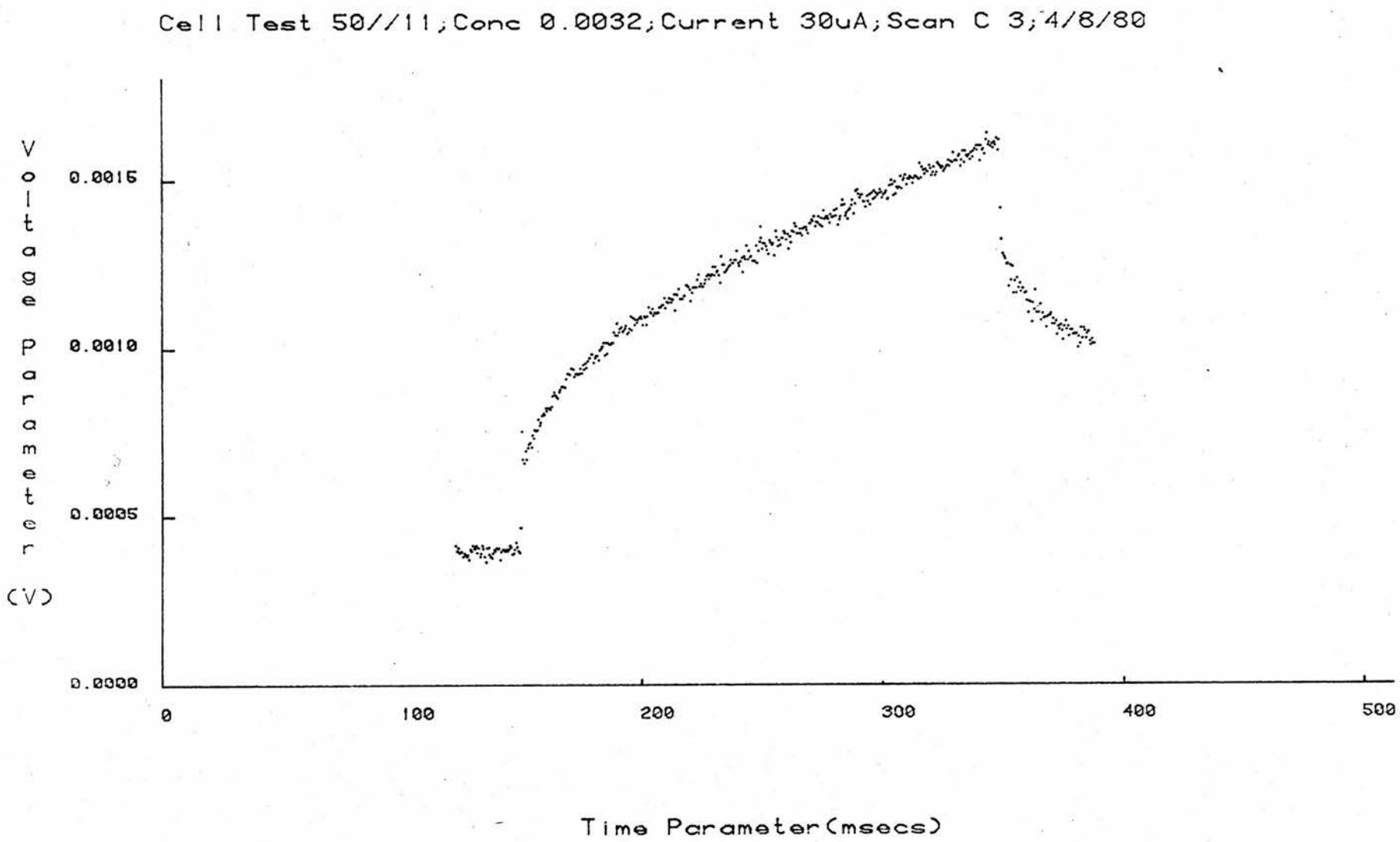

Figure 12: Transient Pulse After Noise Removal

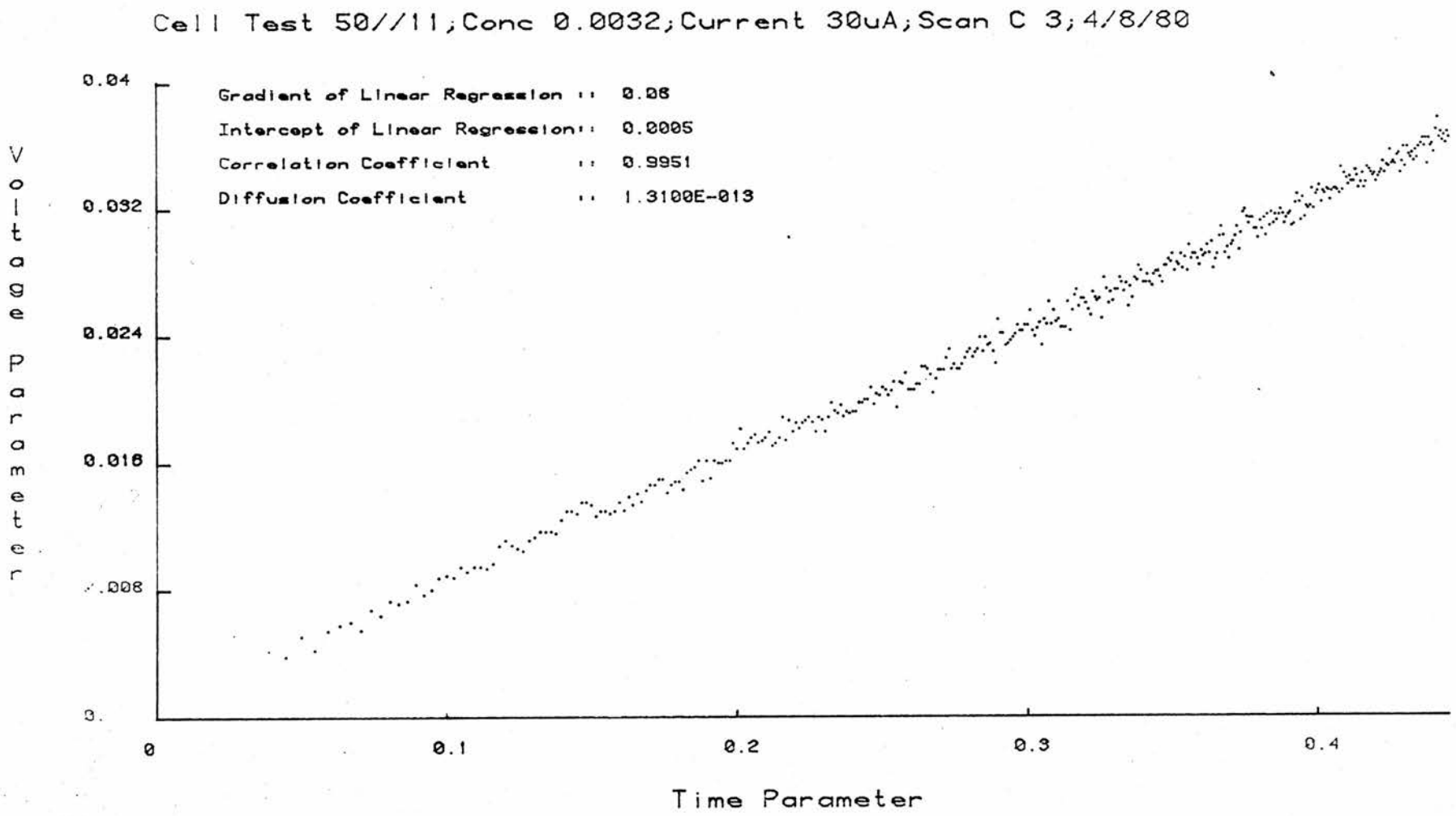

Figure 13: Voltage Parameter versus $t^{\frac{1}{2}}$ After Noise Removal

The secondary data set of noise reduced data, obtained in this way, was written on to a new file on the tape in a suitable format for data plotting of the voltage transient.

A further calculation was then carried out on the section of the data set which contained the voltage transient. Before an appropriate voltage parameter, $(\exp (\frac{\eta F}{RT}) - 1)$ versus time parameter, $(\text{time}^{\frac{1}{2}})$, plot could be obtained the voltage contribution of the IR drop had to be removed from the voltage transient. This was carried out by an iterative method which used a keyboard input parameter as initial value. This approximate IR drop was obtained from the cathode ray tube display on the NS-575. When a linear regression of the transformed data plot obtained an intercept within a preset range of the origin, the calculated values of voltage and time parameters were written onto a new data file. The program then located, loaded and initiated the plotting program.

Program 2; Plotting Program:

The plotting program read "noise reduced" data from a specified file location and converted it to volts. The data was plotted as the total signal obtained by the experiment, including a pre-pulse baseline and post-pulse relaxation.

The program then read data from the transformed plot data file and output the data to the plotter in the format shown in Figure 13 . In both cases a plot was obtained on the Tektronix screen prior to output of a hard copy on the interactive plotter.

A linear regression analysis was performed on this data set and the gradient used to calculate the diffusion coefficient according to the methods detailed in Chapter 5.

3) Pulse Generating Unit

The combination of pulse generator and galvanostat permitted a square wave current pulse of variable height and length to be applied to the cell. A block diagram of the pulse generator components is included in Figure 14.

The unit uses an internal time reference signal to synchronise three timer cards. Card A provides a variable time delay between the initiation signal and the beginning of the first pulse. The

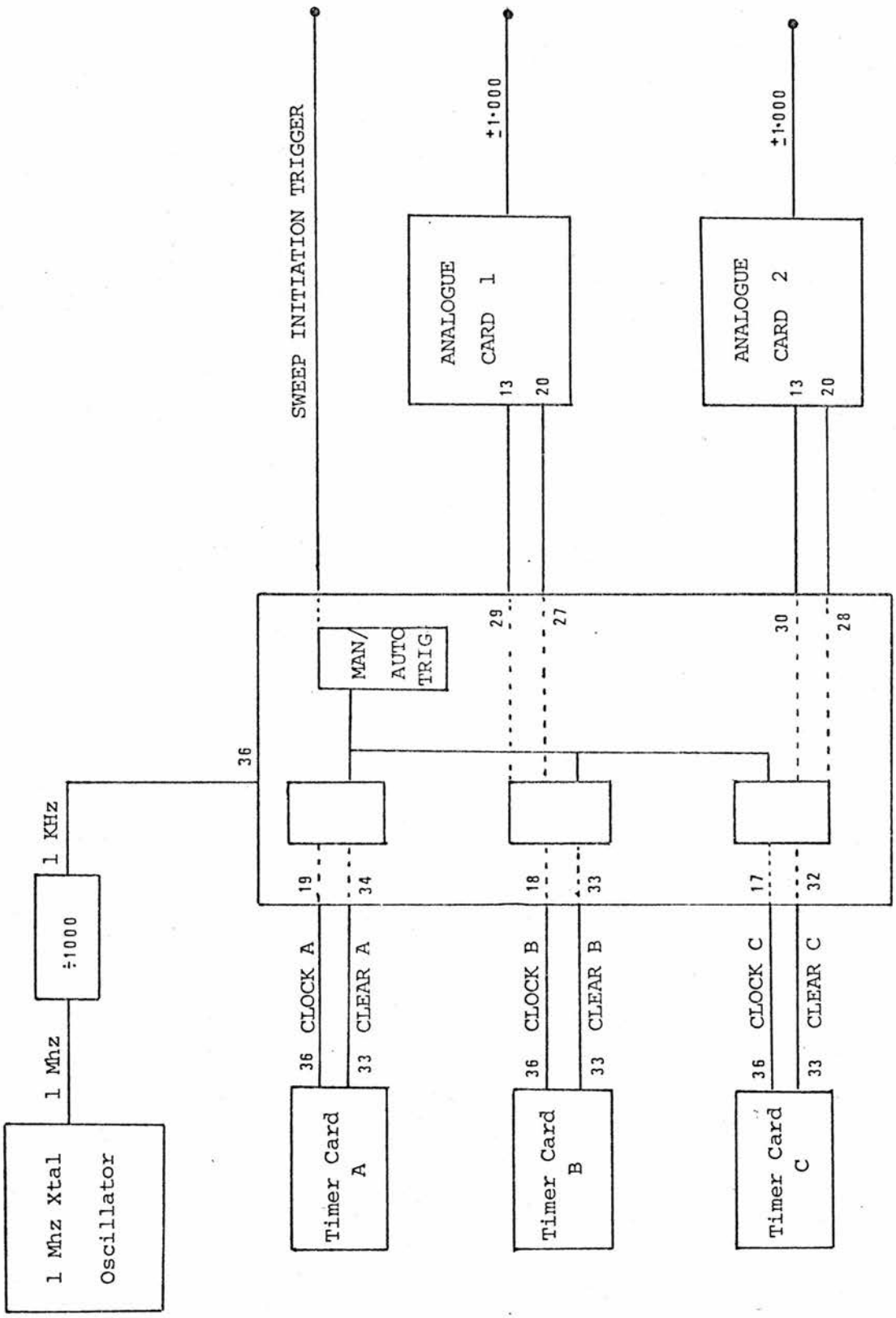

FIGURE 14: Block Circuit Components Diagram of Pulse Generator

initiation may be either manual or automatic. Timer card B controls the length of pulse delivered by the analogue card 1. Timer card C determines the length of the pulse delivered by analogue card 2. Analogue cards 1 and 2 allow the signal generated to be set between ± 1.000V.

The output signal from the pulse generator analogue units was applied to the auxiliary input on the galvanostat at point (A) in Figure 15. The delivery of a 1.000V signal to the auxiliary input resulted in a current, corresponding to the full scale current of the selected scale of the galvanostat, to be applied to the cell. The height of the current pulse the galvanostat delivered to the cell was therefore controlled by the analogue cards of the pulse generator. A variety of signal profiles are therefore available from this experimental setup.

Detail of the timing sequence used in the present experimental procedure is given in Figure 16.

4) Galvanostat/Potentiostat

The galvanostat/potentiostat was designed and constructed in the departmental electronic workshop.

In the present application, use was made of the galvanostatic operating facility, auxiliary input and cell voltage offset facility. These will be discussed with reference to the circuit diagram in Figure 15.

a) Galvanostatic mode

The reference potential circuit and LH002l0k amplifier were used in a standard constant current generating configuration to supply currents as set by the current range selector. Currents applied to the cell in either two electrode or three electrode configuration were measured, either by the internal meter or by using the current output via the current measuring amplifier at (B), Figure 15.

b) Auxiliary input

Auxiliary input from the pulse generator was applied to the summing point (A), of the LH002l0K amplifier. The standing current was set to zero and the current delivered to the cell was therefore controlled by the pulse generator.

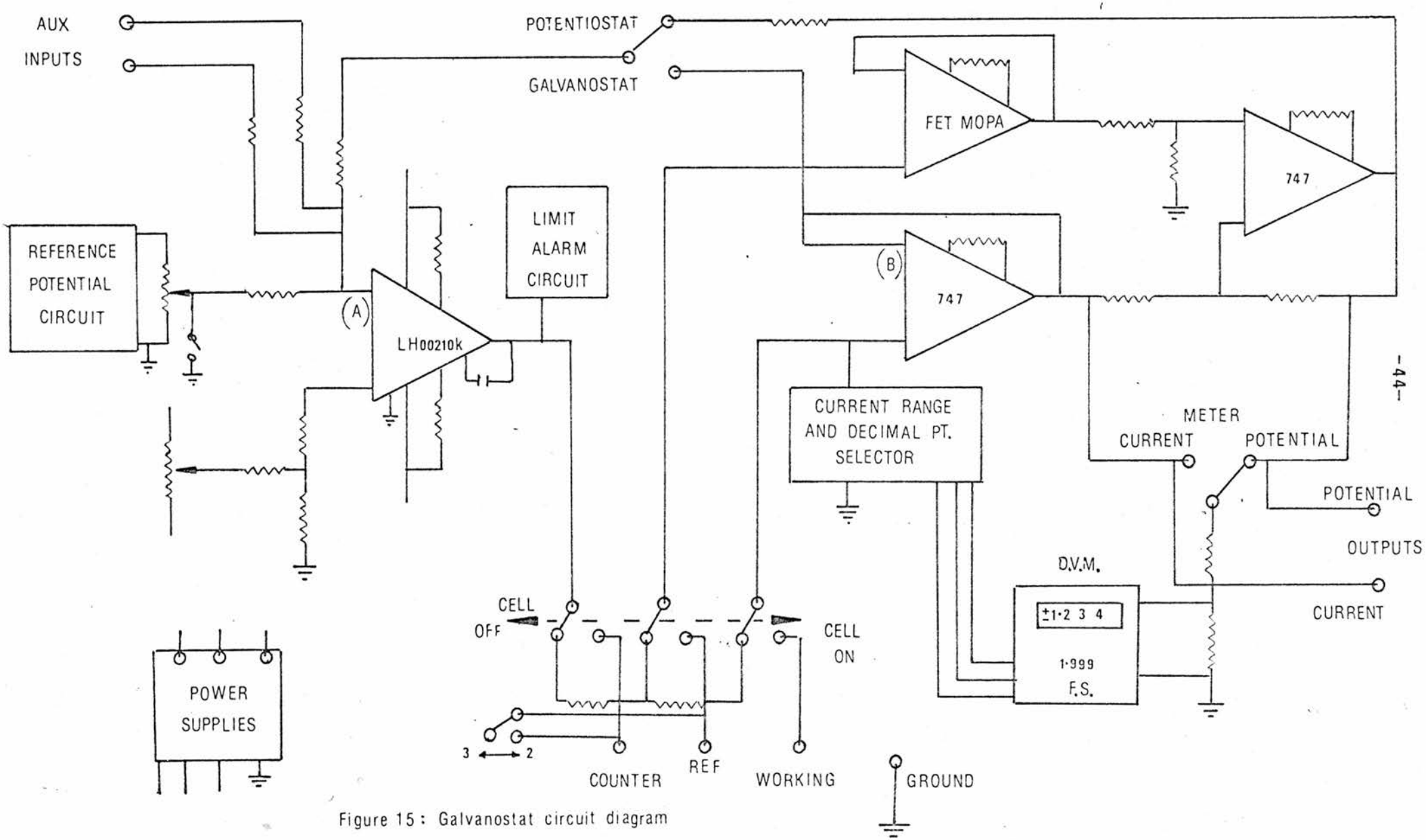

Figure 15 : Galvanostat circuit diagram

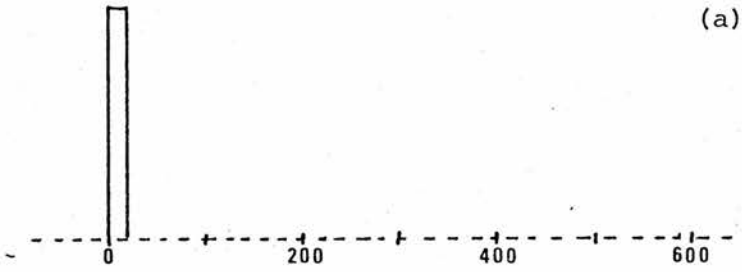

(a) Pulse from trigger output of pulse generator to external trigger input of D.S.A. starts recording sweep at zero time.

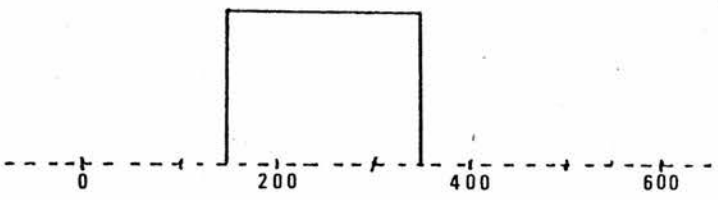

(b) Analogue unit 1 delivers pulse to galvanostat auxilliary input after delay (typically 150 msec).

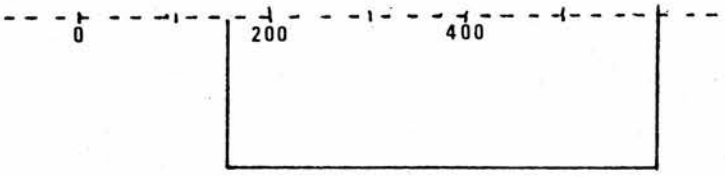

(c) Counterpulse delivered to galvanostat by analogue unit 2

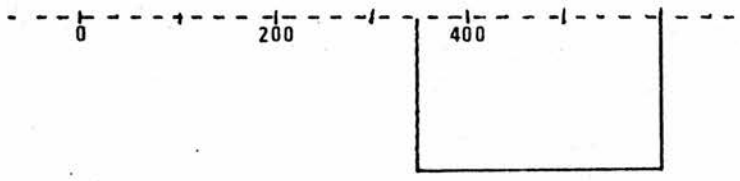

(d) Pulse profile delivered to cell.

FIGURE 16: Timing Sequence

c) Cell voltage offset

For applications in combination with the NS-575 the cell voltage offset was used. This facility is not detailed on the circuit diagram. Its operation permitted the cell voltage to be offset with respect to the potential output to the NS-575, and consequently the most sensitive recording range of the NS-575 to be used for the measurement of the transient. The voltage range of the offset was ± 2.000 volts using a ten turn precision potentiometer.

2.20 b) Experimental Procedure for Diffusion Coefficient Measurement.

Prior to use several instrument checks had to be carried out on the apparatus. The zero standing current in the galvanostat was measured by attaching a dummy cell to the cell connection terminals, and monitoring current through the cell by means of a Solartron 4552 multimeter connected across the current measuring output on the rear panel of the galvanostat. This was brought close to zero by fine adjustment of the current setting potentiometer on the front panel. Further adjustments were carried out with a very sensitive current meter, (minimum measurable current O.OlμA), in series with the dummy cell, using the fine zero adjustment on the front panel.

Periodically the analogue-digital converter of the NS-575 was recalibrated on the appropriate recording scale by application of a known voltage close to the scale maximum to the input of the instrument, after setting the baseline position and clearing memory. The signal height of any record was expressed in counts. This routine provides a calibration of the A/D converter in millivolts/count.

The cell was then connected to the galvanostat and a DVM connected across the potential measuring output on the galvanostat rear panel. The cell was then switched on and the potential offset adjusted to produce an offset at the potential output corresponding to the cell voltage.

The potential output of the galvanostat was then connected to the input of the NS-575 and the "view input" function of the NS-575 selected. Further adjustment of the potential offset of the cell was seldom required to bring the signal to the baseline of the NS-575

screen with the cell switched on. The cell was then switched off temporarily, while the "baseline adjust" function of the NS-575 was selected, and zeroed. With the potential input of the NS-575 removed the baseline adjustment was carried out. The potential input from the galvanostat was then reconnected and the instruments were ready for the beginning of the experiment measurements.

Cell temperature and initial cell voltage was measured using the electronic thermometer and the Solartron DVM respectively. The appropriate current pulse height and length were set on the pulse generator and the cell switched on. The DVM, connected across the potential measuring output of the galvanostat, was used to check the residual voltage difference of the cell and the potential output to the NS-575, when the cell was switched on. The pulse was then applied to the cell and the voltage transient recorded. The cell was immediately switched off. The voltage recovery of the cell, to within a tenth of a millivolt of the original pre-pulse value was usually very rapid as only low currents and short pulse lengths were used. On recovery the pulse measurement was repeated until a suitable total signal was obtained.

The data receive program, program 1, was then loaded and run on the Tektronix. The cell title was input from the Tektronix keyboard, followed by the NS-575 timescale, voltage scale, scan count, temperature and tape file number. Data analysis start and terminate addresses, IR drop approximation, guest concentration, pulse current and number of spurious spike points to be removed were input in the next line, as prompted. "Data readout" was selected on the function select switch of the NS-575 and data transfer initiated on prompting from the Tektronix. From this point the computer carried out the calculations unattended with only page changing on the plotter required.

2.20 c) AC Conductivity

A Solartron 1170 frequency response analyser, (FRA), controlled by the Tektronix minicomputer, was used to obtain the conductivity spectra of samples of the ion conducting glass electrolytes.

Programs for the machine control and parameter input from the Tektronix keyboard, were written by C.A. Vincent, and for data plotting by A.R.Wandless. These programs are not included in the present discussion.

Figure 17 shows a diagrammatic representation of the equipment used. The FRA was used to apply signals of a range of frequencies to the cell which was connected in series with a measuring resistor. The measuring resistor was selected from a range of resistors to be as close to the cell resistance as possible. The ratio of signals, X/Y, was expressed in terms of complex variables, a and b, and output by the FRA. The Tektronix carried out calculations on this data to convert the values to either series, Rs and Cs, or parallel, Rp and Cp, formalism. Plots of log conductivity versus log frequency spectra, based on either series or parallel data, were then obtained on the 4662 interactive plotter. An example of the graphic output is included in Chapter 3. (Figure 1).

2.20 d) D.C. Conductivity Measurements (electronic conductivity)

Potentials in the 50mV to 600mV range were applied to cells using a 1 volt stabilised power supply with precision potentiometers.

The potential applied to each cell was monitored, through a selector switch, with a Kiethley 190 digital multimeter.

The current measurement was carried out using a nanoammeter built in the departmental electronic workshop. The circuit diagram of the nanoammeter is included in Figure 18. The device operates by using a high precision current amplifier with a range of standard resistors and sensitive detection meter.

In general the currents monitored were very low, of the order of nanoamps. After changes in voltage applied to the cells the charging currents were allowed to decay before readings of cell currents were taken. In every case a period of one to three days with no change in current measured was taken to mean the cell had reached the current level due to electronic conduction.

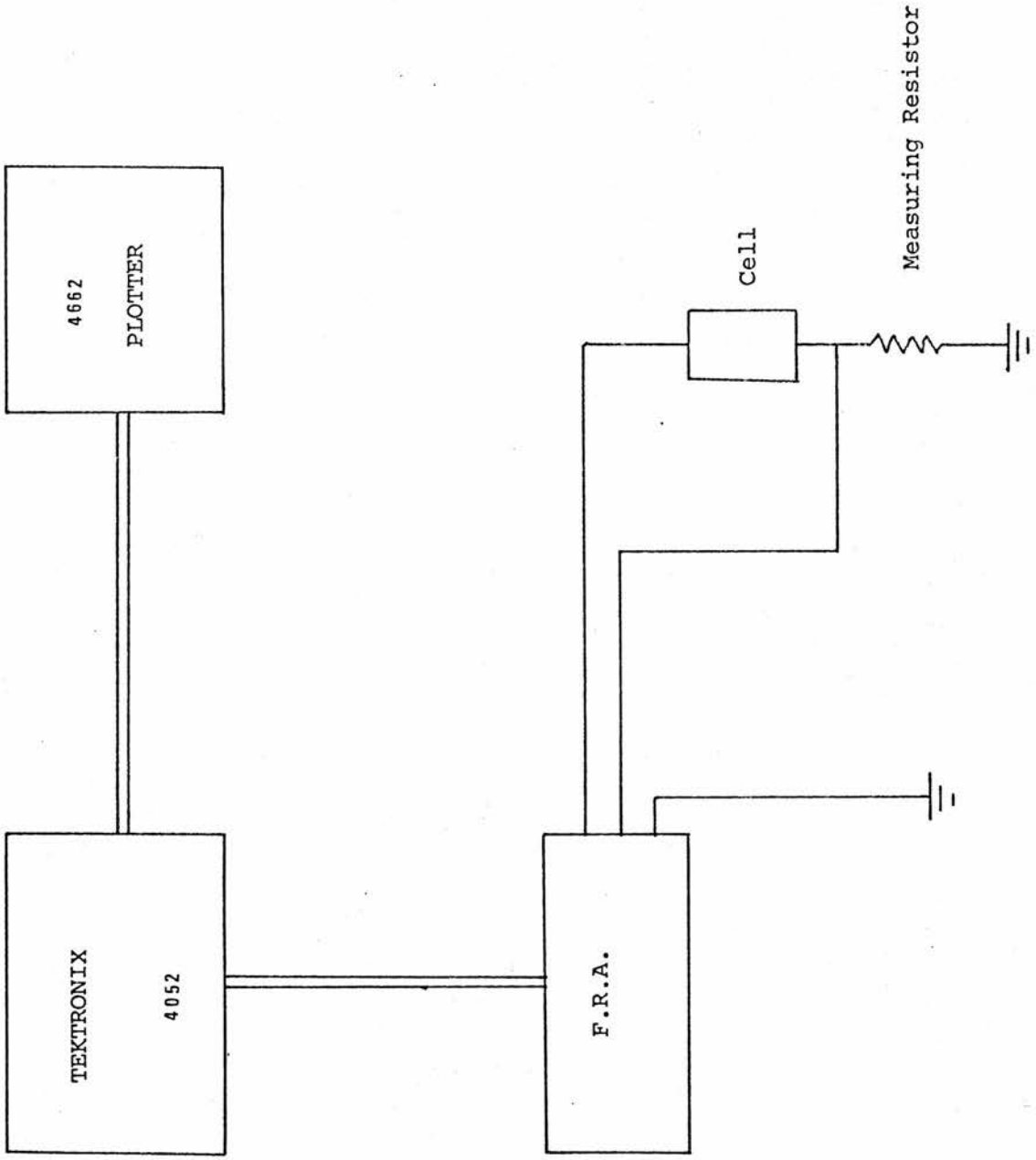

FIGURE 17: Circuit Components used to obtain A.C. Spectra

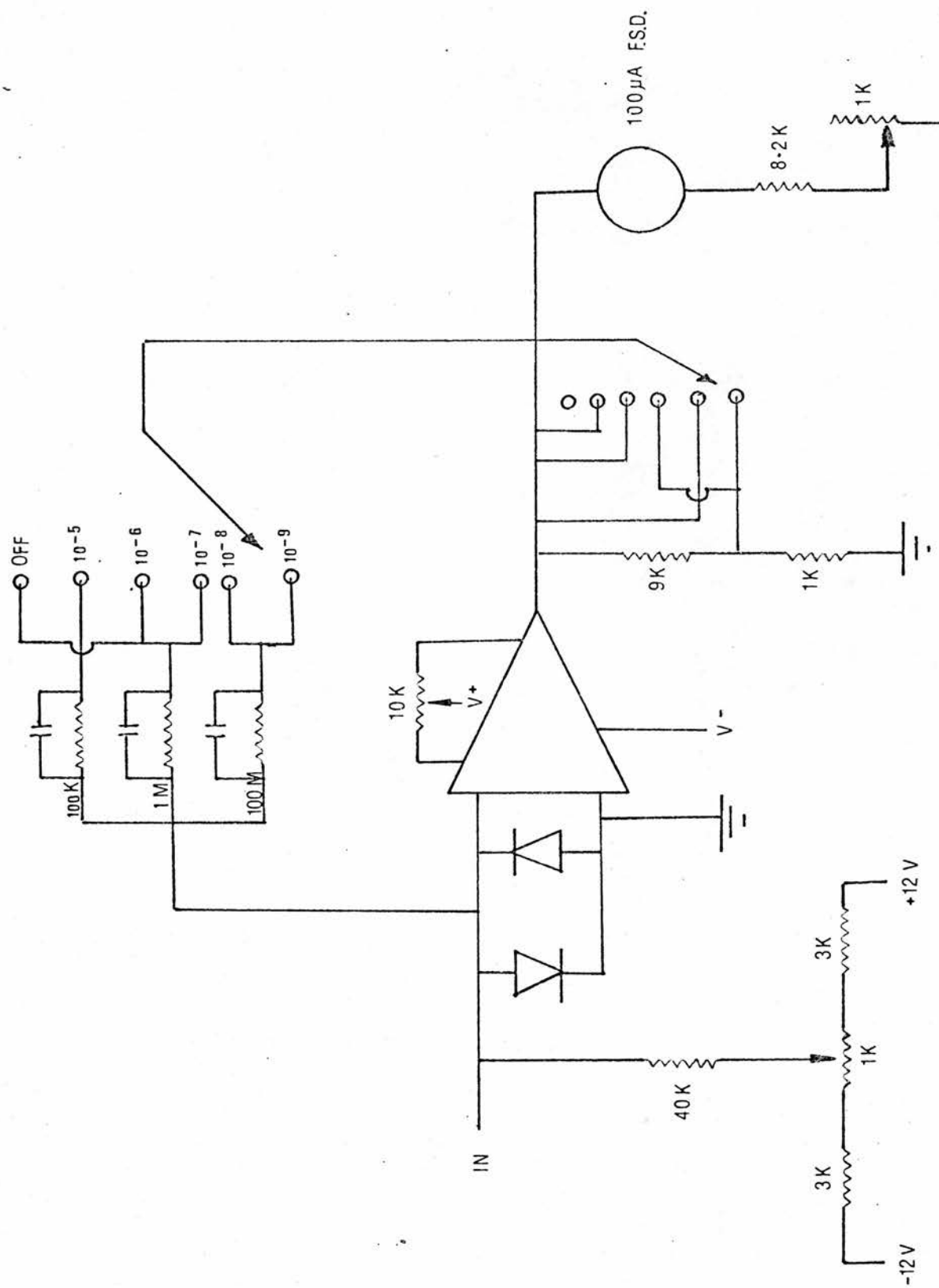

FIGURE 18: Nanoammeter used in D.C. Conductivity Measurements

1. Faurie J.P., Bull. Soc. Chim. France, Vol 44, (1971) 1170

2. Bonino F., Lazzari M., McKechnie J.S., Rivotta B., Turner L.D.S., Vincent C.A., J. Inorg. Nuel. Chem., Vol

3. D'Tvoire F., Bull. Soc. Chim. France, Vol 37, (1962) 1237

4. Takahashi T., Yamamoto O., J. Electrochem. Soc., Vol 120, (1973) 647

5. Chiodelli G., Magistris A., Schiraldi A., Electrochem. Acta, Vol 19 (1974) 655

6. Lazzari M., Papaleo F., Pisoia G., Scrosati B., J. Electrochem. Soc., Vol 122, (1975) 339

7. Jagla M., Private Communication

8. Leith R.M.A., "Preparation and Crystal Growth of Materials with Layered Structures", (D Reidel Publishing Company, Dordrecht, Holland, Boston-USA, 1977)

9. Instituto di Chimica Fisica, Electrochimica e Metallurgia, Politecnico di Milano, Milano, Italy

10. Instituto di Chimica Fisica, Universita degli studi di Roma, Roma, Italy

11. Gamble F.R., Symon C.R., Thompson A.H., Mat. Res. Bull., Vol 10, (1975) 915

12. Barnett W.B., Fernandez F.J., Lumas B.K., Wallace G.F., Atomic Spectroscopy., Vol 2, (1981) 130

13. Carides J.N., Christian P.a., Di Salvo F.J., Murphy D.W., J. Electrochem. Soc., Col 126, (1979) 497

CHAPTER 3: LITHIUM ION CONDUCTING ELECTROLYTE, OPTIMISATION FOR CELL CONSTRUCTION

3.1 Introduction

As a result of the ever increasing list of applications for small, efficient, primary and secondary batteries, considerable interest and research effort has been directed toward the investigation of highly conducting lithium solid electrolytes. The importance of these materials is related to the advantage of high open circuit potentials of cells utilising lithium couples. Recently such advances have been made in electrode technology, with the introduction of lithium alloy and intercalation materials with very encouraging performance characteristics, that there is some justification for the comment that the major remaining obstacle to the viable solid state cell is the absence of an entirely suitable solid electrolyte.[1]

A variety of electrolytes have been proposed for lithium battery applications, several of which have been glasses. In spite of the thermodynamic instability of vitreous phases, many glasses are stable under the conditions of cell operation and offer distinct advantages over crystalline electrolytes with regard to cell fabrication. Unlike cells containing liquid electrolytes, cells utilising solid electrolyte systems have no leakage problems, and sophisticated seals, (with inherent increase in cell container weight, and cost,) are not necessary.

During investigation of certain transition metal dichalcogenides and transition metal oxides as electrode materials the possibility of an extension of the original field of investigation, to include the behaviour of these materials with lithium guest species, made the selection of an appropriate lithium electrolyte necessary. The primary criteria for this selection were ease of electrolyte preparation and cell fabrication. A glass electrolyte based on a lithium fluoride-lithium oxide-aluminium metaphosphate composition,[2] appeared to satisfy these criteria and preliminary experiments leading to the optimisation of conditions of cell fabrication were carried out.

3.2 A.C. Conductivity Measurements.

One of the most powerful techniques available for the investigation of electrolytes is a c frequency response analysis. Typical applications are in the determination of total electrolyte resistance, (due to a combination of contributions of grain boundary and bulk resistances), double layer capacitance and geometrical capacitance. Data obtained by the application of a range of a c frequencies to a cell, and recording the change in the resistance and capacitance of the equivalent circuit of the cell with frequency, may be treated in a variety of ways, to highlight the parameter of interest. While it is possible to use different plots and formalisms to evaluate the components of intergranular and bulk impedances, in the present case the technique was used at its simplest level, as a means of comparison of total resistance of a series of cells with different electrolyte preparation histories. It is generally true that a frequency independent region in the log conductivity versus log frequency spectra corresponds to the d c conductivity of a cell, and in the investigation of the lithium glass electrolyte the value of resistance obtained from these plateau was used to determine electrolyte resistance. The temperature dependence of the log conductivity obtained from these spectra was used to calculate the activation energy of the conduction process.

3.3 Results and Discussion

Early attempts to prepare cells from samples of finely ground electrolyte led to the identification of two serious problems. Cells fabricated using a hydraulic press to prepare 13mm discs, (Chapter 2, Section 2.13) were found to be very fragile. As the intended experimental cell in which the electrolyte was to be used involved a fairly complicated pressing procedure, and was to be firmly mounted during electrode material investigations, this was a major problem.

Log conductivity versus log frequency spectra obtained for the compressed powder samples showed a fairly low conductivity. As the bulk conductivity, obtained from splat formed cells, was considerably higher it seemed probable that the increased resistance of the compressed powder cells was due to the increased grain boundary impedances of this type of cell.

3.3 (a) Oven Pretreatment of Cells

In view of the success of hot pressing and sintering techniques in preparation of the ceramic electrolyte separators used in the sodium sulphur cell, it seemed appropriate to investigate the possibility of reducing the total resistance of the electrolyte and improving pill fracture characteristics using these techniques. An investigation was carried out to determine the feasibility of applying the experimentally more straightforward technique of sintering, or oven pretreatment, to the compressed powder cells.

Preliminary investigations of the effect of oven pretreatment, using an optical microscope with a magnification of 600x, showed that samples retained in an oven at 450 to 500°C for a period of five minutes showed signs of binding between individual conglomerate-like areas of the pill. The optical microscope gave limited information as little detail of intragranular structure could be seen. A considerable improvement in the investigation of the effect of temperature pretreatment was gained with the use of a scanning electron microscope. With the aid of this instrument the range of temperatures between 350 and 500°C was investigated. Several pills prepared over a range of temperatures were sectioned and the sectioned face coated with a very thin film of evaporated gold to improve back scattering of incident electrons and resolution of the scanning electron microscope picture of the surface. Plates 1 to 5 are included to show detail of the pill faces.

Plate 1 is a section of a "green" pill (no oven treatment). The electrolyte chips can be seen to have sharp, well defined edges. A section under increased magnification is shown in Plate 2.

Plate 3 illustrates the effect of a period of five minutes in the oven at approximately 380°C. In this case the effects of the heat treatment are only faintly discernible with some slight rounding of the chip edges. The difference in pill strength however, even at this temperature, was quite remarkable. This suggested that even though no indication of grain cohesion was visible, the effect of the oven treatment was an improvement in intergranular binding.

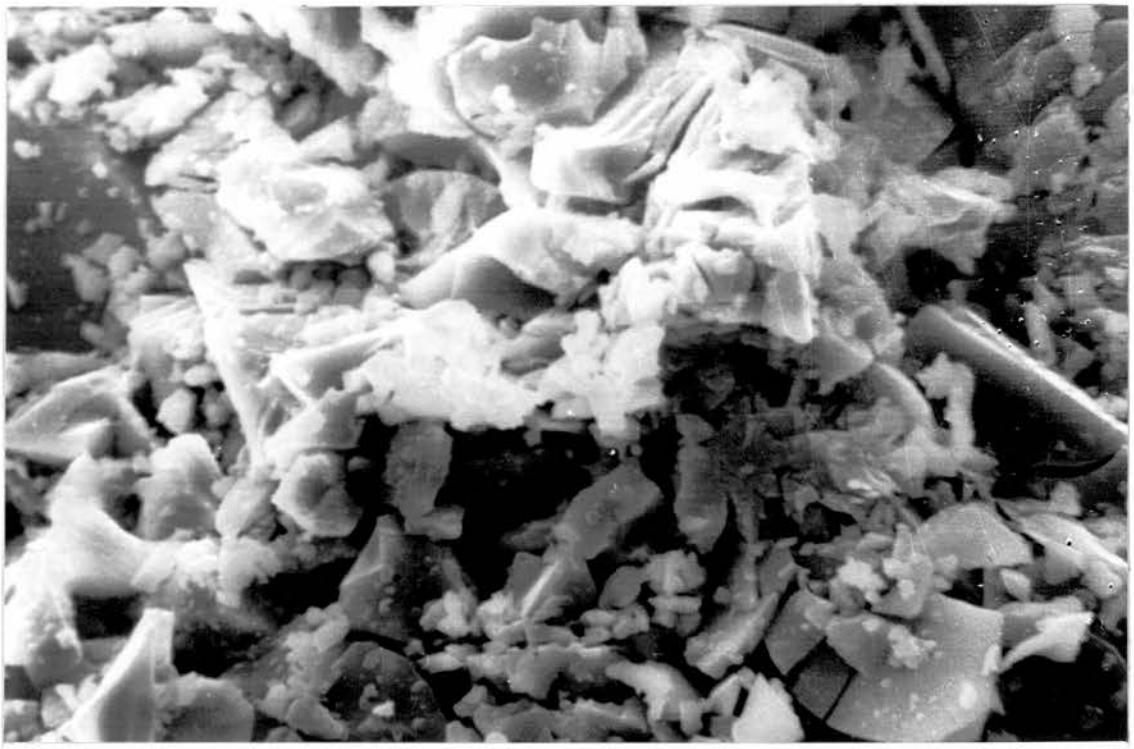

Plate 1: Section of "green" pill, no oven treatment

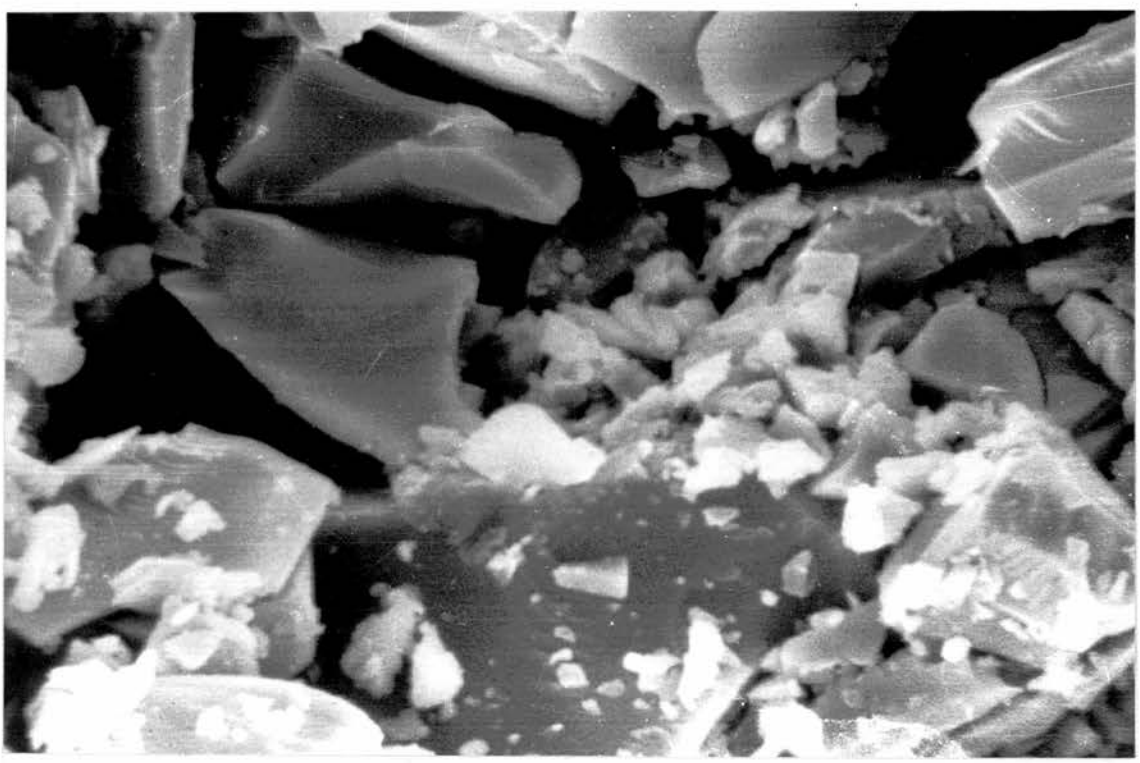

Plate 2: "Green" pill, section under increased magnification

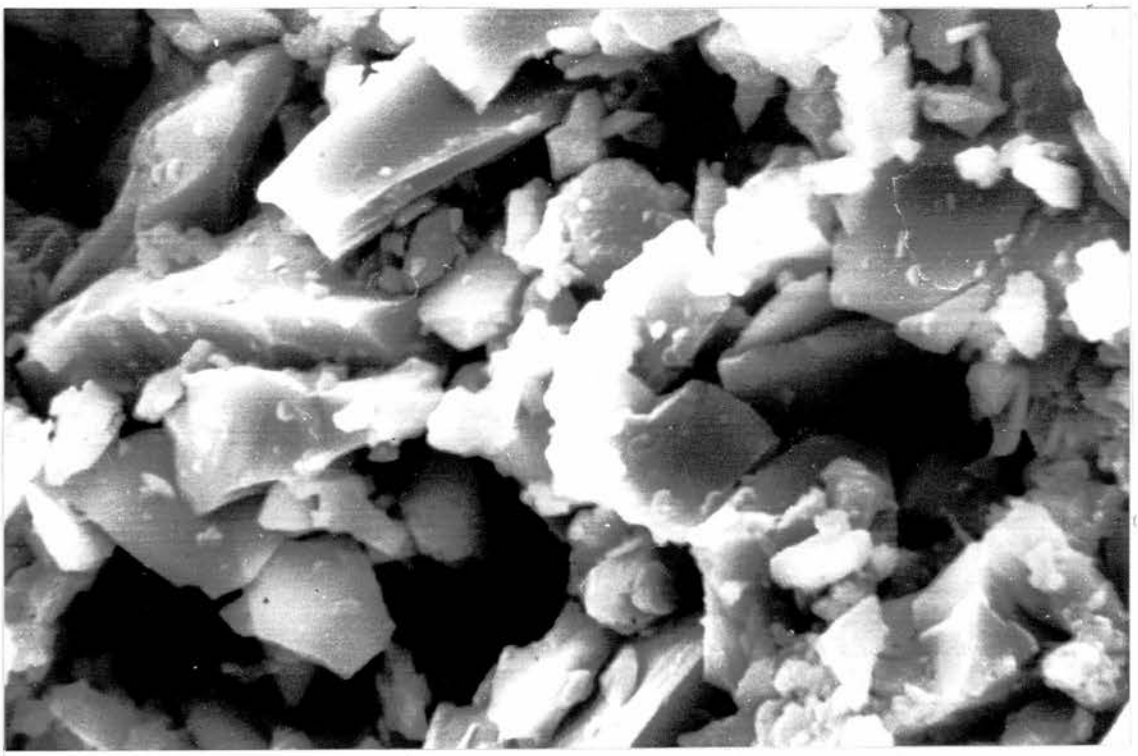

Plate 3: 380°C oven treatment (5 min. duration)

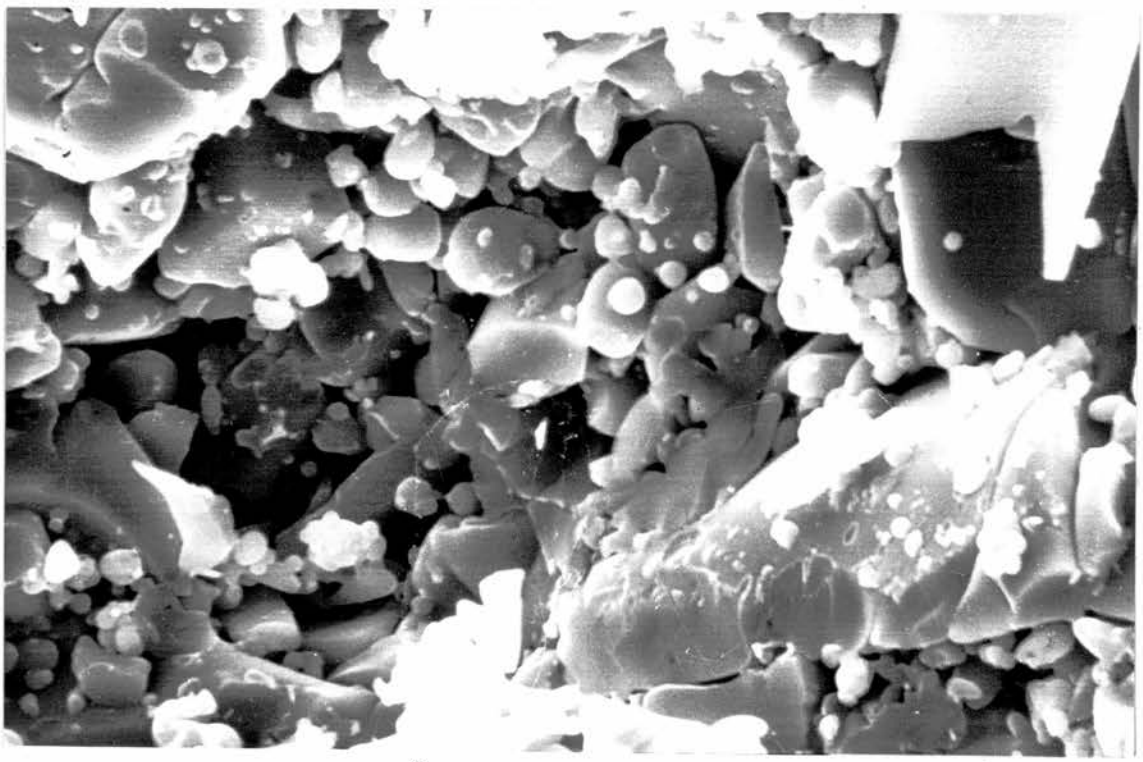

Plate 4: 400-420°C oven treatment (5 min. duration)

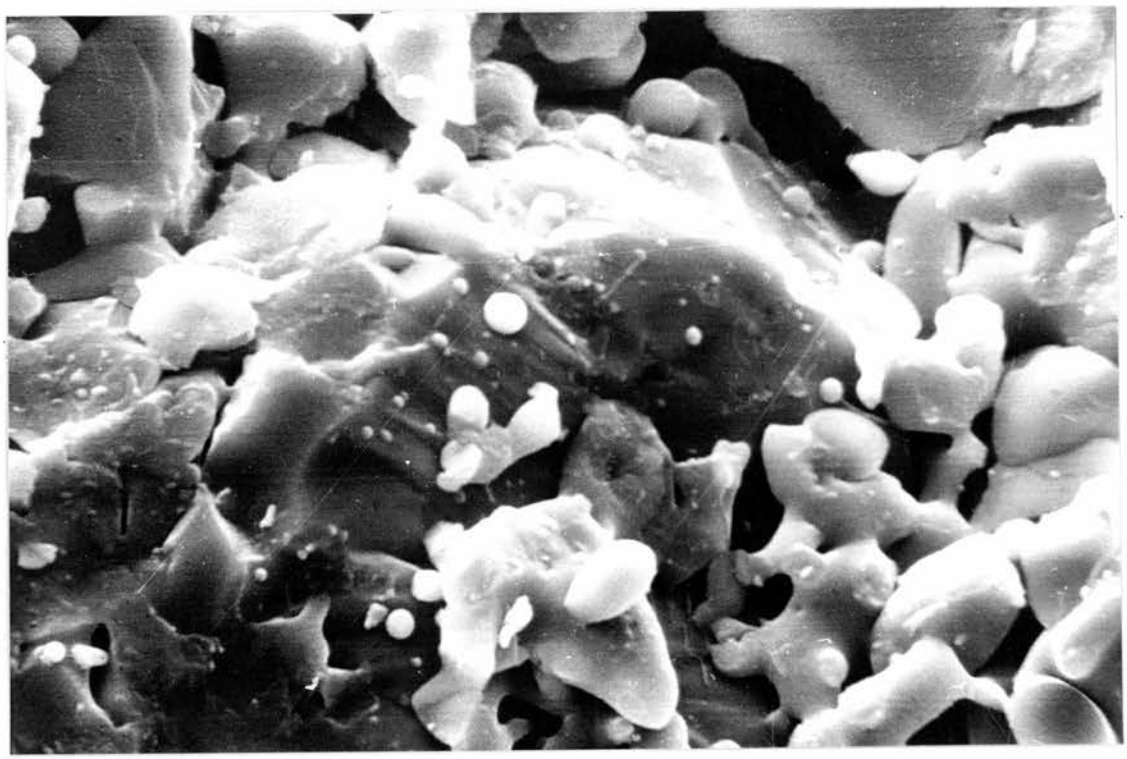

Plate 5: 400-420°C oven treatment, section under increased magnification

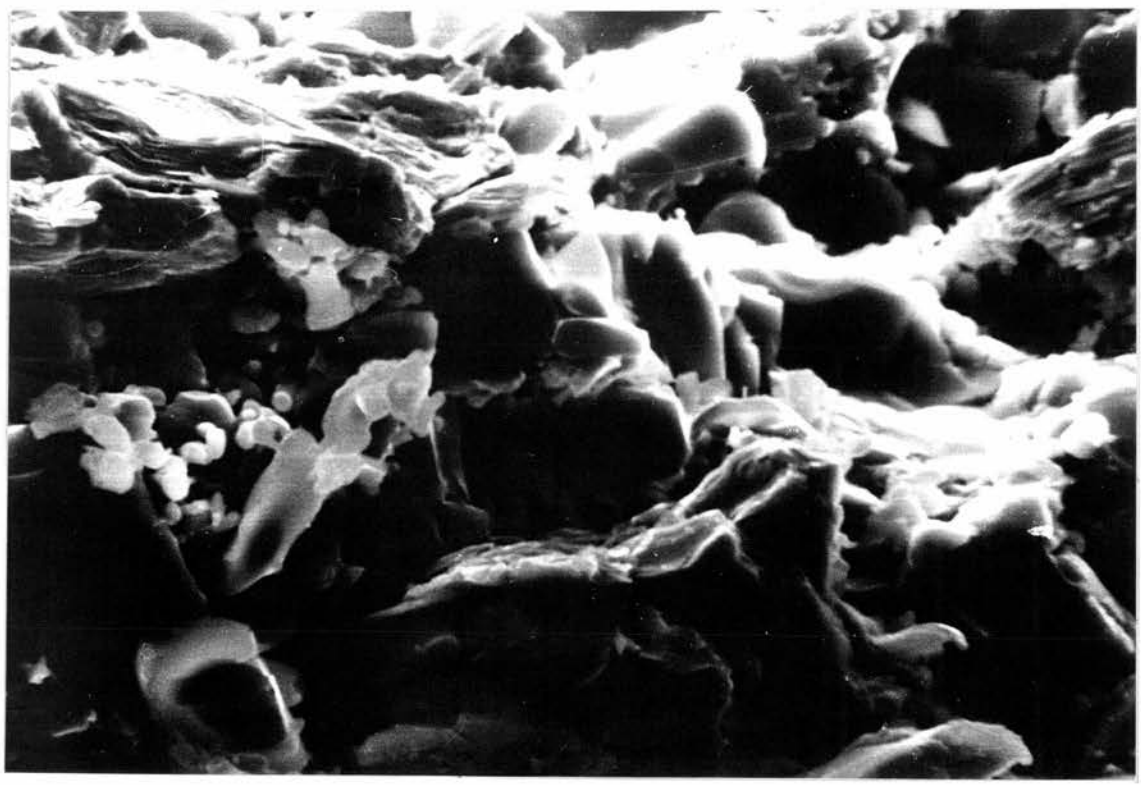

Plate 6: Section of compressed electrode/electrolyte mixture after oven treatment at 415°C

At temperatures between 400 and 420°C, as shown in Plates 4 and 5, there was a sudden change in the effect of temperature, and marked electrolyte chip rounding is clearly visible. Plate 5 shows regions in which the grains have begun to coalesce.

A further increase in the temperature of oven pretreatment led to pill discolouration and distortion. As the cell-holder used to mount the pill relies on the pill being flat, and the experiment requires simultaneous contact between reference and working leads and electrodes in the cell holder (Figures 1 and 2, Chapter 2), oven temperatures which give rise to pill distortion are unacceptable and effectively place an upper limit on the pretreatment temperature.

An investigation of the effect of the duration of the oven pretreatment revealed little change in the cell appearance.

3.3 (b) A C Frequency Response Analysis

Various methods of electrode application for conductivity measurements were investigated. The irregular surface of the compressed powder sample of electrolyte made the use of evaporated aluminium metal blocking electrodes difficult. In order to achieve a low resistance electrode a thick surface coating had to be applied requiring several successive evaporations. The most reproducible results were obtained with electrodes applied to the surfaces as a colloidal silver in an organic solvent. The solvent was removed by drying the cell in a glass oven for a few minutes.

Initial experiments were carried out on splats formed by rapid cooling of a droplet of electrolyte cast onto a polished metal plate and compressed by a descending metal anvil.

Results obtained with a splat-formed cell are reported in Figure 1, and show the plateau in the log conductivity spectra, and the variation of the plateau position with temperature. An activation energy plot obtained from this data is included in Figure 2, and gives values consistent with those obtained by Jagla and Isard[2], Table 1.

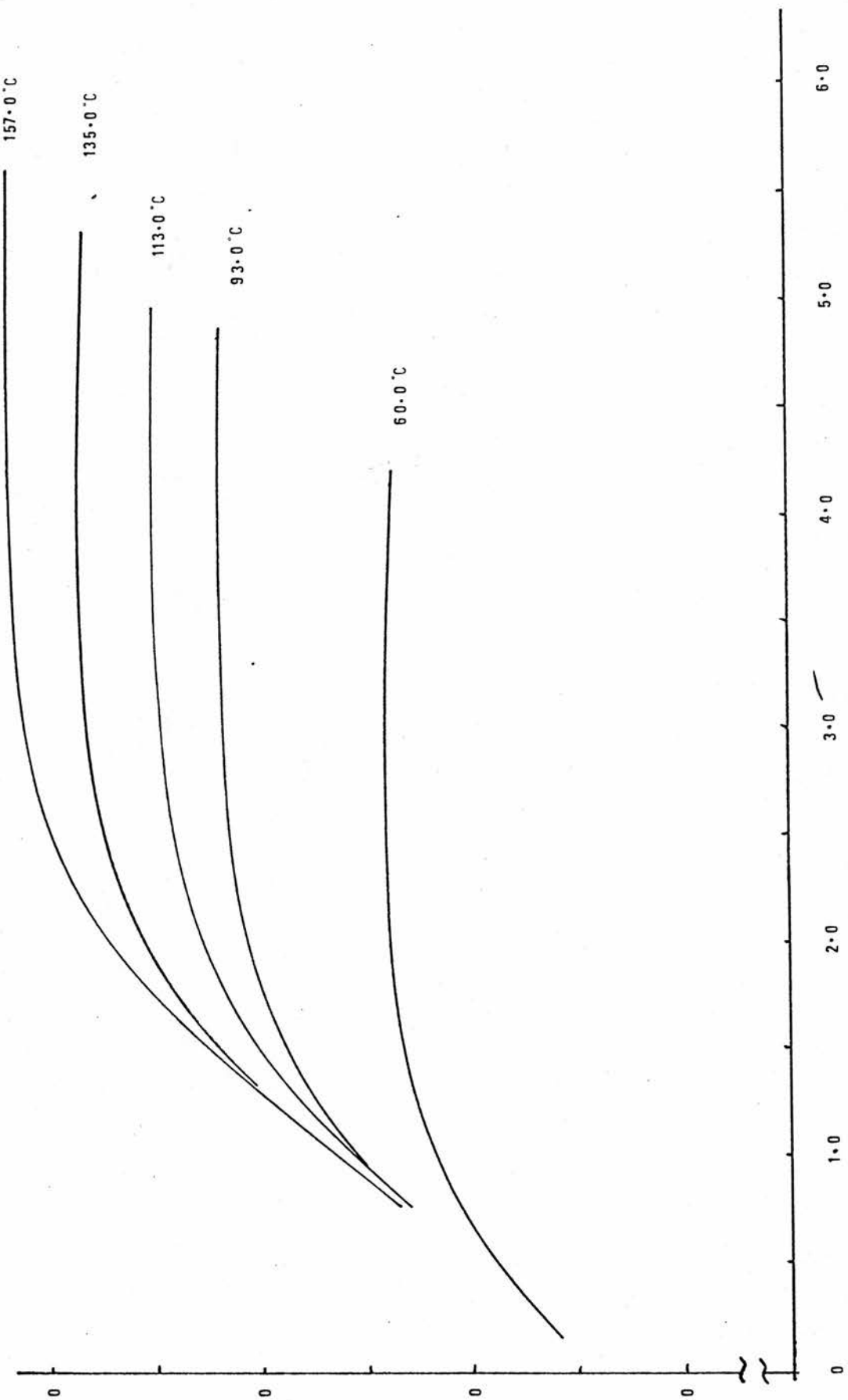

Figure 1: -Log Conductivity versus Log Frequency Spectra

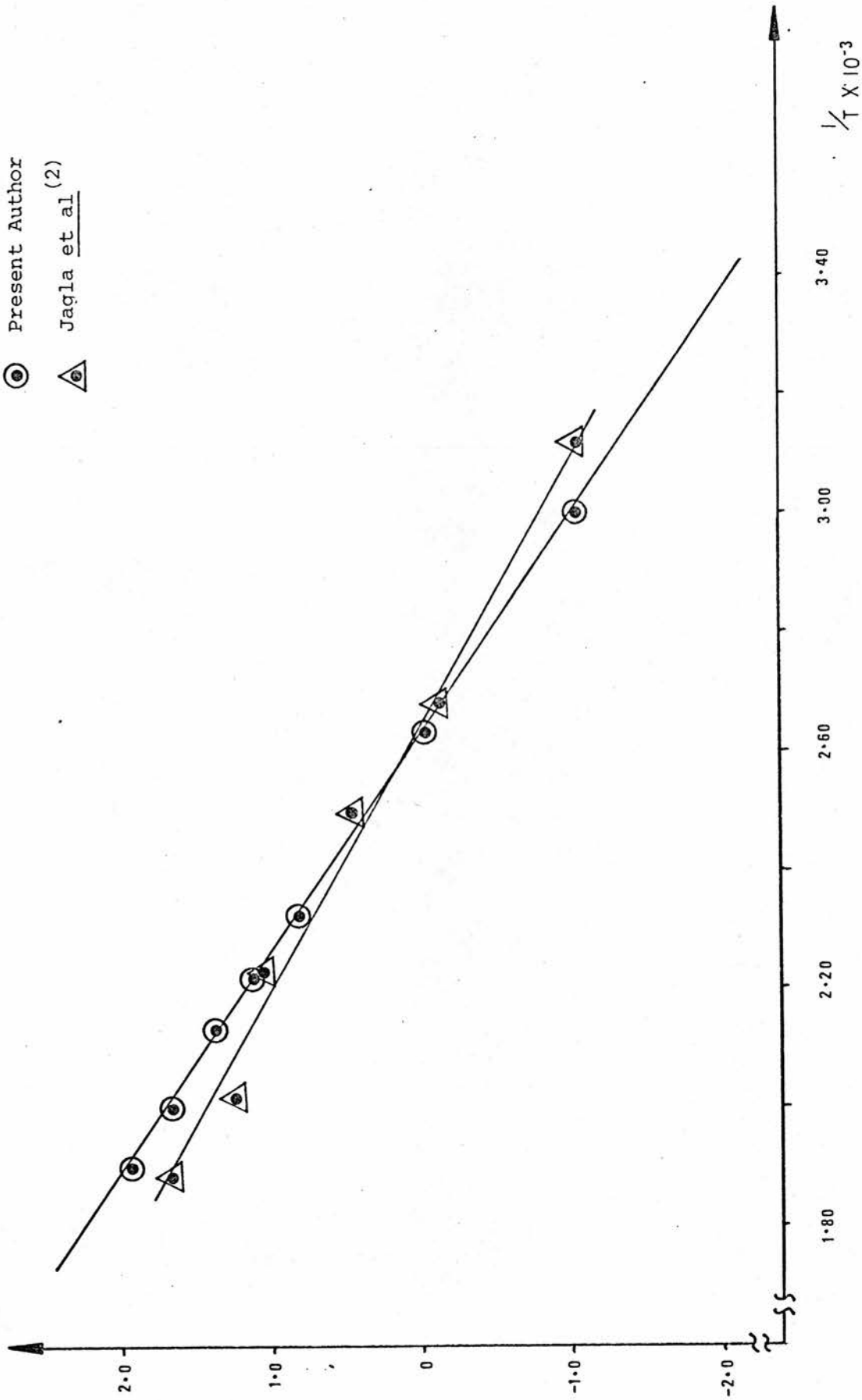

Figure 2: Log σT versus T^{-1} plot for Li conducting glass

Table 1: Comparison of σ_{250^oC} : ΔH_{act}

	σ_{250^oC} ($S.m^{-1}$)	Activation Energy ($kJ.mol^{-1}$)
Jagla et al	0.100	43.92
Present Work	0.166	52.02

Table 2: Effect of Temperature of Oven Pretreatment on σ_{250^oC} and ΔH_{act}

Temp (^oC)	σ_{250^oC} ($S.m^{-1}$)	ΔH_{act} ($kJ.mol^{-1}$)
no oven treatment	0.0201	75
387	0.0317	61
394	0.0325	57
403	0.0474	67
405	0.0474	66
416	0.243	60

Table 3: Comparison of σ_{250^oC} for Oven Treatment Duration

Duration (min)	σ_{250^oC} ($S.m^{-1}$)	ΔH_{act} ($kJ.mol^{-1}$)	Temp (^oC)
2½	0.0263	55.77	412 - 416
5	0.245	59.49	412 - 416
10	0.258	60.64	412 - 416
2½	0.024	57.99	391 - 393
5	0.032	54.66	391 - 395
10	0.034	55.62	390 - 395

The effect of the oven pretreatment on the conductivity of a cell was investigated by subjecting a series of cells to a variety of treatments prior to electrode application and comparing the conductivities of the cells. Table 2 shows the results of this experiment.

These results appear to confirm the data obtained from the scanning electron microscope study. The optimum temperature of pretreatment appears to be about 400 to 420°C. An oven treatment in the range of 380 to 410°C results in a monotonic improvement in the values of conductivity of the electrolyte expected from an improvement of intergranular contact (or decrease in intergranular impedance). At temperatures above 410°C however a sudden improvement is noted, presumably as a result of local melting at intergranular contacts and coalescence of grains giving rise to a further dramatic reduction in intergranular impedance.

The dependence of the conductivity on the duration of the oven pretreatment was investigated at two temperatures by retaining samples in the oven for 2½, 5 and 10 minute periods and comparing the conductivity. As expected, the cells kept in the oven for longer periods showed improved conductivity, (Table 3), but in some cases discoloured and distorted at longer oven times. It was therefore decided that a compromise of oven treatment duration of about 5 minutes be used.

3.4 Conclusions

The present requirements of lithium ion conducting solid for the investigation of various properties of electrode materials are largely met by the glass, examined in this chapter. The glass is readily prepared with a sufficiently high ionic conductivity and low electronic conductivity[2] for the present application. Though very fragile immediately after pressing, once the oven pretreatment has been carried out the cells are quite suitable for installation in the cell holder.

Though it is unlikely that an electrolyte with as low a conductivity at ambient temperatures is likely to be of commercial value, other materials which improve intergranular contact with oven treatment might be of interest. It is possible to visualise a situation in which cells might be assembled and finally subjected to a treatment of this type before final sealing. If during this treatment the electrolyte/electrode interface were subject to a flow of electrolyte then some of the contact area problems which arise in solid state cells might be avoided.

An attempt to illustrate the effect of the oven pretreatment on the electrode/electrolyte interface was only partially successful. In the experiment carried out, in which a finely ground electrolyte/electrode material mixture was compressed and subjected to an oven pretreatment, the difference in physical appearance of the electrolyte and electrode material was the only means of identification of the interface areas. Unfortunately after grinding, heating and evaporating a thin layer of gold onto the surface, clear distinction of these areas was not unambiguously possible. Plates 6 and 7 which are thought to show the interface regions are however included.

While further, more detailed investigation of the effects of the temperature pretreatment on various aspects of the intergranular impedances, by frequency response analysis, would probably yield interesting results, this, not being central to present project, was left unattempted.

Plate 7: Enlargement of electrode/electrolyte section

1. Angell C.A., Boehm L., J. Non-Crystalline Solids, Vol 40, (1980) 83

2. Isard A., Jagla M., Private Communication

CHAPTER 4: THERMODYNAMICS OF SOLID SOLUTION ELECTRODES

4.1 Introduction

Within the last decade a combination of several factors in commercial and scientific spheres has led to an increased interest in the development of solid solution electrode (SSE) materials. A brief survey of the relevant literature demonstrates that practical materials come from a remarkable diversity of structural type. (tunnel compounds, layered compounds, or open framework structures) The fact that there are so many compounds which fulfill the structural criteria, has led to the development of simple test procedures which permit rapid evaluation of candidate compounds.

4.2 Potential Versus Electrode Composition Measurements (Coulometric Titration)

The most readily, and frequently applied test involves the construction of a galvanic cell, as shown in Figure 1. M serves as the source of electroactive species. The electrolyte may be solid or liquid, and the SSE under test, in this case denoted M_xTCh_2, (where T represents transition metal, Ch the chalcogen, and x the molar ratio of guest in the compound) completes the cell. It is assumed that the M and M_xTCh_2 materials are both electronic conductors, and the electrolyte is a purely ionic conductor. Under equilibrium conditions, the open circuit voltage of the cell provides a measure of the activity of M, a_m, in the electrode M_xTCh_2.

$$\Delta G = -nFE = RT \ln a_m \qquad [1]$$

In equation [1], the reference is assumed to be the pure metal M, though in practice this need not be the case, any electrode with a fixed activity of M might be used.

The composition of the M_xTCh_2 electrode is changed by passage of current through the cell. If the number of coulombs transfered is accurately known, and the electrolyte is a pure ionic conductor, with the transference number of M^+ unity, the change in x may be calculated from Faraday's Law. The change in cell potential, or activity of M in M_xTCh_2, may be evaluated by monitoring the potential until the new composition achieves a uniform distribution throughout the electrode material, when

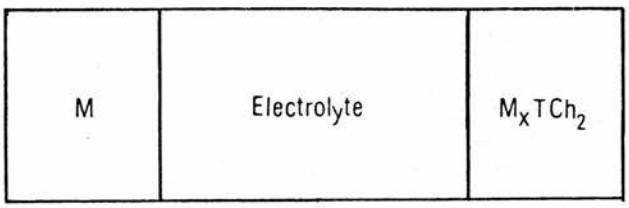

Anode

1. Electronic conductor
2. $M \rightarrow M^+ + e^-$

Cathode

1. Electronic conductor
2. $M^+ + e^- + TCh_2 \rightarrow M_xTCh_2$

Electrolyte

1. Electronic Insulator
2. M^+ conducting electrolyte

Figure 1: Potential versus composition test cell

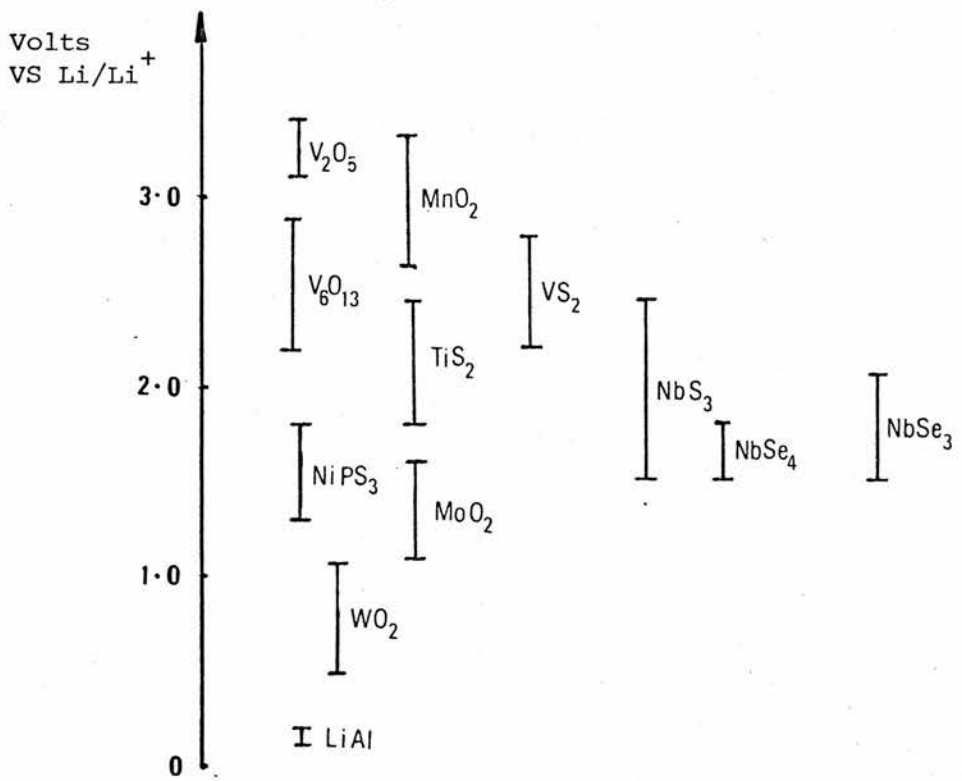

Figure 2: Approximate voltage ranges of reversible operation for various Li/cathode couples[11]

the cell will maintain a time invariant potential.

If the coulometric titration curve is determined in this way, starting from pure TCh_2, the standard Gibb's free energy of formation of M_xTCh_2, or "free energy of intercalation[1]," ΔG_I may be evaluated as a function of composition. This parameter is a useful means by which the energy available during discharge of the concentration cell may be quantified, and compared. The higher the ΔG_I, the greater the energy storage capacity per mole of electrode material.

$$\Delta G_I\ (M_xTCh_2) = -nF \int_o^x E\ dx \qquad [2]$$

Figure 2[2] shows the relative positions of the potentials of several electrode materials with lithium guest species versus a lithium reference. The figure also attempts to give some indication of the working range of the materials. In practical systems these materials are likely to be used in concentration cells, either with a counter electrode of pure guest material or some other intercalation compound. In these applications the most commercially interesting electrodes are those which have a high potential with a shallow voltage versus composition profile in test cells of the type shown in Figure 1. Figure 3[3], is included to show the most promising electrode material so far, TiS_2, with a lithium guest species. The continuous decrease of potential with increasing x is expected for a single phase system and may be related to a number of factors[4]. As may be seen from the figure, the incorporation of a mole of lithium into the lattice results in a voltage decrease of only 0.7 volts, 25% of the initial cell voltage.

4.3 Measurement of ΔH and ΔS of the Cell Reaction

Very little work has been carried out on the thermodynamics of intercalation reactions. In general, only very small entropies of formation have been reported[5], as expected for reactions involving only solids.

The entropy of formation of the intercalation product is obtained from the temperature coefficient of the cell voltage.

$$\Delta S = F \left(\frac{dE}{dT}\right)_p \qquad [3] \qquad \Delta H = F \left\{T \left(\frac{dE}{dT}\right)_p - E\right\} \qquad [4]$$

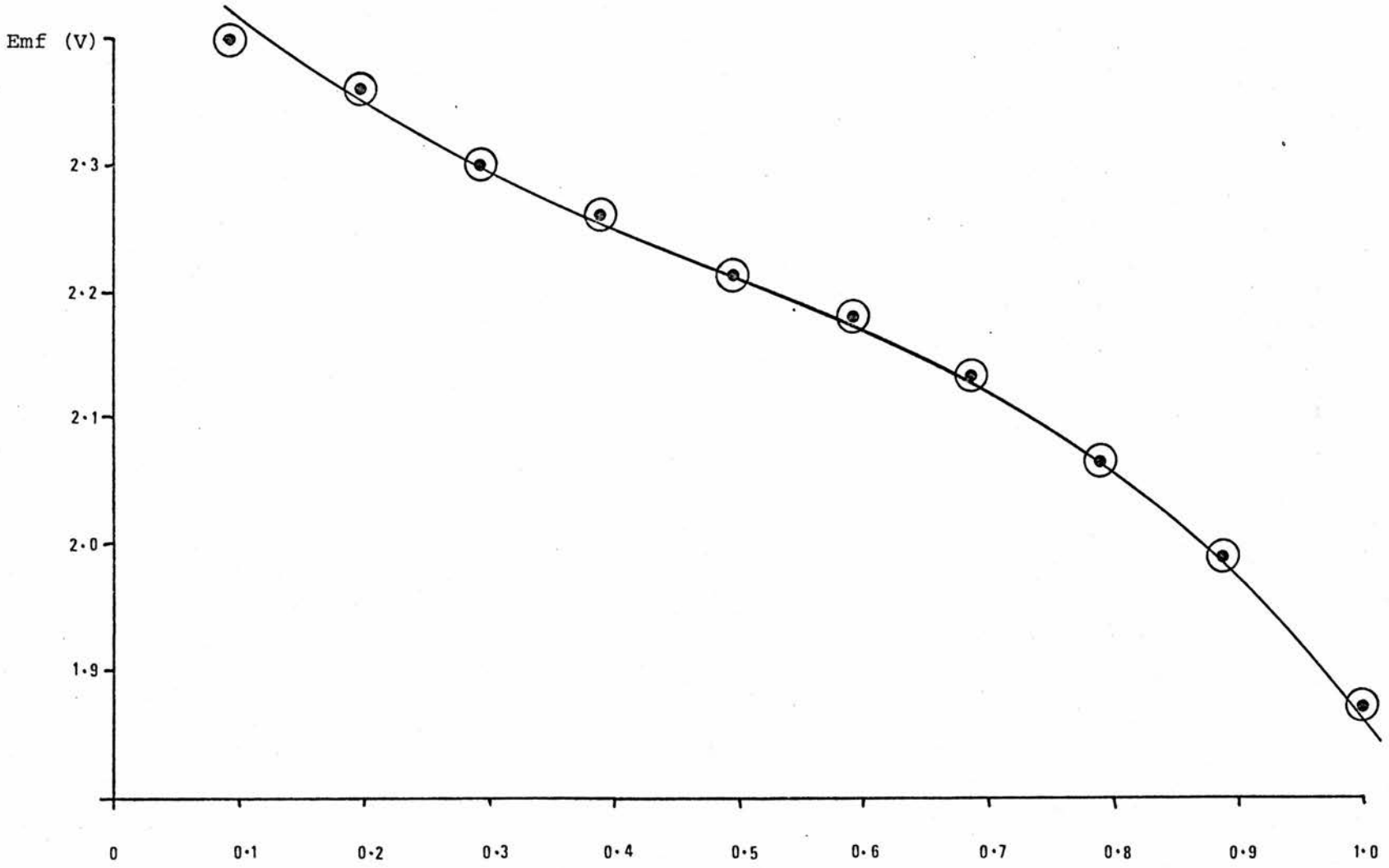

FIGURE 3 : $Li_x TiS_2$ (O x 1.O), Open Circuit Potential Versus Li reference

4.4 Capacity of the Electrode Material; Phase Changes

The number of moles of guest species a mole of electrode material may accomodate is the feature which determines the capacity of an electrode. In practical systems however, there are several reasons why electrode materials may not be used to full capacity. In some cases the cell voltage falls below a useful minimum, (determined by specific applications in the device market) at higher electrode guest concentrations. In general, at compositions approaching the high concentration limit of the electrode material, the cell potential change with increasing concentration becomes much more rapid. Practical cells are unlikely to be used at maximum capacity because of this feature of the electrode performance.

Several examples of electrode materials with working ranges limited by phase changes have been reported. Prior to the occurrence of a phase change the cell potential versus composition profile may show a constant potential region, indicating the simultaneous existence of two phases, in accordance with Gibb's rule. While a region of constant potential in a cell discharge curve may be an attractive feature in certain reference potential applications, the change in rate of cell potential change with concentration in the new phase, which may be very much more rapid, may effectively limit the working range of the cell. Problems may also arise in the cell related to volume changes in the electrode material which makes operation of the cell through a phase change impractical. Thompson et al [6] reported a two phase region extending from approximately $x = 0.1$ to $x = 0.9$ in the primary discharge of the Li_xVSe_2 system. This particular system did not show very promising cycling characteristics but nevertheless draws attention to the possible use of materials showing extended two phase behaviour in voltage reference applications.

Cells of the type shown in Figure 1 have also been used as a sensitive means of detection of phase limits. A suitable illustration of voltage composition profiles used in this way is given for the analogous situation in an alloy, (Figure 4 [7]), by data from the "Li Al" system.

Regions of multiphase behaviour are not always so easily assigned, as shown by consideration of data presented in Figure 5.

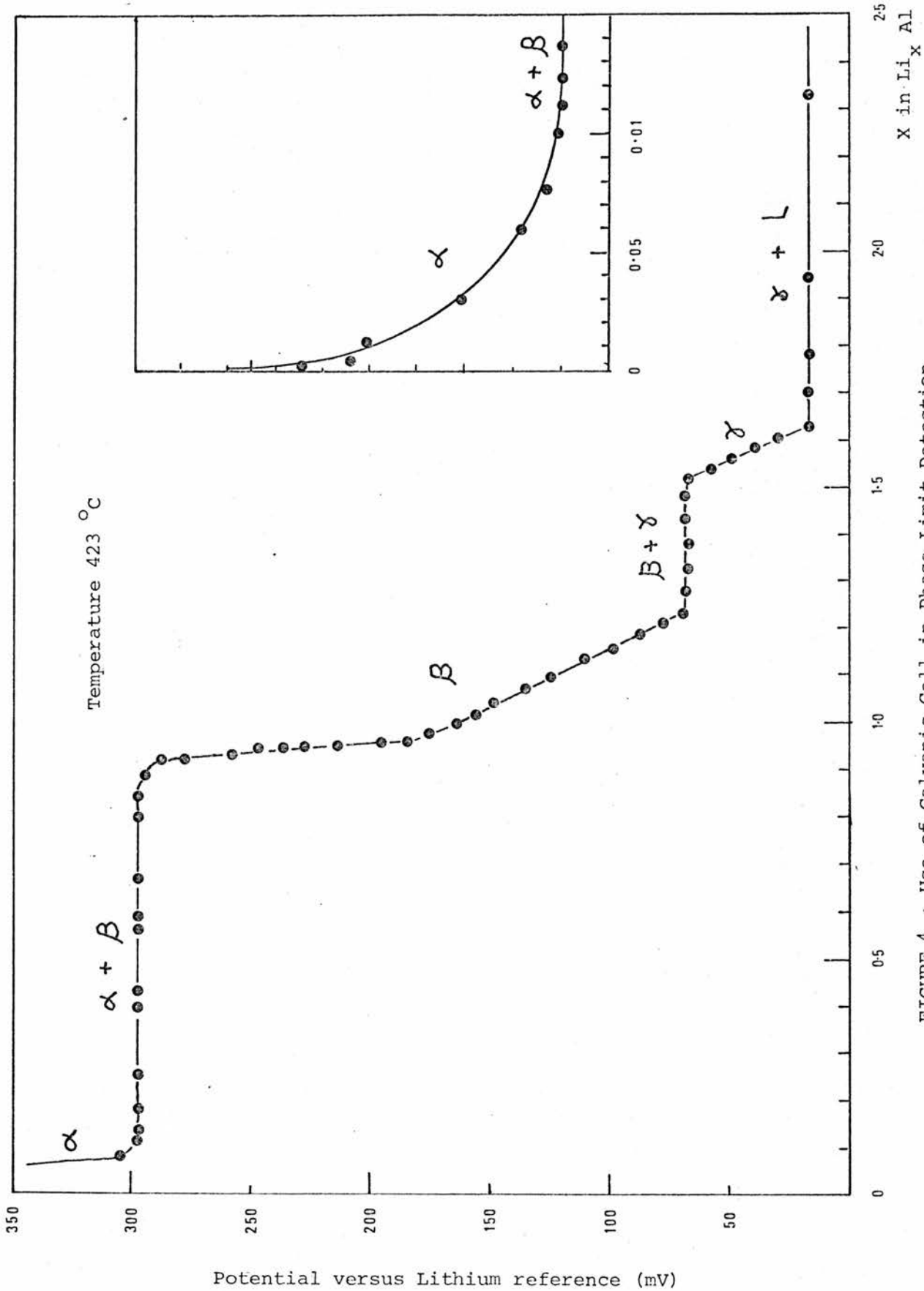

FIGURE 4 : Use of Galvanic Cell in Phase Limit Detection

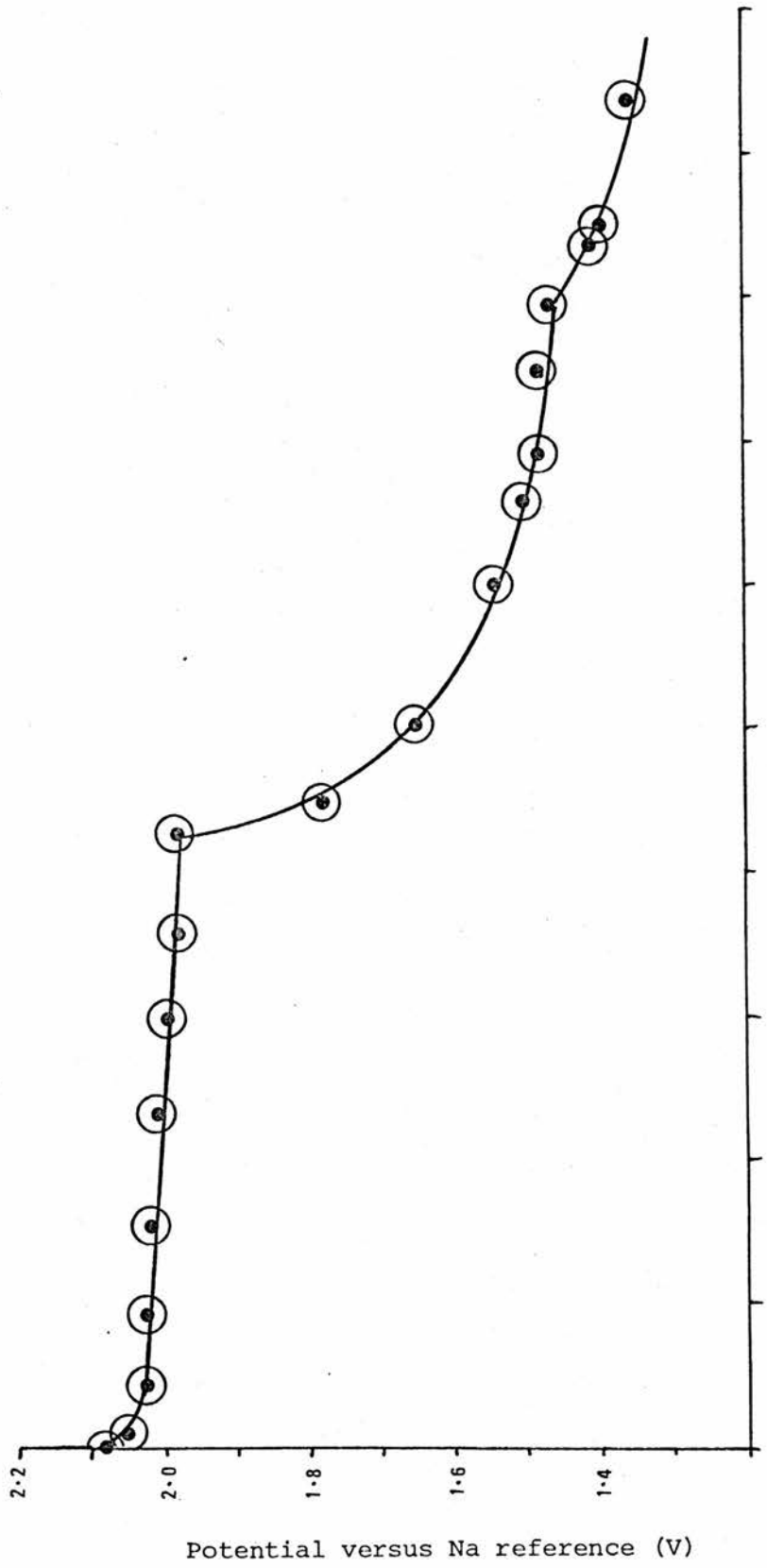

FIGURE 5 : Potential versus Composition, Na TiS_2

This shows the voltage composition profile of the $Na_x TiS_2$ system[8], in which the constant voltage regions are very short. X-ray analysis has shown the presence of second stage, trigonal prismatic and trigonal antiprismatic phases with long two-phase regions that are not confirmed by the voltage versus composition data. Whittingham[4] has suggested that a possible reason for indistinct definition of two-phase regions in layered dichalcogenide systems of this type, is that during the intercalation reaction, where layers of the dichalcogenide host may have to move relative to each other, substantial disorder will occur in the stacking of layers in the electrode material. Under these conditions the phase changes and regions of multiphase behaviour may be partially masked.

4.5 Cyclability of the Electrode Reaction

Where the electrode material, or cell construction, is expensive a cell may nevertheless attain commercial viability if used in a rechargeable configuration.

Several reports are available illustrating the success of TCh_2 compounds as reversible electrodes. TiS_2 in particular has been extensively investigated by several groups[4,9] and found to be capable of undergoing several hundred shallow charge/discharge cycles with good retention of electrode capacity.

Figure 6[9], shows a typical charge/discharge cycle for the Li_xTiS_2 system with a liquid organic electrolyte at room temperature. The reversibility of the cell reaction is clearly shown, the displacement in the cycle being due almost solely to resistance losses in the electrolyte, except at extreme values of x, where polarisation becomes important.

Of particular importance in these results is the absence of significant changes in the diffusion coefficient of lithium in the electrode material as a function of the state of charge.

The performance of dichalcogenide electrodes has been reported to be very dependant on the method of preparation. In general the surface area of an electrode material influences the maximum current density a cell may sustain. For TiS_2 it has been shown that for samples of similar particle size, but different methods of preparation, (and hence different stoichiometry) very different electrode characteristics result[10]. For optimum performance, with respect to current density, TiS_2 electrodes must be prepared in close to ideal stoichiometry. Non-stoichiometric materials, where the excess metal species reside in sites within the van der Waal's

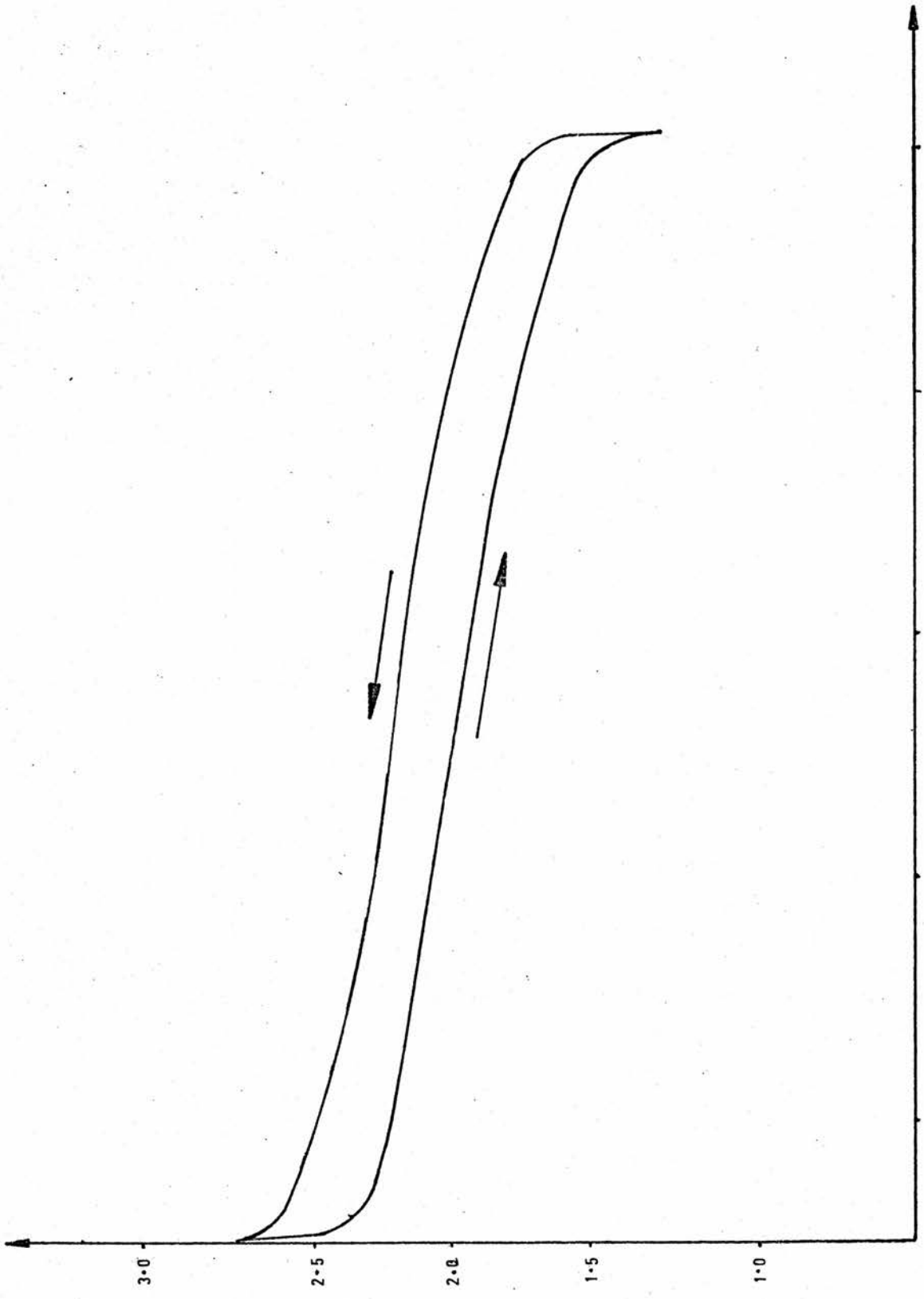

Figure 6: Typical charge/discharge cycle for Li_xTiS_2 (9)

gap in the crystal structure, apparently perform less well as a result of "structure pinning" caused by these metal ions binding to adjacent sulphur layers. The excess host metal species also appear to block the movement of ions diffusing through the electrode material, may cause structure ordered regions in the lattice, and occupy sites which otherwise would have been available to the guest species. (thereby reducing the total capacity of the host)

The importance of electrode material preparation is further emphasised by the issue of patents [10] covering this aspect of cell construction.

4.6 Electronic Conductivity of Electrode Materials

The range of values of electronic conductivity of electrode materials in use in commercial cells suggests that this parameter is not of primary importance. The performance of an electrode deficient in this respect may be improved by the admixture of conducting diluents, with however, an unavoidable reduction in energy density of the cell.

TCh_2 materials have a considerable advantage in this respect over many alternative compounds, as in general their electronic conductivity is high (Table 1), and not significantly dependant on guest concentration. (as is the case with certain metal oxide materials [11]).

4.7 Results and Discussion

Electrode Materials with Silver Guest Species

Figures 7, 8 and 9 show the coulometric titration data obtained for silver guest species with transition metal dichalcogenide systems.

As may be seen from a comparison with earlier figures, the energy density for the cells using silver guest species is very much less than that for lithium and sodium intercalation electrodes. This may not be a severe disadvantage as the voltage requirements of the electronic device market vary over a large range. In some cases multiple cell stacks may be preferred over single and double cells. An example of matching of cell performance to application may be found in the maintenance of calculator memory during power outage. In this instance the necessity for maintenance of a 5 volt level for most of the battery capacity results in a double cell of lower voltage being selected, in preference to a single cell with a greater energy density. The advantage gained in this case was related to a flatter potential versus discharge curve.

Table 1: Electronic Conductivity of TCh_2 Electrode Materials

Compound	Conductivity ($S.cm^{-1}$)
TaS_2	6.04
TiS_2	22.41
$TiS_{1.80}$	17.31
NbS_2	29.94
$Ag_{0.125}TiS_2$	12.09
$Ag_{0.3}TiS_2$	20.27
$Ag_{0.35}TiS_2$	18.73

Table 2: ΔS, and ΔH Values for TCh_2 Electrode Materials

NbS_2 [1] : 25.0°C

X	E (V)	$\frac{dE}{dT}$ $mV.K^{-1}$	ΔS $J.Kmol^{-1}$	$-\Delta H$ $kJ.mol^{-1}$	$-\Delta G$ $kJ.mol^{-1}$
0.00001	.40088	.048	4.63	37.30	38.68
0.0001	.40085	.045	4.34	37.38	38.67
0.001	.39973	.173	16.69	33.59	38.57
0.01	.39183	.118	11.38	34.42	37.81
0.03	.38439	.290	27.98	28.75	37.09
0.05	.37445	.377	36.37	25.29	36.13
0.07	.36384	.406	39.17	23.42	35.10
0.09	.35679	.322	31.07	25.16	34.42
0.11	.35020	——	——	——	33.79
0.13	.32547	.066	6.37	29.50	31.40
0.15	.30992	.059	5.69	28.20	29.90
0.18	.27242	.039	3.76	25.16	26.28
0.20	.25463	.028	2.70	23.76	24.57

NbS_2 [2] : 25°C

x	E(V)	dE/dT mV.K^{-1}	ΔS J.Kmol^{-1}	-ΔH kJ.mol^{-1}	-ΔG kJ.mol^{-1}
0.001	.24125	0.051	4.92	21.81	23.28
0.0066	.22829	0.085	8.20	19.58	22.03
0.01	.21594	0.102	9.84	17.89	20.83
0.0205	.20035	0.144	13.89	15.19	19.33
0.03	.19797	0.086	8.29	16.63	19.10
0.04	.19155	0.117	11.29	15.11	18.48
0.06	.18706	0.117	11.29	14.68	18.05
0.09	.18032	0.112	10.81	14.17	17.39
0.12	.17385	0.117	11.29	13.40	16.77
0.143	.16854	0.123	11.87	12.72	16.26
0.175	.15621	0.121	11.67	11.59	15.07
0.206	.14150	0.097	9.36	10.86	13.65

TaS_2 : 70°C

x	E (V)	dE/dT mV.K^{-1}	ΔS J.Kmol^{-1}	-ΔH kJ.mol^{-1}	-ΔG kJ.mol^{-1}
0.001	0.20406	0.136	13.12	15.78	19.69
0.0048	0.20291	0.140	13.51	15.55	19.58
0.0095	0.20125	0.134	12.93	15.56	19.48
0.020	0.19780	0.132	12.74	15.28	19.08
0.035	0.18963	0.108	10.42	15.18	18.29
0.075	0.16086	0.046	4.44	14.19	15.52

$TiS_{1.8}$: 70°C

x	E (V)	dE/dT $mV.K^{-1}$	ΔS $J.Kmol^{-1}$	$-\Delta H$ $kJ.mol^{-1}$	$-\Delta G$ $kJ.mol^{-1}$
0.00001	0.19230	0.326	31.45	9.17	18.55
0.0001	0.18255	0.327	31.55	8.20	17.61
0.0002	0.18040	0.311	30.00	8.46	17.41
0.0004	0.17785	0.277	26.73	9.19	17.16
0.0008	0.17204	0.303	29.23	7.87	16.59
0.0016	0.16695	0.310	29.91	7.19	16.11
0.0032	0.16072	0.232	22.38	8.84	15.51
0.0064	0.14128	0.256	24.70	6.26	13.63
0.0096	0.12032	0.320	30.87	2.41	11.61

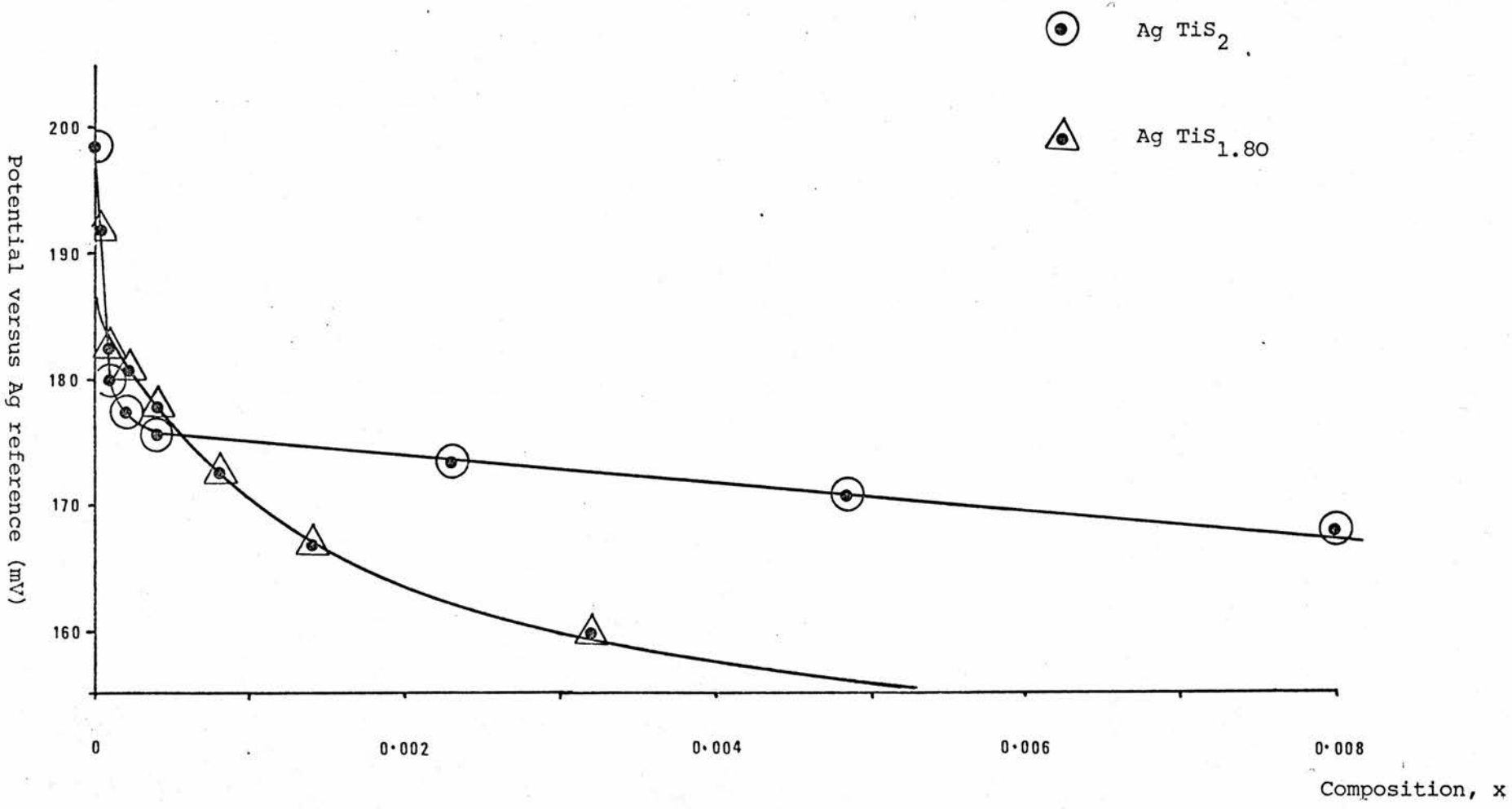

FIGURE 7 : Potential versus Composition Parameter for $Ag_x TiS_2$ and $Ag_x TiS_{1.80}$

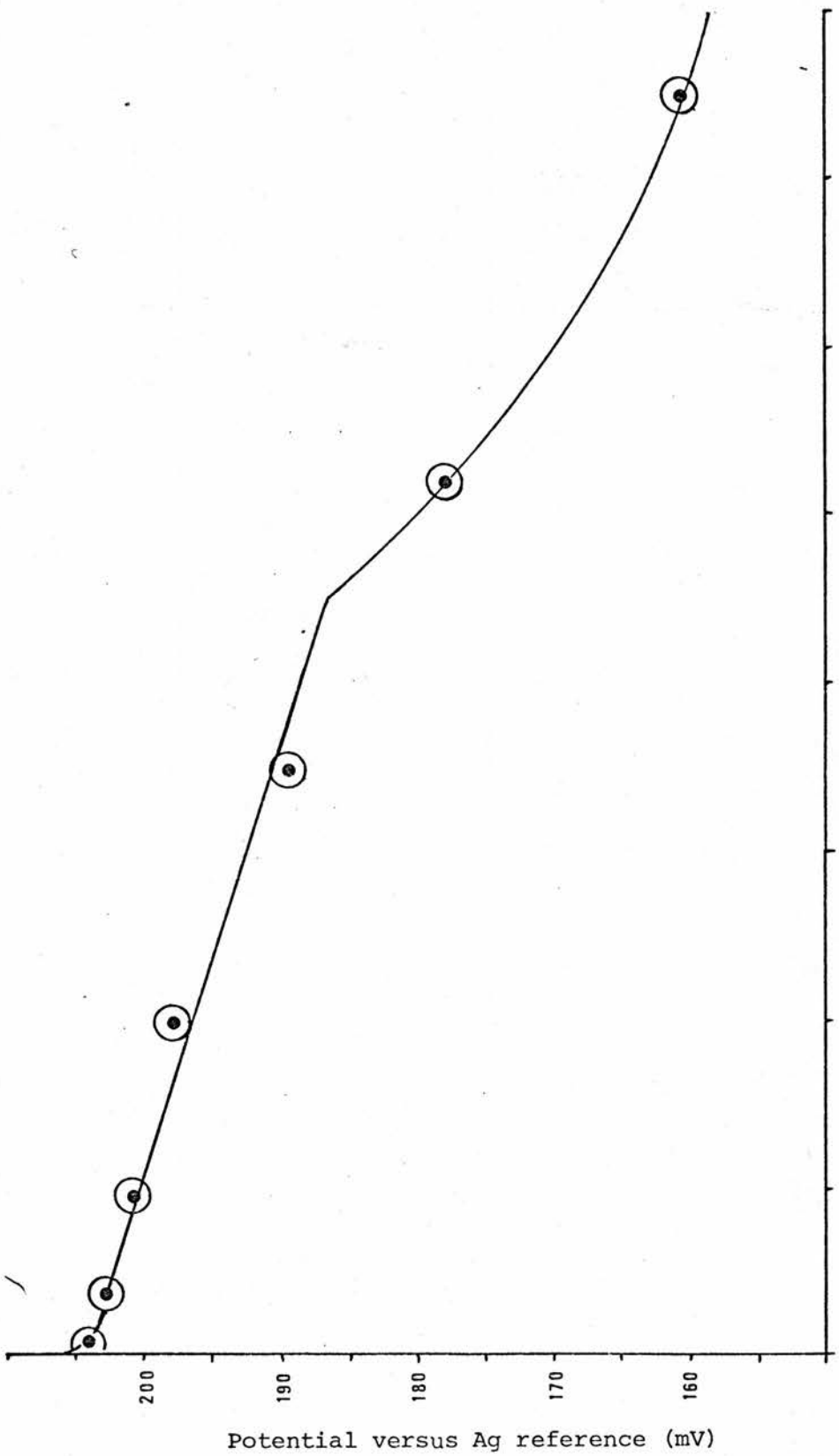

FIGURE 8 : Potential versus Composition Parameter for $Ag_x TaS_2$

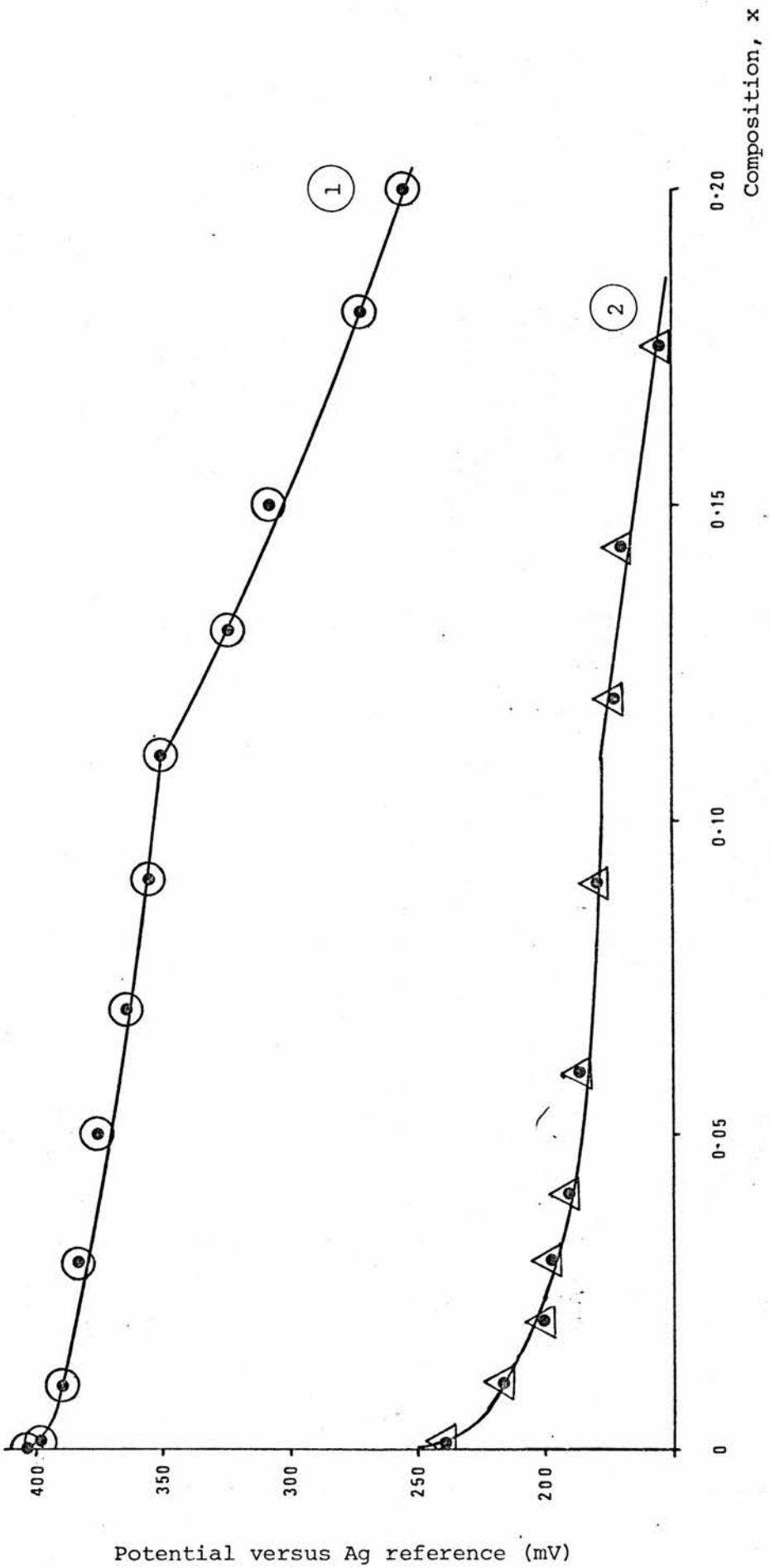

FIGURE 9 : Potential versus Composition Parameter for $Ag_x Nb_{1+y}S_2$, Samples (1) and (2)

An interesting feature of the potential composition profile shown in Figure 7 is the initial rapid decline in potential as a result of intercalation of very small amounts of guest species. In all the cells studied this drop became less severe at higher compositions and adopted an almost linear relationship with composition. These results are similar in trend to those for the Li_xTiS_2 system (Figure 3) but very different from those reported for Li_xVSe_2.[12] A quantitative explanation of the wide variety of voltage composition relationships has been attempted by Armand[13].

Armand discusses the intercalation reaction as a dissolution of M, the guest species, (as M^+ and e^-) in the solvent, host structure. The compounds obtained are classified as

(a) Perfect Non-Stoichiometric Compounds in which x can vary continuously from zero to a maximum value imposed by the host,

(b) Pseudo Two Phase Compounds in which the M_xTCh_2 compounds have narrow non-stoichiometric domains and

(c) Two Phase Compounds in which the intercalation compound initially formed is unstable and disproportionates into two other phases.

In the present study only the first two of these groups are of interest.

The thermodynamics of the intercalation electrode systems are modelled by Fermi-Dirac statistics and are discussed in terms of site occupancy. Armand considers only the case in which the host lattice retains its integrity, fixing the number of available sites for guest species. The basic model he describes considers entropy terms with the incorporation of an energy term which is a linear function of the electrode composition. The magnitude of the energy term is determined by the strength of the guest-guest interactions in the host lattice. If the interactions are weak then the cell potential is a continuous, decreasing function of x, as for example in the Li_xTiS_2 system. (see Figure 3) If however, the interactions are strong, the function has a maximum and minimum as shown in Figure 10. Under these circumstances, according to Armand, the structure will disproportionate, for all x below the maximum, to concentrated and dilute phases. Thus, a two phase, flat region will appear in the potential versus composition profile of the electrode material. An explanation of this kind may account for the extended two phase region in the Li_xVSe_2 discharge curve.

Armand defines pseudo two phase compounds as those in which several regions exist in which the potential versus composition profile is similar to that of a single phase, perfectly non-stoichiometric compound. These

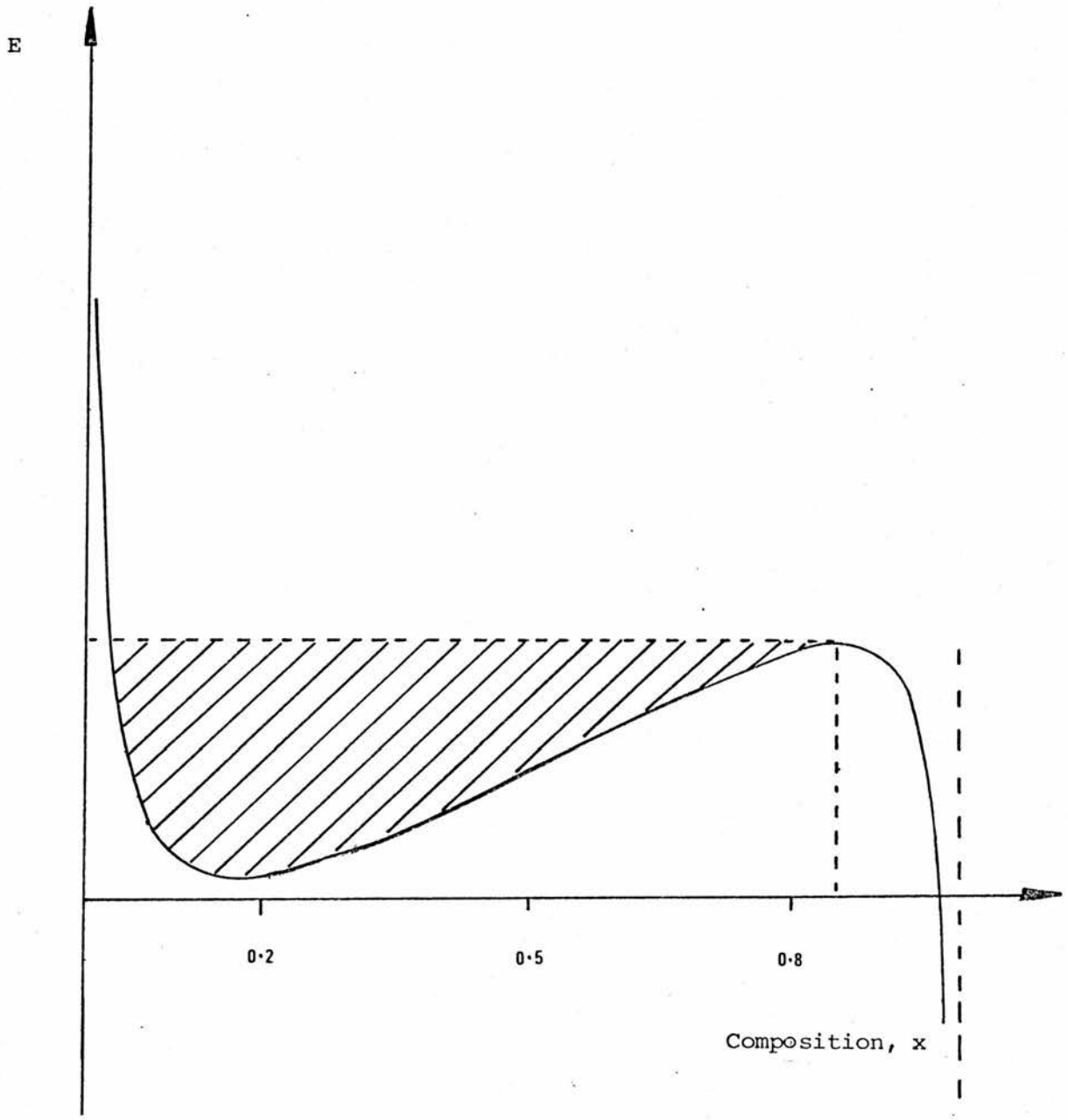

FIGURE 10 : Potential versus Composition Parameter for strong guest-guest Interaction

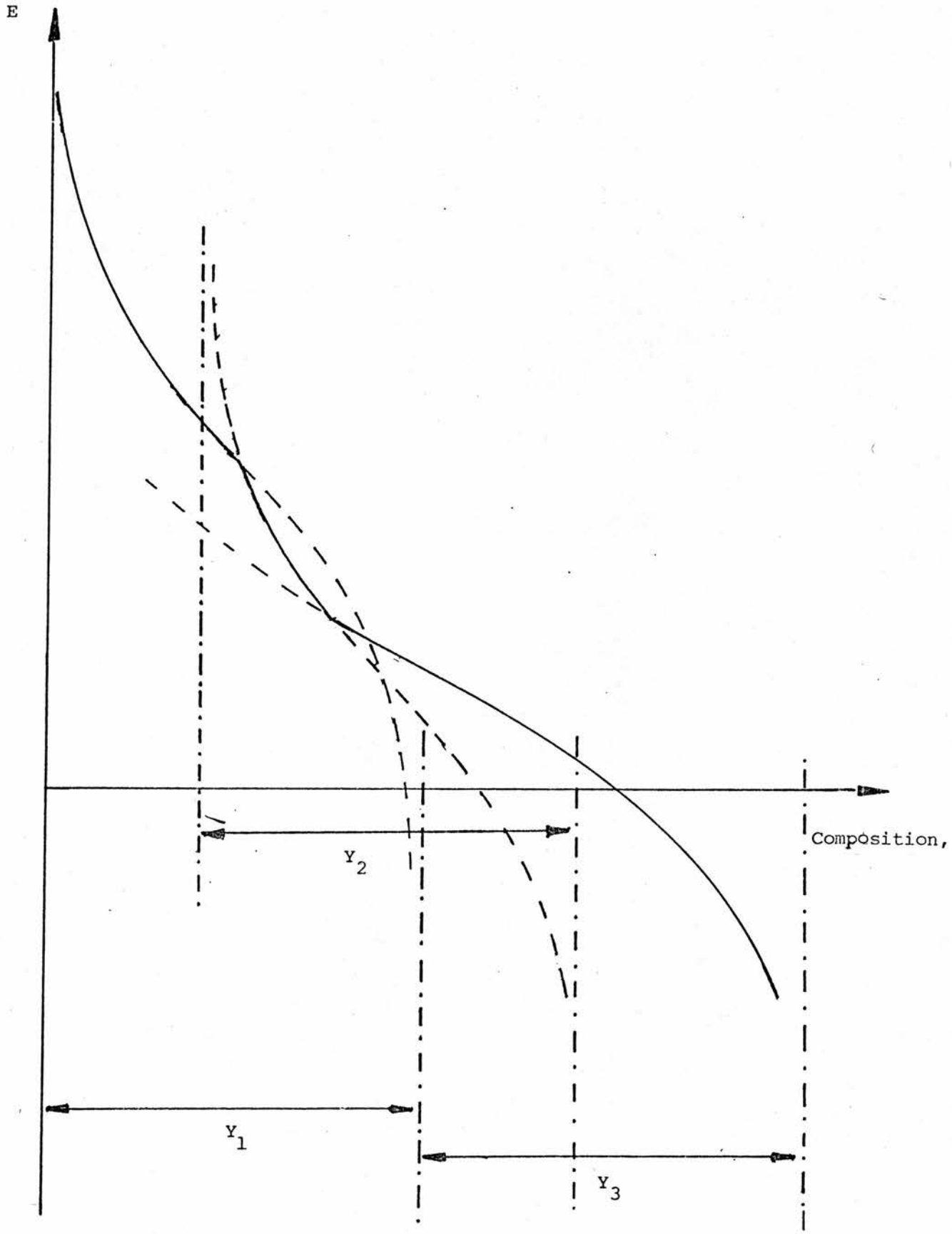

FIGURE 11 : Adjacent domains; Shape of the Potential versus Composition Parameter

phases are filled successively, depending on the site energies within the lattice structure of the phases, and may have different interaction terms giving rise to different forms of potential composition dependance. When the global site occupancy reaches a certain value, the structure disproportionates to form the new lattice structure in which the interactions for the guest composition are less. This type of approach gives a qualitative explanation of the potential versus composition behaviour reported for the Na_xTiS_2 system, (Figure 5), in which three pseudo single phase domains appear to exist. Figure 11 shows this situation with the overlap regions of the pseudo-phases extended to illustrate more clearly the domain structure of the potential composition behaviour. If the overlap is less between phases y_1, y_2 and y_3, then the two-phase regions would be correspondingly less extensive and the behaviour shown in Figure 5 for the Na_xTiS_2 system might be expected.

Comparison of Figures 8 and 9 with Figure 11 leads to the suggestion that phase changes in the Ag_xTaS_2 and $Ag_xNb_{1+y}S_2$ systems may occur at approximately x = 0.04 and 0.11 respectively. In both these systems the rate of change in potential with composition change is very slight, and assignment of phase limits without x-ray confirmation is difficult.

If equations [3] and [4] are used with the temperature coefficients of cell potential, then a list of ΔS and ΔH values may be produced, as a function of x, for each of the electrode systems investigated. These results are included in Table 2. A consideration of these results demonstrates that in general the ΔH_f for the intercalation process is large and negative while the ΔS is small and positive.

Information from magnetic susceptibility and NMR studies suggests that the 2s electron association with lithium in Li_xTiS_2 is donated almost completely to the TiS_2 lattice in the form of essentially free electrons,[4] consistent with a salt-like model, $Li_x(TiS_2)^{x-}$. Data from cell potential versus composition measurements (Figure 3), indicates that the energies of formation of Li_xTiS_2 materials are fairly high, and the activity of lithium in the material low. Similarity between data for other alkali metal, transition metal, and post-transition metal guest species and the Li_xTiS_2 system leads to a general assumption of high ionic character of the guest species in the TCh_2 lattice.

The continuous decrease in the cell open circuit potential with x is expected for a single phase system and, in view of the low entropy associated with reactions between solids, is largely due to the enthalpy change of the reaction. Increased electrostatic repulsion between the

positively charged species in the host as the interlayer sites become filled, partially accounts for an observed decrease in ΔH with increasing x. As the concentration of guest increases the conduction band is filled and the energy of the Fermi level is increased resulting in a larger expenditure of energy being required for the promotion of the electrons associated with the incoming guest species.

An alternative theory is based on the suggestion that a variety of sites, with different site energies, exist in the electrode material. Under these circumstances the incoming guest species, at low values of x, would be expected to occupy the low energy sites. As the guest concentration increases only the higher energy sites are available, with the result that the enthalpy of the intercalation process decreases with increasing x. The justification for the initial assumption of a range of site energies comes from crystallographic evidence and a consideration of the faults within the crystal structure. While reasoning along these lines may explain slight changes in the enthalpy of the reaction it seems unlikely that this theory alone can explain the range of enthalpy values reported and more probable that a combination of several factors leads to the observed trend.

As shown in Table 2, ΔS for the intercalation reaction was small for the materials investigated. Few attempts have been made to quantify the entropy of the intercalation process, however the temperature coefficient of cell potential of the Li_xTiS_2 system was reported to be small.[4]

Steele et al,[14] investigating the $Cu_xMo_6S_8$ system, reported that the entropy varied significantly with x. In this system the range of composition, $0 \leqslant x \leqslant 3.5$, was studied and the entropy was found to be positive at low x and negative at higher concentrations of guest species. This behaviour may be explained simply, in terms of a consideration of the number of available sites for the incoming guest species at low x, as compared to the site availability at high x. As the sites are filled the electrostatic interactions between the guest species cause ordering in the lattice with a negative entropy of formation.

In the investigations carried out on the $TiS_{1.80}$, NbS_2 and TaS_2 systems the range of x studied was very much less. However, in some of these systems the potential versus composition profile obtained suggested the possible occurence of a phase change. The entropy change associated with the intercalation of species into a dilute phase was not as expected. In general the trend of ΔS variation within phases would be predicted to be decreasing with increasing x. The absence of these trends

in the results suggests that theories based on naive site filling models are too simple, and that more accurate description of entropy changes with increasing lattice site occupation must await more detailed structural information.

Table 3 is included to report results of values of ΔG_I, as calculated using equation [2]. These are, as expected, considerably lower than those obtained for the corresponding molar ratio, value of x, in the Li_xTiS_2 system, included for comparison. This method of presentation of the results offers a convenient means of comparison of the systems and quantifies the advantage of the $Ag_xNb_{1+y}S_2$ materials over the others investigated from an energy availability viewpoint.

Cell potential versus composition data may also be used to obtain information about the variation of activity of the guest species in the host at different guest concentrations. Equation [1] relates these parameters. Comparison of Figure 12 which shows the

(a) activity versus concentration, and

(b) potential versus concentration behaviour of an ideal solid solution

with that of the electrode systems investigated, in Figure 13 (a), (b), (c), (d) and (e), illustrates the marked deviation of some of these compounds from ideal behaviour. The variation of a_o with x_o in Figure 12 was obtained by assuming that over the range of concentration plotted, the activity and concentration of guest species in the electrode material were identical. Comparison of the potential versus composition profile obtained for this system with those of the two $Nb_{1+y}S_2$ systems investigated illustrates the shape differences between ideal and experimental systems. More significant is the displacement of one of the $Nb_{1+y}S_2$ curves from the ideal value. In the case of silver guest species this is less severe than for lithium species, as reported by other workers. The reason for this displacement is the strength of the guest-host interaction. The stronger this interaction, the lower the activity of the guest species in the host and the higher the cell voltage with respect to a reference electrode of the guest metal.

Data presented in Figure 7 shows the difference in values of voltage for cells using stoichiometric and non-stoichiometric titanium disulphide hosts. In view of the results obtained by Thompson, [6] in a comparison of voltages of cells using these electrode materials with lithium guest species, a difference in potential versus composition profile was expected. In both cases, for lithium and silver species, the free energy of formation of the compound with the stoichiometric host was higher.

Table 3: $\Delta G_{INTERCALATION}$ of TCh_2 Electrode Materials

System	Mole Fraction, X	Temp (^{o}C)	$-\Delta G$ kJ.mol^{-1}
$Ag_xTiS_{1.80}$	0.01	70	0.15
$Ag_xTiS_{2.0}$	0.01	70	0.16
$Ag_xTaS_{2.0}$	0.01	70	0.20
$Ag_xTaS_{2.0}$	0.08	70	1.4
$Ag_xNbS_{2.0}$ ①	0.08	25	2.9
$Ag_xNbS_{2.0}$ ②	0.08	25	1.7
$Ag_xNbS_{2.0}$ ①	0.20	25	6.6
$Ag_xNbS_{2.0}$ ②	0.20	25	3.6
$Li_xTiS_{2.0}$	0.20	25	46.8
$Li_xTiS_{2.0}$	1.00	25	209.9

FIGURE 12 (a): Activity versus Concentration

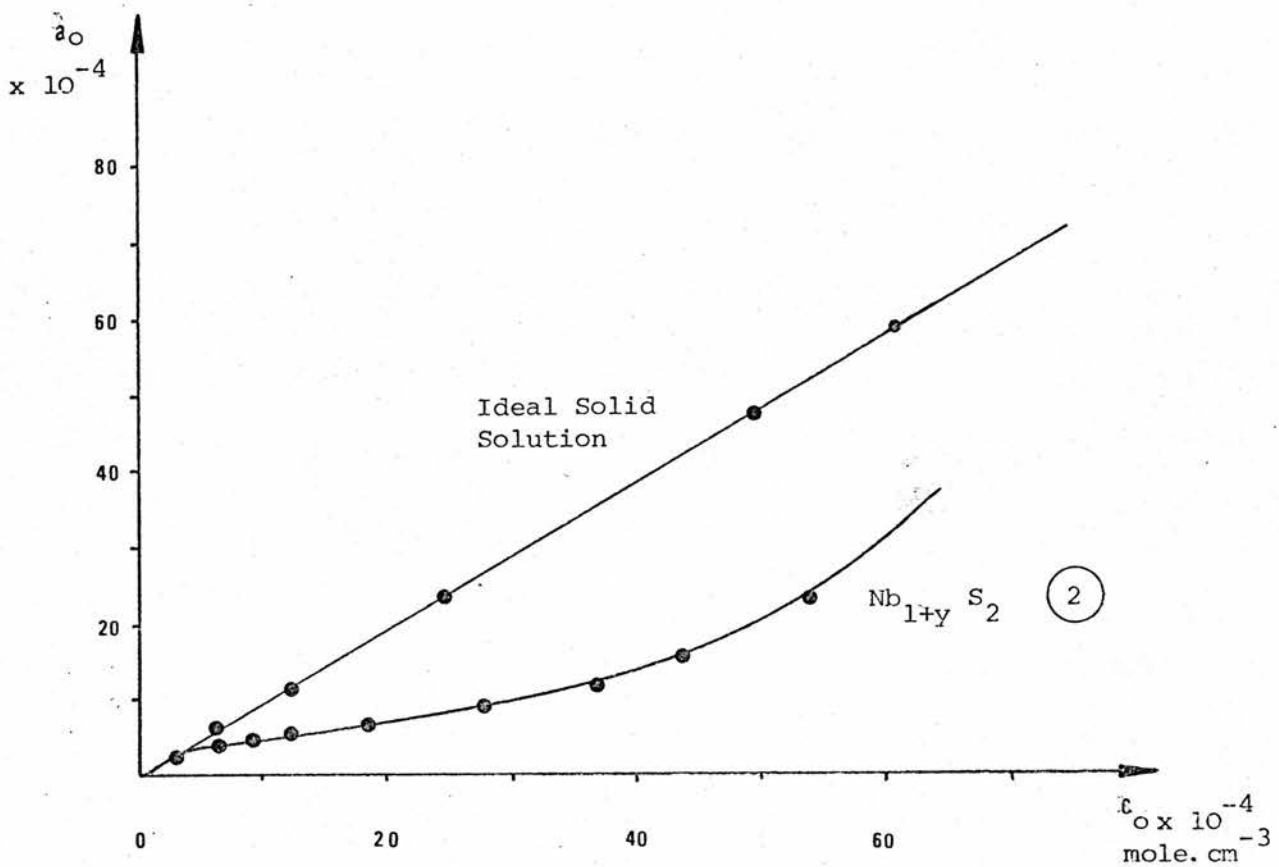

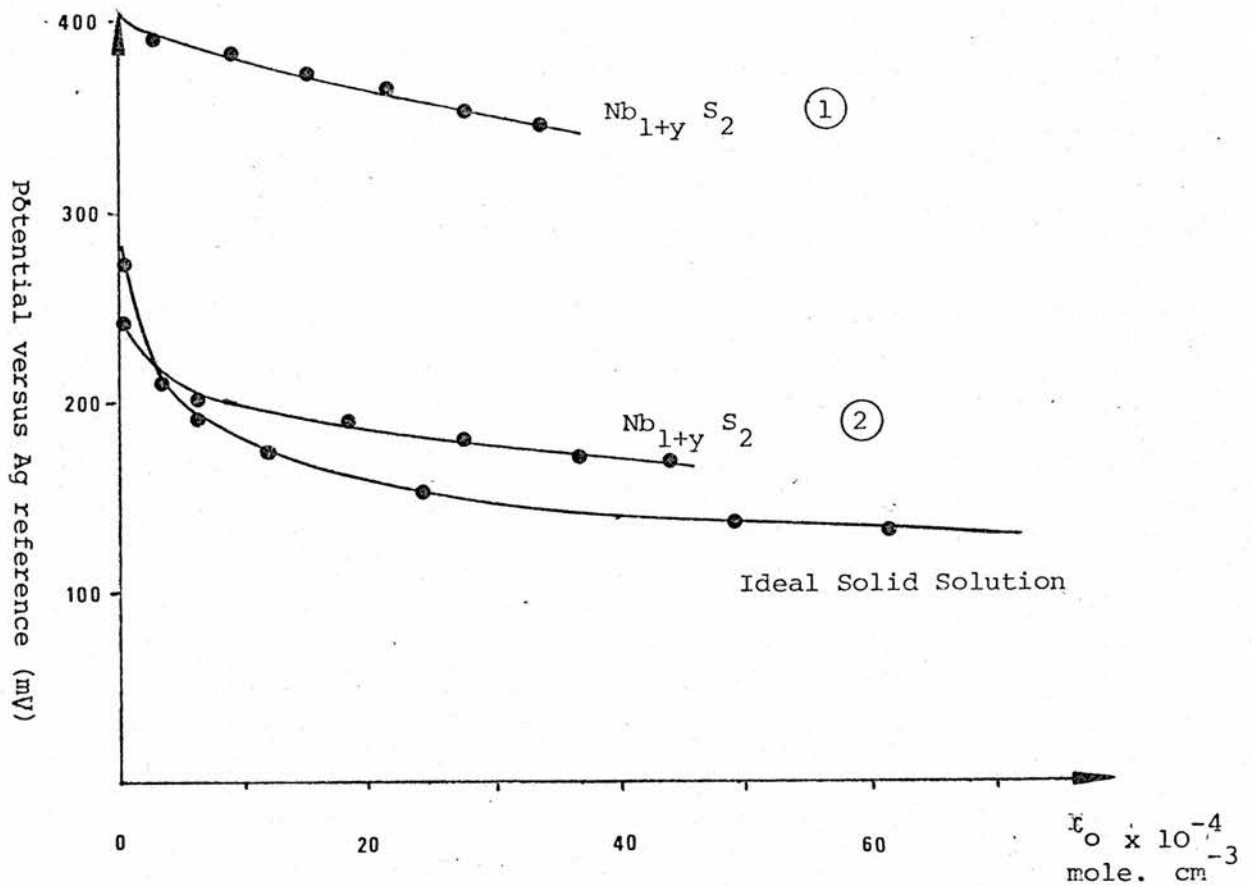

FIGURE 12 (b): Potential versus Concentration

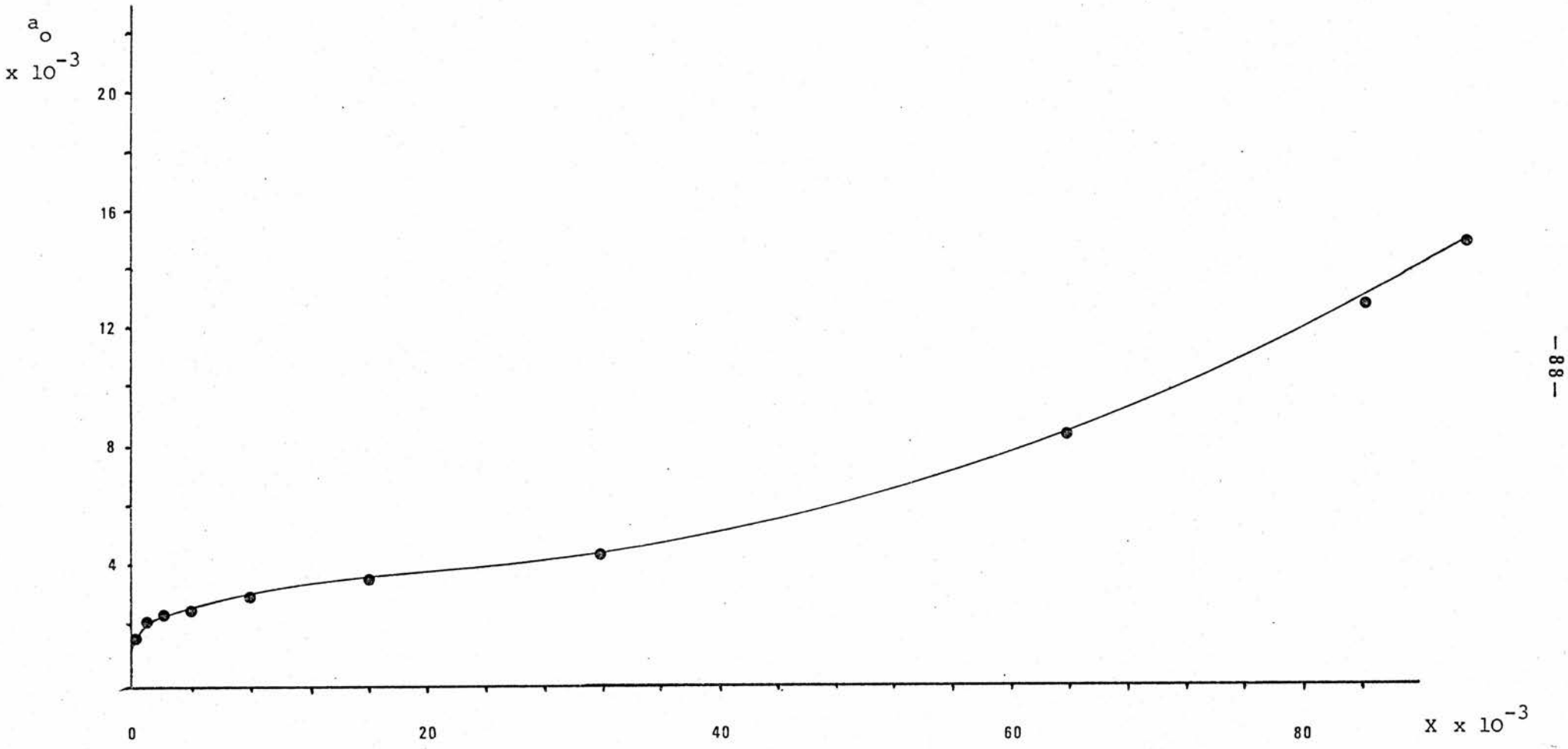

FIGURE 13a: Activity versus Composition Parameter, $Ag_x TiS_{1.80}$

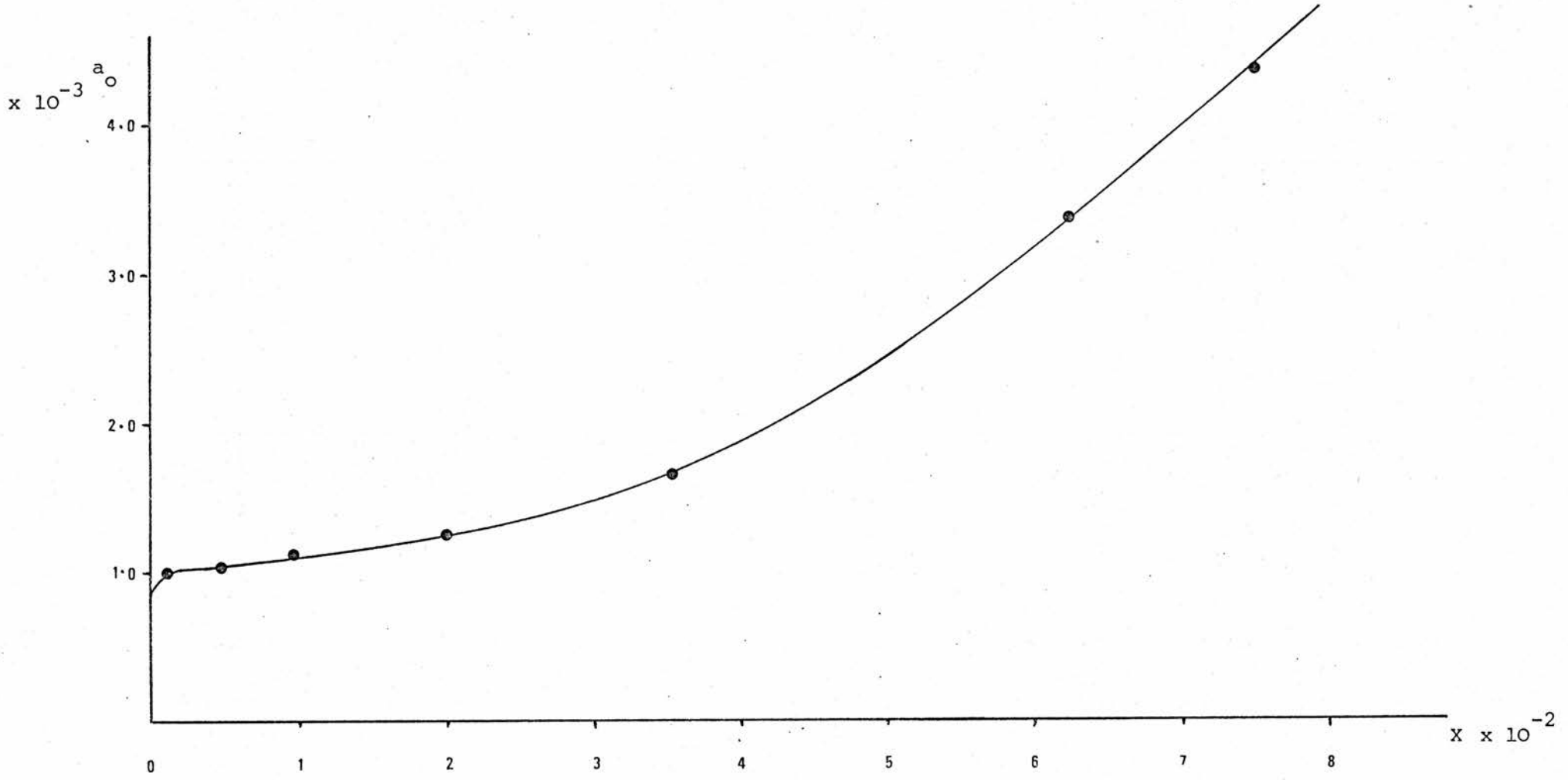

FIGURE 13b : Activity versus Composition Parameter, $Ag_x TaS_2$

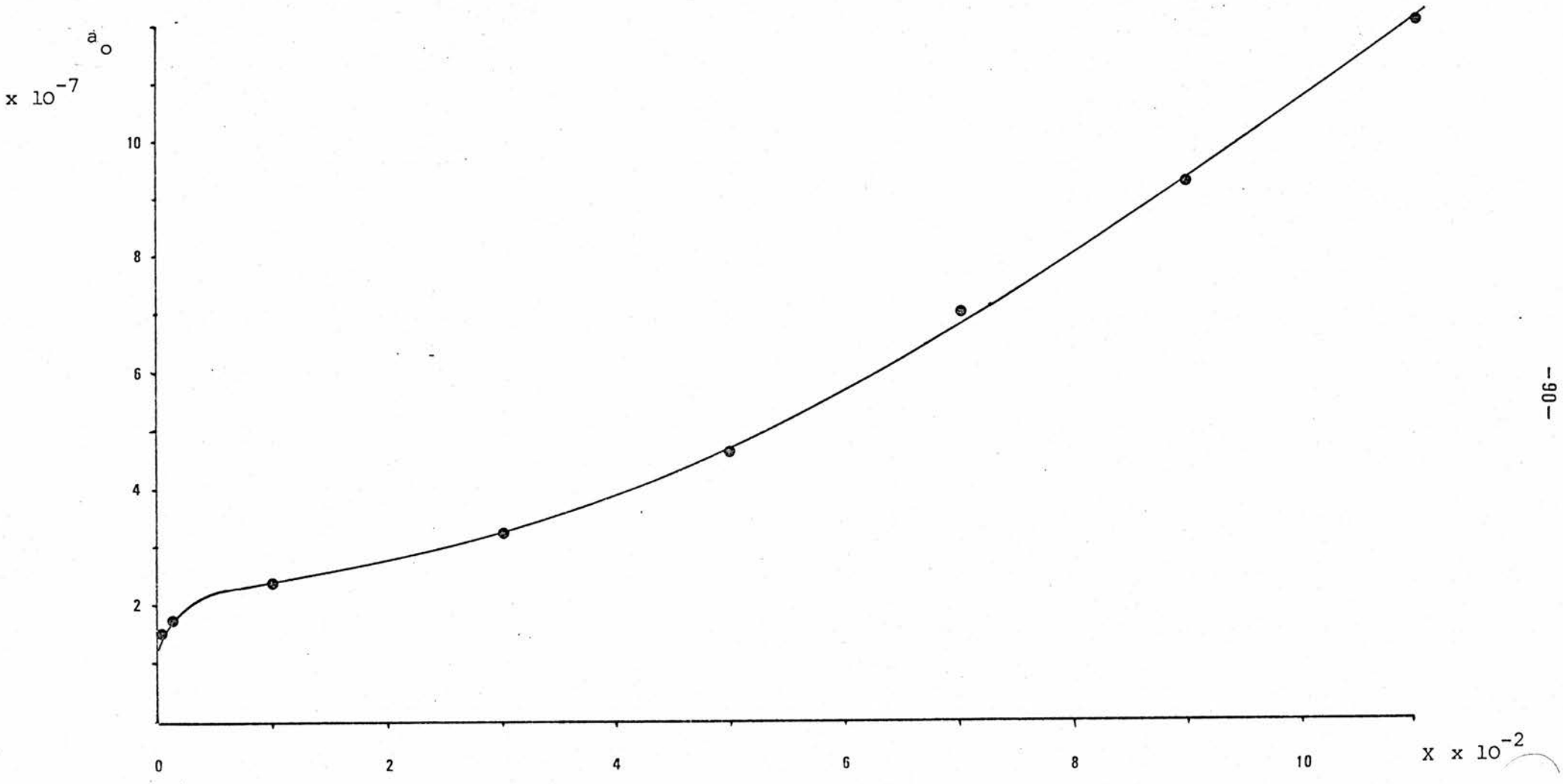

FIGURE 13c: Activity versys Composition Parameter, $Ag_x Nb_{1+y} S_2$ (1)

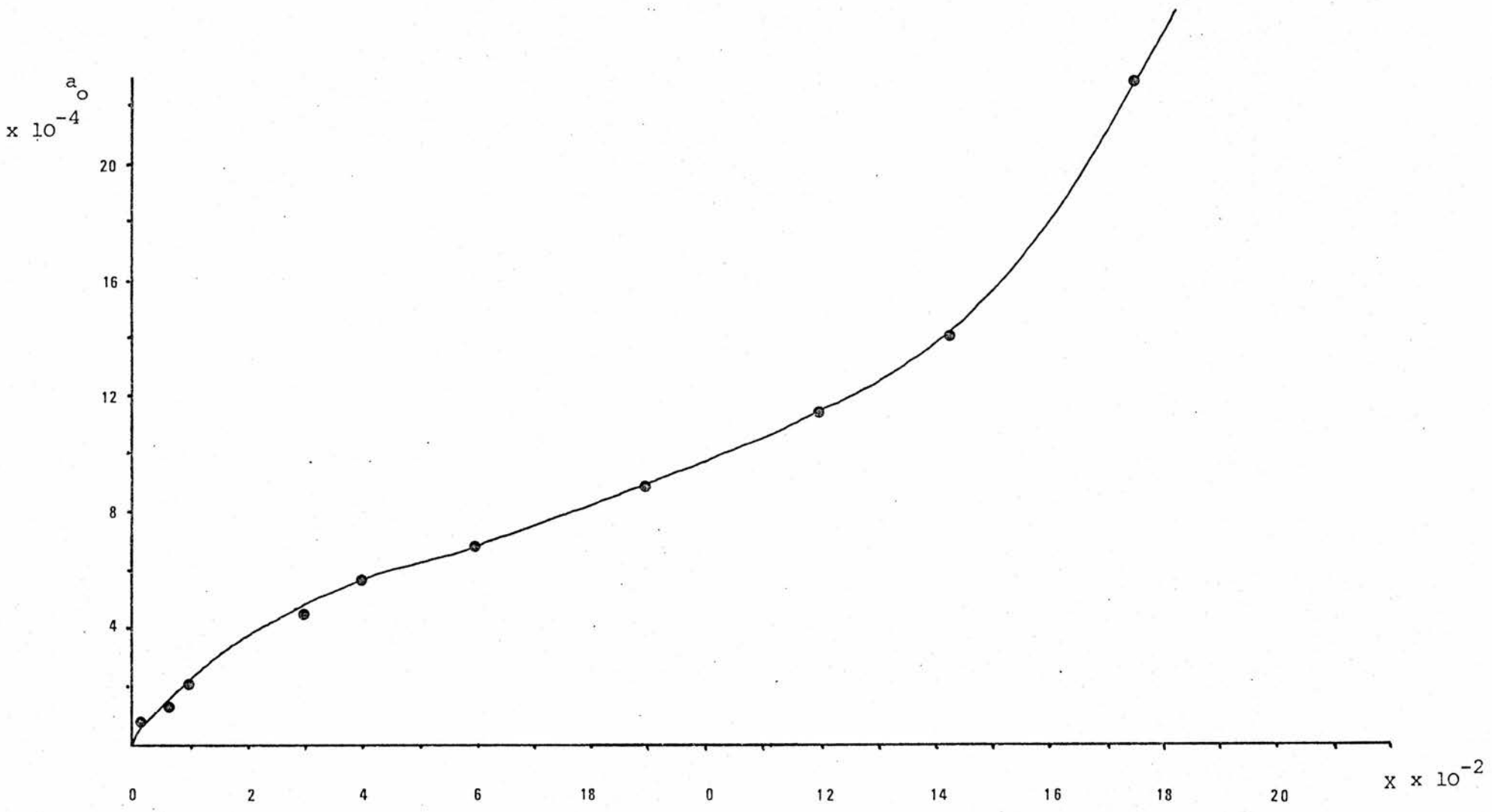

FIGURE 13d: Activity versus Composition Parameter, $Ag_x Nb_{1+y} S_2$ (2)

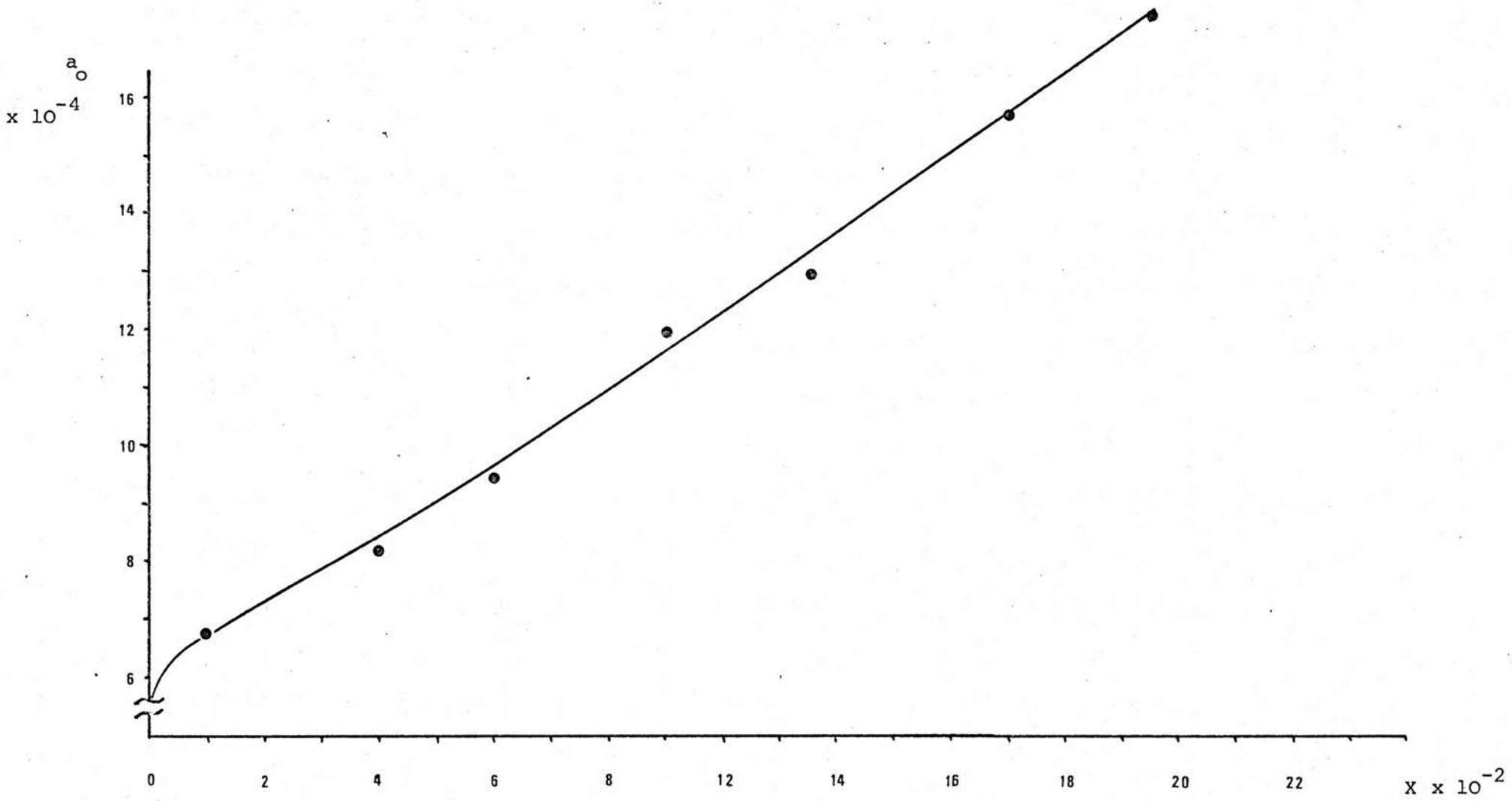

FIGURE13e : Activity versus Composition Parameter, $Ag_x Nb_{1+y}S_2$ (B. Scrosati)[22]

In the case of silver guest species, the decrease in potential with increase in concentration for the stoichiometric host was sufficiently low to suggest the possibility of a two phase region being present.

Various structural investigations of the Ag_xTiS_2 system have been reported. Scholz and Frindt[15] have examined the x-ray diffraction data of thermally prepared samples of Ag_xTiS_2 over a range of x. They conclude that phase changes occur in this system at $0.05 \leqslant x \leqslant 0.15$ and between $0.25 \leqslant x \leqslant 0.35$. They report that the structure below $x = 0.05$ is essentially the same as that of pure TiS_2, with a lattice expansion due to an increase in the van der Waal's gap. This small lattice expansion is reported to be the same as for $Ti_{1+x}S_2$ with $x \leqslant 0.05$.

The data obtained by Lazzari et al[16], Figure 14, confirms the presence of two, two phase regions in the potential versus composition behaviour of both thermally electrochemically prepared materials in the composition range $0.05 \leqslant x \leqslant 0.4$. These results place the phase changes at approximately the same composition ranges as reported by Scholz and Frindt. According to Scholz and Frindt the phases correspond to an expansion in the lattice up to approximately $x = 0.05$, a second stage compound until approximately $x = 0.15$ and a first stage complex thereafter.

In view of this structural information, it seems unlikely that the potential composition data obtained in the $0 < x < 0.01$ range indicate the presence of a two phase region. The gradual change of potential with respect to x is similar to that reported for the Ag_xTaS_2 system shown in Figure 8.

Structural investigations of the Ag_xTaS_2 system reported by Scholz and Frindt, indicate that up to $x = 0.05$ the structure simply undergoes a lattice expansion to accomodate the silver guest species. The region $0.08 \leqslant x \leqslant 0.15$ has been identified as a mixture of this phase and a second stage intercalation compound. The guest concentration is further increased the structure changes to a single stage compound, both single and two stage compounds being present in the region $0.33 \leqslant x \leqslant 0.45$.

The potential composition results obtained for the Ag_xTaS_2 system are only available up to $x = 0.075$ with no decisive indication of a second phase, or two phase region shown.

Results of an investigation of potential versus composition behaviour of the $Ag_xNb_{1+y}S_2$ system are reported in Figure 9. Both sets of data refer to samples of $Nb_{1+y}S_2$ which are apparently close to ideal stoichiometry (i.e. $y = 0$). The higher voltage set of data was confirmed by repetition. In neither sample was there a region which could be ascribed to a flat

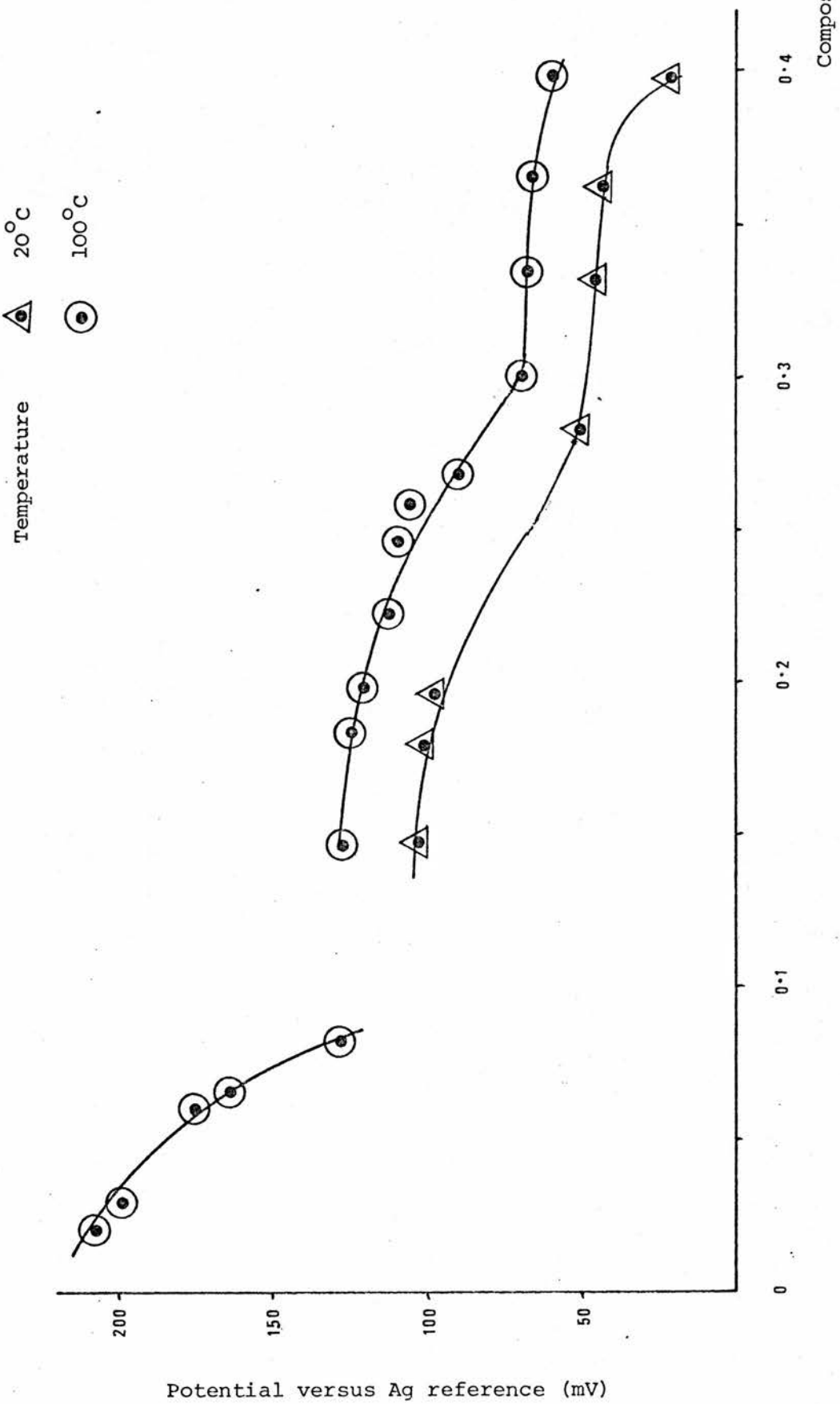

FIGURE 14 : Potential versus Composition Parameter for $Ag_x TiS_2$, Thermally Prepared (6)

voltage region expected to be associated with a phase change, however both samples showed a change in the rate of voltage decrease composition. This may be due to the presence of a phase change with narrow regions of phase overlap, as described by Armand, or due to masking of the two phase regions, as suggested by Whittingham.

An explanation of the differences in the value of potential for materials of the same stoichiometry cannot be derived from a comparison with results reported by Winn et al[8] or Thompson[6], who showed there was a relation between stoichiometry of the host and cell potential. This possibility has been excluded by analysis[17] of the host materials. One of the samples was obtained from laboratories in Milan, the other was synthesised in our laboratory. X-ray analysis showed that the phases present in these two samples were different. The sample from Milan was composed entirely of 2H material, while that prepared in St Andrews was mainly of 3R phase with traces of 2H.

These results lead to the suggestion that the activity of guest species in these two hosts is different as a result of the differences in the intercalate lattice. The implication of this conclusion is that of the electrode materials investigated the most promising from the viewpoint of energy density, is 2H NbS_2.

Electrode Materials with Lithium Guest Species

Measurement of the diffusion coefficients of lithium in transition metal chalcogenides, discussed in Chapter 5, required the development of cell constructional methods using a lithium ion conducting glass, (Chapter 3), and a lithium reference electrode material. In the course of these measurements the voltage composition profile, Figure 15, of a cell with a $Li_{1.05}V_6O_{13}$ reference electrode and $Li_xV_6O_{13}$ ($0 < x < 0.45$) working electrode was recorded. This cell is the lithium analogue of the silver concentration cells studied, with the important difference that the potential of the working electrode was measured not with respect to the pure guest species, but an electrode with a fixed composition of the species. For increasing x the cell may be considered to be under discharge, and during removal of electroactive species, under charge.

Open circuit potentials in the region $0 < x < 0.15$ on the first discharge cycle were found to be increasing with x, a trend opposite to that expected. At x greater than 0.15 the behaviour changed and the potential became a linear decreasing function of x, up to the maximum

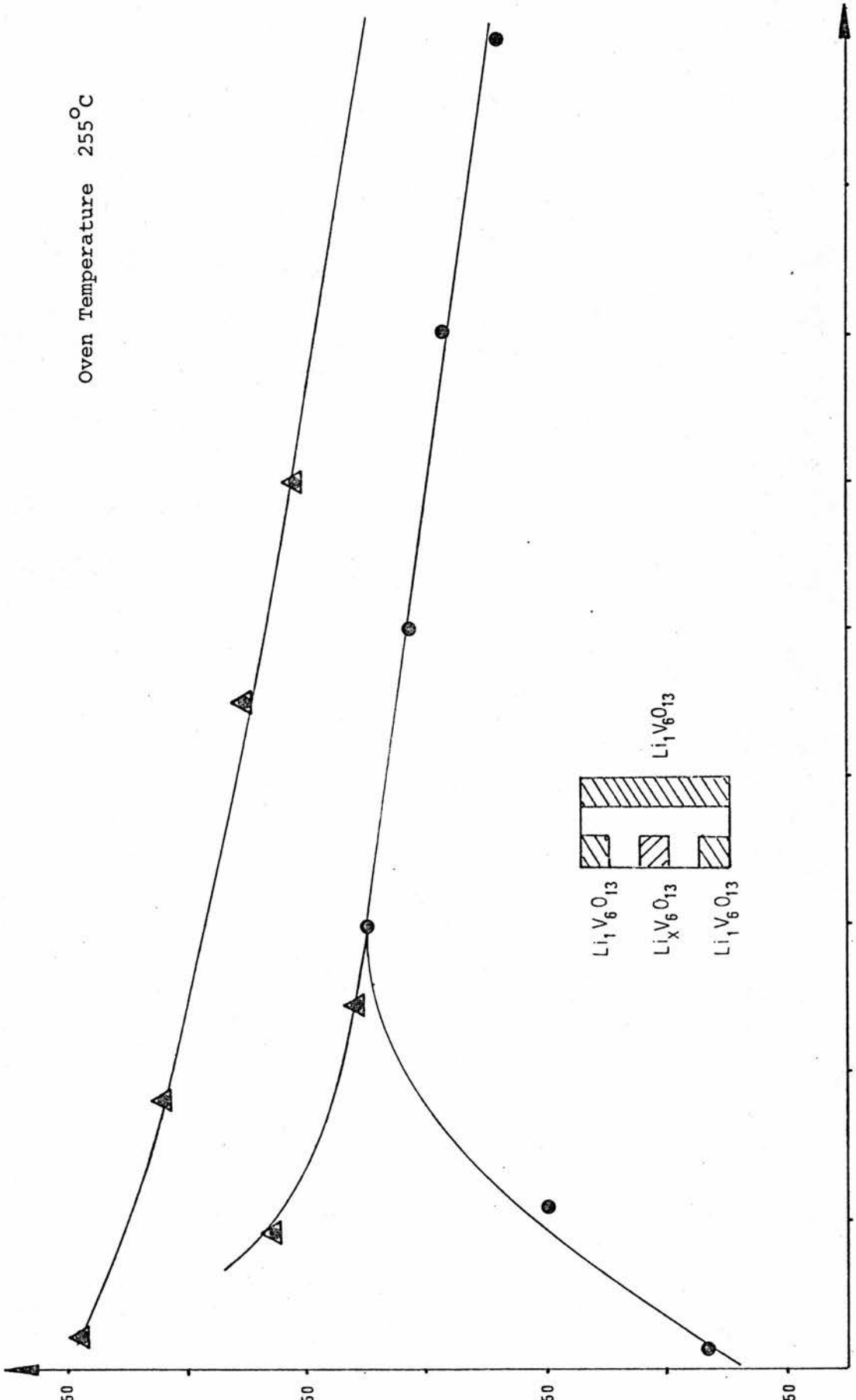

Figure 15: Potential versus composition profile for the $Li_xV_6O_{13}$ system

value of x = 0.45. During the cell charging cycle the voltage was a linear function of x until compositions close to the fully charged composition. A hysteresis in the voltage composition relationship was attributed to non-equilibration of the cell. Immediately after each composition changing coulometric titration the cell voltage recovery was rapid but slowed as the potential approached the equilibrium value. As may be seen from Figure 15, the potential of the cell on the second discharge, in the region $0 < x < 0.15$, was higher than previously, leading to the conclusion that the values in this region on the first discharge had not reached equilibrium, after mounting and heating procedures. The voltage range of the electrode material is within that reported by Murphy et al[11] for a cell using a liquid electrolyte, (1 molar $LiAsF_6$ in propylene carbonate), with a lithium metal reference electrode.

In view of the encouraging performance of this electrode system it was decided that preliminary investigation of a completely solid state cell using two host materials in secondary cell conformation, the so-called "rocking chair" cell, should be undertaken. In this cell the electrode, (Cathode on discharge) which has a high potential with respect to lithium, and therefore a low lithium activity, $Li_{1.05}V_6O_{13}$, was prepared in its fully charged state, thus avoiding problems associated with handling of lithium electrodes. The primary selection criteria in choosing a suitable cathode for this cell was that the total cell voltage should be less than the decomposition potential of the electrolyte. As the decomposition potential of the lithium glass electrolyte was not satisfactorily determined, an electrode potential difference, with respect to V_6O_{13}, Figure 2, of less than 2 volts was imposed. One of the materials which complied with this restriction was MoO_2. The potential versus composition profile reported for this material, in 1 molar $LiClO_4$ in propylene carbonate electrolyte, with a lithium reference electrode, is included in Figure 16[18].

According to the voltage ranges reported for V_6O_{13} and MoO_2 the potential of a secondary cell utilising these electrode materials should be approximately 0.6 volts in the fully discharged state and 1.8 volts at full charge.

Figure 17 shows the potential versus composition profile obtained from experiment. In this figure the percentage of lithium transferred from the $Li_xV_6O_{13}$ electrode is plotted against cell voltage. In the discharged state the solid state cell showed positive voltages. After 25% lithium transfer the cell voltage passed through zero and at higher lithium transfer the voltage was negative, reaching a plateau at - 0.64 volts

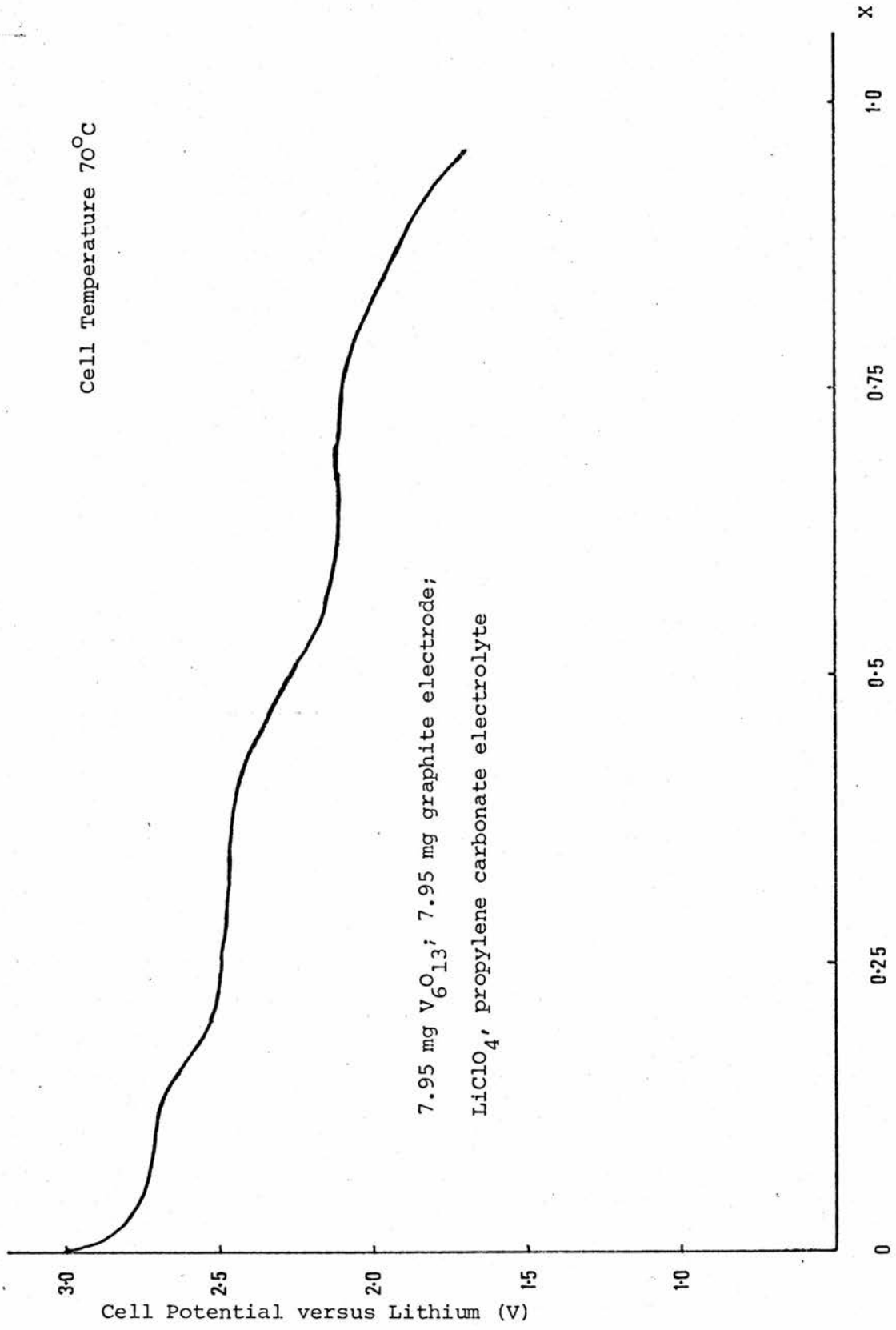

Figure 16: Emf versus Composition, $Li_xV_6O_{13}$ (18)

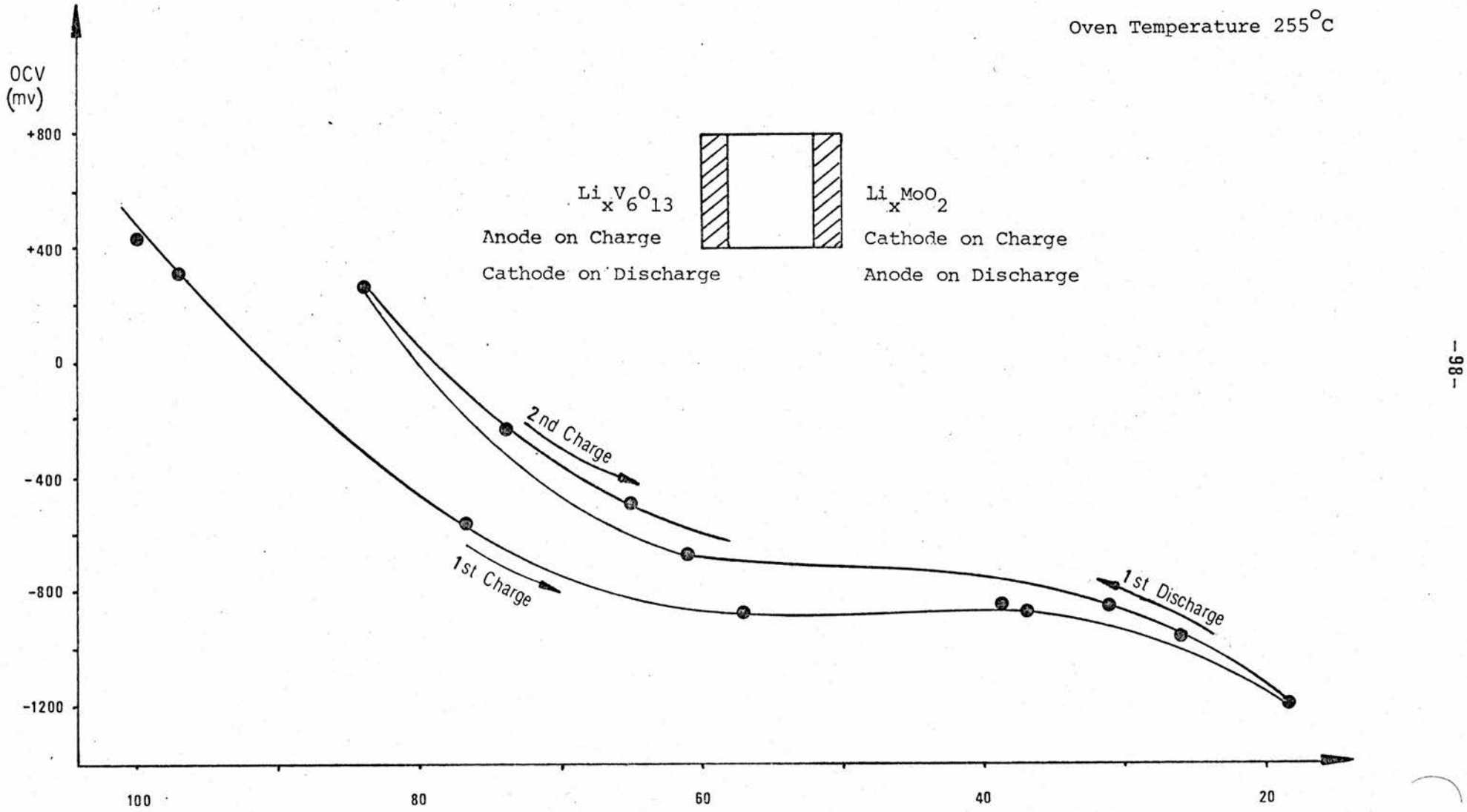

Figure 17: Charge/discharge curves for the $Li_xV_6O_{13}/Li^+$ conducting glass/ Li_xMoO_2 cell

over the range of percentage transfer $30 \leqslant \% t \leqslant 50$. At higher values the voltage began to increase rapidly presumably as a result of the lithium concentration decrease in the $Li_xV_6O_{13}$ electrode. The recharge cycle showed a displacement from the first discharge cycle. This phenomenon, where some cell overcharging occurs on the first, and sometimes subsequent recharge cycles, is quite commonly reported and is frequently attributed to some of the guest species being irreversibly incorporated into the host lattice in a "structure propping" role. Subsequent discharge curves fell close to values obtained for the first recharging cycle. These results suggest that the voltage ranges of the electrode materials were slightly different from those reported by Murphy. (see Figure 2)

During the experiment the total cell resistance was measured by application of short galvanostatic pulses of a range of currents, and recording the cell voltage response. The observed variation of resistance with composition is reported in Table 4. The trend of increasing resistance with decreasing lithium content does not agree with that reported by Murphy et al[11], nevertheless this group did report problems with low electronic conductivity over a range of lithium content. These were overcome by the addition of graphite as conducting diluent.

In view of the simple nature of these experiments with no optimisation of the electrolyte/electrode material ratios in the electrodes, and no addition of current collecting diluents, the results were very good. The cell showed a plateau of approximately 20% of its total capacity over which it could apparently by cycled without loss of capacity, at a voltage of 0.6 volts. While a high temperature cell of this kind is not of immediate commercial value, it illustrates the possibility of similar solid state cells being devloped for low current applications.

Tungsten dioxide and aluminium were also briefly investigated as counter electrodes with $Li_xV_6O_{13}$. Initial open circuit voltages were higher, as expected from Figure 2, but in both cases the voltage decayed, within a period of 72 hours, to a few millivolts. The cause of this cell deterioration was thought to be due to instability of the electrode/electrolyte interface. Further investigation and development of these cells would have been a major project and was not of immediate interest.

Table 4: Variation of Resistance with Composition, V_6O_{13}/MoO_2 Couple

X in $Li_xV_6O_{13}$	Resistance (KΩ)	Cycle
1.05	6.5	
1.02	9.3	
0.82	12.2	1st
0.61	13.3	Charge
0.34	8.2	
0.27	8.0	
0.69	7.6	1st
0.89	7.5	Discharge
0.64	7.7	2nd
0.41	8.2	Charge

4.9 Conclusions

Of the results reported, the most interesting are those of the Ag_xNbS_2 system. A logical extension of this work would be an investigation of potential versus composition profile over the entire range of possible host stoichiometries. Problems associated with the preparation of stoichiometric disulphide have been reported by other authors [4,19] and may be important with respect to diffusion coefficients of the guest species.

There are several ways in which a cell potential versus composition (x and y in $Ag_xNb_{1+y}S_2$) investigation may be carried out. The method used by Lazzari et al[16] in the investigation of the Ag_xTiS_2 system could be readily applied. Thermally prepared samples of $Ag_xNb_{1+y}S_2$, of known phase and composition could be used to construct electrodes in suitable cells, to obtain the variation of potential with x and y. The disadvantage of this technique is the uncertainty in x and y.

An alternative, or preferably concurrent, investigation could be carried out by starting from a series of fixed compositions of known x and y, and intercalating silver electrochemically into the working electrode of a suitable cell. Cells using either liquid or solid electrolytes may be used. The advantage of using a liquid cell is the relative ease with which x-ray or electron microprobe analysis could be undertaken on a single crystal electrode. The major disadvantage encountered with a liquid electrolyte cell is the lack of information regarding the part played by the electrolyte. (cointercalation of solvent has been reported with certain systems)

Advantages of using an entirely solid state cell are related to ease of construction and handling, using techniques already developed. Disadvantages are lack of detailed information about the electrode surface area, and the difficulty of recovering material for analysis.

Both types of cell require low current densities to avoid silver deposition during intercalation and long equilibration times after electrode composition changing titrations. This is necessary to ensure the achievement of a completely uniform distribution of electroactive species throughout the electrode. The major advantage achieved through the use of electrochemically prepared samples is the accuracy with which the guest species concentration is known.

Comparison of the results of potential measurements on Ag_xTiS_2 and Cu_xTiS_2, as reported by Lazzari et al, would suggest that a more interesting investigation from the commercial viewpoint might be carried out on the Cu_xNbS_2 electrode material. A parallel investigation of this system might

prove of greater importance.

Silver and copper occupy a unique position in the class of intercalation electrodes in that they are located in tetrahedral sites within the structure of tantalum and niobium dichalcogenide materials. This may have important implications regarding their capacity and the rate of guest species diffusion. A careful study of diffusion coefficients might yield a useful insight into the identification of diffusion pathways between lattice sites in these materials.

Any cell using silver or copper as electroactive species has the significant advantage of availability of highly conducting solid electrolytes, a situation which has not yet been realised for sodium or lithium at ambient temperatures.

The investigations carried out on the Lithium host materials in secondary cells yielded promising results. Further development of these cells by investigation of the effect of addition of graphite as a current collector in the electrode materials might be of interest.

The electrolyte used in the experiments seems to be incapable of supporting potential differences as high as liquid, non-aqueous electrolytes. This effectively restricts the electrode systems available for coupling to $Li_xV_6O_{13}$. Various other electrolytes might be reviewed with the purpose of extending the range of electrode materials and increasing the potential range of the secondary cell produced.

1. Worrell W.L., Nagelberg A.S., J. Solid State Chemistry, Vol 29, (1979) 345

2. Trumbore F.A., Pure & Appl. Chem., Vol 52 (1980) 119

3. Whittingham M.S., Mat. Res. Bull., Vol 9, (1974) 1981

4. Whittingham M.S., Prog. Solid. St. Chem., Vol 12, (1978) 41

5. Whittingham M.S., J. Electrochem. Soc., Vol 123, (1976) 315

6. Thompson A.H., "fast Ion Transport in Solids" Ed. Mundy., Shenoy, Vashishta, (Elsevier North Holland Inc., 1979)

7. Boukamp B.A., Huggins R.A., Wen C.J., Wepper W., J. Electrochem. Soc., Vol 126 (1979) 2258

8. Shemitt J.M., Steele B.C.H., Winn D.A., Mat. Res. Bull., Vol 11, (1976) 559

9. Whittingham M.S., J. Solid. St. Chem., Vol 29, (1979) 303

10. Whittingham M.S., U.S. Patent No. 4,007.055 (1975)

11. Carides J.N., Christian P.A., Di Salvo F.J., Murphy D.W., J. Electrochem. Soc., Vol 126, (1979) 497

12. Scanlon J.C., Symon C.R., Thompson A.H., Solid. St. Ionics., Vol 1, (1980) 47

13. Armand M.B., "Materials for Advanced Batteries", Ed. Broadhead J., Murphy D.W., Steele B.C.H., (Nato Conference Series, Plenum Publishing Corp., New York 1980)

14. Cheung K.Y., Dudley G.J., Steele B.C.H., J. Solid. St. Chem., Vol 32 (1980) 269

15. Frindt R.F., Scholz G.A., Mat. Res. Bull., Vol 15 (1980) 1703

16. Bottini A., De Felici G., Lazzari M., Razzini G., Rivolta B., Scrosati B., Voso M.A., J. Electroanal. Chem., Vol 96 (1979) 165

17. Lieth R.M.A., "Preparation and Crystal Growth of Materials with Layered Structures", (D. Reidel Publishing Co., Dordrecht, Holland, 1977).

18. Carides J.N., Murphy D.W., Di Salvo F.J., Mat. Res. Bull., Vol 13, (1978) 1395

19. Bayard M., Mentzen B.F., Sienko M.J., Inorg. Chem., Vol 15 (1976) 1763

20. Steele B.C.H., Winn D.A., Mat. Res. Bull., Vol 11, (1976) 551

21. Barnett W.B., Fernandez F.J., Lumas B.K., Wallace G.F., Atomic Spectroscopy, Vol 2, (1981) 130

22. B. Scrosati, University of Rome (Private communication)

CHAPTER 5: MEASUREMENT OF DIFFUSION COEFFICIENTS

5.1 Introduction: Mathematics of Diffusion

Mass transport in a chemical system may occur as a result of various perturbing forces. These may be classified -

(a) Migration, as a result of an applied electric field,

(b) Diffusion, under the influence of a chemical potential gradient, or

(c) Convection, where this class also includes motion as a result of mechanical forces.

In the investigation of any one of these influences, experimental conditions are chosen to minimise the effects of the other two. In the present case transport solely as a result of diffusion processes is of interest.

In general the assumption is made that the driving force of diffusion processes, the chemical potential gradient, may be approximated by the concentration gradient. The fundamental equation which relates the flux of particles to the concentration gradient is known as Fick's first law, and is expressed,

$$J = -D \frac{\partial c}{\partial x} \qquad [1]$$

and defined, "the rate of transfer of diffusing species, through a section of unit area, is proportional to the concentration gradient, measured normal to the section." If the system can be assumed to be ideal, then D, the diffusion coefficient, is independant of concentration.

If a disturbance is imposed on a system which produces a concentration gradient at a point in the system, which was previously at equilibrium with its environment, (with respect to interchange of species), a diffusion process will occur which will eventually reach a new steady state condition. The period of disturbance from the steady state, with respect to variation in concentration with time and distance from an arbitary reference point, is described by Fick's second law. This equation, expressed here in one dimensional form, is fundamental to the solution of many problems of non-steady state diffusion.

$$\frac{\partial c}{\partial t} = D \frac{\partial^2 c}{\partial x^2} \qquad [2]$$

Before equation [2] can be solved it must be transformed into a total differential, the solution of which is a function of a single variable. Various methods and solutions have been described for different experimental

situations with different geometries and boundary conditions. Probably the most commonly used method is that of the Laplace transform.

The use of Laplace transforms may be regarded as a mathematical device which leads to a simplification of the total differential by transformation into another equation the solution of which is a function of only one independant variable. This solution is then transformed back, to reintroduce the second independant variable.

The relevant equation is expressed,

$$\frac{d^2\bar{c}^*}{dx^2} - \left(\frac{P}{D}\right)\bar{c}^* = 0 \qquad [3]$$

where c* is a variable introduced to describe the disturbance from the initial concentration Co.

$$C^* = C - Co$$

where [3], is now second order, linear and homogeneous.

The general solution is

$$\bar{C}^* = \propto \exp - \left(\frac{P}{D}\right)^{\frac{1}{2}}x + \beta \exp \left(\frac{P}{D}\right)^{\frac{1}{2}}x \qquad [4]$$

Consideration of the constraints imposed on the solution by the initial and boundary conditions leads to the evaluation of the constants, $\propto$ and β. These conditions are mathematical descriptions of the system prior to experiment initiation, ($t = 0$), and during the experimental process, at specified boundaries. (normally for $x = 0$, and $x = \infty$) These conditions therefore determine the form of solution that is appropriate.

A brief derivation of the solution for the experimental conditions used in the diffusion experiments carried out in this investigation, will be given. In principle, the method is identical to that used for other experimental procedures discussed elsewhere in this chapter.

Under the present experimental conditions, a short, cathodic, galvanostatic pulse was applied to the cell (Figure 1(a)) working electrode. During the pulse, the voltage transient between working and reference electrodes was recorded (Figure 1(b)) with respect to time. The initial condition therefore is given,

$$\text{at } t = 0, \quad x \geqslant 0, \quad C = Co$$

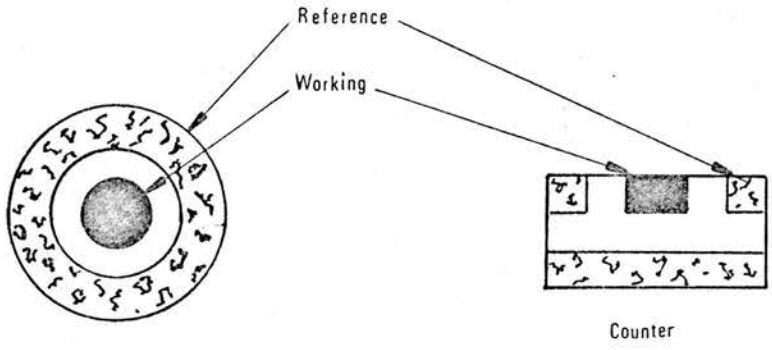

Figure 1 (a): Cell Structure of 3 Electrode Cells

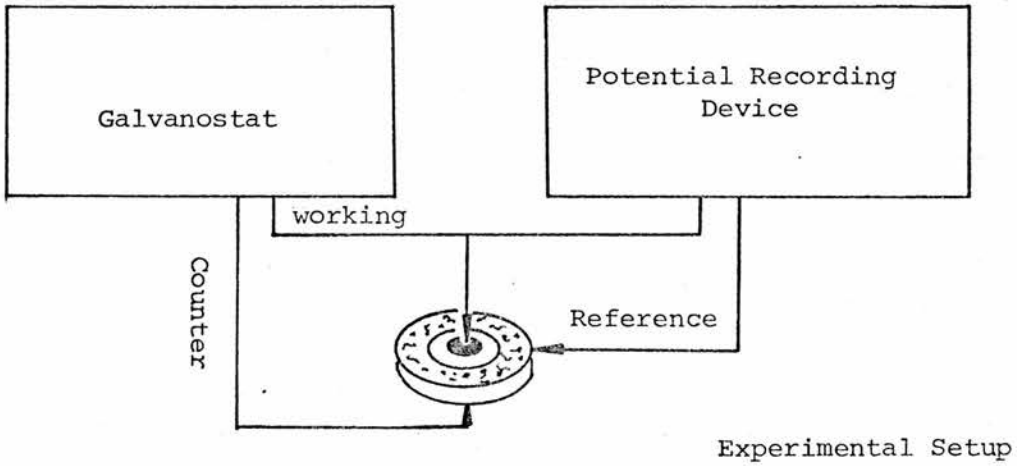

Experimental Setup

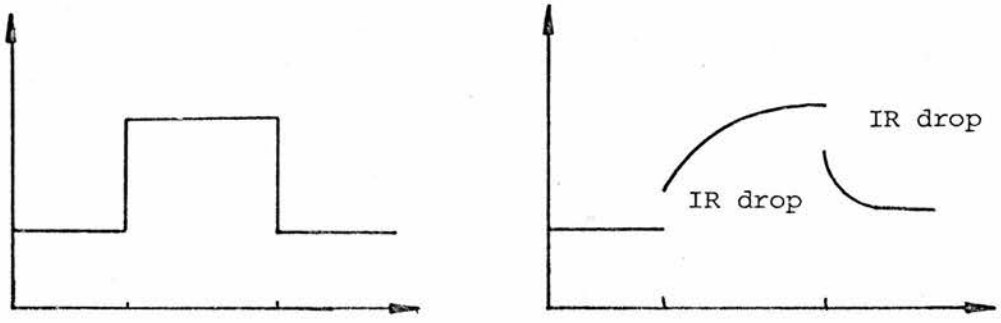

FIGURE 1(b): Transient Recorded During Current Pulse

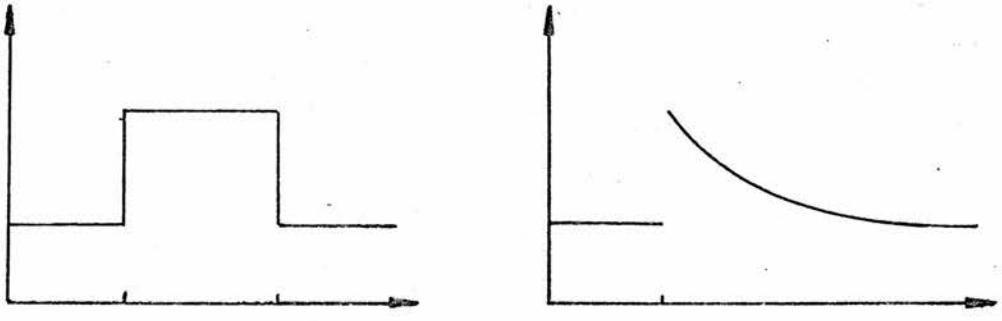

FIGURE 1(c): Transient Record of Relaxation Method

which states the assumption of uniformity of concentration in the electrode, of the diffusing species, at initiation.

The boundary conditions are derived from the assumption that at a sufficiently large distance from the electrode/electrolyte interface, the concentration of the diffusing species is invariant with time during the pulse. (the semi-infinite condition)

$$t > 0, \quad x \longrightarrow \infty, \quad C \longrightarrow Co$$

as $$x \longrightarrow \infty, \quad \bar{C}^* \longrightarrow 0.$$

Applying these conditions to equation [4], it is obvious that for $\bar{C}^*$ to tend to zero as x tends to infinity, the constant β, must be zero. Equation [4] is therefore simplified to

$$\bar{C}^* = \propto \exp - \left(\frac{P}{D}\right)^{\frac{1}{2}} x \qquad [5]$$

The second boundary condition establishes the invariance of the flux of diffusing species at the electrode/electrolyte interface, from Fick's first law,

$$\left(\frac{dc}{dx}\right)_{x=0} = - \frac{i}{nFAD} \qquad [6]$$

As the current is fixed under the experimental conditions used, (Galvanostatic condition), and the total concentration of species generated is proportional to the number of coulombs available at the electrode, (Faraday's law) the total flux of particles across the electrode/electrolyte interface is invariant.

Differentiation of [5] with respect to x gives

$$\left(\frac{d\,\bar{c}^*}{dx}\right) = - \propto \left(\frac{P}{D}\right)^{\frac{1}{2}} \exp - \left(\frac{P}{D}\right)^{\frac{1}{2}} x \qquad [7]$$

which for x = 0 reduces to

$$\left(\frac{d\,\bar{c}^*}{dx}\right)_{x=o} = - \propto \left(\frac{P}{D}\right)^{\frac{1}{2}} \qquad [8]$$

combining [6] and [8] gives,

$$- \propto \left(\frac{P}{D}\right)^{\frac{1}{2}} = - \frac{i}{nFADp}$$

and $$\propto = \frac{i}{nFAD^{\frac{1}{2}} p^{\frac{1}{2}}} \qquad [9]$$

hence substituting [9] into [5] gives,

$$\bar{C}^* = \frac{i}{nFAD^{\frac{1}{2}}p^{\frac{1}{2}}} \exp - \left(\frac{P}{D}\right)^{\frac{1}{2}} x \qquad [10]$$

Using tables to find the inverse transformation of [10], and expressing the equation in terms of C and Co gives,

$$C = Co + \frac{i}{nFAD^{\frac{1}{2}}} \left[\frac{2\,t^{\frac{1}{2}}}{(\pi)^{\frac{1}{2}}} \exp\left(\frac{-x^2}{4Dt}\right) - \frac{x}{D^{\frac{1}{2}}} \operatorname{erfc}\left(\frac{x}{2D^{\frac{1}{2}}t^{\frac{1}{2}}}\right) \right]$$

which is the required solution of Fick's second law for the initial and boundary conditions of the experiment.

This equation gives the profile of concentration of the diffusing species as a function of time and distance from the reference plane. (the electrode surface, at x = O)

For small values of time, when $t << L^2/D$, where L is the distance the concentration profile extends into the electrolyte, the time variation of the concentration of the electroactive species at the electrode/electrolyte interface, the solution can be approximated by

$$C = Co + \frac{2\,i\,t^{\frac{1}{2}}}{nFA\,(D\pi)^{\frac{1}{2}}} \qquad [11]$$

If C - Co may be related to an experimentally measurable parameter, voltage measured during the pulse, then the diffusion coefficient is calculable from [11].

An alternative technique, similar in principle, employed by other groups, uses a slightly different approach. When a small amount of an electroactive species is introduced into the cathode of a cell as a consequence of a short, galvanostatic pulse, the voltage of the cell decreases from the equilibrium value. The rate of diffusion of electroactive species into the electrode bulk will control the recovery of the cell voltage to an equilibrium level. The mathematics of the solution of this situation are similar (with certain important differences[1],) to the derivation given above. The solution for this case, (instantaneous planar sink, semi-infinite geometry) is given by,

$$C - Co = \frac{i\tau}{nFA\,(\pi Dt)^{\frac{1}{2}}} \exp\left(\frac{-x^2}{4Dt}\right) \qquad [12]$$

where τ is the length of the pulse, and all other parameters are as before.

Again, if an experimentally recorded voltage transient may be related to C - Co then evaluation of the diffusion coefficient is possible.

Various authors have approached the evaluation of C - Co in different ways. A review of these methods is now given.

5.2 Evaluation of the Diffusion Coefficient

During the last decade electrochemical techniques have been used by many authors in the evaluation of diffusion coefficients. The development of methods by which diffusion coefficients of guest species in host lattices may be measured has been given priority as a consequence of the direct relationship between cell currents and the diffusion process which may control the kinetics of electrodes. Given a reliable means of measuring the diffusion coefficient, various electrode materials may be screened and the most promising identified for further investigation.

Both galvanostatic techniques discussed in the previous section, the relaxation method in which the voltage is monitored after the pulse, and the alternative in which the voltage is monitored during the pulse, have been used on a variety of systems. Authors have favoured different methods of transforming the solutions, equations [12] and [11] respectively, which are given in terms of concentration, into the voltages recorded under experimental conditions. Weppner[2,3,4] and Worrell[5,6,7] have used a relationship between cell voltage and concentration of electroactive species, determined with the use of a galvanic cell, to permit the evaluation of D, while Bonino[8,9], Bottleberghs[10], Scholtens[11], Scrosati[12] and Winn[13] have used equation [13], to directly relate concentration and voltage.

$$E = Eo + \frac{RT}{nF} \ln \frac{C}{Co} \qquad [13]$$

$$\eta(t) = (E(t) - Eo) = \frac{RT}{nF} \ln \frac{C}{Co} \qquad [13ii]$$

5.3 Results and Discussion

In view of the conclusions drawn by Bonino[8], as a result of a comparative study of chronopotentiometric techniques, it was decided that further investigation of other electrode materials, using the galvanostatic pulse method, should be undertaken. Results obtained using this method appear to be less dependant on experimental factors, such as pulse duration and current density.

It was felt that the "key site blocking" or "anti-cooperative motion" theory proposed by Bonino et al[9] was an inadequate explanation of the apparent rapid fall of the silver species diffusion coefficient in the Ag_xTaS_2 system, but until further information about similar systems was obtained, no alternative proposals could be made.

An investigation was therefore carried out on the Ag_xTiS_2, $Ag_xTiS_{1.80}$, and Ag_xNbS_2 systems, with respect to the composition dependance of the diffusion coefficient of the guest species.

In preliminary investigations equation [13ii] was used to relate the experimentally recorded values of voltage to the concentration parameter, C - Co, in equation [11].

$$C - Co = \frac{2\,it^{\frac{1}{2}}}{nFA\,(D\pi)^{\frac{1}{2}}} \qquad [11]$$

$$E - Eo = \eta(t) = \frac{RT}{nF} \ln \frac{C}{Co} \qquad [13ii]$$

The results obtained for stoichiometric and non-stoichiometric titanium disulphide materials are reported in Figure 2 and those for niobium disulphide in Figure 3. As may be seen from comparison with Figure 4[9], the results in all these systems, using identical experimental procedures, are very similar. While the reported activation energies for the diffusion process in the Ag_xTaS_2 system were almost composition independant, the trend in the other three systems was a slight decrease with increasing guest concentration.

If the structural information, already discussed in Chapter 4, is considered then this trend for the composition dependance of the diffusion coefficient is very different from the expected trend, and that reported by Worrell[5,6,7] for similar layered electrode materials with lithium and sodium guest species. The structural consequences of increasing guest concentration in these materials, a van der Waal's gap dilation, correlated well with the decrease in the activation energy of the diffusion process reported by Worrell. The variation of log D of sodium and lithium species in the TaS_2 host lattice with x, Figures 5 and 6, appears to confirm the predicted increase in diffusion coefficient as the lattice expansion occurs. In contrast, the compositional independance of Log D_{Li} in Li_xTiS_2, (Figure 7), is surprising and no explanation was offered by Worrell.

These results bear little resemblance to those obtained for the Ag_xTaS_2, Ag_xTiS_2, $Ag_xTiS_{1.80}$ and Ag_xNbS_2 systems.

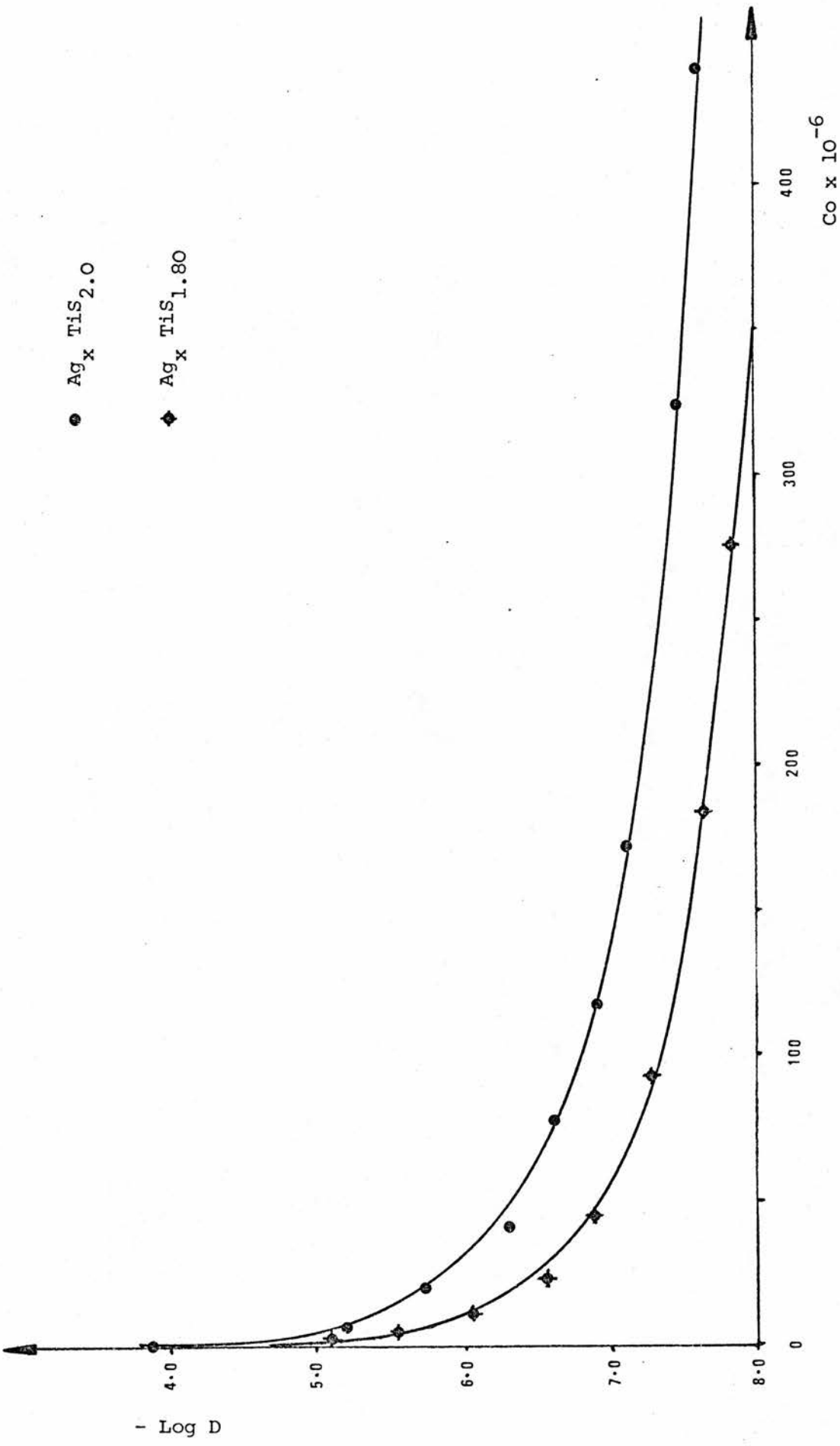

FIGURE 2: Comparison of Log Dcoeff versus Concentration behaviour of $Ag_x TiS_2$ and $Ag_x TiS_{1.80}$

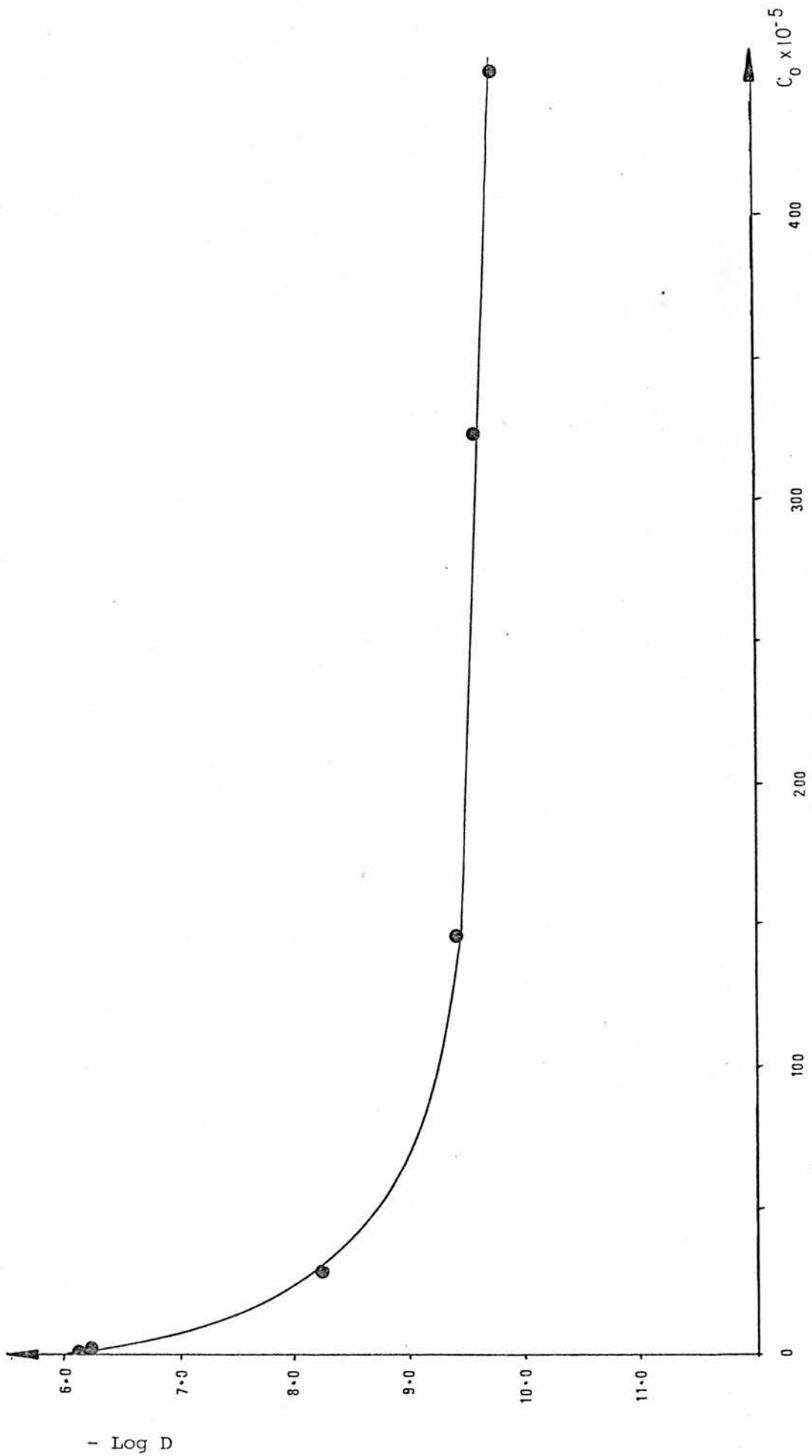

Figure 3: Log Dcoeff versus Concentration, Ag_xNbS_2

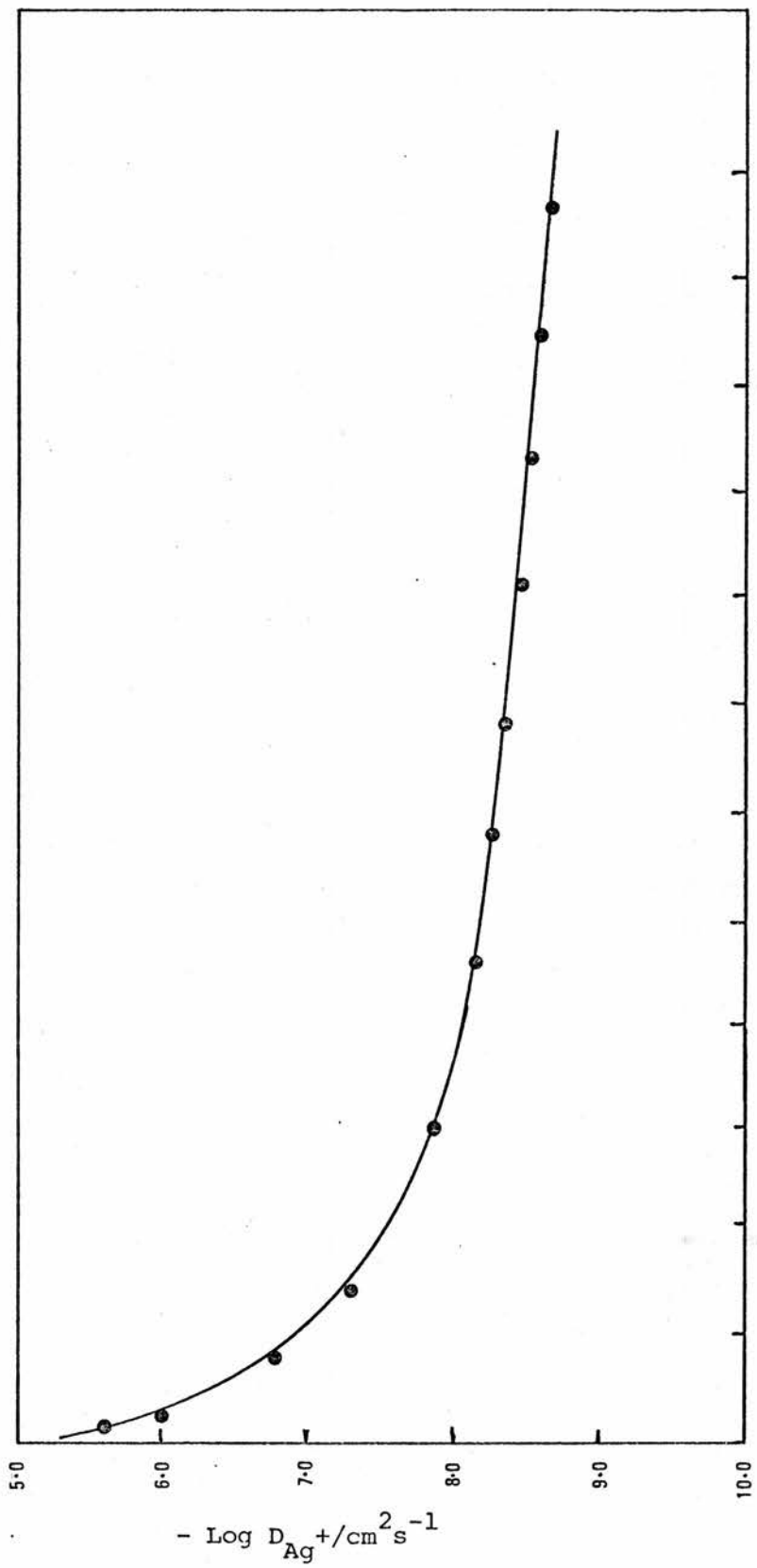

Figure 4: Variation of Log Dcoeff versus Composition of Ag_xTaS_2 [9]

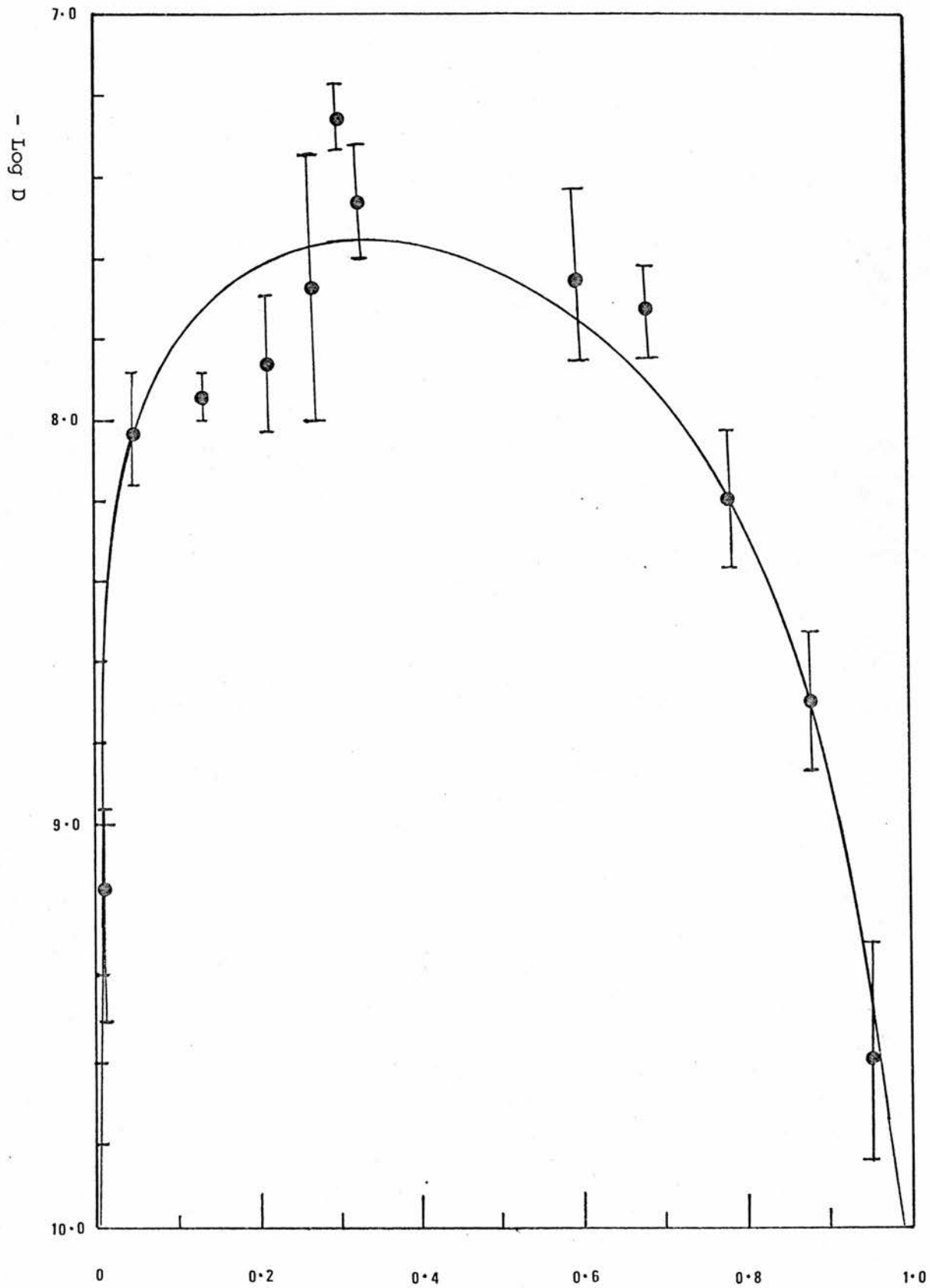

Figure 5: - Log D versus Composition, Na_xTaS_2

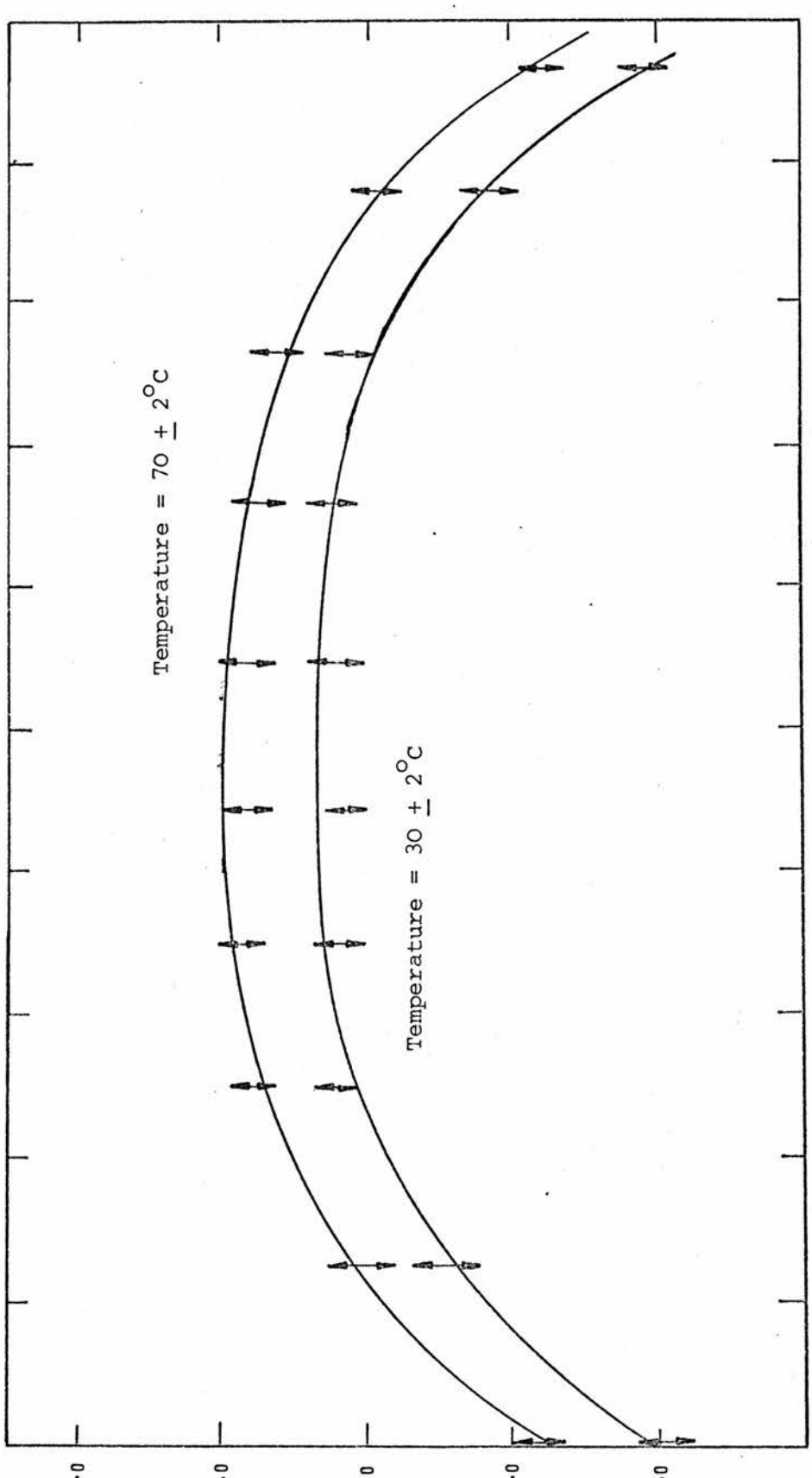

Figure 6 : DIFFUSIVITY OF Li^+ IN Li_xTaS_2

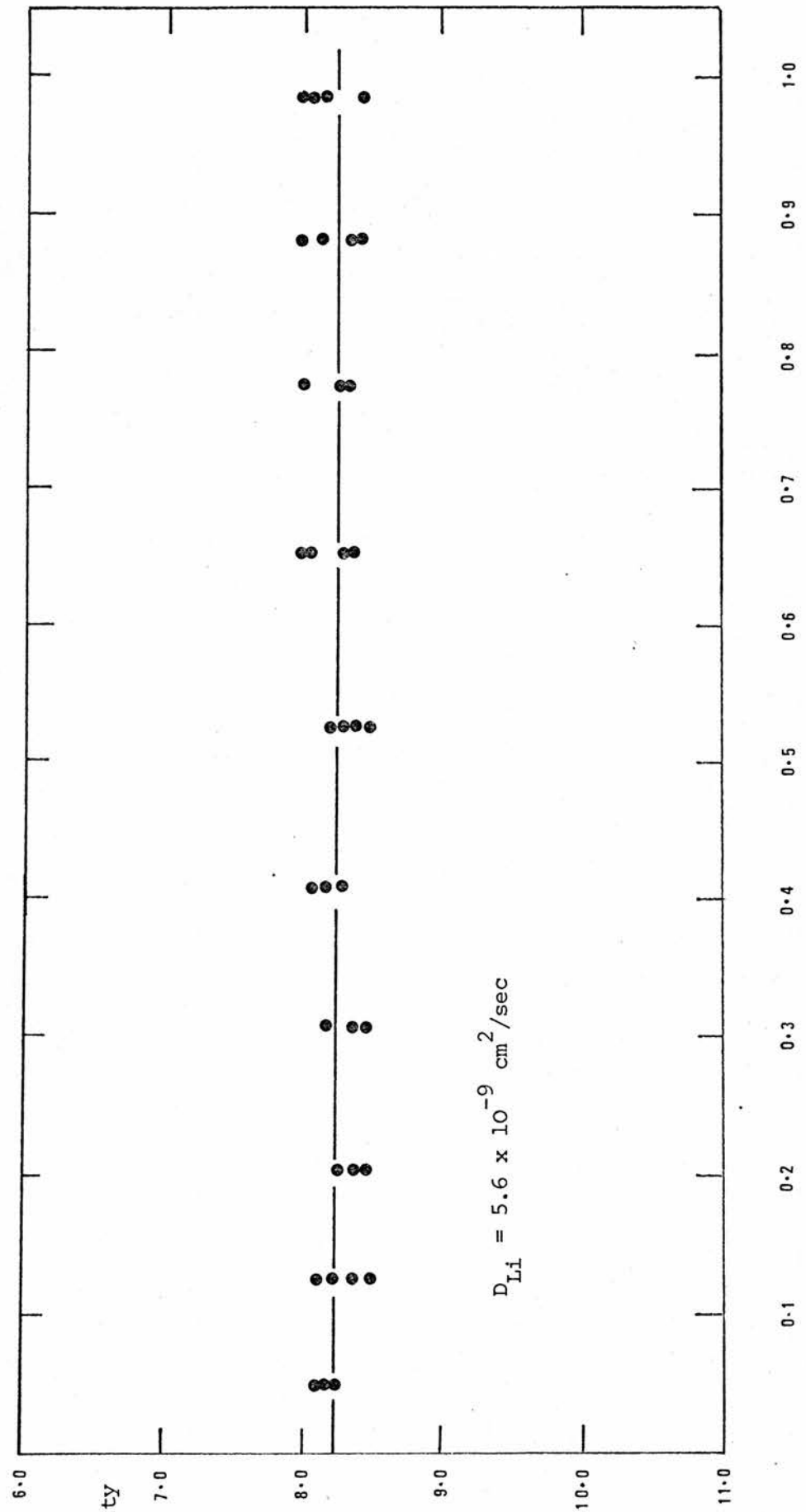

FIGURE 7 : Diffusivity of Li IN Li_xTiS_2 System at 30 $\pm$ 2°C

As thermodynamic data became available and its interpretation considered, it became clear that the intercalation class of electrodes behave as very non-ideal solutions. This point is illustrated by the inclusion of Figure 8 (a) and (b), in which the slope and position of the activity versus composition plot of an ideal solid solution is compared with that for $Ag_xTiS_{1.80}$. In the limit of infinite dilution solutions are assumed to behave in an ideal manner. Clearly the use of equation [13ii] to relate the instantaneous voltages of the recorded transient to concentration is not justified under the present experimental circumstances.

Further consideration of the consequences of using equation [13ii] led to an explanation of the origin of the observed log D_{Ag^+} versus composition relationship. Using equations [11] and [13ii] to evaluate the diffusion coefficient from the gradient of an exp $[(\frac{nF}{RT}) - 1]$ versus $t^{\frac{1}{2}}$ plot, leads to equation [14].

$$Dcoeff = \frac{4\, i^2}{F^2 A^2 n^2 Co^2 \pi m^2} \qquad [14]$$

As the Co parameter in this equation was more dependant on x, (in M_xTCh_2), than any of the other factors, Co dominated the diffusion coefficient. This is shown in Figure 9 where values of log D are plotted as a function of x, with all other factors in equation [14] held constant. This plot shows the source of the log D versus composition behaviour reported by Bonino et al[8,9,12].

As a relationship between the voltages recorded during the galvanostatic pulse and the instantaneous concentration at the interface is necessary to permit the evaluation of the diffusion coefficient, reference was made to the techniques used by other groups. The approach used by Worrell and Weppner employed an empirical relation between open circuit potential and the guest concentration.

Worrell et al[7], working with a non-aqueous, liquid electrolyte cell, used the current pulse relaxation method to obtain the diffusion coefficient of lithium species in Li_xTaS_2 and Li_xTiS_2. Using Fick's second law to describe the diffusion process for an instantaneous planar sink of diffusing species in semi-infinite geometry, the time dependance of the concentration at the electrode/electrolyte interface is given by equation [15].

$$C - Co = \frac{i\, \tau}{nFA\, (\pi Dt)^{\frac{1}{2}}} \qquad [15]$$

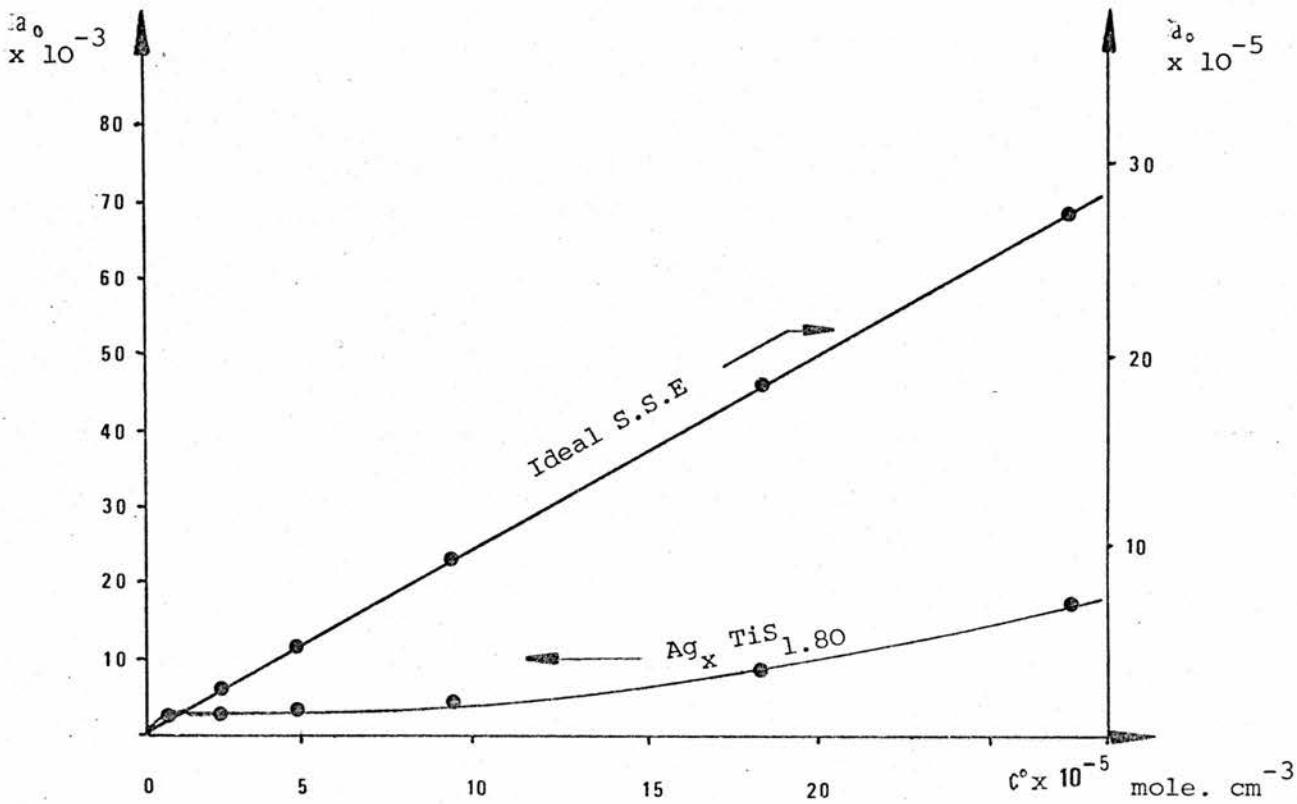

FIGURE 8(a): Comparison of Activity versus C^o behaviour of ideal and $Ag_x TiS_{1.80}$ Electrode Systems

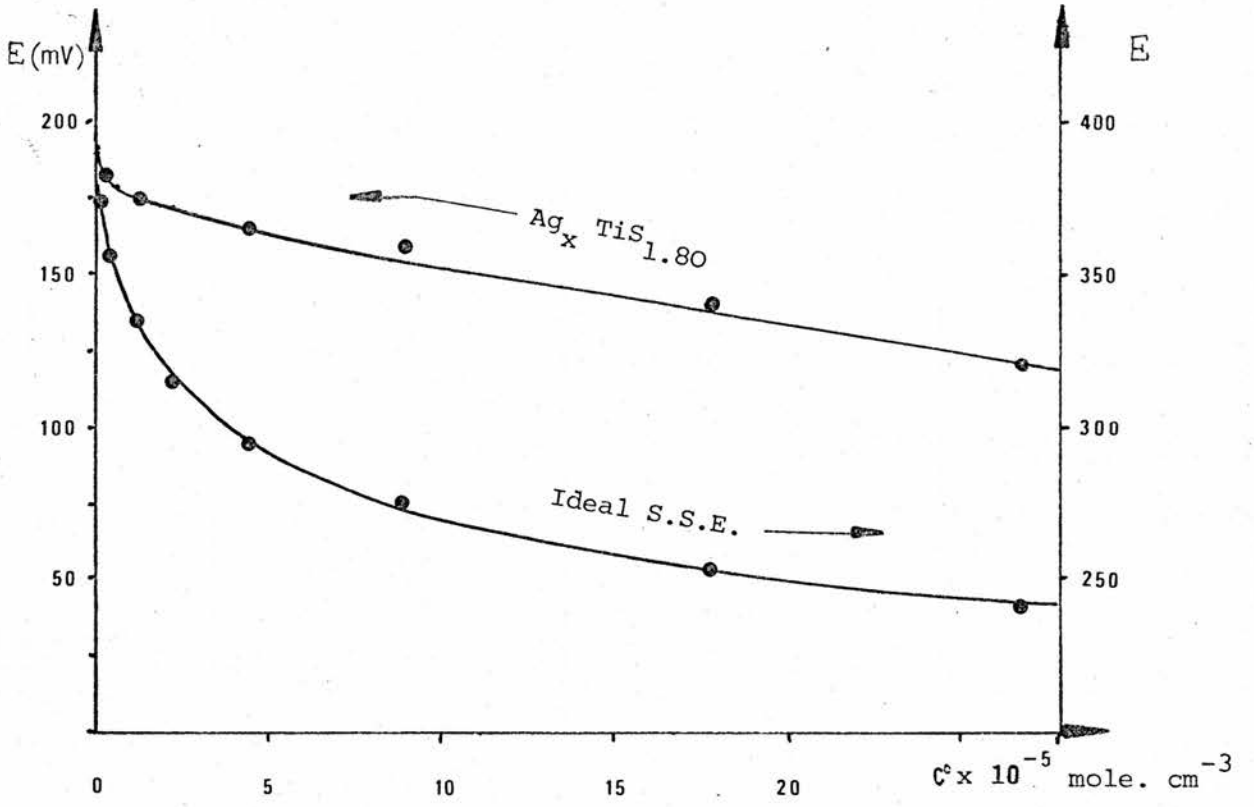

FIGURE 8(b): Comparison of Potential Versus C^o behaviour for ideal and $Ag_x TiS_{1.80}$ Systems

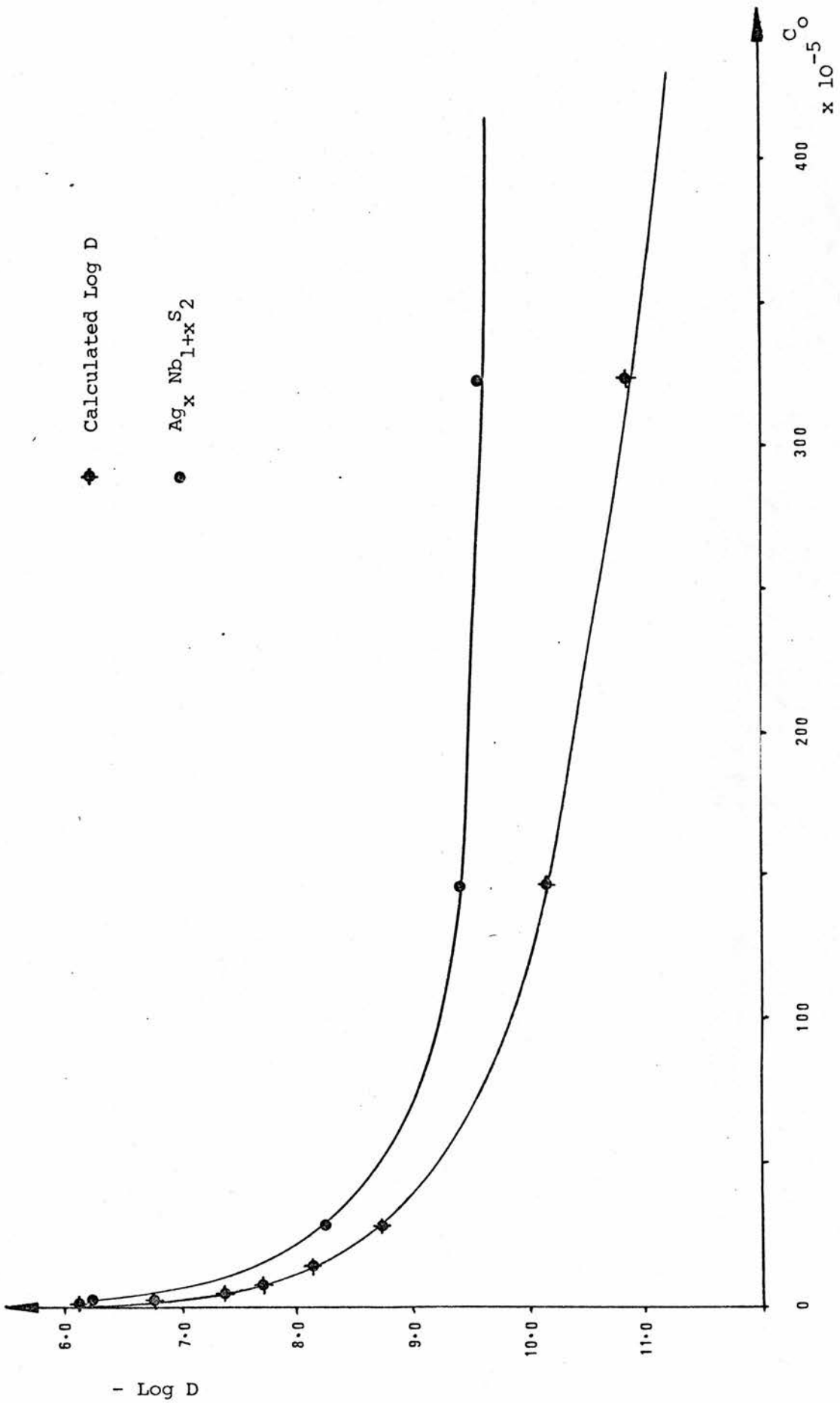

FIGURE 9: Comparison of Log Dcoeff versus Concentration behaviour with that calculated from equation [29]

Worrell used Emf versus composition data[5] to relate C to the voltages recorded after the pulse. The Emf of a galvanic cell was found to be an approximately linear function of composition for Na_xTaS_2, Li_xTaS_2 and Li_xTiS_2 systems, Figures 10 and 11, (details of the Li_xTiS_2 measurements are not yet available) and equations [16], [17] and [18] respectively. The concentration terms C and Co in equation [15] were replaced by voltage using equations [16], [17] and [18] with equation [19].

Table 1

E = mx + c m	c	System	Equation	Reference
2.72	-1.78	Na_xTaS_2	[16]	(5)
2.92	-1.40	Li_xTaS_2	[17]	(6)
2.86	-0.80	Li_xTiS_2	[18]	(6)

$$C = \frac{x}{Vm} \qquad [19]$$

where Vm is the molar volume of the cathode material.

Substituting appropriately, equation [20] may be obtained.

$$E - Eo = \eta(t) = \frac{m\ Vm\ i\ \tau^{\frac{1}{2}}}{FA\ (\pi Dt)^{\frac{1}{2}}} \qquad [20]$$

According to this equation, $\eta(t)$ should be a linear function of $t^{-\frac{1}{2}}$ and D may be evaluated from the slope of this plot.

The typical voltage - time plot reported by Worrell showed marked non-linearity at early time. (Figure 12) Results which correlate poorly with the ideal mathematical solution may be expected with the relaxation technique used by Worrell, as the instantaneous galvanostatic pulse assumed by the theory cannot be practically achieved. Nevertheless, the use of an empirical voltage/concentration relationship offers a possible alternative to equation [13ii].

A similar problem was encountered by Weppner in the application of the "galvanostatic intermittent titration technique". Using a galvanic cell arrangement, Figure 13, Weppner applied a galvanostatic pulse to the cell. This produced a constant concentration gradient at the A_yB/electrolyte interface, giving rise to a voltage transient, Figure 14, which was recorded during the pulse. After a time interval, τ, the current flux was terminated,

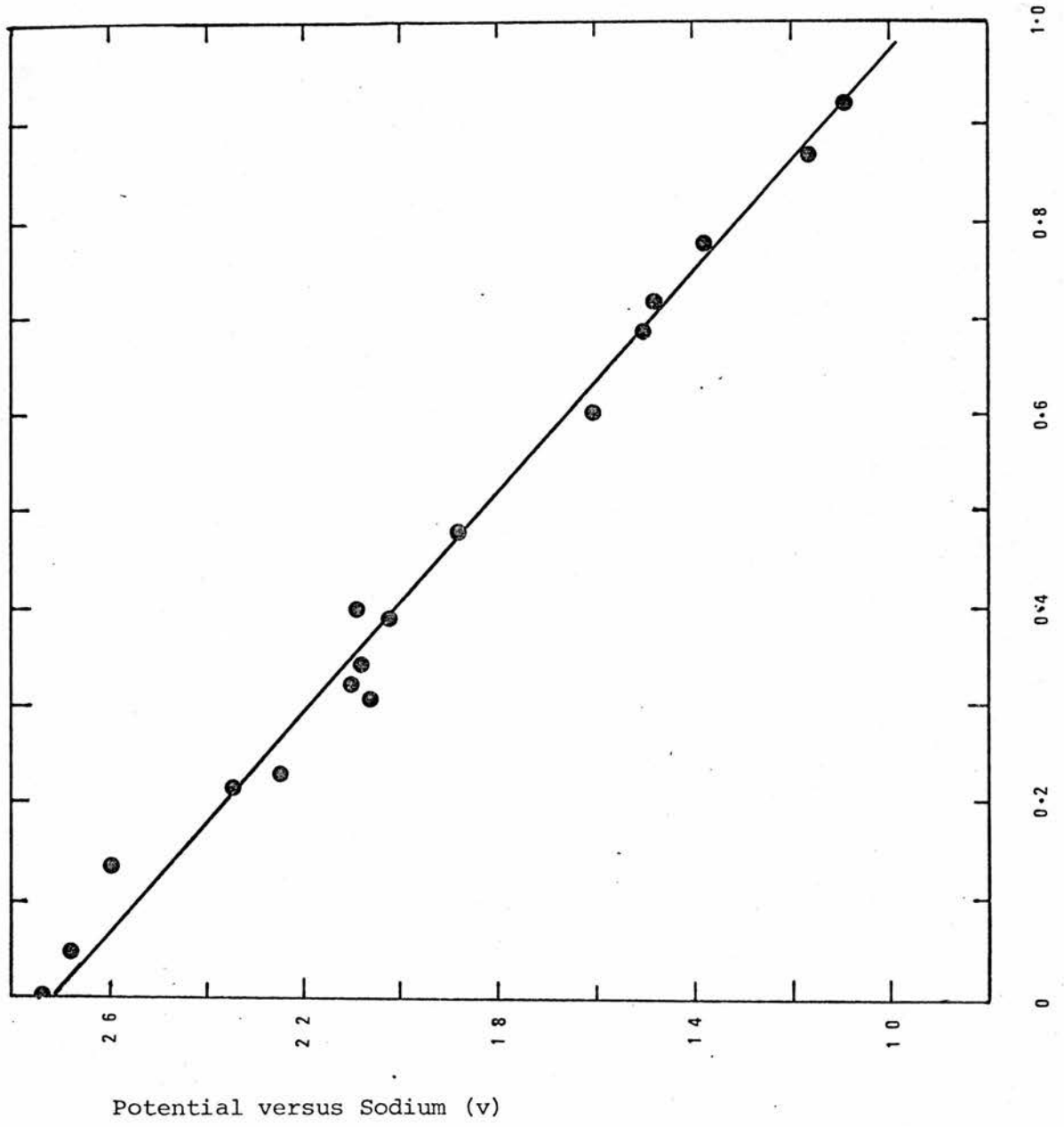

Figure 10: Emf versus Composition, Na_xTaS_2

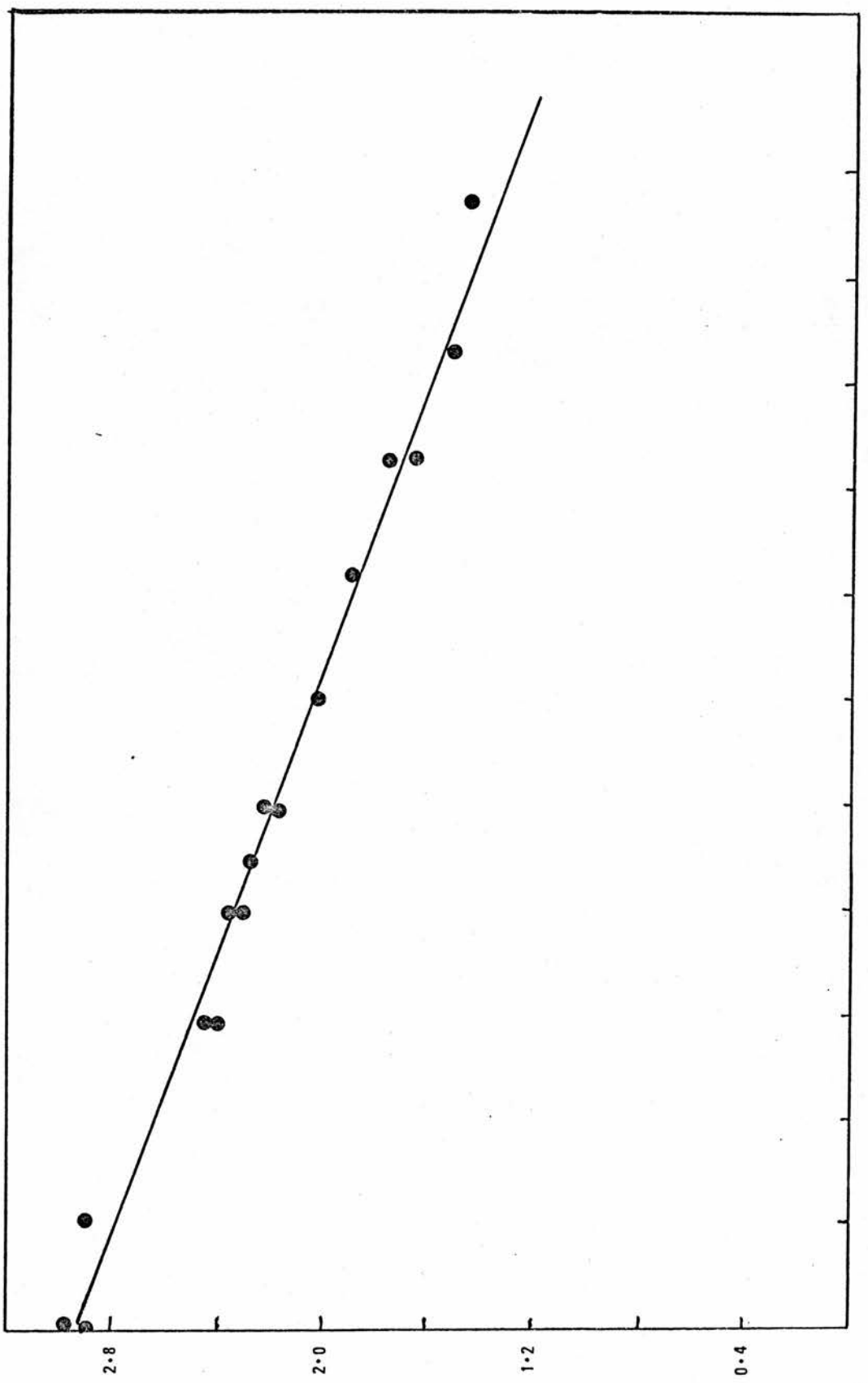

Figure 11: Emf versus Composition, Li_xTaS_2

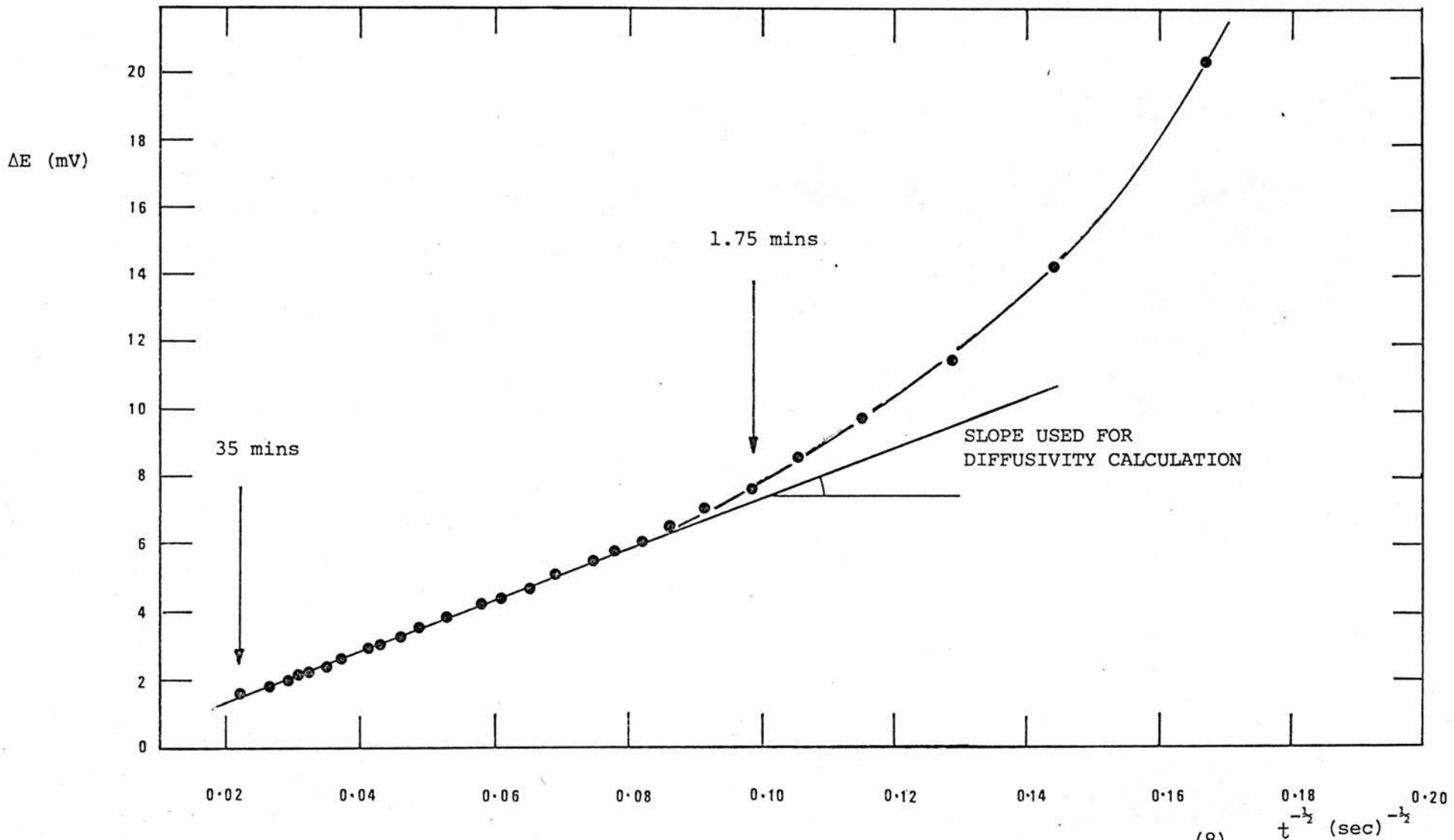

FIGURE 12 : TYPICAL VOLTAGE - TIME RELATION IN CURRENT PULSE METHOD[8]

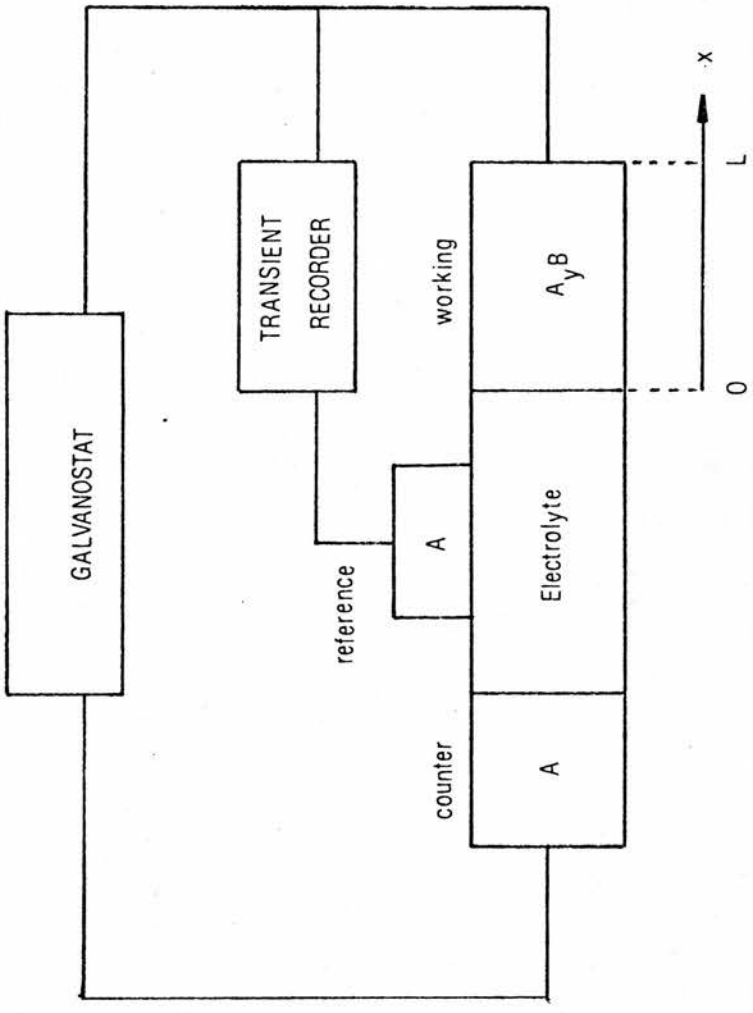

Figure 13: Schematic diagram of experimental galvanic cell arrangement

FIGURE 14 : GITT TECHNIQUE:

CURRENT PULSE AND VOLTAGE TRANSIENT RESPONSE

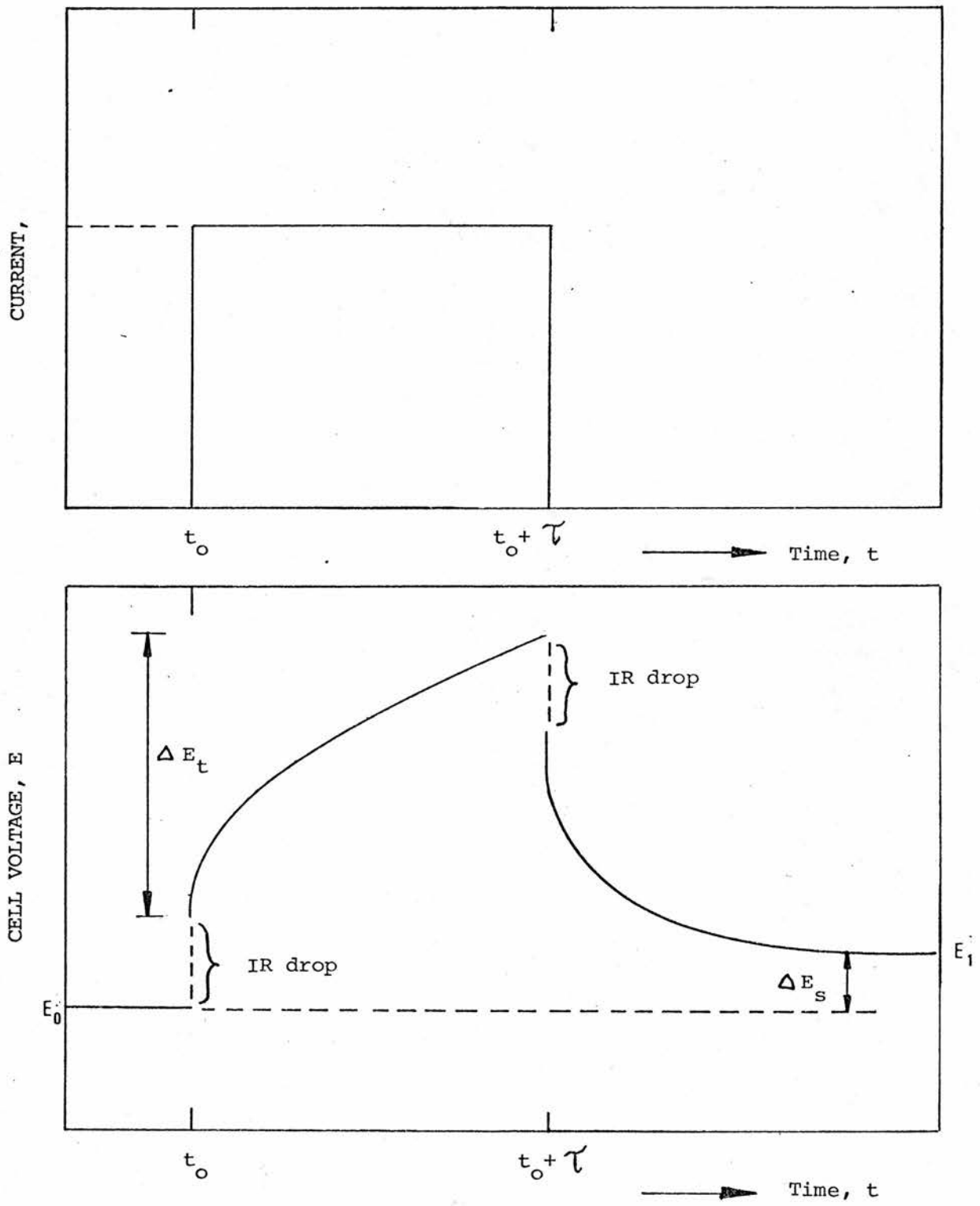

whereupon the composition within the A_yB electrode, (now $A_{y+\delta}B$), tended to become homogeneous again. During this equilibration process the interface composition of the electrode, and therefore the cell voltage, drifted back toward a new steady state value E_1, corresponding to the new activity of A in the sample. The composition change, δ, of the electrode, may be calculated from values of current and pulse duration. After the new steady state was achieved the procedure was repeated. This pulse routine was continued until a phase change occurred in the cathode material.

As may be seen by comparison with the experimental details reported in Chapter 2, this technique is virtually identical with that used by the author. A slight difference arises in the treatment of the results.

The solution to Fick's second law, under the initial and boundary conditions which apply, was given previously, equation [11]. This may be restated in the form,

$$\frac{dc}{d\sqrt{t}\ (x=o,t)} = \frac{2\ i}{AFn\ (D\pi)^{\frac{1}{2}}} \qquad [20]$$

If the molar volume change with composition can be assumed to be insignificant, then the change in concentration and stoichiometry can be related by [21],

$$dc = \frac{d\delta}{Vm} \qquad [21]$$

where δ is the displacement of A_yB from the initial composition, $A_{y+\delta}B$. (This is equivalent to the method used by Worrell to relate concentration to voltage) Inserting [21] into [20] gives [22],

$$\frac{d\delta}{Vm} \times \frac{1}{d\sqrt{t}} = \frac{2\ i}{AFn\ (D\pi)^{\frac{1}{2}}} \qquad [22]$$

which is then converted to [23], by expansion by dE.

$$\frac{dE}{d\sqrt{t}} = \frac{2\ i\ Vm}{AFn\ (D\pi)^{\frac{1}{2}}} \frac{dE}{d\delta} \qquad [23]$$

The parameter $dE/d\delta$ can be obtained from the slope of the coulometric titration curve. All the terms in [23] are therefore known of calculable from experimentally measured parameters, and D may be evaluated.

An examination of typical results of a transient voltage versus $t^{\frac{1}{2}}$ plot, obtained by Weppner for a Li_3Sb sample, Figure 15, shows marked deviation from linearity at long times. Weppner suggested that such a deviation might have its origin either in an incorrect assumption with

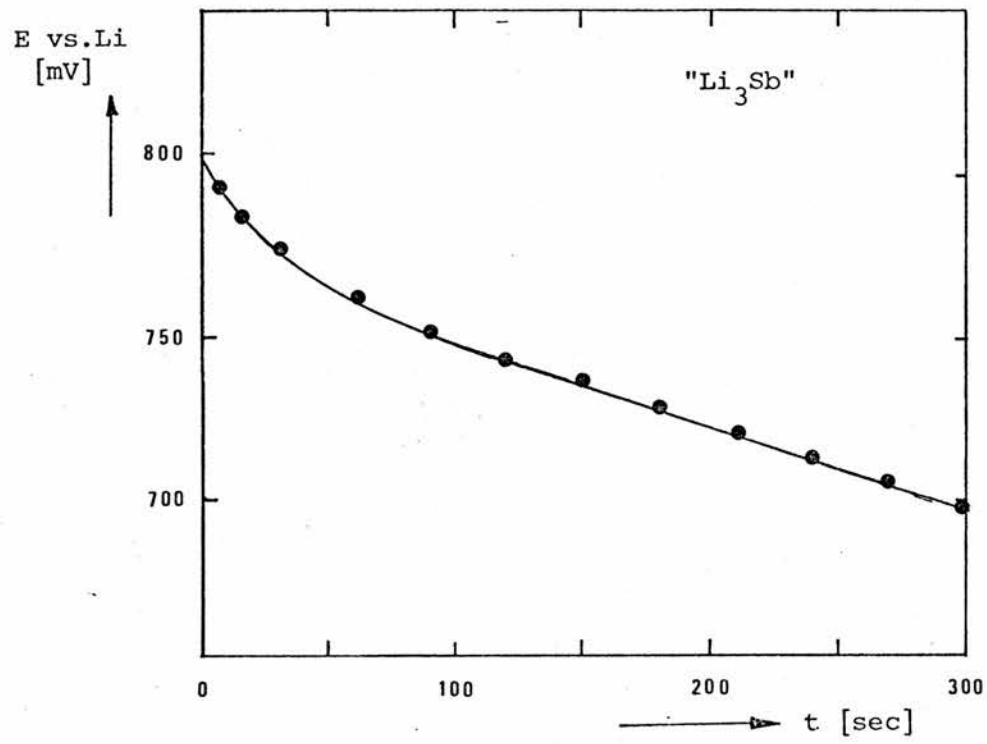

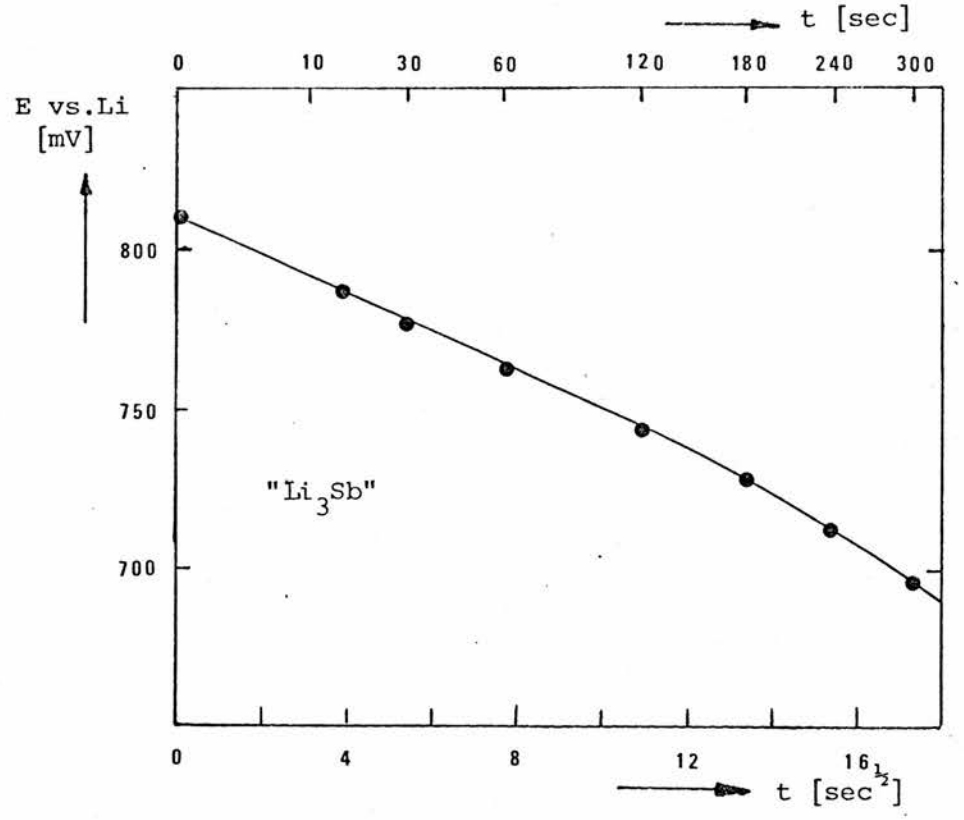

FIGURE 15 : Representation of the Transient Voltage of the Galvanic Cell as a Function of Time and the square root of time

respect to boundary conditions of the differential equations, (finite length effects), or a significant change of the thermodynamic enhancement factor over the composition range covered by the pulse titration.

Having demonstrated the failure of the method of Bonino et al associated with the use of equation [13ii], reference was made to the approaches of Worrell and Weppner. Results obtained on the Ag_xNbS_2 system were replotted according to equation [23], (y = O and δ becomes x), η(t) versus $t^{\frac{1}{2}}$. As reference to Figure 16(a) illustrates, the resulting relationship deviated slightly from linearity at long times. This situation was similar to that reported by Weppner. Consideration of the procedure used in working electrode preparation, (section 2.11) led to the proposal that finite length effects might be implicated in the observed deviant behaviour. The cathode was constructed by compression of a finely ground mixture of electrolyte and electrode material, (Plates 1 and 2) with a view to increasing the electrode surface area. The electrode was therefore a random, three dimensional arrangement of particles of electrode material and electrolyte, such that contact between electrode particles and source of electroactive species may occur at several points. Given a high diffusion of silver from contacts surrounding each electrode particle, and the small volume of the electrode particles, it seems possible that within the time-scale of the pulse the diffusion length may be comparable with the electrode particle dimensions. Under these circumstances the semi-infinite precondition has been violated and a modification of the mathematical description of the behaviour is required.

When $t > \frac{L^2}{D}$, where L is the sample thickness) equation [11] becomes,

$$C - Co = \frac{i\ t}{n\ FAL} + \frac{i\ L}{3n\ FAD} \qquad [24]$$

thus at longer times the concentration change, and also the potential change, at the electrode surface will approach a linear relationship. Reference to Figure 12, Chapter 2, appears to confirm this relationship. It can be seen from equation [24] that an alternative method of calculation of the diffusion coefficient is available as the intercept of a η(t) versus t plot extrapolated to t = O is related to the diffusion coefficient.

Returning to equation [23] and Figure 16(a) it is evident that the mathematics of the solution are such that the more useful data, at early time, is expanded by the square root of time scale in the voltage plot. This initial period contains the most valuable information in this technique because any effects due to finite sample thickness do not become important till later in the experimental timescale.

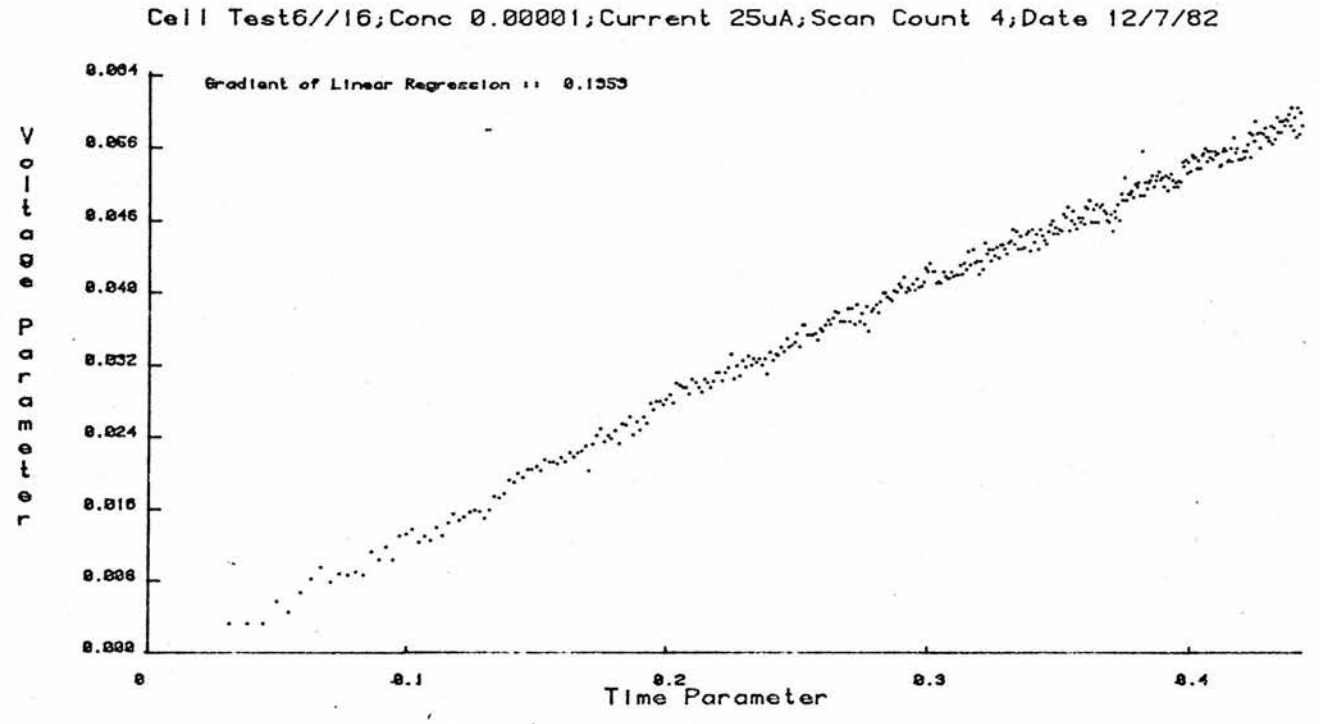

Figure 16(a): E(t) versus (time)$^{\frac{1}{2}}$, complete data

Figure 16(b): 150 data points only

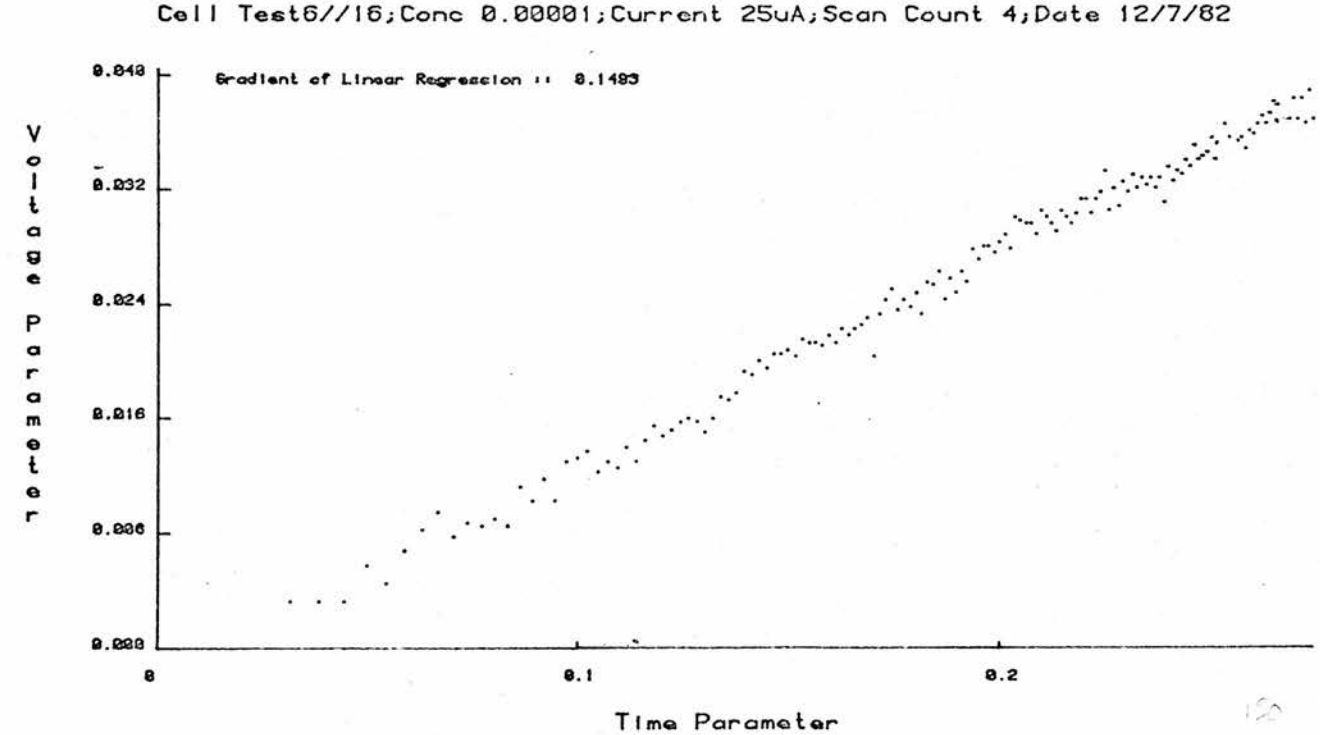

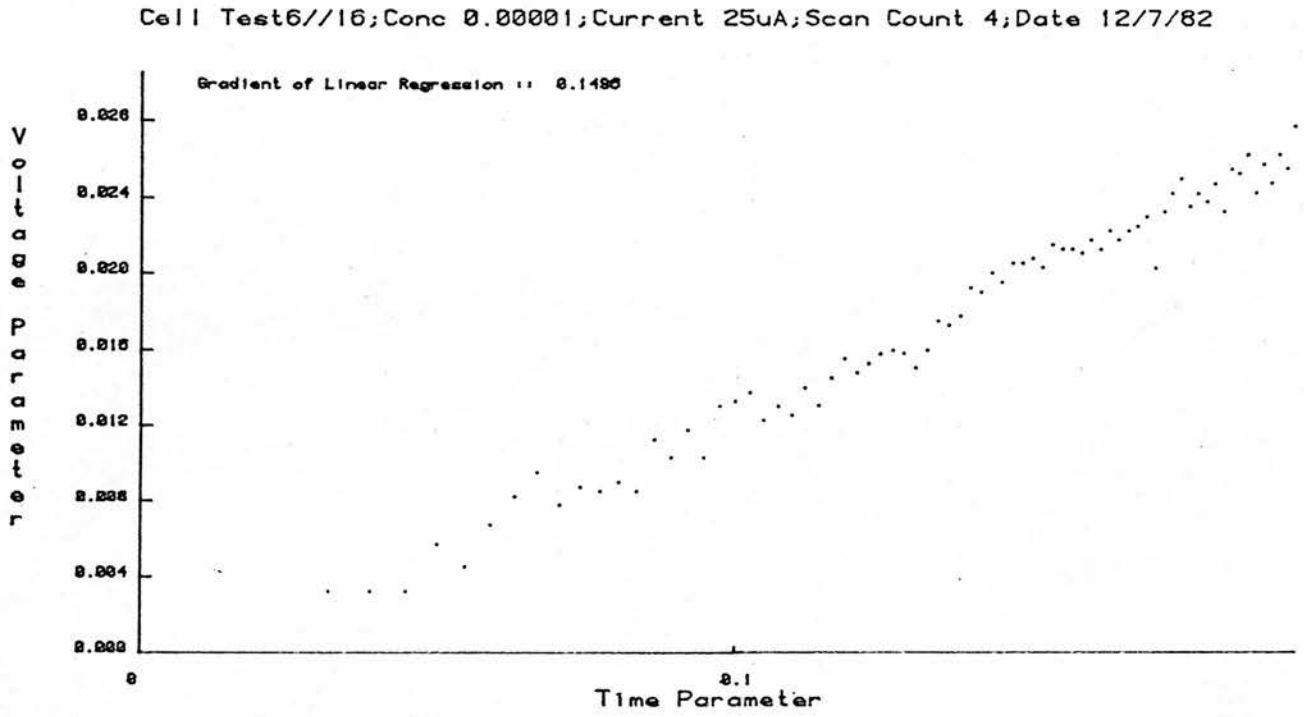

Figure 16(c): 75 data points only

Figure 16(d): Composition x = 0.05, complete data set

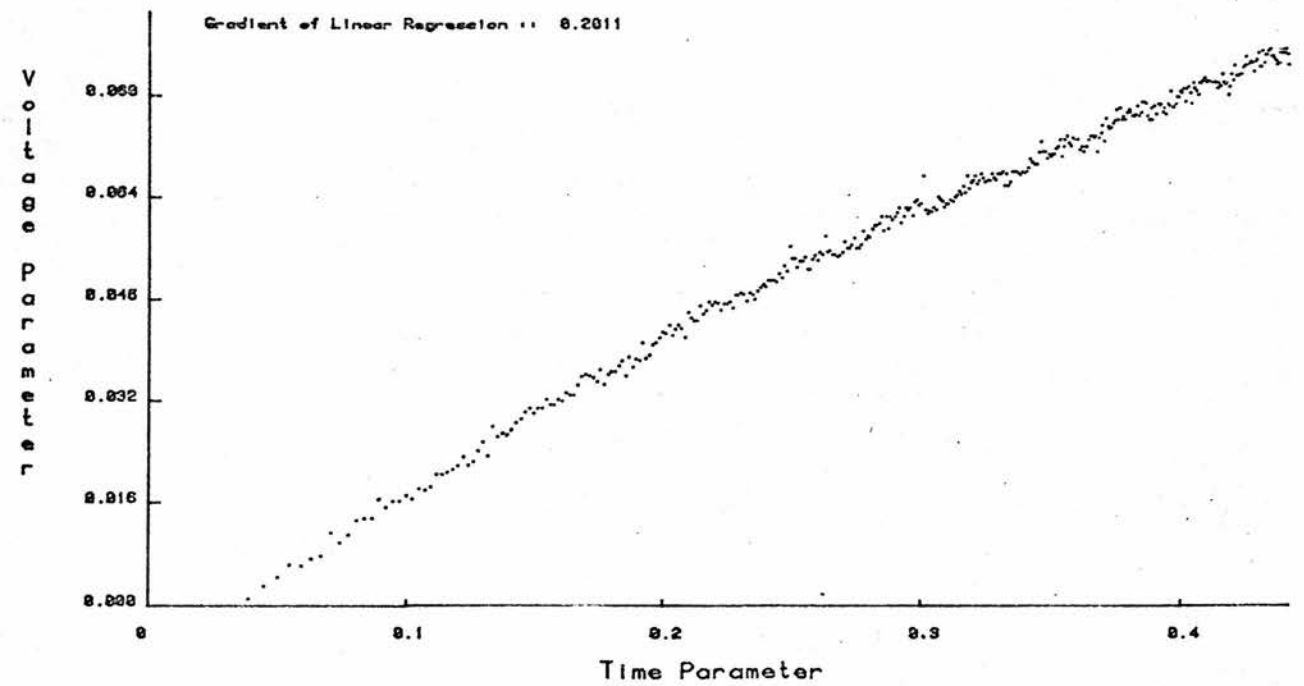

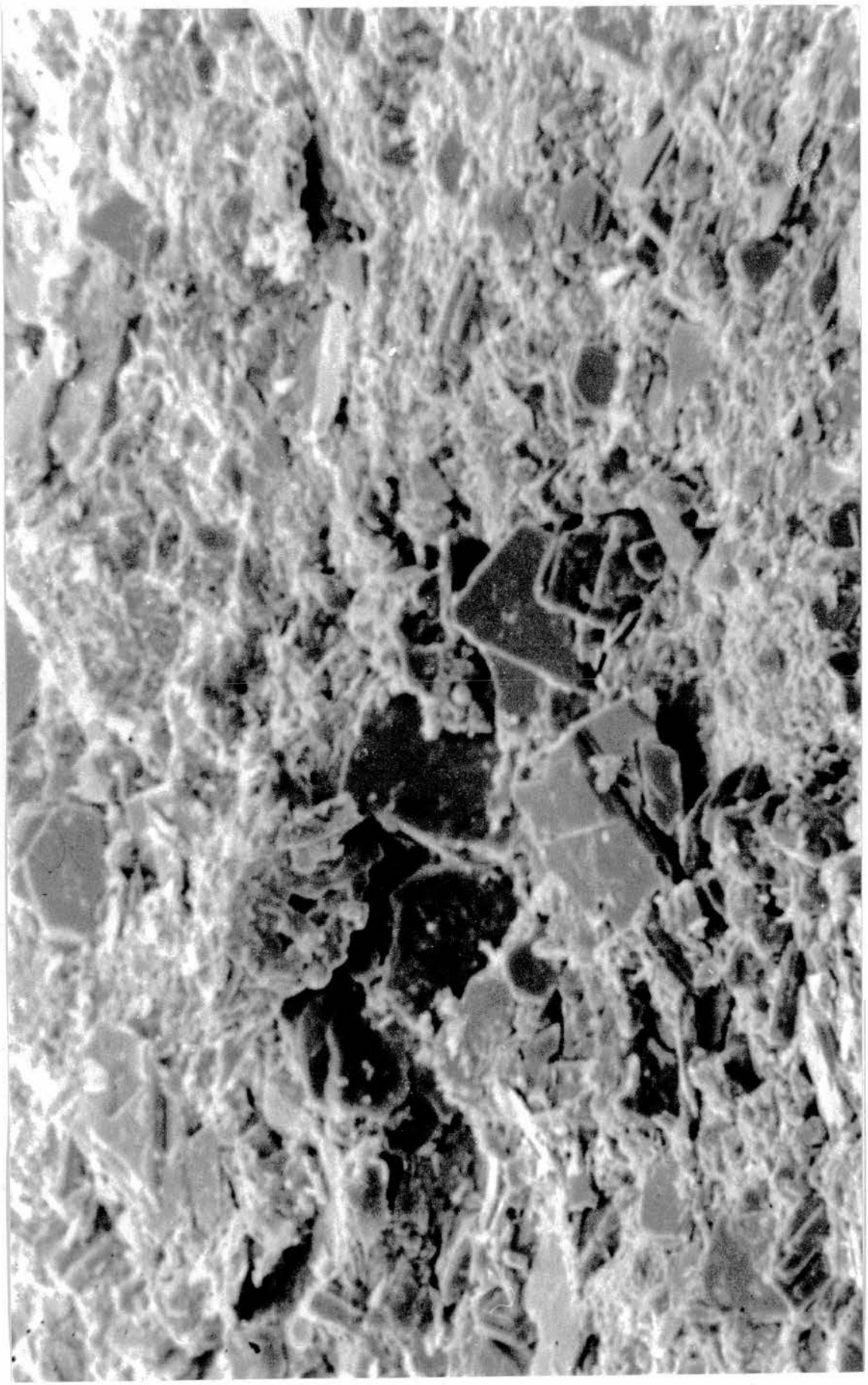

Plate 1: Surface detail of 3 electrode cell

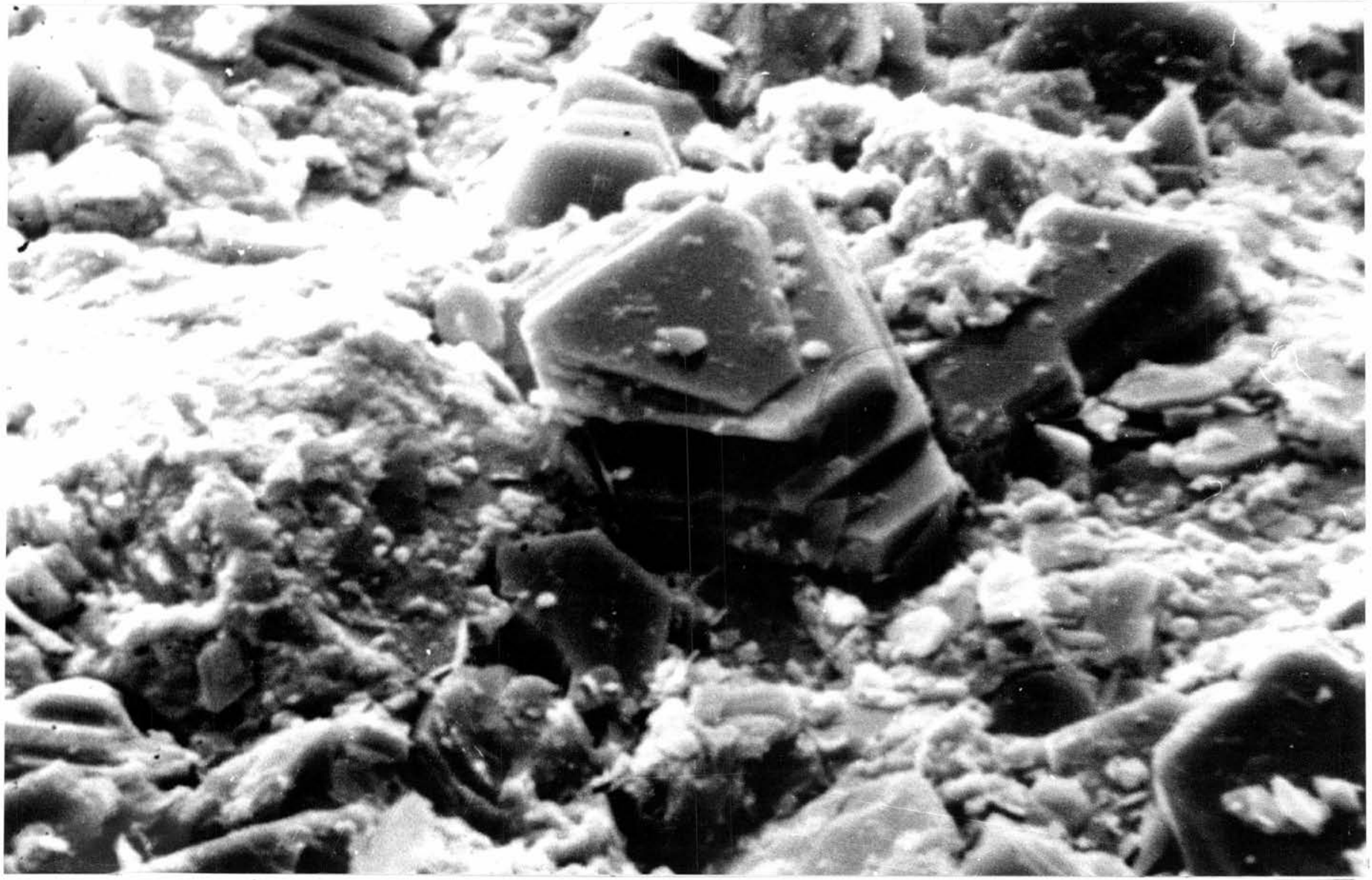

Plate 2: Surface detail of 3 electrode cell, section under increased magnification

Weppner cited the "thermodynamic enhancement, or reduction factor" as another possible influence on experiments of this type. This factor is defined as the ratio of the chemical diffusion to component diffusion coefficients.

Chemical diffusion is a process which, in solids, involves all mobile species within the system. The flux density of species, i, (in particles per square centimeter second) under the influence of an electrochemical potential gradient, $d\eta/dx$, is given for the one-dimensional case by equation [25].

$$\dot{J}_i = - \frac{\sigma_i}{n_i q^2} \frac{\partial \eta_i}{\partial x} \qquad [25]$$

where σ_i is the electrical conductivity of species i,

n_i is the valence of species i,

and q is the elementary charge.

If the electrical conductivity is expressed in terms of concentration, Ci, and electrical mobility, Ui, or the general mobility, bi, equation [26], and the electrochemical potential is expressed in terms of chemical potential μi, or the activity ai, and the electrostatic potential ϕ, equation [27],

$$\sigma_i = |n_i| q c_i u_i = n_i^2 q^2 c_i b_i \qquad [26]$$

$$\eta_i = \mu_i + n_i q \phi = \mu_i^o + kT \ln a_i + n_i q \phi \qquad [27]$$

where μ_i^o, k and T are the chemical potential of species i in the standard state, Boltzmann's constant, and the absolute temperature respectively, equation [25] may be recast as equation [28].

$$\dot{J}_i = - \frac{k T u_i}{|n_i| q} \left[\frac{\partial \ln a_i}{\partial \ln c_i} \frac{\partial c_i}{\partial x} + \frac{n_i q c_i}{k T} \frac{\partial \phi}{\partial x} \right] \qquad [28]$$

The factor in front of the square bracket is the "diffusivity of the species i as a component", D_{ki}, as represented in equation [29],

$$D_{ki} = \frac{k T u_i}{|n_i| q} = b_i k T \qquad [29]$$

The factor $\frac{\partial \phi}{\partial x}$ in the equation [28] cannot be experimentally determined but fortunately can be eliminated by the charge flux balance condition, equation [30]

$$\sum_i n_i j_i = 0 \qquad [30]$$

Rearranging and solving using equations [28] to [30], gives equation [31].

$$j_i = -D_{ki} \left[\frac{\partial \ln a_i}{\partial \ln c_i} - \sum_j t_j \frac{n_i}{n_j} \frac{\partial \ln a_j}{\partial \ln c_i} \right] \frac{\partial c_i}{\partial x} \qquad [31]$$

where $t_i = \frac{\sigma_i}{\sum \sigma_t}$ and t_i is therefore the transference number for species i.

Equation [31] may be transformed into equation [32] which contains activities and concentrations of neutral atomic species.

$$j_i = -D_{ki} \left[(1-t_i) \frac{\partial \ln a_i^*}{\partial \ln c_i^*} - \sum_{j \neq i,e,h} t_j \frac{n_i}{n_j} \frac{\partial \ln a_j^*}{\partial \ln c_i^*} \right] \frac{\partial c_i}{\partial x} \qquad [32]$$

where i*, e, and h represent neutral species, electrons and holes respectively.

Equation [32] has a form similar to the familiar expression of Fick's law, equation [1],

$$j_i = -D_i \frac{\partial c_i}{\partial x} \qquad [1]$$

and the factor which relates equation [1] and [32] is

$$W = \left[(1-t_i) \frac{\partial \ln a_i^*}{\partial \ln c_i^*} - \sum_{j \neq i,e,h} t_j \frac{n_i}{n_j} \frac{\partial \ln a_j^*}{\partial \ln c_{j^*}} \right]$$

For the case in which there is only one ionic and one electronic mobile species this factor is simplified,

$$t_e = 1 - t_i,$$

and hence the enhancement factor becomes

$$W = te \frac{\partial \ln a_i^*}{\partial \ln c_{i^*}} \qquad [34]$$

If te << 1, for an electronic insulator, for example, the case of a solid electrolyte, and as equation [35] relates activities of ions and electronic species to neutral species, we can obtain equation [36], and therefore W tends to zero.

$$d \ln a_i + n_i \, d\ln a_e = d\ln a_i - n_i \, d\ln a_h = d\ln a_{i*} \qquad [35]$$

$$W = te \left[\frac{\partial \ln a_i}{\partial \ln C_i} + n_i \frac{\partial \ln a_e}{\partial \ln c_i} \right] \qquad [36]$$

from $d c_e = n_i \, dc_i$

$$W = te \left[\frac{\partial \ln a_i}{\partial \ln c_i} + n_i^2 \frac{c_i}{c_e} \right] \qquad [37]$$

As a consequence of this, chemical diffusion of ions in solid electrolytes tends to be very sluggish. There are many cases in which electronic conductivity predominates, yet $C_i >> C_e$, and as the electrons have a much greater mobility, W can be very large. This large enhancement factor has been explained by the more mobile species moving ahead of the less mobile species, creating an internal electric field which tends to accelerate the slower particles, in order to maintain local charge flux neutrality.

The enhancement factor can be determined from the local slope of the coulometric titration curve, equation [38], and the change plotted as a function of composition. The local gradient dE/dx, was calculated for the Ag_xNbS_2 and $Ag_xTiS_{1.8}$ systems by means of a statistical package, MLP[14]. This routine optimised constants to permit the observed cell Emf to be expressed as a function of composition.

$$\frac{d \ln a^*_i}{d \ln c^*_i} = \frac{F \, x(dE)}{RT \, (dx)} \qquad [38]$$

For the present purpose the enhancement factor need not be evaluated, it is sufficient to observe that dE/dx is strongly dependant on composition at low x. This point is made by the inclusion of Figures 17 and 18, for the Ag_xNbS_2 and $Ag_xTiS_{1.8}$ systems respectively. These results suggest that the composition change which occurs during the pulse may be accompanied by a change in the enhancement factor and therefore in the diffusion coefficient, giving rise to an observed non-linearity in the voltage versus square root time plot.

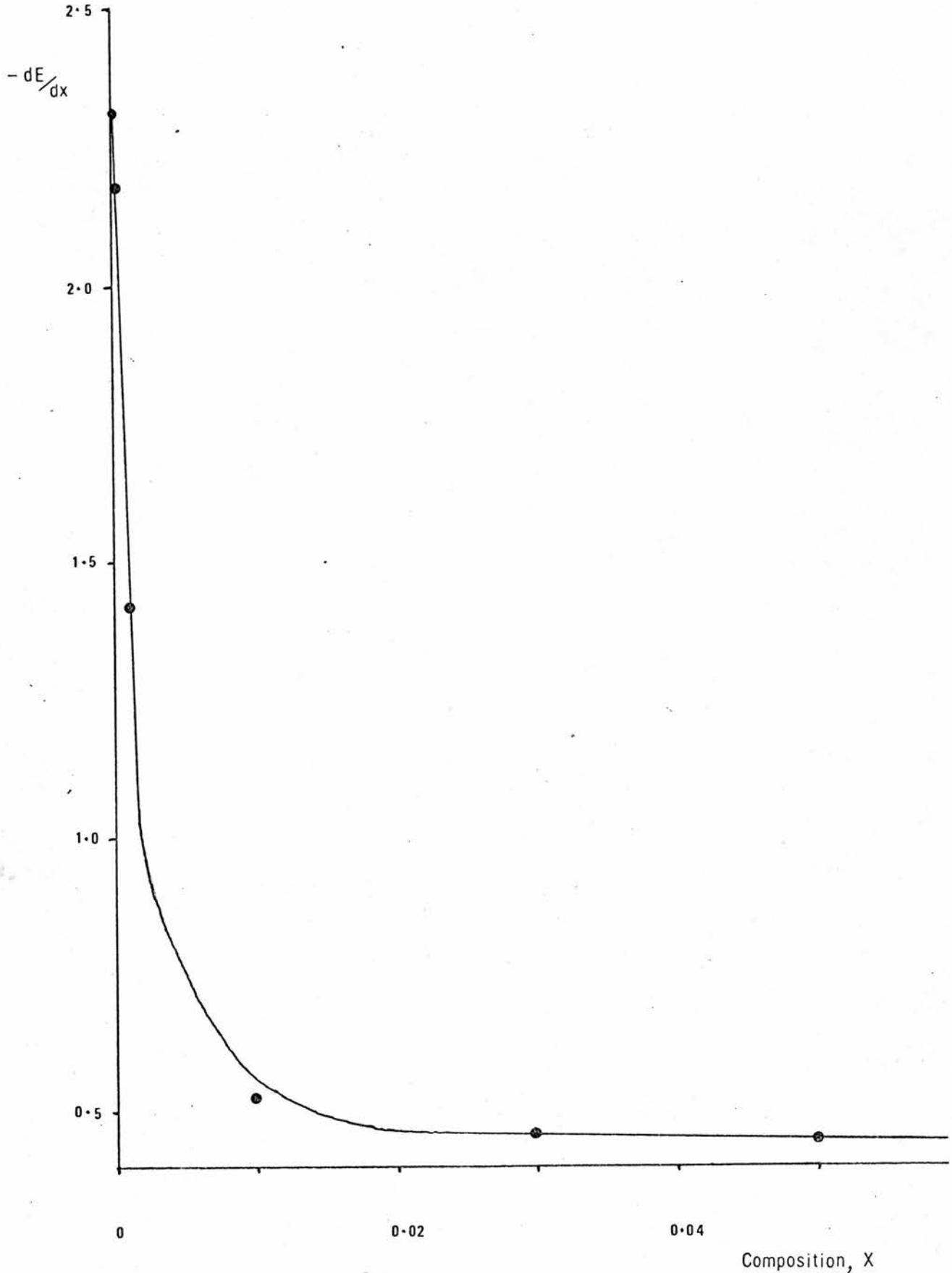

Figure 17: dE/dx versus composition, $Ag_x Nb S_2$

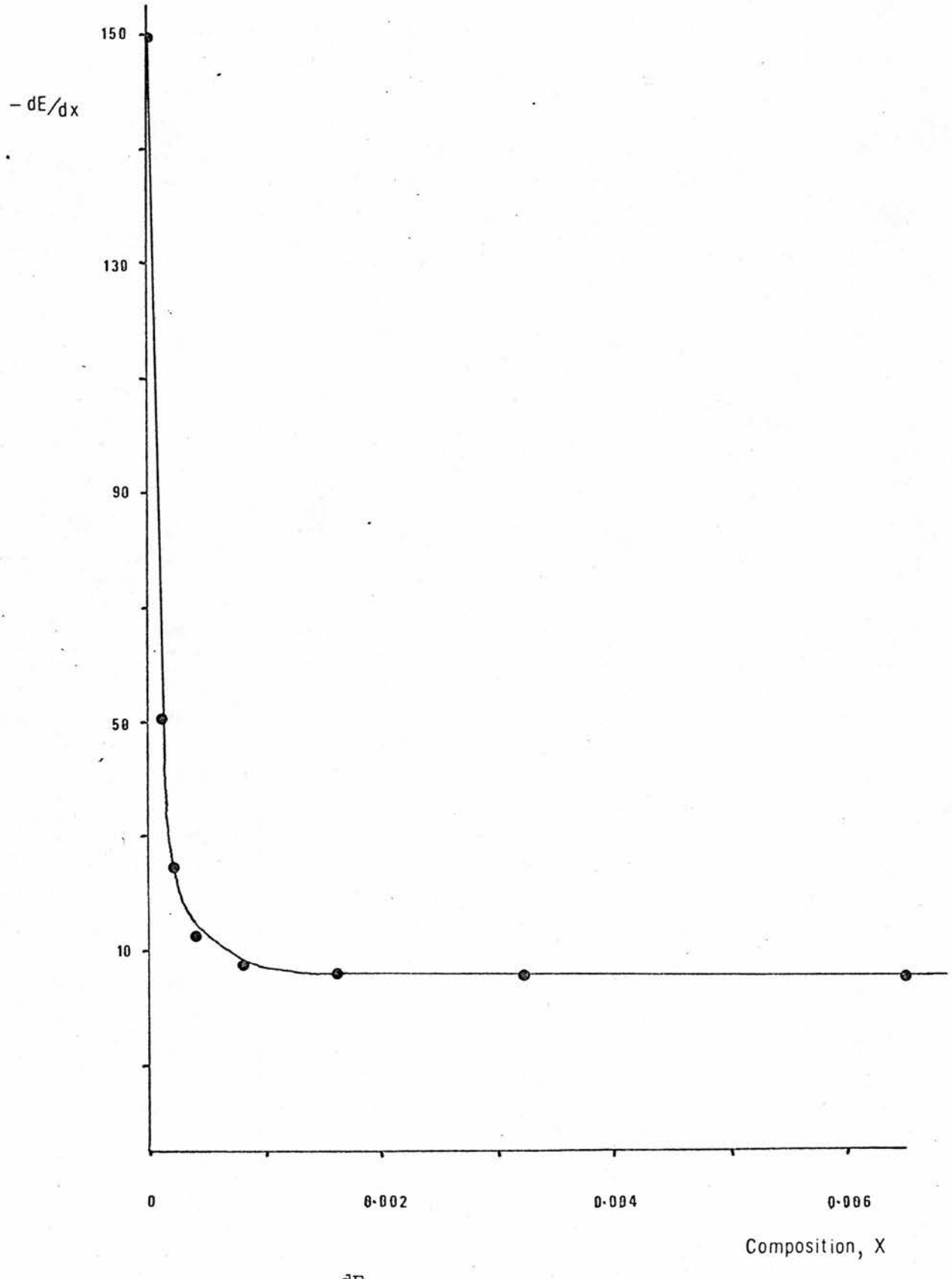

Figure 18: $^{dE}/_{dx}$ versus composition, $Ag_x Ti S_{1.8}$

As the composition of the electrode material is changed by extended galvanostatic titrations, regions are reached where the enhancement factor is no longer a strong function of composition. Under these circumstances the explanation of observed deviation from linearity in the voltage versus square root of time plot must be in terms of finite length effects.

Figures 19 and 20 are included to show the variation of the observed diffusion coefficients with composition in the Ag_xNbS_2 and $Ag_xTiS_{1.8}$ systems respectively.

Tables 2 and 3, and Figures 21 and 22, present activation energy dependance upon composition data for these systems and appear to indicate that there is little variation over the very dilute region of composition investigated.

Comparison of these reported diffusion coefficients with values available in the literature[12] leads to an apparent contradiction. Patriarca et al report values of D_{Ag} in Ag_xNbS_2, available in Table 4, considerably faster than those found in the present study. However, in the same paper, this group comment that experiments, in which NbS_2 electrodes were subjected to cathodic and anodic cycling, showed greater polarisation than might be expected on the basis of their reported diffusion coefficients. The method used by Patriarca et al to calculate the diffusion coefficient was reported in an earlier paper. Equations [13ii] and [15] were combined leading to equation [39], and the gradient of a plot of [exp (nF/RT)-1] versus $t^{-\frac{1}{2}}$, m, being used in equation [40].

$$\eta = \left(\frac{RT}{F}\right) \ln \left[1 + \frac{i\tau^{\frac{1}{2}}}{AF(\pi Dt)^{\frac{1}{2}}Co}\right] \qquad [39]$$

$$D = \frac{i^2\tau^2}{F^2\pi Co^2A^2m^2} \qquad [40]$$

As the Co^2 term in the denominator varies more strongly with respect to x than the value of m, a concentration dependance for the diffusion coefficient of the form reported by Patriarca et al would be expected.

These authors also comment that the observed dependance on concentration must be due in part to the variation of the thermodynamics factor. In this respect these authors are in agreement with the results reported above. According to the data obtained in the present study however, a much more rapid decrease as a consequence of very low levels of guest species and a subsequent approximate independance, as reported in Figure 19, would be expected.

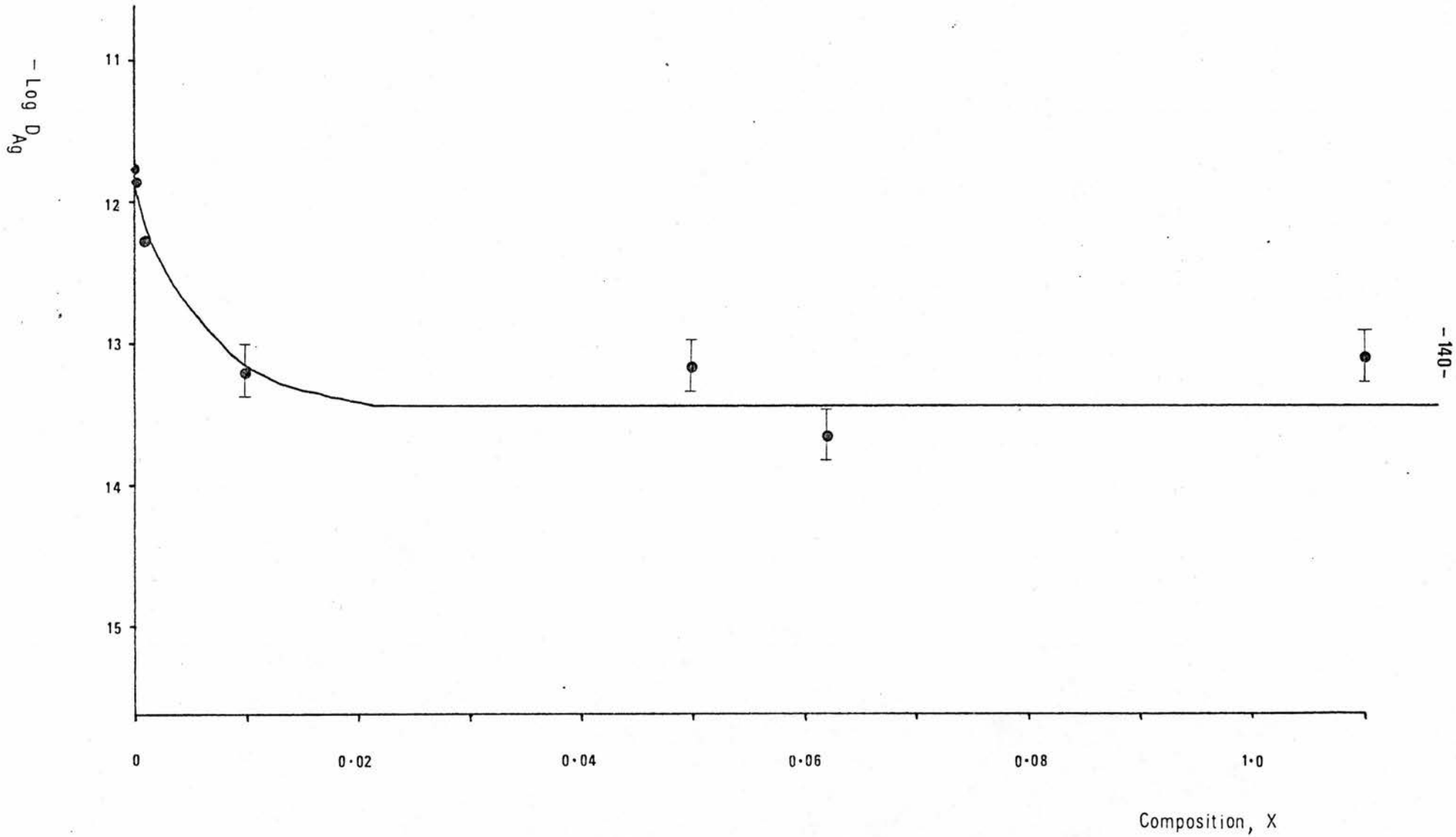

Figure 19: -Log D_{Ag} versus composition, Ag_x Nb S_2

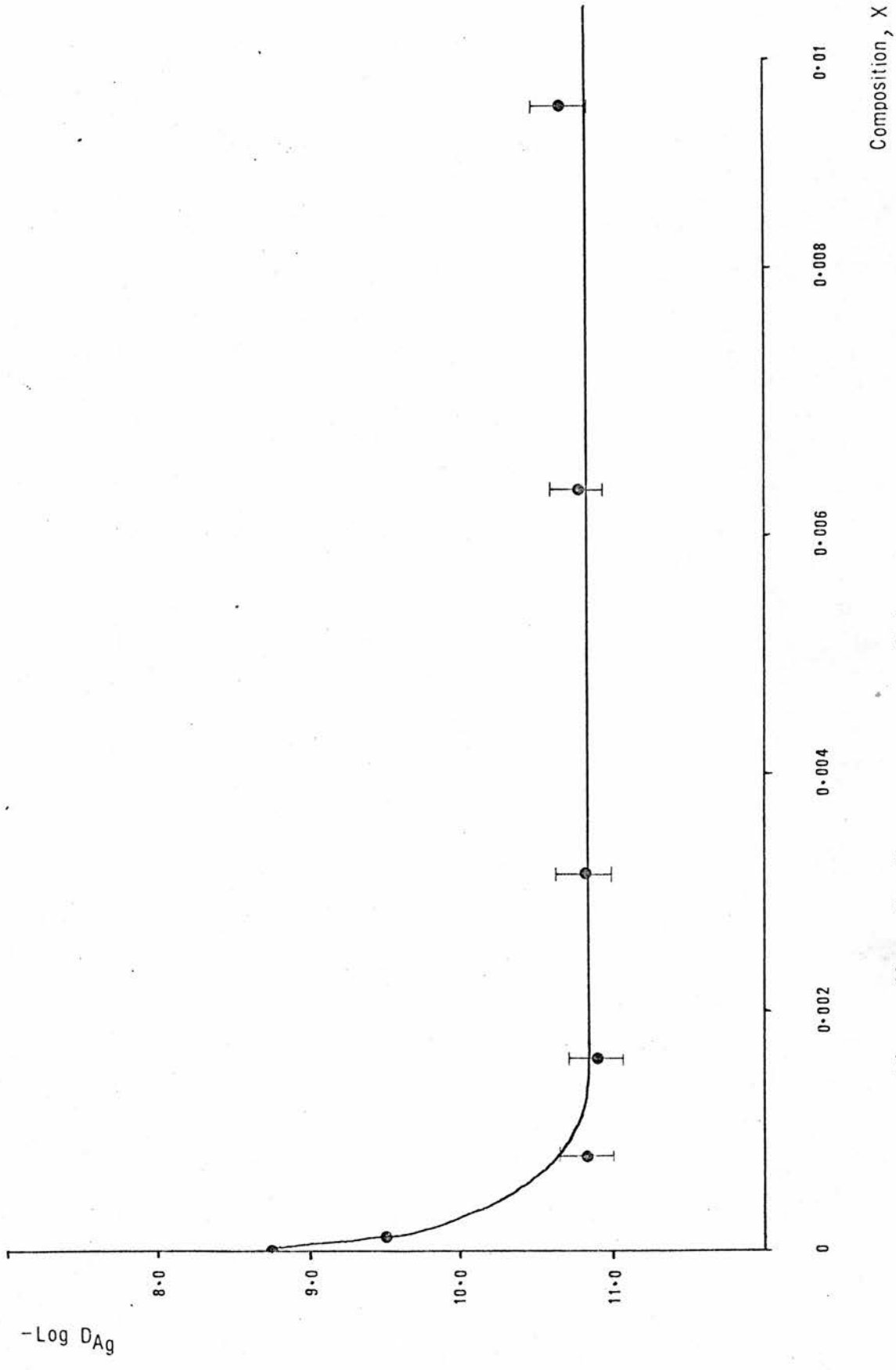

Figure 20: -Log D_{Ag} versus composition, Ag_x Ti $S_{1.8}$

Table 2: Activation Enthalpy Variation with Composition, Ag_xNbS_2

Composition, X	ΔH_{ACT} (KJ. mol^{-1})
0.0001	34.4
0.001	32.8
0.01	23.0
0.05	23.6

Table 3: Activation Variation with Composition, $Ag_xTiS_{1.8}$

Composition, X	ΔH_{ACT} (KJ. mol^{-1})
0.0001	32.0
0.0008	26.8
0.0016	30.6
0.0032	30.5
0.0064	31.6
0.0096	28.7

Table 4: Comparison of Diffusion Coefficients in Ag_xNbS_2

Composition, X	D_{Ag} (12) ($cm.^2\ s^{-1}$)	D_{Ag} Smith ($cm.^2\ s^{-1}$)
0.00001	———	1.82×10^{-12}
0.0001	———	1.35×10^{-12}
0.00013	7.52×10^{-5}	———
0.001	1.68×10^{-7}	5.5×10^{-13}
0.007	2.09×10^{-9}	———
0.010	1.36×10^{-9}	6.17×10^{-14}
0.030	2.4×10^{-10}	———
0.05	———	6.92×10^{-14}
0.06	1.55×10^{-10}	———
0.10	1.60×10^{-11}	———
0.15	8.3×10^{-12}	———

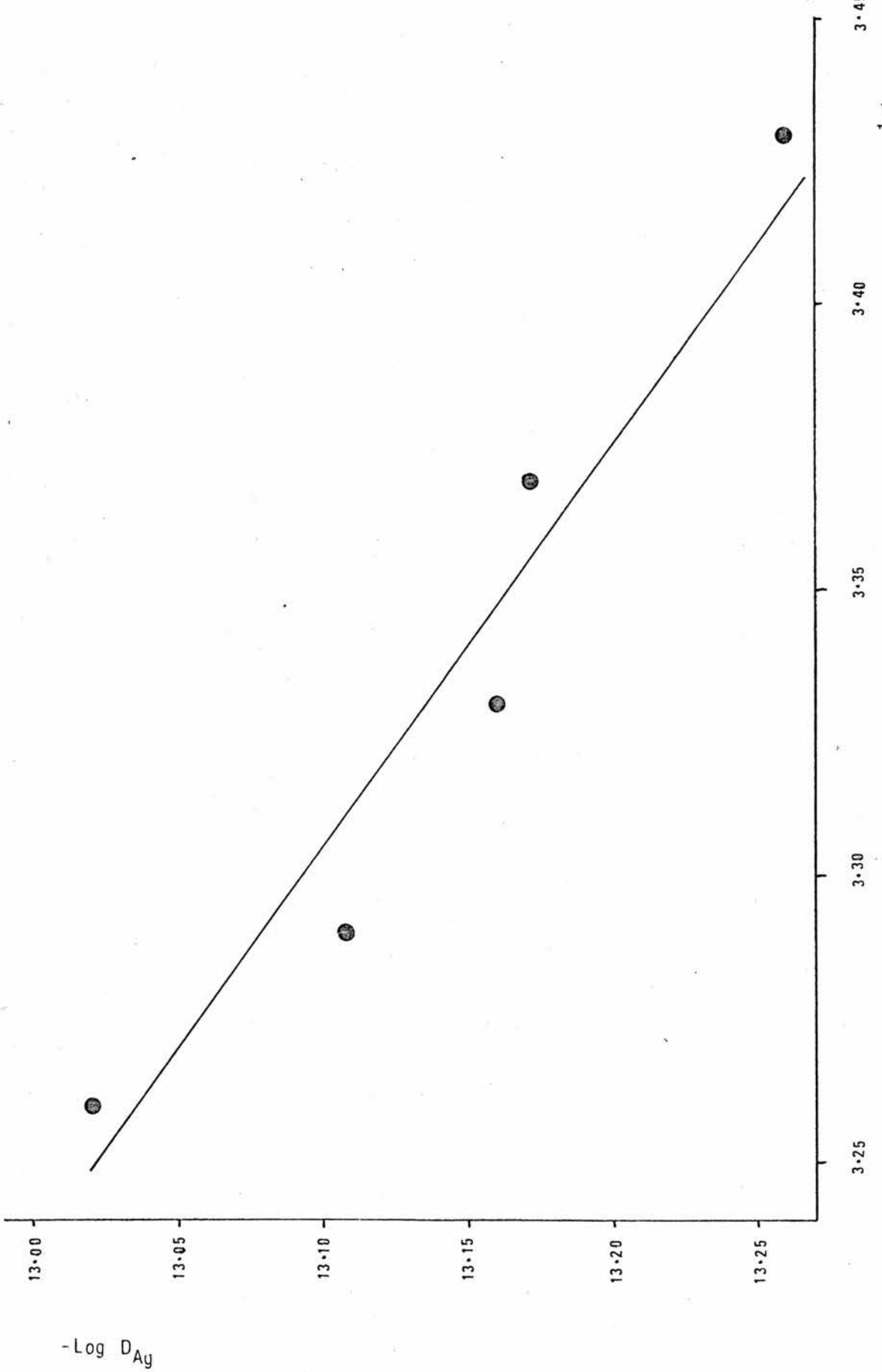

Figure 21 : -Log D_{Ag} versus $\frac{1}{T}$, Ag_x Nb S_2

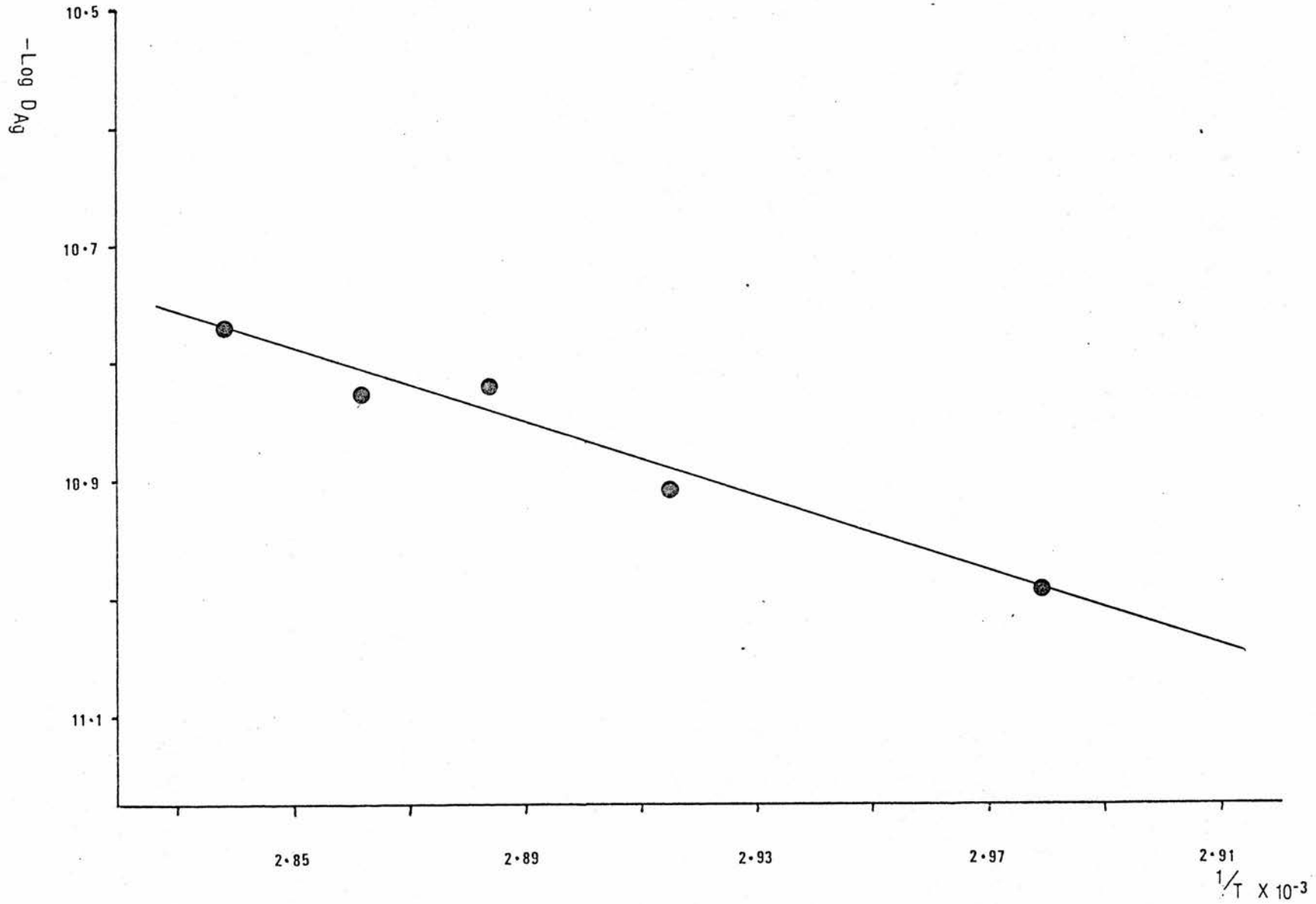

Figure 22: -Log D_{Ag} versus $^1/_T$, $Ag_x S_{1.8}$

This rapid decrease of diffusion coefficient has been experimentally verified during the course of Emf versus composition determinations. The working electrode of the cell was cathodically polarised for extended periods during which a small current was passed to change the electrode composition. The cell was permitted to recover, under open circuit conditions, when the next target composition was reached. The period of recovery was observed to increase with concentration of host species in the electrode. This observation is consistent with a decrease in the diffusion rate in the bulk electrode material[7]. If the intercalation process were continued to higher guest concentrations a further decrease in diffusion coefficient might be expected as a consequence of increasing site occupancy. In the Ag_xNbS_2 and $Ag_xTiS_{1.8}$ systems the measurements were stopped before the region of composition in which a new phase formation (expected from the thermodynamic results) was encountered. Over the dilute composition range investigated the variation of diffusion coefficient was as expected.

Results reported by other authors also investigating diffusion in transition metal dichalcogenides are less directly comparable than those of Bonino et al. Basu, Nagelberg and Shemilt all carried out experiments with sodium or lithium electroactive species. These species occupy different sites in the host lattice and have different dimensions and therefore some differences in diffusion performance may be predicted. However, there are some anomalies which warrant further discussion. In all the papers published by the Basu, Nagelberg, and Worrell group [5,6,7,15] a linear function is used to represent the voltage versus composition data. This approximation neglects the effect of the variation of the dE/dx component on the thermodynamic enhancement factor at low guest concentrations. Though the diffusion coefficient reported by Basu et al[7] for Li_xTaS_2 (Figure 6), appears to correlate well with structural information regarding van der Waal's dilation, this may be partly due to the above approximation. If the dE/dx values reported by Thompsom[16] were used to calculate the diffusion coefficient in a modified expression, a variation similar to those obtained in the present work might be obtained.

Various authors working with electrochemical pulse techniques have reported results with a broad error bar on their diffusion coefficients. Errors from a variety of sources are unavoidable under the experimental conditions used. With compacted polycrystalline electrodes in solid electrolyte cell systems it is very difficult to define the true electrode/electrolyte surface area and the appropriate boundary conditions associated with the diffusion equation. When the electrode is constructed from an electrolyte/electrode

investigation on single crystals and their results may therefore be expected to differ from those obtained with compressed polycrstalline samples. Values of diffusion coefficient, estimated from optical front movement at $80^{o}C$, were within the range $10^{-9} \rightarrow 10^{-10}$ cm^{2} sec^{-1}. Although the concentration range investigated was not reported, as the product was identified as Stage 1, the levels are probably of the same order as the present investigation.

Of particular interest in the preliminary report of Frindt et al[17] is the comment that a crystal thickness effect was noted. These authors considered that thin crystals may enhance the diffusion of guest species as a consequence of electric fields within the crystal. This may have important implications for electrode construction in high power miniature cells. If it were possible to prepare crystals of controlled thickness this might provide the basis of a useful study.

material mixture, as in the present case, the use of the electrode cross sectional area is only an approximation. This estimate is however maintained constant throughout the experiments and it should be possible to compare systems under closely reproduced experimental conditions. The use of mixed electrodes of this type, while increasing the electrode surface area, may also lead to some reduction in the weight of electrode material actually utilised, through isolation of particles with no conducting path to the external contacts. This loss is assumed to be negligible.

The use of liquid electrolytes introduces other problems, (electrolyte penetration of the electrode, wetting effects, etc) and while single crystal work would provide additional information of grain boundary and orientation effects it is plagued by other problems[13]. (crystal mounting, contact problems, etc)

In the method of calculation of the diffusion coefficient used for the Ag_xNbS_2 and $Ag_xTiS_{1.8}$ systems there are additional sources of error. The use of a "stopping procedure" in the acquisition of a gradient from the transient voltage versus square root of time plot, and of an equation to model the voltage versus composition behaviour of the electrode material in order to obtain the dE/dx term, introduces further uncertainty. These parameters are combined in equation [23], but whether their variation is independant or dependant is not known. A relationship between these paramaters would affect the total error involved in the final diffusion coefficient. At low concentrations of guest species in the host lattice the dE/dx term is strongly dependant on composition and the gradient fitted has larger errors caused by covariance of the fitted parameters. Contributions to these errors may be reduced by using sufficient data from thermodynamic investigations and adopting a consistent routine for calculation of gradients from transient voltage versus square root of time plots. Uncertainty in diffusion coefficients calculated necessarily results in uncertainty in activation energies quoted for the diffusion process.

The development of the lithium ion conducting electrolyte was intended to lead to a comparison of results obtained with the present method and those of other authors in the Li_xTiS_2 system. A three electrode cell was prepared using $Li_xV_6O_{13}$ as a counter and reference electrode material and TiS_2 as working electrode. However, although cell construction difficulties were overcome, the cell voltage between the two electrodes was apparently too high, leading to decomposition of the electrolyte. Investigation of a three electrode cell with $Li_xV_6O_{13}$ counter and reference electrodes and a V_6O_{13} working electrode was also attempted. Unfortunately the thermodynamic data

for this cell was not as detailed as required for confident evaluation of dE/dx, and as the voltage drop between reference and working electrodes was high the data obtained during experiments cannot be considered to be accurate. (The estimated diffusion coefficient range is 5×10^{-12} - 2×10^{-12})

5.4 Conclusions and Further Work

In conclusion, considering the degree of approximation involved in their calculation diffusion coefficients obtained by the methods described cannot be considered to be absolute values. The advantage of the technique is in the ease of comparative studies under closely reproduced experimental conditions. In the absence of alternative methods electrochemical techniques represent the most accurate means of assessing candidate solid solution electrode materials.

The field of diffusion coefficient determination still presents some inconsistencies. It would be of interest to investigate other lithium ion conducting electrolytes with a view to achieving the comparison attempted between the present reported method and those of other groups. In principle it is only the absence of a convenient electrolyte which prevents this comparison.

Investigation of silver guest species is much more simply undertaken because of the availability of several highly conductive, room temperature, electrolytes. Shemilt et al[13] attempted a comparison of stoichiometric and non-stoichiometric titanium disulphide electrode materials, but unfortunately there was an error in their analytical technique[5]. Such an investigation could be carried out using the present experimental set up.

While the present method uses voltages recorded during the perturbing galvanostatic pulse, and therefore requires the use of fast recording devices, the technique reported by Basu et al[7] is more easily applied and should be reinvestigated. A slight modification of equation [15] would permit an improved result to be obtained. It may prove convenient to operate this technique in conjunction with the present technique and thereby obtain a confirmatory value of the diffusion coefficient.

$$\frac{dE}{dt}^{-\frac{1}{2}} = \frac{i \tau Vm}{nFA (\pi D)^{\frac{1}{2}} dx} \frac{dE}{dx} \qquad [41]$$

Recently the process of silver species intercalation and the structural consequences on crystals of TaS_2 and TiS_2 has been investigated by optical and scanning electron microscopy[17]. Frindt et al carried out this

1. Crank J., "The Mathematics of Diffusion", (Oxford University Press, London 1975)

2. Huggins R.A., Weppner W., J. Electrochem. Soc., Vol 124, No 10, (1977) 1569

3. Boukamp B.Á., Huggins R.A., Wen. C.J., J. Electrochem. Soc., Vol 126, No 12, (1977) 2258

4. Huggins R.A., Weppner W., J. Solid State Chemistry, Vol 22, (1977) 297

5. Nagelberg A.S., Worrell W.L., "Proceedings of the Symposium on Electrode Materials and Processed for Energy Conversion and Storage" (Eds) McIntyre, Srinivasan and Will, (Electrochem. Soc., Princeton. 1977)

6. Basu S., Worrell W.L., ibid., (1977) 861)

7. Basu S., Worrell W.L., "Fast Ion Transport in Solids", (Eds) Vashishta, Mundy and Shenoy, (North-Holland, Amsterdam 1979)

8. Bonino F., M.Sc. Thesis, University St Andrews (1979)

9. Bonino F., Lazzari M., Vincent C.A., Wandless A.R., Solid State Ionics, Vol 1, (1980) 311

10. Bottelberghs P.H., Broers G.H.J., Electrochemica Acta., Vol 21 (1976) 719

11. Scholtens B.B., Mat. Res. Bull., Vol 11 (1976) 1533

12. Bonino F., Lazzari M., Patriarca M., Scrosati B., Voso M.A., Solid State Ionics, Vol 6, (1982) 15

13. Shemilt J.M., Steele B.C.H., Winn D.A., Mat. Res. Bull., Vol 11, (1976) 559

14. Ross G.J.S., "Maximum Likelihood Program", (Rothamsted Experimental Station 1980)

15. Nagelberg A.S., Worrell W.L., J. Solid. State. Chemistry, Vol 29, (1979) 345

16. Thompson A.H.,"Fast Ion Transport in Solids", (Eds) Vashishta, Mundy and Shenoy, (North-Holland, Amsterdam 1979)

17. Frindt R.F., Jöensen P., Reyes J.M., Scholz G., Physica B, Vol 105, (1981) 214

CHAPTER 6: ELECTRONIC CONDUCTIVITY

6.1 Introduction

For more than a century solid materials capable of conducting electricity by ionic transport have been known. Prior to 1966[1], as far as electrochemical applications were concerned, it was generally believed that the high resistance of these compounds, designated solid electrolytes, made their employment unlikely.

Within a year however, discoveries by three separate groups, Bradley and Greene[2], Owens and Argue[3], (with electrolytes based on silver iodide, of the general formula M Ag_4I_5), and by Yao and Kummer[4], (in single crystal ßalumina) had entirely altered the electrochemists' view of solid electrolytes. Some electrolytes bases on silver iodide show conductances of up to 10 Sm^{-1} at room temperature and the diffusion coefficients reported for sodium ions in ß alumina are comparable with that of sodium in molten sodium nitrate. These results initiated an upsurge of interest in solid electrolytes which continues today.

In practical devices solid electrolytes have several obvious advantages related to the absences of leakage problems and ease of cell construction, but also have some disadvantages, the most important of which is probably the presence of electronic conductivity. All solid electrolytes suffer this handicap though the range of values reported for different materials is very large. Ionically conducting materials which show high electronic conductivity may find use as solid solution electrodes, discussed in previous chapters, while those with very low levels are of most interest as electrolytes.

The total conductivity of a material is a sum of the ionic and electronic conductivities, (equation [1]).

$$\sigma_{TOTAL} = \sigma_{IONIC} + \sigma_{ELECTRONIC} \qquad [1]$$

which may be expressed in terms of transference numbers,

$$t_i = \frac{\sigma_i}{\sigma_{TOTAL}} , \qquad t_e = \frac{\sigma_e}{\sigma_{TOTAL}}$$

in fact a more important relationship is that between the amount of charge passed ionically with electron transfer through the external circuit Q ionic, and the amount passed by internal electronic conduction, Q electronic.

$$Q\ TOTAL = Q\ IONIC + Q\ ELECTRONIC$$

The faradaic efficiency of a cell, η_F, is given by equation [2]

$$\eta_F = \frac{Q\,i}{Q\ \text{TOTAL}} \qquad [2]$$

This parameter depends upon the rate at which charge is drawn from the storage device. The extreme example is a cell maintained in open status until total discharge. The faradaic efficiency of this cell would be 0%. This example illustrates the importance of evaluation of the electronic conductivity when considering an electrolyte for a primary storage cell application.

Initial assessment of the electronic conductivity of a novel electrolyte should be carried out by the Tubandt transference method. The use of this technique establishes whether mixed conduction, (where the electronic conductivity is greater than a few percent of the total conductivity), or co-ionic conduction, (where there is more than one mobile ion), occur to a significant extent. The experiments are limited in the accuracy of the results they provide and where the electronic conductivity of the sample is less than about 1% the most effective method of measurement is by the Hebb-Wagner technique[6,5]. To understand the restrictions in application of this technique a full description of the method is necessary.

6.2 Wagner Method for the Determination of σ_e

This technique, sometimes referred to as the d c polarisation method, was described by Wagner[5] in 1933. Numerous examples of the evaluation of the electronic conductivity of binary compounds using this method are available in the literature. One of these, AgBr[6], will be used to illustrate the application of the technique, and derive the relationship between current and voltage due to excess electron and hole carriers.

If a d c potential is applied to the cell shown in Figure 1, the bromine reversible electrode polarised positively with respect to the carbon blocking electrode, and the potential across the cell is less than the decomposition potential of the electrolyte at the bromine electrode pressure, there can be no discharge of metallic silver at the cathode. Under these circumstances the activities of both components are fixed, at the blocking electrode, by the potential and the activity of the components may be derived, from consideration of the situation in a "concentration cell" of either of the electrolyte components.

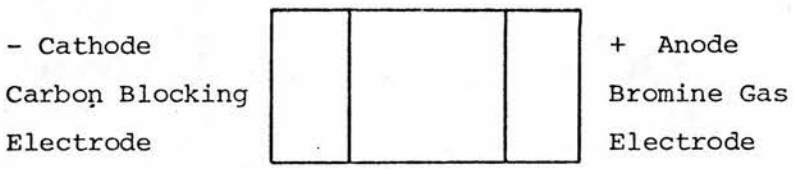

Electrode 1: Non-reversible Blocking Electrode

Electrode 2: Reversible Bromine Electrode

Figure 1: Electrode configuration used by Raleigh[6]

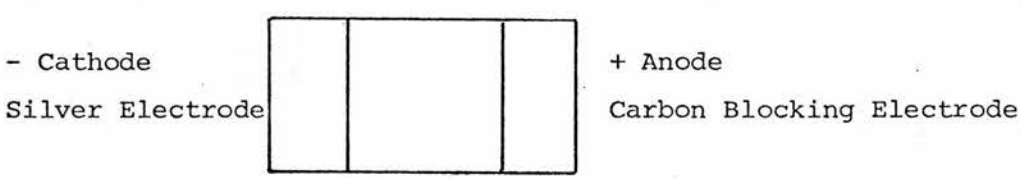

Electrode 1: Reversible Silver Electrode

Electrode 2: Non-reversible Blocking Electrode

Figure 2: Electrode configuration used by Illschner[7]

$$a_{Ag^+} = \exp\ [-\ (Ed - E)F/RT\ ] \qquad [3]$$

$$P_{Br_2} = P^{\circ}_{Br_2} \exp\ (-2EF/RT) \qquad [4]$$

When the polarising potential is first applied to the cell there will be transient ionic migrations in the electrolyte in response to the electric field. Some period after the cell polarisation a steady state condition will be reached, when the motion of the ions in the electric field has given rise to a deficit of the mobile ion at the blocking electrode, which is of course a poor source of this species. During the steady state condition the migration of ions due to the field will be balanced by the counter diffusion due to the concentration gradient. The current measured in the external circuit will be exclusively due to the movement of either excess electrons, or excess holes, depending on which predominates under the experimental conditions in the electrolyte.

Equation [4] shows that there will be a steady state of gradient of bromine pressure across the cell. As bromine vapour induces hole formation according to equation [5],

$$\tfrac{1}{2}\ Br_2 \rightleftharpoons Br^{-}\ \text{(in AgBr)} + \oplus\ \text{(in AgBr)} \qquad [5]$$

the potential across this cell will result in a hole concentration gradient across the cell. This will give rise to a diffusion flux, which may be treated by Fick's law, thus,

$$j_{\oplus} = -D_{\oplus} \frac{d\,n_{\oplus}}{d\,x} = D_{\oplus} \frac{(n^{\circ}_{\oplus} - n_{\oplus})}{L}$$

where $n_{\oplus}$ is the concentration of holes, and L is the length of the cell.

$$j_{\oplus} = \frac{D_{\oplus}\, n^{\circ}_{\oplus}}{L} \left(1 - \frac{n_{\oplus}}{n^{\circ}_{\oplus}}\right), \text{ from [4]}$$

$$j_{\oplus} = \frac{D_{\oplus}\, n^{\circ}_{\oplus}}{L} \left(1 - \exp\ \left(\frac{-EF}{RT}\right)\right)$$

but using,

$$D_{\oplus} = \frac{RT}{F} \mu_{\oplus}, \quad i_{\oplus} = q\, j_{\oplus} \quad \text{and}$$

$$\sigma^{\circ}_{\oplus} = n^{\circ}_{\oplus} \, q \mu_{\oplus}$$

where q is the electronic charge and $\mu_{\oplus}$ is the mobility, equation [6] is obtained,

$$i_{\oplus} = \frac{RT}{LF} \sigma^{\circ}_{\oplus} \left[1 - \exp \left(\frac{-EF}{RT}\right)\right] \qquad [6]$$

which relates the current to the applied potential in a cell with a reversible bromine electrode. As the applied potential increases the current will approach a plateau region. If the contribution from excess electrons is derived (in an identical manner), using the fact that the concentration of excess electrons varies inversely with the concentration of holes, equation [7] is obtained.

$$i_{\ominus} = \frac{RT}{LF} \sigma^{\circ}_{\ominus} \left[\exp \left(\frac{EF}{RT}\right) - 1\right] \qquad [7]$$

As equation [7] shows the current increases in a quasi-exponential manner with potential. In principle then, an electrolyte with suitable values of $\sigma^{\circ}_{\oplus}$ and $\sigma^{\circ}_{\ominus}$ might be expected to show a constant current region at low potentials and an exponential rise at higher potentials. At still higher applied potentials a decomposition current would be recorded.

In none of the electrolytes investigated up to the present time has it been possible to obtain $\sigma^{\circ}_{\oplus}$ and $\sigma^{\circ}_{\ominus}$ with the same cell arrangement. Complementary cell arrangements must be used to obtain these parameters separately. Illschner[7] used the cell shown in Figure 2 to obtain $\sigma^{\circ}_{\ominus}$. Analogous current expressions, to equations [6] and [7], which show reversed roles for electrons and holes, that is, a plateau due to $\sigma^{\circ}_{\ominus}$ and an exponential rise due to $\sigma^{\circ}_{\oplus}$, are obtained with this arrangement.

Where silver ion conducting electrolytes are used in primary cells[8], it is of interest to know the magnitude of electronic conduction. In this work the value of σ_e in the silver iodide based iodotungstate and iodoarsenate electrolytes were investigated. While in simple binary electrolytes it is possible to use both cell arrangements, in the present cases, where the function of the silver tungstate and silver arsenate components of the electrolytes, and the decomposition products of the electrolytes, have not been identified, it was decided to restrict the investigation to the current-voltage relationship of the cells using a reversible silver electrode arrangement. Under these circumstances equation [8] is appropriate.

$$i_{TOTAL} = i_{HOLES} + i_{ELECTRONS}$$

$$i_T = \frac{RT}{LF} \left[\left[\sigma^{o}_{\oplus} \left(\exp^{(EF/RT)} - 1 \right) \right] + \sigma^{o}_{\ominus} \left[1 - \exp^{(-EF/RT)} \right] \right] \qquad [8]$$

6.3 Results and Discussion

Preliminary work on the decomposition products of the iodoarsenate electrolyte implicated oxygen as a gaseous product at the anode, and prompted the investigation of the influence of an oxygen atmosphere on the electronic conductivity. Using the cells and experimental set up described in Chapter 2, sections 2.18 and 2.20 respectively, the effect of environment on the current voltage relationship was investigated. The currents recorded are plotted as a function of applied potential in Figures 3 to 6.

A significant feature of these results is the low level of excess electron conduction. These results are in contrast to those reported by Minami et al[8] for the pseudo-binary AgI - $Ag_2 MoO_4$ electrolyte in which conduction due to electrons was reported to be approximately 9×10^{-9} S.cm.$^{-1}$. These electrolytes, being based on silver iode, with similar methods of preparation, might have been expected to show similar conduction characteristics. The results obtained for the iodoarsenate and iodotungstate systems indicate that the electron conductivity is less than 2×10^{-11} S.cm.$^{-1}$ at 40°C for both electrolytes.

If the electrolytes behave according to equation [8], as predicted by Wagner, the currents registering at approximately 500 and 590 mV for iodoarsenate and iodotungstate respectively, are due to the presence of hole conduction, and by plotting log i versus E, the parameter $\sigma^{o}_{\oplus}$, the hole conductivity may be calculated, (equation [8a]).

$$I_T = I_{\oplus} = \frac{RTA}{LF} \sigma^{o}_{\oplus} \left[\exp \left(\frac{EF}{RT} \right) - 1 \right] \qquad [8a]$$

Under the condition that EF >> RT, this may be simplified to give equation [9].

$$i_T = i_{\oplus} = \frac{RTA}{LF} \sigma^{o}_{\oplus} \exp \left(\frac{EF}{RT} \right) \qquad [9]$$

Values of $\sigma^{o}_{\oplus}$, and conditions of measurements, are reported in Table 1. These results were calculated from currents measured near the

Table 1: Electronic Conductivities, Conditions of Measurement and Limits of Confidence for Iodoarsenate and Iodotungstate Electrolytes

Electrolyte	Flow Gas	Temp (^{o}C)	σ (S. cm^{-1})	σ Range (S.cm^{-1})
Iodoarsenate	N_2	40.0	2×10^{-19}	1.6×10^{-19} - 2.5×10^{-19}
	N_2	25.0	4×10^{-20}	1.3×10^{-21} - 2.3×10^{-19}
	O_2 (wet)	35.6	8.5×10^{-20}	1.9×10^{-20} - 2.6×10^{-19}
	O_2	25.0	6.5×10^{-21}	3.4×10^{-22} - 3.9×10^{-20}
Iodotungstate	N_2	40.7	1.4×10^{-19}	3.5×10^{-21} - 4.4×10^{-19}
	N_2	25.4	7×10^{-20}	5×10^{-20} - 4×10^{-19}
	O_2 (wet)	39.3	3×10^{-19}	3.5×10^{-20} - 1.3×10^{-18}
	O_2	25.0	5×10^{-20}	3.5×10^{-22} - 8×10^{-19}

Table 2: Electronic Conductivity due to Holes Reported for Other Electrolytes

Electrolyte	σ_e S.cm^{-1}	Temp (^{o}C)
$RbAg_4I_5$	7×10^{-19}	25
$RbCu_3Cl_4$	2×10^{-16}	25
ß-PbF_2	1.7×10^{-20}	125
Li_3N	1×10^{-12}	200
CaF_2	1×10^{-8}	600
$C_6H_{12}N_4RX$-CuX X=I, Br, Cl R=H, CH_3	1×10^{-11}	100
Li/Al_2O_3	5×10^{-27}	300

detection limit of the current amplifier and are reported with large error bars. This in turn gives rise to limits of confidence with which the hole conductivity can be quoted.

The results, Figures 3 to 7, demonstrate the prevalence of electron hole conduction, but do not provide conclusive evidence of the involvement of oxygen in the electronic conduction process.

Table 2[13] is included to provide comparison with electronic conductivity due to electron holes in other solid electrolytes. The table demonstrates the large range of conductivities reported.

Various authors have commented on the problems encountered in the measurement of electronic conductivity. In many cases marked deviation from the behaviour predicted by Wagner's equation has been observed[7] and various explanations have been offered. Schoonman et al[8] reported the formation of lead oxide at the cathode interface in a cell constructed to determine the nature of the electronic conduction process in lead bromide. These authors suggested the incomplete blocking of the Faradaic process during polarisation was a possible source of deviation from the ideal gradient in the Log i versus E plot.

Joshi et al[9] proposed that non-ideal Log i versus E behaviour was a consequence of the application of polarisation voltages in excess of a critical voltage E_c, which was defined according to equation [10].

$$E_c = - \frac{2.303\ RT}{nF} \log \frac{\sigma_{\oplus}^{o}}{\sigma_i} \qquad [10]$$

Joshi suggested that at polarisation above this critical voltage the condition $\sigma_i >> \sigma_e$ is violated and Wagner's theory is no longer valid. The E_c value was not, for Joshi's experiments, near the decomposition potential. Experimentally the upper limit at which measurements are stopped to avoid electrolysis is a somewhat arbitary decision which restricts the the range of voltage investigated and means that the evaluation of hole conductivity may be subject to considerable error.

In several electrolytes electronic conductivity is sensitive to environment, and the importance of the Wagner technique is that it defines the conditions under which the electronic conductivity applies. The electronic conductivities, $\sigma^{o}_{\oplus}$ and $\sigma^{o}_{\ominus}$, of the cell are defined as those which would be observed in a cell M / electrolyte / M, (where M^{n+} is the mobile ion responsible for conduction), under zero applied voltage. This evaluation of the electronic conductivity is obtained by extrapolation of the current voltage relationship to zero voltage, as the "standard"

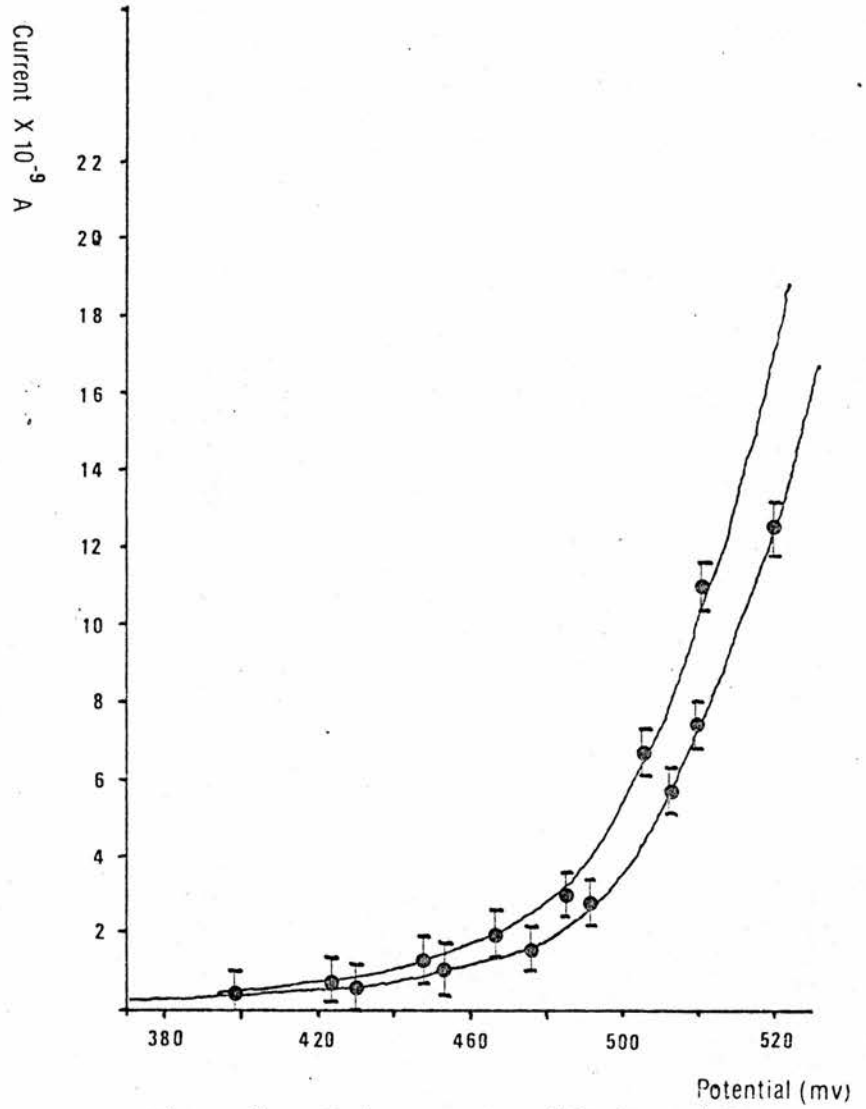

Figure 3a: Iodoarsenate with O_2 and N_2 flow gas

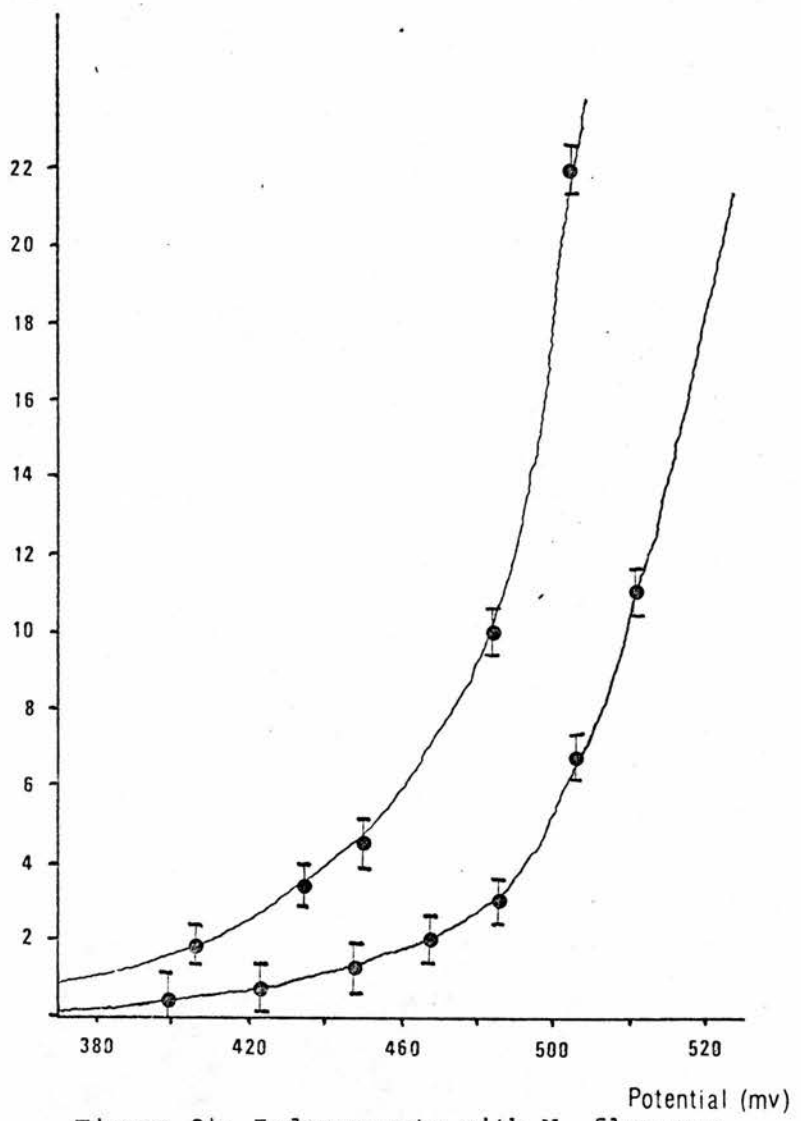

Figure 3b: Iodoarsenate with N_2 flow gas at 25°C and 40°C

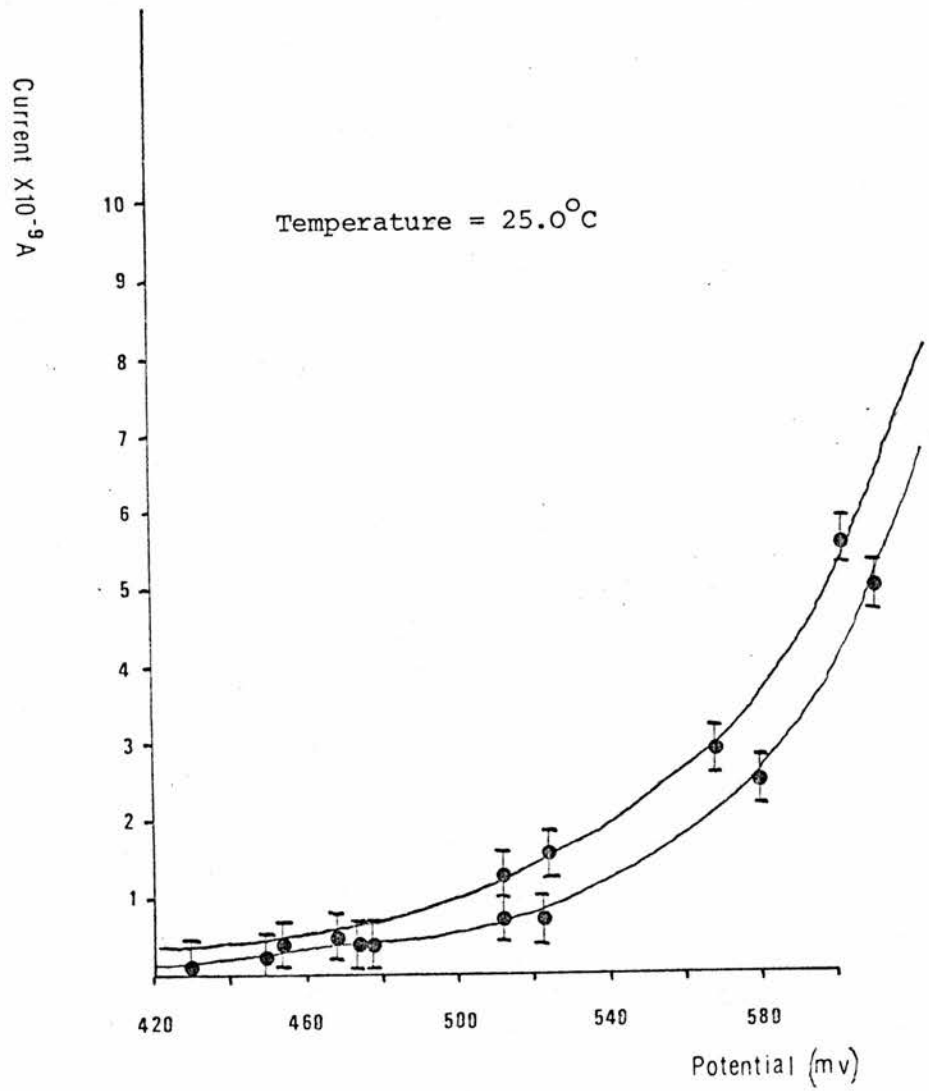

Figure 4a: Iodotungstate with potential O_2 and N_2 flow gas

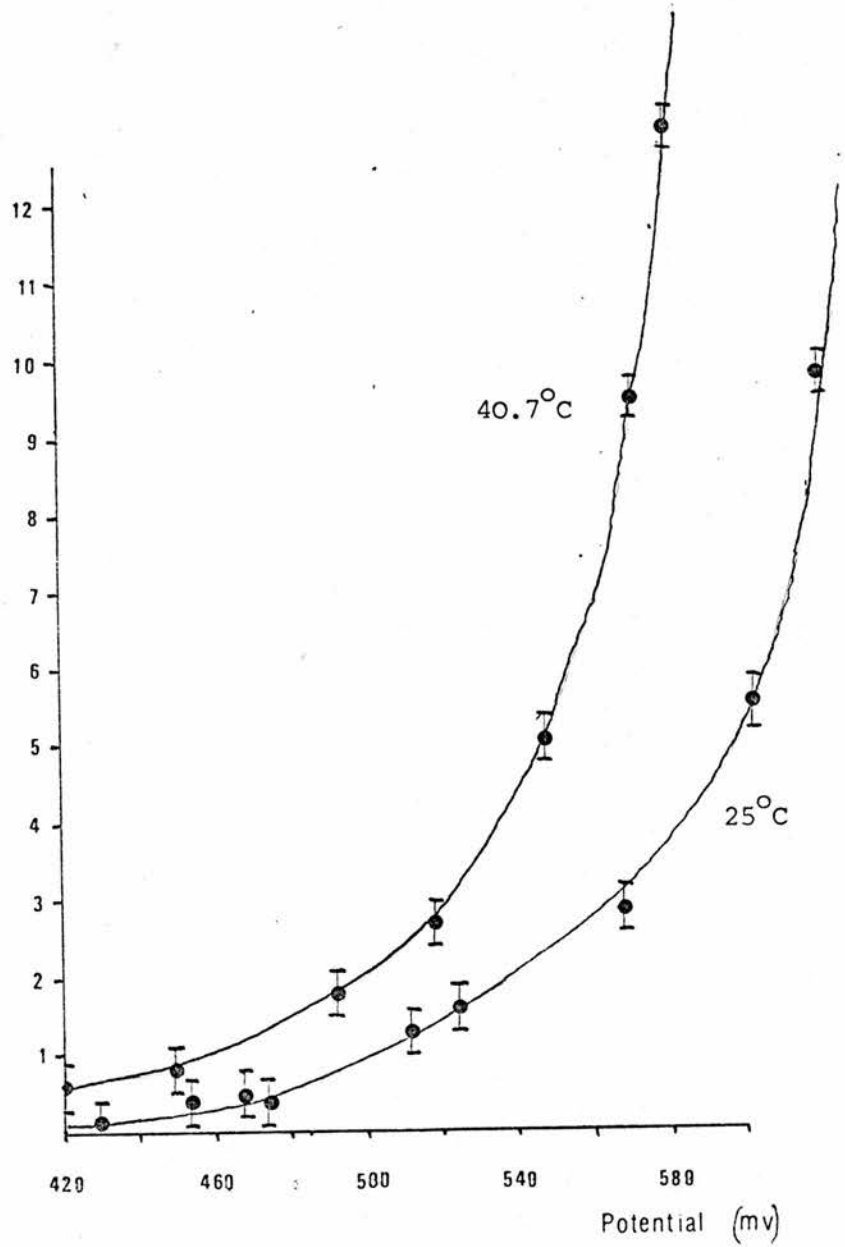

Figure 4b: Iodotungstate with N_2 potential flow gas at 25°C and 40.7°C

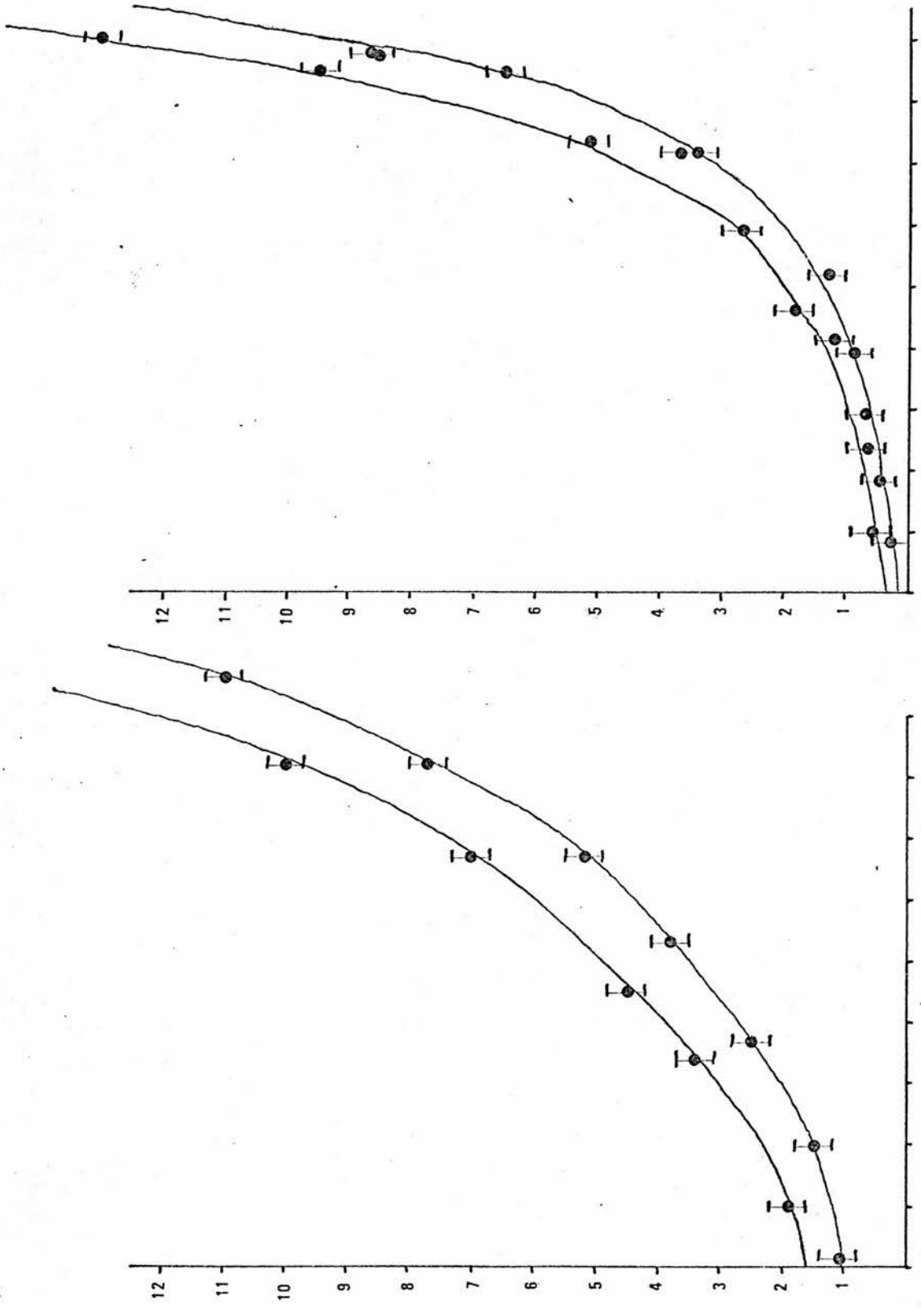

Figure 5: Iodoarsenate with "wet" O_2 and N_2 flow gas

Figure 6: Iodotungstate with "wet" O_2 and N_2 flow gas

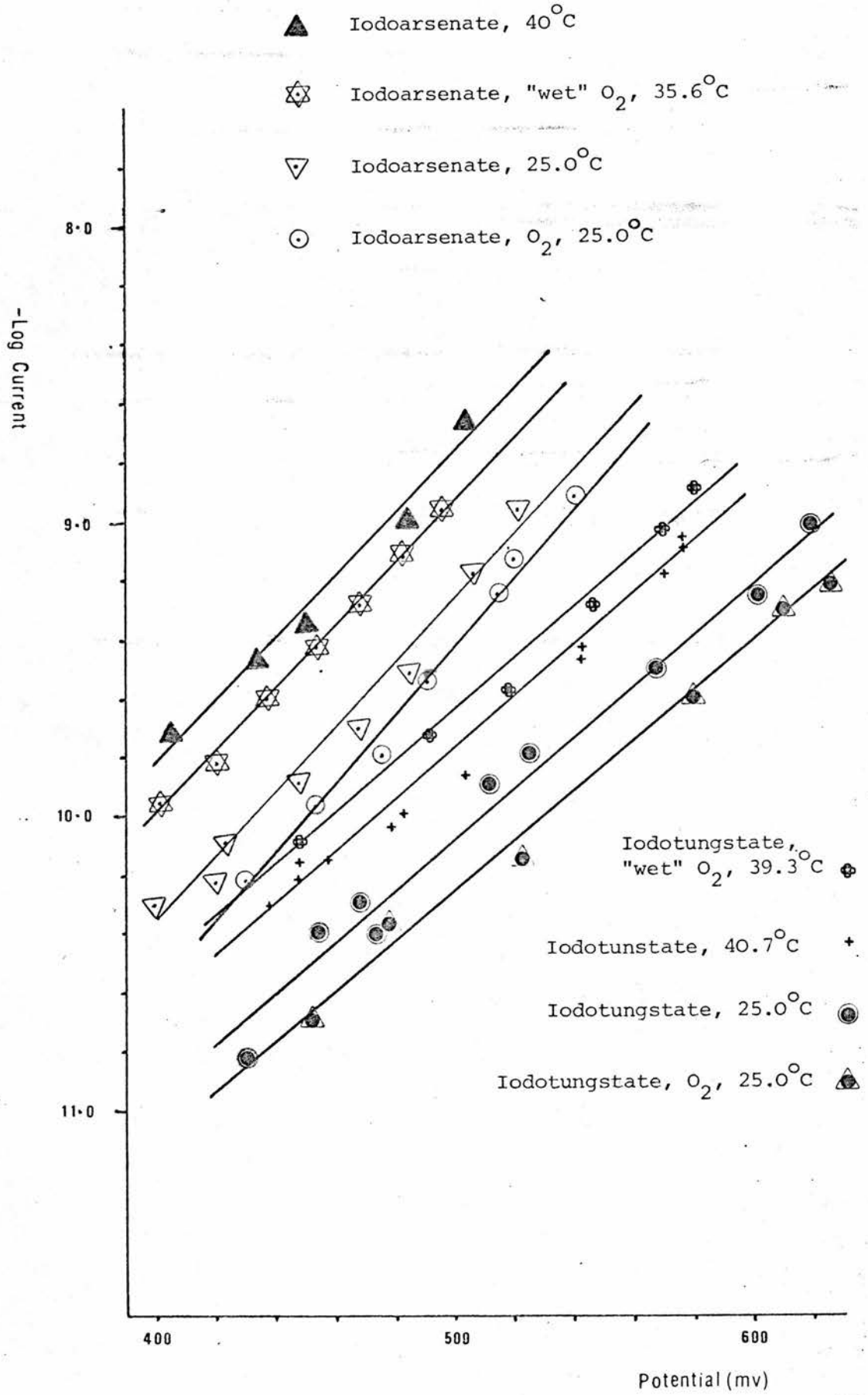

Figure 7: -Log i versus applied potential plots

voltage at which σ_e is quoted. It is important to realise that for $\sigma^{\circ}_{\ominus}$ this is the maximum value that $\sigma_{\ominus}$ assumes, while for $\sigma^{\circ}_{\oplus}$ the quoted value will be very much less than that shown by the electrolyte under cell operating conditions. This led to the proposal, by Kennedy[10], that in electrolytes in which hole conductivity is observed, a more useful parameter to report would be an "electronic decomposition potential". An alternative proposition from Joshi et al[11] is that an "electronic leakage current", calculated on the basis of $\sigma_{\oplus}$ under conditions of potential and temperature which an operational cell might experience, should be quoted. This would provide a more accurate indication of the magnitude of the cell self discharge current.

An example to illustrate this latter proposal might be found in the cells used in Chapter 4. At 400 mV, 25°C and under nitrogen atmosphere, the leakage current of the iodotungstate electrolyte would be less than 2×10^{-11}A. Under these conditions the electrolyte performs satisfactorily.

6.4 Conclusions and Further Work

Other authors have reported a composition dependance of electronic conductivity of crystalline solid electrolytes based on silver iodide. As the ionic conductivities of these electrolytes are strongly dependant on composition, a variation in electronic conductivity might be expected. This may lead to optimisation studies with respect to electronic conductivity.

During the last decade several vitreous electrolytes based on silver iodide have been reported[12]. Thorough investigations of the Wagner type have been carried out on very few of these. A comparative study based on the electronic conductivity of these electrolytes may be of interest.

1. Raleigh D.O., Progr. Sol. St. Chem., Volume 3 (1966) 83

2. Bradley J.N., Greene P.D., Faraday Soc., Volume 63 (1967) 2516

3. Owens B.B., Argue G.R., Science, Volume 157 (1967) 308

4. Yao Y.-F., Kummer J.T., J Inorg, Nuclear Chem., Volume 29 (1967) 2453

5. Wagner C., Z. Phys. Chem., Volume B21 (1933) 25

6. Raleigh J., Phys. Chem. Solids, Volume 26 (1965) 329

7. Ilschner B., J. Chem. Phys., Volume 28 (1958) 1109

8. Macke A.J.H., Schoonman J., J. Sol. St. Chem., Volume 5 (1972) 105

9. Joshi A.V., Liang C.C., J. Phys. Chem. Solids, Volume 36 (1975) 927

10. Kennedy J.H., J. Electrochem. Soc., Volume 124 (1977) 865

11. Hamilton N.E., Joshi A.V., Liang C.C., J. Applied Electrochem., Volume 8 (1978) 445

12. Broers G.H.J., Bronwer A., Schottens B.B., J. Applied Electrochem., Volume 8 (1978) 165

13. Gurevich Yu.Ya., Ivanov-Shits A.K., Electrokhimiya, Volume 16 (1980) 3

APPENDIX

Program 1: Data Receive and Formatting

```
4 RUN 100
44 PRINT @37,26:0
45 PRINT @51,11:0
46 END
80 PRINT @37,26:1
81 LIST @51:
82 PRINT @37,26:0
83 END
100 REM ************************************************************************
101 REM *****  Keyboard Data Input of Parameters                            *****
102 REM ************************************************************************
110 PRINT "↓Enter Cat Data Title (max 70 characters)::↓"
120 INPUT A$
130 PRINT "↓↓Enter Timescale(msec/address),Voltage scale(mV/count),"
140 PRINT "↓Number of Scans,Celsius Temperature,and Tape File Number.↓↓"
150 PRINT @37,0:32,255,255
160 INPUT %31:T4,V,N1,T1,N
170 PRI "↓↓↓Enter Analysis start,and Terminate Addresses,Baseline count"
180 PRINT "↓      Guest concentration ,Pulse current and Nignore.↓↓"
190 INPUT %31:S,X,B,C5,B1,L
200 PRINT @37,0:13,255,255
210 PRINT @32,26:0
211 REM ************************************************************************
212 REM *****  Initiate Data Communications                                 *****
213 REM ************************************************************************
220 REM L$ is a lf
230 C$=CHR(13)
240 REM C$ is a CR
250 CALL "RSTRIN","↓",C$,"↓↓↓↓↓↓"
260 CALL "RATE",1200,0,2
270 CALL "RCRLF",1,0,1
280 PRINT "↓Start Cat Output at 1200 baud rate after the two beeps."
290 FIND N
300 PRINT "↓↓"
310 CALL "WAIT",0.5
320 PRINT "↓"
330 CALL "DIRECV"
340 CLOSE
350 CALL "WAIT",5
360 ON EOF (0) THEN 400
370 FIND N
380 INPUT @33:X$
390 GO TO 380
400 PRINT @33:"**"
410 KILL N+2
420 FIND N+2
430 PRINT @33:A$
440 PRINT @33:T4,V,N1,T1,C5,B1
450 T=T1+273.15
455 Z=EXP(V*96487/(8.314*T*1000*N1))-1
457 L=L+1
```

```
458 S=S+1
460 DIM A$(66),M(1030),F(250)
461 REM ************************************************************************
462 REM *****  Create Primary Data Array                                  *****
463 REM ************************************************************************
470 FIND N
480 ON EOF (0) THEN 560
490 FOR J=1 TO 1023 STEP 8
500 INPUT @33:Y,M(J),M(J+1),M(J+2),M(J+3),M(J+4),M(J+5),M(J+6),M(J+7)
510 NEXT J
560 GOSUB 2000
570 GOSUB 3500
580 KILL N
590 FIND N
591 REM ************************************************************************
592 REM *****  Write Data for Voltage Time Plot                           *****
593 REM ************************************************************************
600 FOR I=1 TO 1022
610 WRITE @33:M(I)
620 NEXT I
630 CLOSE
640 GOSUB 4000
730 DELETE F
731 REM ************************************************************************
732 REM *****  Remove IR Drop by Iterative Routine                        *****
733 REM ************************************************************************
740 DIM M1(700)
750 FOR K=S TO X
760 M1(K-S+1)=EXP((M(K)-B)*96487*V/(8.314*T*1000*N1))-1
770 NEXT K
771 GOSUB 2500
772 PRINT "&Output Values of count and intercept"
773 PRINT B,B1
775 IF B1<Z THEN 778
776 B=B+1
777 GO TO 740
778 IF B1<0 THEN 781
780 GO TO 1340
781 B=B-1
782 GO TO 740
783 REM ************************************************************************
784 REM *****  Write Data for Voltage Time Parameter Plot                 *****
785 REM ************************************************************************
1340 KILL N+1
1350 FIND N+1
1360 FOR I=1 TO X-S+1
1370 WRITE @33:M1(I),T2(I)
1380 NEXT I
1390 FIND 2
1400 OLD
1401 REM ************************************************************************
1402 REM *****  Subroutine Outputs Hard Copy of Data                       *****
1403 REM ************************************************************************
2000 PRINT @51,11:1
2010 PRINT @37,26:1
2020 PRINT @51:A$,"@"
2030 PRINT @51:"Timescale  Voltage scale  Scan Count  Temp@"
2035 PRINT @51:"   ";T4;"          ";V;"          ";N1;"     ";T
```

```
2040 PRINT @51:
2050 PRINT @51:
2060 FOR I=1 TO 1024 STEP 20
2070 PRINT @51: USING "4D,3X,S":I-1
2080 FOR J=I TO I+19
2090 IF J<1024 THEN 2120
2100 J=I+19
2110 GO TO 2130
2120 PRINT @51: USING "2X,4D,S":M(J)
2130 NEXT J
2140 PRINT @51:
2150 NEXT I
2160 PRINT @51:
2170 PRINT @51:
2180 PRINT @37,26:0
2190 RETURN
2191 REM ************************************************************************
2192 REM *****  Linear Regression Analysis                                  *****
2193 REM ************************************************************************
2500 DELETE T1,X1,X2,X3,Y1,Y2,Y3,P2,C
2510 RESTORE
2520 DATA 0,0,0,0,0,0,0,0
2530 READ X1,X2,X3,Y1,Y2,Y3,P2,C
2540 FOR I=1 TO 40
2550 X1=X1+T2(I)
2560 X2=T2(I)*T2(I)
2570 X3=X3+X2
2580 Y1=Y1+M1(I)
2590 Y2=M1(I)*M1(I)
2600 Y3=Y3+Y2
2610 P1=M1(I)*T2(I)
2620 P2=P2+P1
2630 C=C+1
2640 NEXT I
2650 A1=P2-X1*Y1/C
2660 A2=X3-X1*X1/C
2670 A3=A1/A2
2680 A3=INT(A3*10000)/10000
2690 B1=Y1/C-A3/C*X1
2700 B1=INT(B1*10000)/10000
2710 R1=P2-X1*Y1/C
2720 R2=R1*R1
2730 R3=X3-X1*X1/C
2740 R4=Y3-Y1*Y1/C
2750 R5=R2/(R3*R4)
2760 R6=R5*R5
2770 R6=INT(R6*10000)/10000
2780 RETURN
3000 PRINT @51,11:1
3010 PRINT @37,26:1
3020 FOR I=1 TO 24 STEP 8
3030 FOR J=I TO I+7
3040 IF J=>24 THEN 3090
3050 PRINT @51: USING "2X,2D.7D,S":M1(J)
3060 NEXT J
3070 PRINT @51:
3080 NEXT I
3090 PRINT @37,26:0
```

```
3100 RETURN
3101 REM ************************************************************************
3102 REM ***** Noise Reduction Subroutine                                  *****
3103 REM ************************************************************************
3500 M2=0
3510 FOR I=2 TO 242
3520 M2=M2+M(I)
3530 NEXT I
3540 M2=INT(M2/240)
3550 M(1)=M2
3560 FOR I=1 TO 241
3570 F(I)=M(I)-M2
3580 NEXT I
3590 S1=1
3600 FOR I=1 TO 5
3610 FOR J=1 TO 240
3620 M(S1)=M(S1)-F(J)
3630 S1=S1+1
3640 IF S1=1022 THEN 3670
3650 NEXT J
3660 NEXT I
3670 RETURN
3671 REM ************************************************************************
3672 REM *****  Routine Sets up Time Parameters Arrays                    *****
3673 REM ************************************************************************
4000 DELETE T1,T2
4010 DIM T1(400),T2(400)
4020 D=L*5.0E-4
4030 T1(1)=D
4040 T2(1)=SQR(T1(1))
4060 FOR I=2 TO X-S+1
4070 T1(I)=T1(I-1)+5.0E-4
4080 T2(I)=SQR(T1(I))
4090 NEXT I
4100 RETURN
```

Program 2: Plotting Program

```
  4 GO TO 100
 80 PRINT @37,26:1
 81 LIST @51:
 82 PRINT @37,26:0
 83 END
 97 REM ************************************************************************
 98 REM *****  Keyboard Input of Data File Number                          *****
 99 REM ************************************************************************
100 PRINT "£@@Enter Raw Cat Data File Number ";
110 INPUT N
120 PAGE
130 DIM A$(66),M(1024)
140 ON EOF (0) THEN 190
150 FIND N
160 FOR J=1 TO 1024
170 READ @33:M(J)
180 NEXT J
190 FIND N+2
200 INPUT @33:A$
210 INPUT @33:T,V,N1,T1,C5,B1
220 V=V/1000
230 M7=-1.0E+100
240 FOR I=1 TO J-1
250 M(I)=M(I)*(V/N1)
260 M7=M(I) MAX M7
270 NEXT I
280 M7=M7+M7/10
290 M5=5.0E-4
300 N7=M7/M5
310 IF N7<0 THEN 365
320 M5=M5*2
330 GO TO 300
365 L=32
366 X=123
367 V$="Voltage Parameter"
368 H$="Time Parameter"
370 GOSUB 3000
760 INPUT S$
770 L=1
780 X=145
790 GOSUB 3000
1170 INPUT S$
1210 A=0.1256637
1220 B=B1
1230 T7=T1+273.15
1250 DELETE T,V,M,M1,T1
1260 DIM A$(66),X$(1),T(1024),V(400)
1270 ON EOF (0) THEN 1330
1280 FIND N+1
1290 FOR I=1 TO 693
1300 READ @33:V(I),T(I)
1310 Z=I
```

```
1320 NEXT I
1330 T1=T(Z-1)
1340 V1=V(Z-1)+V(Z-1)/10
1350 V2=10↑INT(LGT(V1))
1360 V3=V2/5
1380 IF V1/V3=>5 THEN 1410
1390 V3=V3/2
1400 GO TO 1380
1410 IF V1/V3>10 THEN 1430
1420 GO TO 1495
1430 V3=V3*2
1440 GO TO 1410
1495 X=123
1496 L=32
1497 PAGE
1500 GOSUB 3500
1520 DATA 0,0,0,0,0,0,0,0,0
1530 READ X1,X2,X3,Y1,Y2,Y3,P2,C
1535 GOSUB 2000
1540 GOSUB 4000
1870 INPUT S$
1880 X=145
1890 L=1
1900 GOSUB 3500
1910 GOSUB 4000
1913 REM*****************************************************************************
1914 REM *****  Linear Regression Analysis                                      *****
1915 REM*****************************************************************************
1920 END
2000 FOR I=1 TO Z
2010 X1=X1+T(I)
2020 X2=T(I)*T(I)
2030 X3=X3+X2
2040 Y1=Y1+V(I)
2050 Y2=V(I)*V(I)
2060 Y3=Y3+Y2
2070 P1=V(I)*T(I)
2080 P2=P2+P1
2090 C=C+1
2100 NEXT I
2110 A1=P2-X1*Y1/C
2120 A2=X3-X1*X1/C
2130 A3=A1/A2
2140 A3=INT(A3*10000)/10000
2150 B1=Y1/C-A3/C*X1
2160 B1=INT(B1*10000)/10000
2170 R1=P2-X1*Y1/C
2180 R2=R1*R1
2190 R3=X3-X1*X1/C
2200 R4=Y3-Y1*Y1/C
2210 R5=R2/(R3*R4)
2230 R6=INT(R5*10000)/10000
2240 C1=4*B*B+4
2242 C2=96487*96487*A*A*PI*A3*A3*C5*C5
2244 C3=C1/C2
2246 RETURN
```

```
2765 REM*************************************************************
2766 REM *****  Voltage Versus Time Plot                          *****
2767 REM*************************************************************
3000 VIEWPORT 18,X,17,86
3010 WINDOW Ø.1Ø24,Ø,M7
3020 AXIS @L:2ØØ,M5
3025 PRINT @L,17:1.17,1.88
3030 FOR I=Ø TO 1Ø24 STEP 2ØØ
3040 MOVE @L:I,Ø
3050 PRINT @L:"ØØ";I*Ø.5
3060 NEXT I
3070 FOR I=Ø TO M7 STEP M5
3080 MOVE @L:Ø,I
3090 PRINT @L: USING """#########"",1D.4D":I
3100 NEXT I
3105 PRINT @L,17:1.79,2.82
3110 MOVE @L:Ø,7*M7/8
3115 PRINT @L:"#########";
3120 FOR I=1 TO LEN(V$)
3130 X$=SEG(V$,I,1)
3140 PRINT @L:X$;"#Ø";
3150 NEXT I
3160 PRINT @L:"##Ø";" (V)";
3170 MOVE @L:35Ø,-M5
3180 PRINT @L:h$;"(msecs)";
3190 FOR I=245 TO J-1
3200 MOVE @L:I,M(I)
3210 DRAW @L:I,M(I)
3220 NEXT I
3230 MOVE @L:Ø,M7
3240 PRINT @L:"KK";A$
3250 RETURN
3253 REM*************************************************************
3254 REM *****  Voltage Versus Time Paramaters Plot               *****
3255 REM*************************************************************
3500 VIEWPORT 18,X,17,86
3510 WINDOW Ø.T1,Ø,V1
3520 AXIS @L:Ø.1,V3
3525 PRINT @L,17:1.17,1.88
3530 FOR I=Ø TO T1 STEP Ø.1
3540 MOVE @L:I,Ø
3550 PRINT @L:"ØH#";I
3560 NEXT I
3570 FOR I=Ø TO V1 STEP V3
3580 MOVE @L:Ø,I
3590 PRINT @L: USING """#######"",1D.3D":I
3600 NEXT I
3605 PRINT @L,17:1.79,2.82
3610 MOVE @L:Ø,7*V1/8
3615 PRINT @L:"#########";
3620 FOR I=1 TO LEN(V$)
3630 X$=SEG(V$,I,1)
3640 PRINT @L:X$;"#Ø";
3650 NEXT I
3660 MOVE @L:Ø.4*T1,Ø.7*-V3
3670 PRINT @L:H$
3680 FOR I=1 TO Z
3690 MOVE @L:T(I),V(I)
```

```
3700 DRAW @L:T(I),V(I)
3710 NEXT I
3720 MOVE @L:0,V1
3730 PRINT @L:"##";A$
3740 RETURN
3744 REM*************************************************************
3745 REM *****  Data Output Calculation Results                  *****
3746 REM*************************************************************
4000 MOVE @L:T1/20,V1
4010 PRINT @L,17:1.17,1.88
4020 PRINT @L:"0";"Gradient of Linear Regression ::";"  ";A3
4025 MOVE @L:T1/20,V1
4030 PRINT @L: USING 4040:B1
4040 IMAGE "@@@Intercept of Linear Regression::  ",fd.fd
4045 MOVE @L:T1/20,V1
4050 PRINT @L:"@@@@@";"Correlation Coefficient       ::";"  ";R6
4060 IMAGE 39A,1X,4E
4065 MOVE @L:T1/20,V1
4070 PRINT @L: USING 4060:"@@@@@@@Diffusion Coefficient          ::";C3
4080 PRINT @L,17:1.79,2.82
4090 RETURN
```